EXPERIMENTAL INVESTIGATION OF THE FACTORS AFFECTING THE WETTABILITY OF AQUIFER MATERIALS

by

Jodi L. Ryder

A dissertation submitted in partial fulfillment
of the requirements for the degree of
Doctor of Philosophy
(Environmental Engineering)
in The University of Michigan
2007

Doctoral Committee:

Associate Professor Avery H. Demond, Chair
Professor Kim F. Hayes
Professor Philip A. Meyers
Associate Professor Terese M. Olson
Professor Linda M. Abriola, Tufts University

“Believe that with your feelings and your work you are taking part in the greatest; the more strongly you cultivate this belief, the more will reality and the world go forth from it.”

-Rainer Maria Rilke

ACKNOWLEDGEMENTS

For all her patience, instruction and direction, I can never thank my advisor, Avery Demond, enough. You've been a transformative presence in all aspects of my scholarship and, despite my apparent stubbornness, I've appreciated your gentle encouragement. Thank you for going above and beyond to share your experiences and knowledge about the academic institution as well as the practical aspects of research.

Thanks to Hsin-Lan Hsu for many years of friendship and collaboration.

Thanks are due to Dr. Francis P. Miknis for the collection of NMR spectra. Thanks to Michela Arnaboldi and Basamm Almasari for instruction is the collection of bulk elemental composition. Thanks to Dr. Walter J. Weber for the use of the FTIR equipment. This research was supported in part by Grant No. DE-FG07-96ERI4702 from the Environmental Management Science Program, United States Department of Energy (DOE). Any opinions, findings, conclusion, or recommendation expressed herein are those of the author and do not necessarily reflect the views of DOE.

I have been fortunate to be surrounded by several students who gave survival advice, scholarly input, and friendship. Many thanks to Denis O'Carroll, Tom Phelan, Tanya Gallegos, Hans Tritico, Andrew Henderson, Karlin Danielson, Eduardo de Silva, John Christ, and Leonardo de Oliviera. Several people in EWRE have supported my work over the years, including, Nancy Osuigi, Rick Burch, Tom Yavarski, Jill Miller, and Janet Lineer.

I would not have made it without the love and support of my family at St. Clare's: Chuck and Vickie Hatt, David Treadwell, Leslie De Pietro, David Clifford, Jayin Rhodenheiser, Fr. Marianna Groenik, Barry Fuller and Christine Modey, Mary and Jan Barber, Karen Slagell, and Gail Jungbluth. There were many days that I would have quit if not for the encouragement of my friends at the Ann Arbor Rowing Club: Catherine Frieman, Robin Schultz-Purves, Merrill Mullis, Amy Stone, Jen Shifferd, Mike Taft, Ron Woodman, Sandy Rutherford, and Tom Kraft.

I have the best family ever, who refuse to let me be anything but my best: Travis and Rachel Dahl, Kimi Ryder (sister, nanny and friend), Sharon and Brooks Ryder, Ken and Chris Dahl, and Jen Bowers Williams.

And finally, I would not have made it this far without the financial support of my Grammy, Grammy Ryder, and Great Grandma Neva who have believed in me and inspired me. I am honored to belong to such a tradition of strong, intelligent and resourcesful women.

TABLE OF CONTENTS

LIST OF FIGURES

LIST OF TABLES

LIST OF APPENDICES

ABSTRACT

EXPERIMENTAL INVESTIGATION OF THE FACTORS AFFECTING THE WETTABILITY OF AQUIFER MATERIALS

by

Jodi L. Ryder

Chair: Avery H. Demond

The correlation between the wettability of soil materials and soil chemical composition and surface energy is examined. Wettability, as measured by the contact angle, is a governing parameter of capillary flow in the subsurface. The contact angle is determined by the intermolecular forces at the intersection of a drop with a surface and surrounding fluid. It was previously assumed that although most soil materials are water wet, similar to quartz sands, some organic-carbon containing materials may be hydrophobic. However, this work determines that some common subsurface media may have radically different wetting behavior depending on the past wetting history even in the absence of surface active agents. The wettability of four organic carbon containing natural soil materials (Ann Arbor II sand, Lachine shale, Garfield shale, and Waynesburg Coal), three carbon containing mineral materials (graphite, dolomite, and calcite), and two pure mineral materials (quartz and talc) was measured by bottle tests and sessile

contact angle measurements. The liquid systems examined included air-water, perchloroethylene-water, and carbon tetrachloride-water. The wettability of soil materials is shown to depend on the order of fluid contact with the surface such that some soils (talc and organic carbon-containing materials) are non-water wet if contacted by a non-aqueous phase first. This relatively unexplored phenomenon is termed wettability hysteresis and may indicate that the wettability of some soils will differ depending on the saturation of the system. The effect of the surface composition on the contact angle and degree of hysteresis was quantified by measuring the surface energy components of the surface. It is shown that oxygen indices are a better predictor of contact angle and wettability hysteresis than carbon content. The surface energy components (dispersion, polar, and total) of each solid are determined by the van Oss-Chaudhury-Good method and the polar surface energy component is shown to determine wettability hysteresis. Evidence that a water film forms when water is the first fluid to contact the surface, causing wettability hysteresis, is provided from multiple approaches. The estimation of contact angle and wettability hysteresis based on the polar surface energy component is presented.

CHAPTER 1

INTRODUCTION, OBJECTIVES, AND BACKGROUND

1.0 DNAPLs in the subsurface

Dense Non-Aqueous Phase Liquids (DNAPLs), such as tetrachloroethylene, also known as perchloroethylene (PCE), are a major concern for groundwater quality. Chlorinated solvents have been used since the development of the synthetic chemical industry in the 1940's. They have been employed as degreasers for civilian and military use, automobile repair, aircraft service, dye manufacturing, machining, asphalting, electronics, and dry cleaning as well as ingredients in paints and paint thinners, dyes, adhesives, septic tank treatments, and many household products (Schwille, 1988). Production for industrial uses continues at an estimated 318 million pounds per year (U.S. Department of Health and Human Services, 2007). A 1992 study of 91 Department of Energy (DOE) waste sites and 18 DOE facilities revealed that nearly 80% of DOE facilities report the presence of chlorinated hydrocarbons in ground water samples, with PCE reported at more than 50% of DOE sites (Riley and Zachara, 1992).

Chlorinated solvents are a particular problem because they have toxic properties at high concentrations and are carcinogens at low concentrations and can cause harm by ingestion, inhalation, and dermal contact. Most chlorinated solvents have Maximum Contaminant Limits (MCLs), defined as the maximum allowable concentration in drinking water to produce less than 1 in a million additional cancers per year, that are orders of magnitude below their solubility limit. For example, PCE has a solubility of 150 mg/L and the MCL is 0.005 mg/L (Code of Federal Regulations, 2002). Health concerns with chlorinated compounds include their moderate persistence in fatty tissues that allow them to build up high concentrations in the body over time, causing neurological damage, toxicity, and possible synergism with other carcinogens. A further

concern with chlorinated solvents is their co-solvent properties. Trace compounds which were removed during the solvent's initial use as a cleaner or degreaser can remain in the waste. An examination of DOE sites revealed that chlorinated hydrocarbons carry trace quantities of other contaminants such as fuel hydrocarbons, PCBs, metals, and radio nuclides once the DNAPLs enter the subsurface (Riley and Zachara, 1992).

DNAPL distribution in the subsurface is dependent on the wettability of the soil solids. Wettability is the property of three-phase fluid-liquid-solid systems that describes which fluid or liquid preferentially spreads over the solid surface. It is important to note that the term water-wetting means that water spreads over the surface and has a contact angle less than 90° measured through the water phase regardless of the second fluid. The terms non-water wet or NAPL-wet refer to surfaces that have a contact angle through the water phase greater than 90°. The terms hydrophilic and hydrophobic are also used to indicate water wet or non-water wet solids respectively. Pump and treat remediation methods have been shown to be largely ineffective (Hunt and Sitar, 1988; Wilson and Conrad, 1990; Commission on Geosciences, Environment and Resources, 1994) because the distribution of the NAPL in the subsurface can prevent mobilization and prolong the dissolution timescale (Bradford et al., 1999). In a study of 93 sites, pump and treat methods were found to be satisfactorily effective at only the most homogenous, as heterogeneity in soil particle shape, size, and material all influence the distribution of immiscible liquids. Dwarakanath et al. (2002) concluded that more attention needs to be given to wettability and its effects in remediation after studying NAPL transport in five real NAPL-soil systems. This may improve the ability to account for heterogeneity in fluid distribution when planning remediation actions.

1.1 Soil heterogeneity

Heterogeneity in soil materials can exist at the macroscopic level in the form of layers or regions of varying soil composition. At the smaller scale, outwash deposits may contain a mixture of many grains of different composition. At the microscale, a single soil pore may be bounded by multiple types of grains. Figure 1 illustrates heterogeneity in the subsurface. Thus, a waste liquid will not necessarily be present as a uniform,

continuous source of contamination to surrounding groundwater but may be distributed heterogeneously according to the horizons or regions of certain types of soil materials.

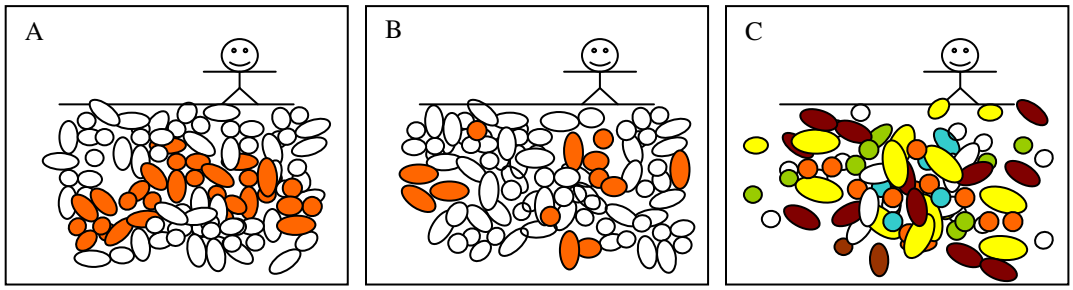

Figure 1.1, Spatial heterogeneity of soil grains in the subsurface. A) layers of varying composition, B) blocks of varying composition, C) outwash of varying composition.

The impact of hydrophobic sand grains is not necessarily proportional to their fraction of the total soil mass. In a tightly packed uniform sand, a single soil grain contacts up to 12 other grains (Hillel, 1980). Thus, a single grain contributes to the pore walls of several pore spaces. Hence, the fluid interface between the two liquids may be influenced by the presence of hydrophobic grains in several pores. Hydrophobic grains were shown to constitute a single soil size fraction in a sample by Bisdom et al. (1993). Indeed, Bauters et al. (2000) calculated that 37% of the pore spaces will have at least one hydrophobic pore wall in a soil containing 3.1% hydrophobic grains. Combes et al. (1998) used environmental scanning electron spectroscopy to show that wettability heterogeneity does occur at the pore scale. Two types of cores, mixed wettability sandstone and carbonate, were observed as pressurized fluid was introduced into the cores. In both cases, there appeared to be two simultaneous routes of fluid movement in a single core. In the carbonate, the large pores had become oil-wet while the small pores remained water-wet. In the mixed wettability sandstone, zones of kaolinite provided a network of oil-wet pores. Thus, both cores demonstrated spontaneous imbibition of the oil phase.

1.2 Influence of wettability on residual distribution of NAPLs

The main source of continued NAPL input to downstream water resources are blobs and ganglia of residual NAPL residing in the subsurface. The residual NAPL is the result of the combined effects of wettability and pore morphology. The immobilized blobs of NAPL comprise the residual phase which is usually between 15 and 50% NAPL saturation (Mercer and Cohen, 1993). Blobs of residual NAPL form by snap-off and by-passing. By-passing occurs when pores branch and have irregular geometry. In some cases, a stable interface between the two fluid phases cannot form at the entrance to the pore and one fluid remains connected to the source while the other is isolated in the pore. Snap-off occurs when the non-wetting fluid moves between two large pores via a narrow pore throat. Snap-off depends largely on the aspect ratio of the pore diameters. The smaller the contact angle between the wetting phase and the solid, the less severe the aspect ratio has to be to cause snap-off. In intermediate wetting systems, there is less snap-off and by-passing which is why it is an ideal condition for NAPL or oil recovery (Morrow et al., 1988).

In addition to increasing the amount of residual saturation, soil texture and wettability heterogeneity also influence the interfacial area between the fluids and hence, the rate of mass transfer between the NAPL to the water phase. Powers (1992) showed experimentally that assuming local equilibrium may over-estimate the interphase transfer of NAPL to the water phase and underestimate the length of time and volume of water necessary to remove the NAPL. Bradford et al. (2000) paired experimental and numerical simulation of fractionally wet sands to show that PCE dissolution and remediation time are influenced by both the magnitude and spatial distribution of wettability heterogeneities. Wilson and Conrad (1990) showed that the position of the blob within the pore space can influence interphase mass. Since wettability can have a profound impact on many subsurface processes involving DNAPLs, this study will examine several soil materials which are expected to have variable wettability.

Yet, it is not clearly understood which soils are expected to have differing wettability. Most wettability studies have focused on pure mineral phases such as quartz sand, although anecdotal evidence abounds citing organic carbon-containing soil materials as water repellent, NAPL-wet, or hydrophobic. In the literature, water

repellency usually refers to air-water systems, such as the vadose zone and ground surface, and indicates a soil that is not easily wetted or resists the imbibition of water. Water repellency does not connote a specific contact angle. Similarly, the contact angle of water against a hydrophobic soil is not necessarily greater than 90°. The term hydrophobic is used in the literature to refer to both water repellant and non-water wet soils. It is also used to refer to non-polar chemical characteristics independent of their influence on the wettability of a surface. Because of the ambiguity in the literature it is best to use the contact angle as the definitive definition of wettability. Thus the goal of this study is to understand how the chemical composition of soil materials determines the contact angle.

1.3 Natural soil composition and wettability

Mineral soils are primarily composed of mineral grains. Although the most common mineral phase is quartz silica, other oxide minerals, carbonates, inorganic carbon, and clays are also present. Organic carbon may be present in two forms: direct contributions from the surface and geologically processed materials from parent rocks. The contributions of organic carbon from the surface may include leaf litter, plant roots, decaying organisms, algae, and extracellular material. As these materials age, they form humic solids which are large, condensed molecules with a large variety of chemical functional groups. Humic materials accumulate over geologic time to form coal and shale solids which are typically a mix of organic components and fine grained minerals. In air-water systems such as the vadose zone, mineral components are considered water-wet but organic carbon containing particles are believed to be less water wet. In the saturated zone, the wettability of non-silica soil materials is largely unknown. The wettability of some natural solids from the literature is shown in Table 1.1. Coals B2, Y1, and Y3, as well as the organic rich soil, were reported to have air-water contact angles that are intermediate wetting, supporting the claim that soils containing organic matter are less strongly water wet than quartz. However, air-water contact angles for some minerals, most notably the clay minerals hectorite, playgorskite, pyrophilite, and talc were also reported in the intermediate water wetting range, 60-90º. All of the

materials shown on Table 1.1 are wet by the droplet phase in air-dry systems and water-wet in NAPL-water systems, although the contact angles vary considerably.

Solid	Surrounding Phase	Droplet Phase	Contact Angle	Source
Calcite	Air	Water	0	1
Calcite	Air	Water	40.0	2
Coal B2	Air	Water	75.0	3
Coal Y1	Air	Water	62.0	3
Coal Y3	Air	Water	61.0	3
Hectorite	Air	Water	63.0	4
Kaolinite 1	Air	Water	46.1	5
Kaolinite 2	Air	Water	42.0	5
Organic rich soil	Air	Water	62.0	6
Playgorskite 1	Air	Water	61.0	5
Pyrophilite	Air	Water	79.2	4
Quartz	Air	Water	0-15	1
Quartz	Air	Water	29.0	2
Shale B3	Air	Water	31.0	3
Smectite 1	Air	Water	33.1	5
Smectite 2	Air	Water	20.5	5
Smectite 3	Air	Water	45.7	5
Smectite 4	Air	Water	21.7	5
Talc	Air	Water	80.4	4
Calcite	Air	Benzene	0	1
Calcite	Air	Benzene	18.0	2
Calcite	Air	Carbon tetrachloride	13.0	2
Calcite	Air	Ethylene glycol	72.0	2
Hectorite	Air	Ethylene glycol	57.3	4
Pyrophilite	Air	Ethylene glycol	46.1	4
Quartz	Air	Benzene	0	1
Quartz	Air	Benzene	12.0	2
Quartz	Air	Carbon tetrachloride	9.0	2
Quartz	Air	Ethylene glycol	35.0	2
Talc	Air	Ethylene glycol	48.8	4
Calcite	Benzene	Water	0	1
Ca-Montmorillite	Decane	Water	61.3	8
Ca-Montmorillite	Hexadecane	Water	64.8	8

Solid	Surrounding Phase	Droplet Phase	Contact Angle	Source
Ca-Montmorillite	Octane	Water	61.5	8
Mica	Benzene	Water	25.0	7
Mica	Carbon tetrachloride	Water	25.0	7
Mica	Chloroform	Water	30.0	7
Mica	1,2 Dichloroethane	Water	35.0	7
Mica	Dichloromethane	Water	29.0	7
Quartz	Benzene	Water	0-15	1

Table 1.1, Contact angles of some solids in the absence of surface active agents. Contact angles are given in degrees, measured through the droplet phase. Sources: 1) McCaffery and Mungan, 1970; 2) Ethington, 1990; 3) Miyamoto et al., 1977; 4) Giese et al., 1991; 5) Wu, 2001; 6) Sparks et al., 1999; 7) Schultz et al., 1978; 9) Jouany, 1991.

1.4 Objectives

The overall goal of this study is to understand the relationship between solid aquifer material composition and wettability. The first objective, explored in Chapter 3 and Appendices A and B, is to determine the wettability of natural soil materials and what conditions affect the wettability of these materials. Qualitative bottle tests and quantitative contact angle measurements were used to determine soil material wettability under a variety of conditions including air-dry solids, solids immersed in water, and solids immersed in non-polar NAPLs. The second objective is to relate the composition of aquifer materials to wettability, which is covered in Chapter 4. Bulk elemental composition is compared to contact angles and wettability hysteresis to determine which composition parameters are important in wettability and to develop predictive relationships for the wettability of natural materials based on composition. Surface specific FT-IR and NMR measurements are used to examine the surface functional groups of both organic and mineral solids. The third objective of this study is to apply surface free energy measurements to the aquifer materials to determine the source of wettability hysteresis and develop predictive relationships that can relate the contact angle for one system to another on the basis of surface energy. Surface free energy components for each solid were measured based on sessile contact angles following the method of van Oss (1988a). From these values, traditional and modified Zisman plots were created. Predictive relationships for the contact angle of an untested liquid on a

solid based on surface energy were then determined from an analysis of the solid surface energy component values.

Background

1.5 Capillary forces

Wettability controls the distribution of NAPLs in the subsurface because the fluid that wets the soil solid (most often assumed to be the aqueous phase) will coat the soil grains and is drawn by capillary forces into the smallest pores. The non-wetting phase is then limited to larger pores and often becomes immobilized as isolated blobs, which cannot be removed by a method such as pump and treat except under extreme pressures or flow rates (Morrow and Chatzis, 1988). The degree of capillarity depends on the contact angle, the angle formed by a tangent passing through the three phase point of contact. Figure 1.2 shows the contact angle of a droplet resting against a smooth surface and the analogous contact angle formed by the meniscus between two fluids in a capillary tube. The contact angle is described by Young's equation:

$$\gamma_{SL1} - \gamma_{SL2} = \gamma_{L1L2} \cos\Theta \qquad \textbf{Eqn. 1.1}$$

where γ indicates the interfacial tension between two phases and the subscripts S, L1, and L2 refer to the solid, the surrounding or immersion liquid phase, and the droplet phase respectively.

The capillary pressure, P_c, is the difference between the non-wetting and wetting fluid pressures across the curved interface. Capillary pressure depends on the contact angle through the relationship assuming a spherical meniscus:

$$P_c = \frac{2 * \gamma_{L1L2} \cos\Theta}{r} \qquad \textbf{Eqn. 1.2}$$

where r is the effective pore radius. The interfacial tensions γ_{SL1} and γ_{SL2} will depend on the surface free energy of the solid phase which, in turn, depends on the solid composition.

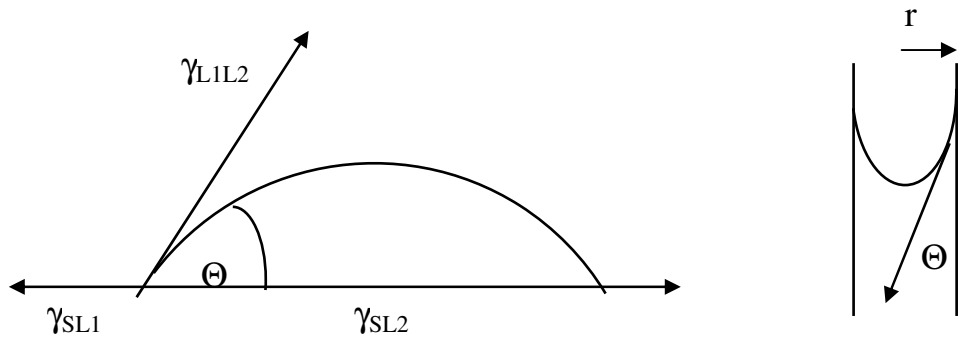

Figure 1.2, Contact angle made by a sessile drop and by a meniscus in a capillary tube.

1.6 Free surface energy

The Young equation given in equation 1.1 is essentially a force balance among the liquid and solid interfacial tensions. The magnitude of the contact angle indicates which liquid spreads over the surface. If the contact angle is less than 90º, measured through the water phase, the system is water-wet. To further divide the wettability scale, contact angles up to about 60º are usually interpreted as wetted by the droplet fluid. Contact angles of 60º to 120º denote neutrally wet or intermediate wet systems. Contact angles of 120º or above indicate non-wetting behavior by the droplet (Anderson, 1986). It is apparent that for a given solid, the wettability can only be reversed if the magnitude of the interfacial tensions between the solid and each liquid are reversed, that is if γ_{SL2} becomes larger than γ_{SL1}.

All molecules exert forces upon one another. These forces can be divided into two categories depending on whether the interacting bodies are permanently charged (Coulomb forces) or intermittently charged (van der Waals forces) due to the fluctuations of the electron cloud surrounding each molecule (dipoles). A permanent charge is an ion, a molecule that has more or less electrons than are needed to fill the outer valence shell. Even if a molecule has the exact number of electrons needed, the electrons are constantly moving around in an electron cloud. At any given moment, the electrons may be unevenly distributed giving rise to a dipole. A molecule such as methanol, CH_3OH, for

example has an uneven distribution of charge, called a permanent dipole, because the electronegative oxygen atom pulls the electron cloud toward itself. By contrast, PCE (C_2Cl_4) is completely symmetric in the location of electronegative atoms (chlorine) and has no permanent dipole. The Coulomb and van der Waals forces are described as occurring between pairs of molecules but the theory has been extended to describe forces interacting at surfaces (Israelachvili, 1992).

The Coulomb force is the strongest of the intermolecular forces discussed here but acts over a short length, on the order of the inverse square of the separation distance between the two bodies. Coulomb forces may be attractive or repulsive; an example is the electrostatic repulsion of colloidal particles in solution at pH extremes. Van der Waals forces act over longer distances, on the order of the inverse separation distance to the sixth power which is typically about 0.2 to 10 nm. Van der Waals forces can be further divided into three types; Keesom, Debye, and London dispersion forces. The Keesom force arises from the interaction between two permanent dipoles. Hydrogen bonding is a special case of Keesom attraction and is expected to play a large role in mineral wetting as the protons of the aqueous phase are attracted to electronegative oxygen in silica (SiO_2) and other oxide minerals. The Debye force is the result of a permanent dipole inducing a dipole in another molecule. The London dispersion force is present between all molecules as the result of the constantly shifting electron cloud. Momentary dipoles induce a momentary dipole in neighboring molecules. Figure 1.3 illustrates the types of forces possible between molecules in a fluid-liquid-solid system. The polar fluid, such as water, is the surrounding phase. The droplet is a non-polar NAPL, such as PCE. The magnitude of the Coulomb, Keesom, Debye, and London forces is unique to each fluid-fluid-or fluid-surface pairing.

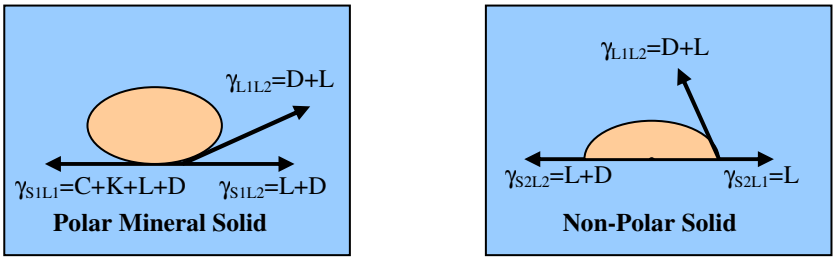

Figure 1.3, Forces present between two fluids and a solid where C, K, D, and L refer to Coulomb, Keesom, Debye, and London dispersion forces, respectively.

1.7 Measurement of free surface energy

Interfacial tensions can also be thought of as energy terms describing the energy necessary to create an interface between two phases. As such, they can be broken into components arising from the attraction or repulsion of molecules on opposite sides of the interface. Fowkes (1964) demonstrated that for most surfaces and liquids, the forces can be divided into polar and non-polar components. van Oss, Good, and Chaudhury (van Oss et al., 1988b) extended this model to describe both the positive and negative polar forces at a surface as shown in:

$$\gamma = \gamma^{D} + \gamma^{AB} \qquad \textbf{Eqn. 1.3}$$

where the superscript AB refers to the total polar (acid-base) energy of the material while D refers to the total non-polar (dispersion) surface energy of the material. The total non-polar component, γ^{D}, is a single term and present in all material. The total polar component, γ^{AB}, is the combination of the acid and base character of the surface as given by:

$$\gamma^{AB} = 2\left(\gamma^{A}\gamma^{B}\right)^{1/2} \qquad \textbf{Eqn. 1.4}$$

where γ^{A} and γ^{B} are the Lewis acid and base components of the surface. The acidic forces are those associated with electronegative groups such as oxygen functionalities like phenols and carboxyls (Lopez-Ramon et al., 1999) and most natural solids are

believed to be enriched in acid groups relative to basic groups. The basic energy is due to electron rich groups such as ethers and carbonyls.

In a vacuum, the interaction between two phases such as a solid and liquid can be described as a sum between the interfacial energy minus each individual surface tension:

$$\Delta G_{SL} = \gamma_{SL} - \gamma_S - \gamma_L \qquad \textbf{Eqn. 1.5}$$

The interfacial dispersion energy between two materials is then given by:

$$\gamma_{SL}^{D} = \left(\sqrt{\gamma_S^D} - \sqrt{\gamma_L^D}\right)^2 \qquad \textbf{Eqn. 1.6}$$

and the polar interfacial energy is given by:

$$\gamma_{SL}^{AB} = 2\left(\sqrt{\gamma_S^A \gamma_S^B} + \sqrt{\gamma_L^A \gamma_L^B} - \sqrt{\gamma_S^A \gamma_L^B} - \sqrt{\gamma_L^B \gamma_S^A}\right) \qquad \textbf{Eqn. 1.7}$$

Van Oss et al. (1988b) showed that a geometric form was necessary for the polar (acid-base) components because each force is only present when the force with the opposite sign is also present across the interface. The total interfacial energy between two materials is then the sum of the dispersion and polar interfacial energies and can be either positive or negative. Although many researchers have attempted to use a single polar component or a combination of polar terms similar to equation 1.6 for the dispersion term, this approach does not allow for negative polar energies, γ^{AB}. In other words, the total interactive energy of equation 1.7 is only allowed to be attractive when, in reality, it can be either attractive or repulsive (van Oss, 1993). These single interfacial energy components describing the interaction between two materials can be combined with the Young equation to produce a form relating the contact angle to polar and non-polar surface energy components:

$$\frac{1+\cos\Theta}{2}\gamma_L = \left(\gamma_S^D \gamma_L^D\right)^{1/2} + \left(\gamma_S^A \gamma_L^B\right)^{1/2} + \left(\gamma_S^B \gamma_L^A\right)^{1/2} \qquad \textbf{Eqn. 1.8}$$

where the subscripts S and L refer to solid and liquid phases respectively. Note that the interaction described here is between a surface and a single liquid in a vacuum.

The scale of surface energy component values is based on water which has equal acid and base components of γ_L^A=25.5 and γ_L^B=25.5 in units of mJm^{-2}. Water has the highest polar (γ_L^{AB}) component of any material yet tested. One way to determine the solid phase surface energy component values is to measure the contact angle for three different liquids (as a liquid drop surrounded by air) against a single solid. Equation 1.8 is then written for each solid-liquid system with the appropriate liquid interfacial energy values and the measured contact angle. This defines a system of three equations which can be solved for the three unknowns, γ_S^D, γ_S^A, and γ_S^B. Surfaces can then be compared on the basis of the solid dispersion or polar components. The surface energy components for several liquids are tabulated (van Oss, 1993). Two of the probe liquids must be polar; traditionally water, formamide, and glycerol are used. The traditional apolar liquids are α-bromonaphthalene (ABN) and di-iodomethane (DIM) because of their high surface tensions. However, any liquids that form a sessile drop can be used provided the interfacial energy components are known. This method was first described by Fowkes (1964) and has been utilized successfully for many types of materials to determine the solid surface energy components. One limitation to this method is that it may be difficult to find a liquid that forms a droplet for high energy solids because, if the surface tension of the liquid is lower than the surface tension of the solid, the liquid will spread.

This model does not account for the presence of a second surrounding fluid phase. Equation 1.1 specifies a unique contact angle for each liquid-solid pairing. Traditionally, the spreading pressure, π_e, is a term used to account for the reduction in the apparent solid surface energy, γ_S, due to the presence of condensed vapor from the droplet (Adamson and Gast, 1997), as shown in:

$$\gamma_{LV} \cos \Theta = \gamma_{SV} - \pi_e - \gamma_{SL} \qquad \textbf{Eqn. 1.9}$$

where γ_{LV} is the surface tension of the droplet liquid in equilibrium with the vapor phase, V, and γ_{SV} is the surface tension of the solid in equilibrium with the vapor phase. Fowkes

(1964) showed that when a sessile drop could be formed, that is when $\gamma_L > \gamma_S$, the spreading pressure is negligible.

Van Oss (1993) presented a method for examining the interaction between two phases immersed in a third phase which can be applied to liquid-liquid-solid systems. Following Dupre (1869), a third material can be added to the system such that two materials are interacting in the presence of another. This is analogous to a drop of liquid 1 (L1) and solid (S) interacting with a second, surrounding, liquid phase present (L2). In this case, the interaction is a sum of interfacial energies:

$$\Delta G_{SL2,L1} = \gamma_{SL1} - \gamma_{SL2} - \gamma_{L1L2} \qquad \textbf{Eqn. 1.10}$$

Allowing for the presence of the surrounding liquid to affect the interfacial tension between the drop and the solid in three phase systems is somewhat analogous to assuming that the drop vapor affects the solid surface tension in two phase systems.

1.8 Zisman approach

A second method to examine competitive wetting is through the Zisman approach (Fox and Zisman, 1952). A Zisman diagram, shown in Figure 1.4, consists of the cosine of the contact angle of several different liquid droplets on a single surface plotted against the surface tension of the droplet fluid. For a homologous series of fluids (for example, a series of n-alkanes) a straight line relationship is expected. From the fitted straight line relationship, the surface tension at which the contact angle equals zero is estimated. This is termed the critical surface tension of the solid and represents the maximum surface tension for a liquid to spontaneously spread over the surface. Based on Figure 1.4, the critical surface tension for n-alkanes on Teflon appears to be about 20 mJm^{-2}. For many natural materials, this value is expected to be about 45 mJm^{-2} (Parekh and Aplan, 1978). In accordance with the geometric combining rule for interfacial energies, it is actually more appropriate to plot the square root of the interfacial energy (Good, 1992). This approach is typically only applied to the dispersion component of the surface free energy, γ_L^D.

Guy et al. (1996) expanded the Zisman method from single liquid-solid systems to liquid-liquid-solid systems. In three phase systems, the contact angles on each solid did not plot as a straight line versus interfacial tension but rather exhibited threshold value where the profile began to curve. Examining coals in contact with a variety of probe liquids while immersed in a water phase, they observed that the critical interfacial tension increased as the rank of the coal (defined as the atomic carbon to oxygen ratio) increased. In other words, as coal became more mineralized, the organic liquid had to be more polar to displace water from the surface and form a spreading organic drop. Furthermore, they found that for advancing (increasing) oil drops immersed in water the maximum oil-water interfacial tension that would allow the oil drop to spread was lower (i.e., the oil had to be more polar) than in the case of an oil drop that was receding (shrinking).

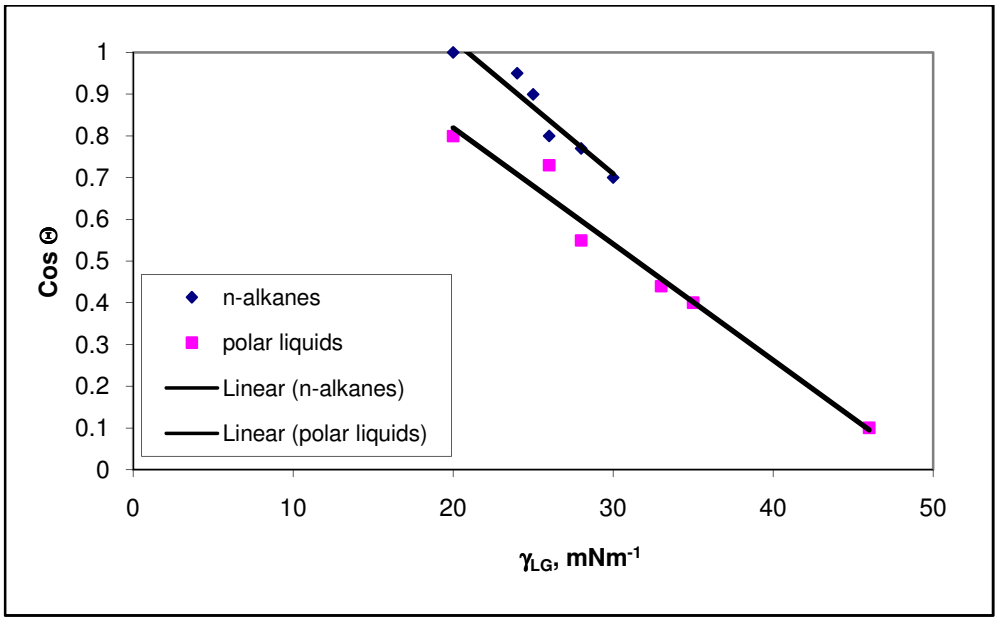

Figure 1.4, Zisman diagram for dry Teflon (Adamson and Gast, 1997).

1.9 Direct contact angle measurement

The most unambiguous measure of wettability is the contact angle. If possible, it is desireable to measure the contact angle directly so as to avoid the complicating effects of pore shape distribution, tortuosity, and system heterogeneity. A goniometer can be used in combination with a microscope to view a droplet placed on the smooth solid surface. A quartz slide is often used as a surrogate for natural sands. For materials other

than quartz, a polished surface of a rock face may be used as a surrogate for the soil surface.

Alternately, a digitized image of the drop can be processed by Axissymetric Drop Shape Analysis (ADSA) (Cheng, 1990). In this method, a computer program digitally analyzes each image to fit a curved line to the drop profile. It then calculates and compares the distance from the center of the drop to the edge of the drop profile repeatedly. With the viscosity and relative density between the two fluids input by the user, the contact angle is then determined.

There are limitations to using a direct measurement of contact angle. For consistent, repeatable measurements, the solid surface should be molecularly smooth. This is difficult to achieve with natural materials. For crystalline materials a freshly cleaved surface can be used. For other materials, a polishing process can produce a smooth surface, but it is unlikely to be molecularly smooth. However, if the scale of the roughness of the solid surface is similar or smaller than the scale of the natural soil particle roughness then the tendency of surface roughness to exaggerate the contact angle toward either wetting extreme (shown in Figure 1.5) can be considered inconsequential in determining an effective contact angle that is appropriate for the material. However, if the intrinsic contact angle is intermediate wetting, roughness may have a significant influence on the effective contact angle (Morrow, 1975). A second problem with surface roughness is that the edges of crystal planes have different surface energy than the planar surfaces. Thus, to get an absolute surface energy value, the edges of the drop should not touch the edges of the crystal. In practice however, a soil particle surface will not be a single crystal face thus the surface energy determined through the use of sessile drops and through porous media infiltration methods are typically in agreement with one another, with the sessile drop measurement having a smaller error associated with the method (Siebold et al., 1997).

Figure 1.5, Surface roughness exaggerates contact angle toward wettability extremes.

1.10 Limitations of contact angle measurement

In addition to differences in particle wettability, soil materials of differing composition also may have different particle size distribution, shape, density, and porosity. Equation 1.2 is derived for a meniscus formed inside a smooth cylindrical capillary tube. The parameter r in equation 1.2 thus represents an average pore radius in a straight, smooth capillary. In a soil, the pore radius fluctuates from pore to pore and different soils will have varying degrees of spread around the average pore radius. The shape of the meniscus will vary from spherical as well. So, in applying equation 1.2 to a soil, the term r becomes an effective radius called the hydrodynamic radius. The capillary pressure-saturation relationship is also dependent on these features. Contact angle measurements by displacement or imbibition into a porous sample are unable to differentiate between changes in surface forces and the effects of pore shape and size distribution unless the porous medium remains constant in all ways except composition.

Macroscopically measured contact angles may differ from the intrinsic contact angle due to contact angle hysteresis. Hysteresis is the condition where the state of a system depends in part on the history of the system. As a drop advances over the surface, it presents a larger angle through the drop. As a drop recedes, there is a smaller angle. The intrinsic contact angle is the angle measured on an ideal, uniform, smooth surface. The apparent contact angle, Θ', is the contact angle measured on a non-ideal surface and it may differ significantly from the intrinsic contact angle (Morrow, 1975). Surface roughness and chemical heterogeneity are also associated with hysteresis. One explanation for this phenomenon is that the advancing edge gives the contact angle against the low energy areas of the surface while the receding edge gives the contact angle of the high energy areas (Hiemenz and Rajagopolan, 1997). Figure 1.5 shows how roughness creates surfaces that are not parallel to the apparent surface of the material so

that although the angle of intersection of the two-fluid boundary and the solid is the same, the measured angle appears to be different. Roughness causes the contact angle of a non-wetting fluid drop to increase while a wetting fluid appears more wetting. Morrow (1975) demonstrated that roughness causes contact angle hysteresis by systematically roughening the insides of PTFE capillaries. This effect is often incorporated by using a roughness factor, R, as shown in equation 1.11 (Adamson and Gast, 1997).

$$\cos \Theta' = R * \cos \Theta \qquad \textbf{Eqn. 1.11}$$

Gosiewska et al. (2002) showed that the patterning of chemical heterogeneity of the solid surface can influence the macroscale wettability as measured by contact angle. Using scanning electron microscopy, they mapped inorganic inclusions on rock surfaces. Advancing and receding contact angle drops were then measured. The advancing drops corresponded to the more hydrophobic material wettability while the receding drop corresponded to the hydrophilic mineral inclusions. By choosing locations with varying size and distribution of mineral inclusions they were able to show that the measured contact angle also changes with the patterning of the surface.

1.11 Wettability alteration

Roughness and contact angle hysteresis may affect the contact angle in the absence of surface active solutes within the liquid phases. However, several researchers have also shown that contact with crude oil or NAPLs can cause the sorption of hydrophobic compounds at the soil surface rendering it less than strongly water wetting. Denekas (1959) presented evidence that crude oil components influence rock wettability. Powers and Tamblin (1995) showed that synthetic gasolines containing polar additives created intermediate-wet surfaces in both the water-wet and organic-wet regimes. Buckley and Liu (1998) examined the contribution of bitumens, insoluble components of crude oil, to surfaces and showed that they influenced reservoir wettability. In many cases, the liquid components cited are polar organic molecules that sorb to solids over extended equilibration times. However, it is important to note, that the concentration of additives, as shown by Hsu and Demond (2007), does not need to be high to alter

wettability. The alteration of wettability by surface active agents can also create regions of wettability heterogeneity in the subsurface.

1.12 Alternative methods of measuring wettability

Although a directly measured contact angle is the most definitive measurement of wettability, it is not always feasible. Several alternative methods exist to obtain an estimated value of the contact angle or wettability.

Bottle test

The bottle test is a visual method to determine which liquid phase preferentially wets a soil surface. It gives no information about the contact angle on the soil surface and works best for strongly-wetted systems (Anderson, 1986). The basic procedure is as follows: clean sand or soil a material of a specific particle size is placed into a small bottle or tube. A NAPL is added to completely cover the sand and shaken to coat the sand. A period of equilibration is allowed and then the aqueous phase is added to the bottle. An alternate method that can be used to better approximate the typical chronological order of contact for immiscible contaminants is to add the water first and then the non-aqueous phase (Anckner and Powers, 1996).

Water drop penetration time and molarity of an ethanol drop

Water drop penetration time (WDPT) is a field test method used in agricultural soil science to examine the water repellency of surface soils. This test is carried out by placing a single drop of water on the smoothed surface of a dry soil sample measuring how long it takes for the drop to imbibe. A variation on the water drop penetration time method is the molarity of an ethanol drop test or MED test (King, 1981). Drops of water containing a known molar amount of ethanol are placed on the soil. The ethanol concentration of a drop that imbibes within a set time is the MED value of the soil. The higher the MED value is, the more hydrophobic the soil.

These methods are popular in water repellency studies. For example, Roy (1999) based the hydrophobicity of oil contaminated sand on MED values in a study that showed that the hydration of soil organic matter affects wettability. WDPT has been used to

assess the wettability of coal mine spoils (Miyamoto et al., 1976). Doerr (1998) reports that WDPT and MED are only correlated to one another for highly hydrophobic materials. Buczko et al. (2002) found that soil organic matter was positively correlated to WDPT. The key difficulties are that the imbibition of the droplet into the soil depends on the soil pore size and shape and that dynamic wetting effects result in a slow lowering of the drop imbibition rate (Watson and Letey, 1970).

Several spontaneous imbibition and capillary rise methods have been reported in the literature. These methods are based on the idea that the wetting fluid will spontaneously flow into a capillary tube or soil column while a non-wetting fluid will not flow spontaneously and a minimum pressure, described by the Young-Laplace relationship:

$$\Delta P = \Delta \rho g h = \frac{2\gamma_{LV} \cos\Theta}{r} \qquad \textbf{Eqn. 1.13}$$

is required to force the non-wetting fluid to enter the largest pores. A plot of the pressure difference between the non-wetting and wetting fluids versus the percent saturation of the wetting fluid forms a curve that is characteristic for each material. A method for collection capillary pressure-saturation curves is given in Appendix C. According to equation 1.13, if two porous media samples have similar porosity and tortuosity then a difference in pressure at a given saturation must be due to a difference in contact angle. Thus, capillary methods are more applicable to estimating the contact angle between a second pair of fluids in the same medium.

Imbibition rate

To measure wettability by imbibition rate, a plot of the average saturation of imbibing fluid in a core or packed cell versus time is created and a steep slope indicates samples that are wetted by the imbibing fluid. This test has been used in the petroleum industry for cores of oil reservoir rock very successfully (Anderson, 1986), and in friable media by Powers and Tamblin (Powers and Tamblin, 1995). To alleviate the effect of pore structure differences, Denekas et al. (1959) suggested treating a soil or core sample

with a chemical application to render it completely water wet without changing the pore geometry. Then a single term, the relative imbibition rate R, can be used to compare samples. A variation of the imbibition rate test, which eliminates the problems associated with the combination of fluid properties, pore geometry, and packing heterogeneities, is the imbibition time method developed for use with powders (Mohal and Chandler, 1986). A sensitive balance is placed beneath the fluid surface. Particles are videotaped as they drop through the surface and a plot of 75 to 100 particles against imbibition time on a log scale produces characteristic curves for each sample which may be compared to solids of known wettability. For mixed media samples, where particles may vary in composition from one another, this method may provide a better assessment of wettability than a packed column where each pore may have walls of different wettability.

Water entry value or pressure of displacement

The water entry pressure is the critical soil water potential where water starts to displace the non-aqueous fluid in the porous matrix. Water entry pressure can be determined in a capillary pressure-saturation cell by starting with zero water saturation and measuring the pressure necessary to cause infiltration of water. If the pore radius is unknown, it can be calculated iteratively by using fluid systems with known contact angles solid first. Wang et al. (2000) were able to show that organic matter content and initial moisture content affected the wettability of soil in air-water systems using this method. Variations of this method include Bartell and Osterhof's (1933) pressure of displacement method, and Bahrani et al.'s (1973) capillary rise method.

Amott-Harvey and USBM

The Amott-Harvey and USBM (United States Bureau of Mines) methods are widely used in the petroleum industry to measure the average wettability of cores. The Amott-Harvey method (Anderson, 1986) takes advantage of the fact that the wetting fluid will spontaneously imbibe but the non-wetting fluid must be forced to imbibe. The volume of water displaced by spontaneous imbibition of oil divided by the total volume of water that can be displaced is δ_o, the displacement by oil ratio. The volume of oil spontaneously displaced by water divided by the total volume of oil that can be displaced

is δ_w, the displacement by water ratio. I is the Amott-Harvey relative displacement index:

$$I = \delta_w - \delta_o = \frac{V_{osp}}{V_{ot}} - \frac{V_{wsp}}{V_{wt}} \qquad \textbf{Eqn. 1.14}$$

The Amott-Harvey index ranges from –1, completely oil wetting, to +1, completely water wetting. The Amott-Harvey method is sometimes sensitive to mixed or fractional wettability but fails near neutral wettability (Anderson, 1986).

The USBM method is more sensitive near neutral wettability and is based on the idea that the area beneath a capillary pressure-saturation curve is proportional to wettability (Gatenby and Marsden, 1957). The wettability number, W, is calculated, as shown:

$$W = \log\left(\frac{A_1}{A_2}\right) \qquad \textbf{Eqn. 1.15}$$

using the ratio of the area under the oil displacement curve, A_1, to the area under the water displacement curve, A_2. A positive wettability number indicates a water-wet sample. The Amott-Harvey and USBM wettability test methods provide a usable scale to compare the combined effects of porosity variation, pore geometry, and intrinsic contact angle but they do not produce an estimate of contact angle. A drawback to using these methods is the time required, 7-21 days for packed soils.

1.13 Conditions affecting wettability

Several groundwater conditions can affect wettability. The factors cited in the literature include pH (Barranco et al., 1997; Zhou et al., 1998; Fuerstenau and Colic, 1999; Gribanova et al., 2000), ionic strength (Barranco et al., 1997), sorption to the surface (Denekas et al., 1959; Toledo et al., 1996) and the order of fluid contact (Perwuelz et al., 1999). In examining the forces that can occur at fluid-solid interfaces, it is important to note that if one of the materials is non-polar then there will only be dispersion forces between the two materials. Since PCE is non-polar, only dispersion

forces can occur between the PCE and the surface. Water may have an additional polar attraction if the surface is also polar.

pH

pH affects the dissociation of surface groups in contact with the aqueous phase. As the pH increases, more of the surface sites are charged due to the loss of surface hydroxyls. Since PCE is a non-polar NAPL, there are only dispersion forces at a PCE interface. The negative electrostatic force between the surface and water may overcome the van der Waals attraction between the NAPL and the solid surface. A thin film of water may be attracted and retained at the surface due to electrostatics and hydrogen bonding between the water molecules and the surface, preventing NAPL contact with the surface (Hirasaki, 1990). However, at the isoelectric pH of the surface, there is no net charge and electrostatic attraction will be at a minimum allowing the wettability to be governed only by the relative van der Waals forces between the solid and NAPL versus between the solid and water. pH dependent contact angles and particle flotation have been observed in the literature (Zhou et al., 1998; Fuerstenau and Colic, 1999; Gribanova et al., 2000). Sessile drop contact angle systems and particle flotation systems are related in that the van der Waals, polar, and permanent charge forces determine the wetting or particle stability within the immersion phase. Barranco et al. (1997) reported that the maximum water-PCE contact angle on glass slides occurred near pH 2, which is the isoelectric point for quartz. In studies of suspended colloids, Fuerstenau and Colic (1999) report that the pH of maximum aggregation and hydrophobicity occurs near each solid's isoelectric point because the Coulomb forces generated by permanent surface charges are minimized. Dubey and Doe (1993) showed that the pH of wetting reversal in crude oil sand systems occurred near the isoelectric pH.

Zeta potential

While zeta potential does not indicate exactly which species are present on the surface, it does give the potential at the shear plane which can be converted to the charge of the surface using an electric double layer model. The zeta potential of a surface is the charge at the edge of the electrical double layer (Hiemenz and Rajagopalan, 1997). It is

usually a function of the pH of the surrounding solution, as surface groups protonate and deprotonate depending on the availability of protons (or other charged species) in solution. The charged surface groups result in a charge at the edge of the double layer. This charge is also a function of the ionic strength of the surrounding solution. A particle immersed in water of a given ionic strength will have no surface charge at a specific pH. This pH is the isoelectric point, or IEP. Below the IEP, the surface has a positive charge due to the preponderance of protons in solution. Above the IEP, the surface has a negative charge. The isoelectric of quartz is near 2 (Hirasaki, 1991) so its surface is negatively charged at typical groundwater pH values. At the IEP, the wettability may change to a more organic wet state since the attraction between water and the surface is minimized since only the van der Waals forces are acting. Gribanova (2000) showed this to be the case for drops of water in air on diamond, graphite, and pyrocarbon surfaces. Isoelectric points reported for coals are in the pH range of 5-6 by Orumwense (1998) who also found that the maximum contact angle occurred near the isoelectric point of each coal material. Isoelectric points for shale do not seem to have been measured so it is possible that their IEPs fall within the pH range typical in groundwater systems. Ward et al. (1999) found that an aqueous film separating a hydrocarbon drop from a solid surface collapsed near the isoelectric point of the quartz. Thus, a material that is water wetting near the isoelectric point is likely to be water wet at all pH values. Table 1.2 shows the IEP for several minerals that may be components of natural soils.

Mineral	**pH of IEP**	**Source**
Quartz and Silica	2-3	Parks and de Bruyn, 1962
Hematite	7-9	Kosmulski, 2001
Calcite	7-10	Kosmulski, 2001
Graphite	1.3-1.5	Gribanova et al., 2000
Coal	5	Orumwense, 1998

Table 1.2, Isoelectric points of some natural soil materials.

Redox condition

Wang and Guidry (1994) found that the redox condition of cores influenced the surface charge which resulted in altered sorption of the polar crude oil components that highly influence wettability. Because of this finding, they recommended that water-wet

materials be stored under reducing conditions. The redox-dependent behavior occurred in the presence of iron minerals at the surface of the material. Near surface aquifers are generally oxidized.

Ionic Strength

Ionic strength affects the thickness of the electrostatic double layer surrounding soil particles in solution. This, in turn, affects the range of influence of electrostatic forces to attract water molecules to the surface and displace the NAPL molecules. For example, Svitova et al. (2002) found that KCl did not strongly affect the wettability of three surfaces in oil-water systems but $CaCl_2$ did change the zeta potential values of the surfaces and hence the wettability. In a study using carbon tetrachloride and trichloroethylene drops immersed in water, Barranco and others (1997) demonstrated that increasing the ionic strength caused quartz slides to become more water-wet as the quartz-water interfacial tension was reduced.

Sorption

Natural soil materials may sorb many trace materials from the air or aqueous phase rendering their surfaces different from the acid-washed laboratory-prepared materials sometimes studied. It is well known in petroleum engineering that the sorption of crude oil components to rock surfaces influences reservoir wettability (Denekas et al., 1959). Gonzalez (1986) showed that resins and asphaltenes sorbed to uncharged components of reservoir rocks, leaving the electrophoretic mobility of quartz and feldspar samples unchanged. Many oil-wet reservoir surfaces become water-wet if the sorbed oil components are stripped away by vigorous cleaning processes. For example, Toledo et al. (1996) used X-ray photoelectron spectroscopy (XPS) to demonstrate that cleaning a series of oil-wet reservoir cores using different procedures resulted in the solid surfaces containing different groups and different wettabilities. They observed that cores with Si-CH groups present, indicating chemical bonding of organic carbon to the surface, were more hydrophobic while those with Si-O groups, a surface similar to silane treated slides, were more water-wetting. Buckley (2001) stated that the wettability of oil cores should not be assessed in the dry state because it would not realistically represent the sorption of

crude oil components to the surface. Despite the presence of a pre-existing brine layer at the solid surface, Buckley noted that oil cores vary in wettability from completely water wet to completely oil wet; thus, the water does not always shield the surface from oil. Lord and Buckley (2002) used atomic force microscopy to show that the topography of mica surfaces changed before and after exposure to crude oil, reflecting the sorption of polar compounds from the oil phase. Standal et al. (1999) showed that model polar compounds, meant to mimic asphaltenes and other polar components of crude oil, altered the wettability of clean surfaces in differing amounts depending on the fluid in contact with the surface. Morrow (1973) showed that quartz, calcite, and dolomite were susceptible to sorption of polar compounds. Sorption of cyclopentane-carboxylic acid and octanoic acid caused a reversal of the dolomite wettability to oil-wet but quartz was always water-wet.

Order of wetting

A surface in contact with a very polar solvent like water can become charged. Iler (1979) performed heat of wetting measurements and concluded that the hydration state of silica was the most significant factor determining the wetting of silica by organic liquids. Hair and Hertl (1969) asserted that sorption of organic vapors to silica surface actually increased when two layers of water cover the surface. The surface charge may result in a film of water that prevents contact between the NAPL and the surface. In a water-NAPL solid system, the soil material may always be water wet. However, if the NAPL first contacts the soil material when it is air dry, the soil may remain NAPL wet even after water is added to the system. Ward et al. (1999) showed that the stability of a water film separating hydrocarbon drops from quartz depended on the pH and the ionic strength. Perwuelz et al. (1999) observed that a larger force was necessary to pass a polyester fiber from the oil phase to the water phase than to move the fiber from the water phase to the oil phase. Guy et al. (1996) described wetting as a balance between the oleophilicity and hydrophilicity of a surface whereby the solvent must have a minimum polar characteristic to displace the water from the surface. This suggests that there is an energy difference between the displacement of water from the surface and the displacement of oil that results in an order of wetting phenomenon. There are theories of the same nature

regarding the order of fluid contact and the degree of sorption of organic molecules from oil phases (Standal et al., 1999; Daughney, 2000). Daughney and co-workers (2000) reported that sorption of crude oil components from a solvent mixture onto quartz surfaces was reduced by the presence of water. They attributed this to a change in the electrostatic forces at the surface. However, Daughney cited two other studies where the opposite occurred and pre-wetted material sorbed more from solvent phases (Brown and Neustadter, 1980; Lagerge et al., 1993). Similarly, the orientation of molecules sorbed to the solid surface has been shown to change depending on hydration state (Kramer and Somasundaran, 2002) and Miranda et al. (1998) showed that the surrounding solvent affects surfactant conformation. These findings are in agreement with those of Roy (1999) who found that the water repellency of surface soils at oil spill sites varied with hydration state and Poulenard et al. (2004) who showed that soils containing long-chain fatty acids and non-polar alkanes also became hydrophobic after drying. pH, ionic strength, sorption of surface active species and wetting order are liquid phase properties that influence wettability. Equation 1.1 showed that γ_{SL1} must be larger than γ_{SL2} to produce a wetting drop. Thus, the degree that pH, ionic strength, wetting order, and sorption affect the contact angle depends in part on the liquid phase conditions but also on the native solid surface composition.

1.14 Soil composition

Soils are composed of both mineral and organic fractions. Quartz is the predominant soil mineral in the form of silica (SiO_2). Most investigations into the distribution of subsurface liquids use silica sands as the model porous medium. However, it is known that soils are also comprised of other minerals and organic carbon. The wettability of soil minerals is not well documented with the exception of a few select model materials (Table 1.1). Talc is often highlighted as a hydrophobic mineral although contact angle data suggest that this means it is less water wet than quartz but not necessarily NAPL-wet (Giese, 1991). Graphite, which is mineralized carbon, is a completely non-polar material that is also cited as being hydrophobic (Adamson and Gast, 1997). With the exception of coal, the wettability and surface energy of carbon containing rocks and soil materials are absent from the literature.

Soils are composed of particles from parent rocks and organic matter from decaying plants and animals. The parent rocks contain combinations of the primary and secondary minerals described in Sections 1.15 and 1.16 but may also contain organic matter which is described in Section 1.17. Shales, siltstones, and mudstones are examples of carbon containing parent rocks that contribute particles to soils. Organic carbon may also be input directly from the surface in the form of humic materials.

1.15 Primary soil minerals

The most common elements in soils are: O, Si, Al, Fe, C, Ca, K, Na, Mg, and Ti (Sposito, 1989). The most abundant primary minerals are silicates such as quartz and aluminum-silicates such as feldspars, which are found in 60% of the earth's crust. These materials are composed of SiO_4 tetrahedra arranged in rigid ionic crystalline structures (McBride, 1994). Feldspars have aluminum substituted for silicon in some of the tetrahedras but all four points of the tetrahedra still share their oxygen atom, making a rigid structure. Soil particles generated from these materials are typically rounded and can be any size from gravel to clay although the proportion of primary soil minerals to secondary soil minerals decreases as the particle size decreases.

1.16 Secondary soil minerals

Secondary minerals are formed by the weathering of parent rocks. They include the clay minerals. Clay minerals are formed of layers of tetrahedral silica sheets and octahedral aluminum substituted sheets. Because of the fragility of the sheets, clay minerals do often occur as clay size particles although they can also remain as larger particles with platy shapes. 1:1 clays such as kaolinite have alternating tetrahedral and octahedral sheets. Kaolinite is common but has a low surface area thus it is not a highly sorptive or reactive soil material (McBride, 1994). 2:1 clays are very common including talc, illites, vermiculites, smectites, and chlorites. Talc ($Mg_3Si_4O_{10}(OH)_2$) is representative of the 2:1 group as a charge neutral 2:1 clay with an octahedral silicate layer containing magnesium sandwiched between two tetrahedral silicate sheets (McBride, 1994). Other cation substitutions in the 2:1 layers produce clays with swelling properties and increased sorptive area.

Oxides of iron, aluminum, and manganese occur in soils as well due to their abundance and low solubility at typical soil pH values (Sposito, 1989). Goethite (α-FeOOH) is a thermodynamically stable iron oxide and, thus, the typical form in weathered clay-size fractions. Like many oxide minerals, it may occur as a massive octahedral structure or a coating on other primary minerals.

Precipitates are another group of rocks that contribute materials to soils and consist of minerals that precipitated from aquatic environments, usually in an ionic structure with a large cation opposed by an oxygen anion group such as carbonate or sulfate. Calcium carbonate ($CaCO_3$) is often sandwiched between geologic layers of other materials such as shales or siltstones. The carbonate is highly soluble and thus may weather away faster than its surroundings, leaving karst formations where large fractures or cavities are present. Secondary carbonates may also occur as coatings on other materials. Dolomite is a very common bedrock material; in fact, it is the primary bedrock material in much of North America. Dolomite is limestone ($CaCO_3$) that has been substituted with magnesium ($CaMg(CO_3)_2$) producing a harder, less soluble material. Although these materials contain carbon, it is mineralized and does not have organic, non-polar functional groups at the surface. Fifty percent of the world's petroleum reserves exist in carbonate reservoirs (Roehl and Choqette, 1985, in Austad and Standnes, 2003); thus, several researchers have reported that carbonates are oil-wet or intermediate wet. Austad and Standnes (2003) present compelling evidence that the wettability of carbonate cores is influenced by the presence of acidic components in the crude oil and depends on the history of contact with the oils.

1.17 Soil carbon

The organic carbon found in soils arises from the decay of biological material over geological time scales (Killops and Killops, 1993). It may be directly supplied from the surface or may arise from the breakdown of organic carbon-containing-parent rocks such as shales and peats. Glacial outwash materials may contain a mix of many materials including particles from carbon containing rocks. Also, shales formations are often highly fractured due to the laminar nature of their sedimentary formation and the dissolution of included calcites; thus, they can be productive aquifers.

The term maturity refers to how much processing a soil material has undergone transforming it from native plant and animal matter to mineralized carbon. The maturity of the carbon in soils and rocks is indexed using the elemental ratios of hydrogen to carbon (H/C) and oxygen to carbon (O/C), both of which tend to decrease as a material ages (Killops and Killops, 1993). As geologic processes age the material, it loses oxygen and hydrogen groups to surrounding aqueous solutions, plants, microorganisms, and other minerals (Weaver, 1989). The disappearance of functional groups is believed to progress in the order: methoxyl, carboxyl, carbonyl, phenolic, alchoholic, etheric (Hatcher et al., 1985). A Van Krevelen diagram, shown in Figure 1.6, is typically used to depict the aging process (Killops and Killops, 1993). At the geologically young end of the scale, soils are made up of a quartz particle coated with humic acids derived from the decay of plant litter (Huang, 1997). This type of soil material is typical of agricultural topsoils. The endpoint of maturation is pure carbon which may be mineralized into graphite (Weaver, 1989).

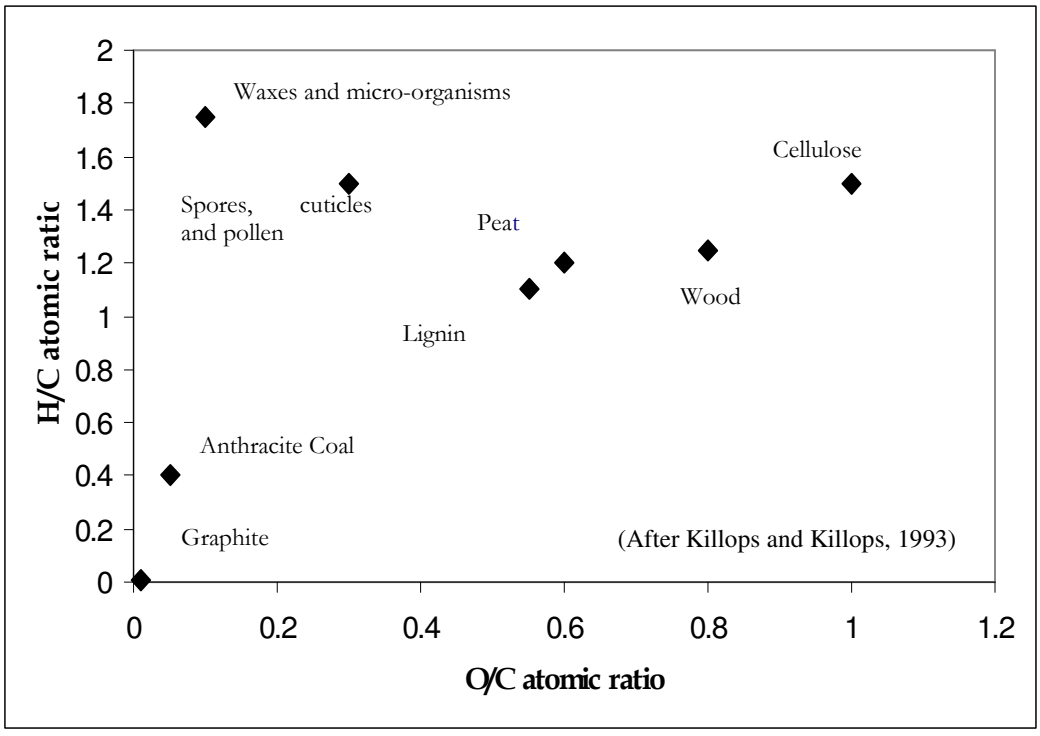

Figure 1.6, Van Krevelen diagram of selected carbon containing materials.

Geologically young material supplied from the surface takes the form of humic matter. Humin is typically considered to be composed of heterogeneous biopolymers such as polysaccharides and lignins that are too complex to describe completely but are typically defined by their aromatic rings and hydroxyl functional groups (Aiken, 1985). The residue that dissolves in a basic solution is humic acid. The fulvic acid fraction of soil organic matter is soluble in acid solutions (McBride, 1994). Humic matter is oxidized and may contain oxygenated functional groups such as carboxylic acids, carbonyls, and phenolic structures (Tschapek, 1976; Aiken, 1985; Karnok, 1993; Killops and Killops, 1993). Humic acids have more oxygen containing functional groups than the other forms of humic matter. Humic acids are typically found as a coating on mineral grains and metal ions may play a role in binding humic matter to the surface of mineral soils (Aiken, 1985). Many mollisols and alfisols present an organic surface but have overall carbon contents less than one percent (Aiken, 1985). Hajnos et al. (2002) showed that the migration time of water in kaolin soils enriched with varying amounts of humic acid was related to changes in the free surface energy of the solid.

Kerogen is the most abundant form of soil organic matter and accounts for most of the organic matter found in sediment and sedimentary rocks (Bouska, 1981; Littke, 1993). Kerogen is a more aged insoluble material formed when humic materials condense under reducing conditions such as the bottom of an ocean or lake. Kerogen typically exists as macerals embedded with mineral matter in the form of shale or other rocks (Killops and Killops, 1993). The carbon content of shales varies from 5 to 40%.

There are four types of kerogens. The differentiation of kerogens depends on the source material and the conditions of diagenesis (Killops and Killops, 1993). Type I kerogen has a high H/C ratio and low O/C ratio. It contains few aromatic structures but has a high lipid content. The major carbon source for type I kerogen is vascular plant cell walls and biopolymeric compounds that are difficult to degrade, giving it a tendency toward n-alkyl chain structures (Pratt, 1992). Type II kerogens have many ketone and carboxylic acid functional groups. They have a high H/C ratio and a low O/C ratio. In contrast to type I kerogens, they contain a high proportion of polyaromatic structures. Type II kerogen contains more animal and bacterial matter. Type III kerogens have a low H/C ratio but a high O/C ratio. Source materials include vascular plants and straight

chain hydrocarbons from leaf waxes. Large amounts of oxygen may be present at the surface in many forms of functional groups. Type IV kerogen has a very high carbon content. It is often reflective of partially degraded plant matter that was transported to a reducing deposition site (Killops and Killops, 1993). Organic matter that accumulates from surface deposition at a rapid rate in reducing conditions eventually condenses to coal and typically has a carbon content greater than 50% (Killops and Killops, 1993). Coals can vary in the amount of soluble organic matter. Bitumen is organic matter that is soluble in hydrocarbon solvents (Littke, 1993), while anthracite is insoluble or hard coal with a very low oxygen content. Humic coals arise from peats formed by vascular plant debris while sapropelic coals are generated by aquatic organisms such as algae and the humin of non-vascular plant debris under very reducing conditions (Hatcher et al., 1985).

Graphite is a mineralized form of carbon that can form from organic carbon through processes such as fires or directly from volcanic activity. After the organic processing of coal ends, the remaining carbon can also become graphitized. Graphite is made up of sheets of carbon atoms joined by three sigma bonds and one pi bond to four other carbons (Snoeyink and Weber, 1972). The sheets are not bonded to one another and have no net charge; thus, graphite is a soft mineral and utilized for its lubricating properties. Zhang and Lee (2003) showed that the wettability of graphite could be improved by adding Al_2O_3/SiO_2 gel coatings because the native graphite has limited hydrophilic groups present at the surface.

1.18 Previous studies of soil composition relative to wettability

Organic matter has been linked to water repellency in soils. Water repellency is the condition where dry soils resist the imbibition of water. This is an agricultural term applied to air-water-soil systems and is not consistently connected to a definitive contact angle. Debano et al. (1970) determined that the organic matter content was not the only factor causing water repellency because some soils with high organic contents are water wetted. Coniferous, eucalyptus, and citrus trees have been cited as contributors to water repellency, probably due to the wax-like coatings present in the leaf and fruits which protect the vegetation from dehydration in arid conditions (Wallis and Horne, 1992). Soil micro-organisms, including fungi, have been implicated in the production of toxins and other extracellular material that renders surface soils water-repellent in other locations

(Savage, 1969). These substances are long-chain hydrocarbons with few polar groups. Franco et al. (2000) showed that the polar wax materials in eucalyptus leaf litter were similar to the waxes found in hydrophobic soils and, in the arid Australian location of the study, micro-organisms were shown to have only a minor effect. Ma'shum and Farmer (1985) determined that the state of organic matter coatings on soils could influence the degree of water repellency. They extracted material from hydrophobic sands and found it was characterized by long-chain polymethylene chains and fatty acid groups. Similarly, Roy et al. (1998) showed that coatings of oil residues following surface spills of crude oil in Alberta sands caused variable repellency depending on the thickness of water films at the surface. Studies of water repellency have examined the chemical nature of the organic matter by spectroscopic or chromatographic methods but most dissolve the soil organic matter (which, for humic materials, exists as a coating around mineral grains) into an organic solvent such as di-methyl-sulfoxinate (DMSO) or aliphatic alcohols such as isopropanol and do not examine the organic matter in-situ. The unifying discovery of these experiments (Tschepek, 1976; Ma'Shum and Farmer, 1985; Roy, 1998) has been the discovery that the polarity of the organic matter influences degree of water repellency. However, no attempts have been made to correlate the surface chemistry to quantitative measures of wettability or to surface energy measurements.

Agricultural scientists have investigated the chemical functionality of soil surfaces. Organic matter can be a heterogeneous component of soils occurring in bedding layers, mixed materials such as gravels, or as patches on material surfaces. Organic carbon can occur in high concentrations, 0.5-5% in surface soils and up to 100% in organic soils such as peat (Sparks, 1995). Sandy soils containing humic and fulvic acid coatings with carboxylic and hydroxyl groups seem more hydrophilic in air-water systems than those without such functionality (Karnok et al., 1993). Capriel (1995) used FT-IR to examine the hydrophobicity of arable soils and found that methyl, methylene, and methine groups were associated with hydrophobicity. Similar to Tampy et al. (1988), Capriel found that alkyl carbons were more hydrophobic than other types. One limitation of Capriel's study, however, is that how hydrophobicity was determined was not presented.

Petroleum and chemical engineers have looked at the wettability of oil-water systems as well. It is frequently assumed that the mineral phase of aquifer and oil reservoir surfaces is quartz (Anderson, 1986) which, in its pure state, is water-wet at pH values greater than 2. The adsorption of hydrophobic components onto mineral surfaces is frequently assumed if there are deviations from a completely water-wet state (Denekas et al., 1959; Rixey and Fuerstenau, 1994). Denekas et al. (1959) showed that sorption of crude oil components is selective for reservoir surfaces. It has also been acknowledged that some minerals such as calcite, talc, and pyrite may display a less water-wet condition in the absence of sorbed hydrophobic components (Anderson 1986; Fuerstenau and Colic, 1999).

Coal is one carbon-containing material that occurs in soils whose wettability has been investigated in depth. The separation and collection of fine dust during coal processing is often accomplished by utilizing the hydrophobic tendencies of coal compared to minerals such as silica that may be mixed with the mined products (Fuerstenau, 1983; Somasundaran et al., 2000). Coal rank describes the level of biological and geochemical processing the organic matter has undergone in becoming coal. The contact angle of single fluids on coal has been correlated to coal rank and the pH of the solution (Horsely and Smith, 1951; Fuerstenau, 1983). The wettability of coal has been examined by FT-IR (Tampy et al., 1988) and by the Zisman approach (Guy et al., 1996). Guy et al. (1996) showed that, as coals increased in rank (had lower bulk O/C and H/C ratios), the soil materials became more strongly wet by non-polar solvents.

1.19 In-Situ composition measurement

Most natural organic carbon-containing soil materials have an amorphous structure that cannot be described by a chemical formula like a mineral phase. Thus, in order to draw conclusions about the influence of the solid phase on wettability, it is necessary to characterize the soil material composition experimentally.

Infrared spectroscopy has been used extensively to examine the composition of organic materials. The concept is relatively simple. Energy, in the form of infrared radiation (IR), is applied to the sample. The energy causes covalent bonds in the sample molecules to rotate or vibrate. The resulting spectrum of vibration frequencies is

indicative of specific bonds and atomic combinations that can be compared to standard libraries and identified. The sample can be a thin film applied to a slide or powdered soil pressed into a pellet with KBr as a carrying medium. One disadvantage of using IR methods is that the penetration into the sample is deeper than with XPS. X-ray photoelectron spectroscopy (XPS) is a method that can be applied to look specifically at solid surface composition. However, the ease of sample preparation and data interpretation in IR methods is a significant advantage. Capriel (1995) used diffuse reflectance infrared Fourier transform spectroscopy (DRIFT) to examine the composition of plants and leaf materials. He created a hydrophobicity index (HI) based on the amount of C-H to the total alkane region in the FT-IR spectra. Haberhauer and Garzabek (1999) traced forest litter decomposition with FT-IR and Zodrow et al. (2003) used FT-IR to show that soil carbon sources could be identified by the CH_2/CH_3 ratio. McKissoc et al. (2003) attempted to correlate water repellency based on the molarity of an ethanol droplet (MED) test to the aliphatic carbon peak; however, they were not successful in a linear correlation between the two parameters. A better fit was given for the aliphatic carbon peak versus the results of a water drop penetration test.

In XPS analysis, an x-ray beam is applied to the solid surface. The energy from the x-ray causes electrons to scatter from the surface. The kinetic energy of each ejected electron is related to the binding energy of that electron to its source element. The binding energy is characteristic of each element so it can be used to determine the elements present at the surface. XPS is a surface specific measurement because electrons more than 5 nm deep are scattered and not reflected in the information collected (Rouxhet et al., 1993). A higher electron density around an atom causes a lower binding energy allowing different functional groups to be discerned for the same element (Rouxhet et al., 1993). XPS has been used to examine soil surface composition by Yuan et al. (1998), and Gerin and Dufrene (2003) who combined XPS with atomic force microscopy to map soil surfaces in nanoscale detail. Toledo et al. (1996) were able to group oil-wetting and water-wetting materials based on the carbon content determined by XPS and the Amott-Harvey index, although they did not report a predictive model. XPS was also used in conjunction with nuclear microanalysis (Mercier, 1999) to show that nitrogen-bearing compounds influence the formation of crude oil films on mineral surfaces.

Nuclear Magnetic Resonance (NMR) Spectroscopy is a surface specific analysis method that relies on the ability to measure the vibrations from excited molecules. A powerful magnet is applied to the sample. Atoms that resonate or spin under magnetic fields send off vibrations indicating their motion. The frequency of vibration is calibrated to the type of bond of which the atom is part. These vibrations are recorded and quantified to produce the resulting spectra which describes the bond for that atom. Carbon 13 is used to get a spectrum of carbon bonding for a material. Thus, NMR is more specific than FT-IR in that it produces a spectrum for bonds of a specific atom. The composition of pristine and hydrophobic oil contaminated soils in Alberta was examined by NMR and the hydrophobic soil was shown to have more aliphatic and carbohydrate type groups (Litvina et al., 2003).

1.20 Summary

The distribution of NAPLs, such as chlorinated organic solvents, in the subsurface is an important factor in the success of contaminated subsurface remediation. The organic liquid distribution is determined by wettability and pore structure, which in turn are both functions of the solid phase. Thus, in this study, the wettability of several natural materials is is measured both quantitatively and qualitatively. The organic content and type of soil materials has been shown to influence water repellency and is believed to affect water-NAPL wettability as well. Alkane groups have been associated with increased water repellency while oxygen- containing groups have been associated with water-wetting soils. Thus, this research considers the influence of solid phase composition on wettability by examining the correlation between contact angle and composition as measured by elemental analysis, FT-IR, and NMR. The mechanism of wettability hysteresis is examined by free surface energy analysis, which provides a quantitative method to relate the contact angle to dispersion and polar surface forces and can be applied to dry solids as well as those immersed in liquids.

CHAPTER 2

MATERIALS AND METHODS

2.0 Liquid phases

Throughout this dissertation, the terms aqueous solution, water, and water phase refer to the model groundwater solution which was composed of 0.01 M sodium chloride in Milli-Q ultrapure water. The ultrapure water was created by passing deionized, distilled water through a series of four Milli-Q filters (Millipore, Bedford, MA). Sodium chloride was selected as the background electrolyte for the model aqueous phase because groundwater is typically dominated by mono-valent ions such as Na^+ and Cl^- which must be balanced in solution (Domenico and Schwartz, 1998). Secondly, the use of an electrolyte background at 0.01 M minimized changes in electrolyte concentration when pH adjustments were made to the samples. pH adjustments to the samples were made by the drop-wise addition of sodium hydroxide solution or hydrochloric acid solution at concentrations of 1 M, 0.1 M, or 0.01 M as appropriate for the degree of pH change desired. An Orion pH meter (Thermo Fisher Scientific, Waltham, MA) calibrated to 0.01 pH units was used to measure the pH of samples during the addition of acid or base solutions. If the sample being adjusted held only an aqueous solution, a Teflon coated stir bar was used to mix the solution. If two phases (for instance PCE and water) were present, a 1 mL pipette tip was used as a clean stirring apparatus to gently agitate the aqueous phase without forming trapped blobs on the sides of the sample container or otherwise contaminating any surfaces in the container with a second liquid. Table 2.1 lists the materials and suppliers used to create the model groundwater and adjust the pH of aqueous samples.

Fluid	Type	Source
Milli-Q Water	Aqueous phase	Millipore, Bedford, MA
Sodium Chloride	ACS grade, granular	Sigma, St. Louis, MO
Sodium Hydroxide	Anhydrous pellet	Fisher Scientific, Hanover Park, IL
Hydrochloric Acid	1 N solution	Fisher Scientific, Hanover Park, IL
pH Calibration Buffer	pH 4, 7, and 10	Fisher Scientific, Hanover Park, IL

Table 2.1, Materials used to create model groundwater solutions.

Four chlorinated solvents were used as model NAPL phases. All four are denser than water and thus classified as DNAPLs. Perchloroethylene (PCE, 99% purity, Acros Organics, Morris Plains, NJ), also known as tetrachloroethylene, was chosen as the primary NAPL because it is one of the most common and persistent groundwater pollutants. Trichloroethylene (TCE, 99.5+% purity, ACS reagent grade, Sigma Aldrich, St. Louis, MO), carbon tetrachloride (CTET, 99.9+% purity, Chromasolve HPLC grade, Sigma Aldrich, St. Louis, MO), and 1,1,2-trichloroethane (TCA, 97% purity, Aldrich Chemical, Milwaukee, WI) are also common groundwater pollutant DNAPLs. The carbon backbone in PCE and TCE is made up of two carbons with a double covalent bond between them, also known as a pi bond. PCE contains four equally spaced, highly electronegative, chlorine atoms bonded covalently to the ethylene carbons. TCE has three chlorines and one hydrogen atom bonded to the ethylene carbons and thus is slightly polar. TCA is a chlorinated alkane with a backbone of two carbons with a single covalent bond between them. TCA has two chlorines and a hydrogen atom bonded to one of the carbons and one chlorine and two hydrogens on the second carbon making it more polar. Carbon tetrachloride shares similar properties to PCE in that it is non-polar, chlorinated, and a common groundwater pollutant; however, its structure is a single carbon bonded to four chlorines. These four model NAPLs often occur together at sites due to the fact that they were historically very popular solvents with many industrial applications. Table 2.2 lists the chlorinated solvents used as model DNAPL phases along with some properties that may be relevant to wettability, the liquid surface tension, σ, the NAPL-water interfacial tension, γ, and the dipole moment, μ.

Fluid	Density, g/cm^3	σ, mNm^{-1}	γ, mNm^{-1}	μ, Debye
Tetrachloroethylene (PCE)	1.6	31.7	47.5	0.00
Carbon Tetrachloride (CTET)	1.6	27.0	45.0	0.00
Trichloroethylene (TCE)	1.5	28.8	34.5	0.80
1,1,2 Trichloroethane (TCA)	1.4	34.0	29.6	1.55

Table 2.2, Model DNAPL phase properties (Riddick, 1986).

Table 2.3 lists the probe liquids used to measure the surface free energy components of the solid aquifer materials. Water (Milli-Q), glycerol (99.5% purity, spectrophotometric grade, Acros Organics, Morris Plains, NJ), and formamide (99.5+% purity, Sigma Aldrich, St. Louis, MO) served as polar probe liquids. α-Bromonaphthalene (abbreviated ABN, 97+% purity, Alfa Aesar, Ward Hill, MA) and di-iodomethane (DIM, 99+% purity, packaged with silver to prevent spontaneous degradation, Acros Organics, Morris Plains, NJ) were chosen as non-polar fluids. These five liquids are typically used because the surface tension of the probe liquids must be high enough to allow the drop to form a raised profile rather than to spread completely over the surface. σ is the total liquid surface tension, γ^D, γ^A, and γ^B are the dispersion, acid, and base components of the liquid surface tension, respectively.

Fluid Phase	Density, g/cm^3	σ, mNm^{-1}	γ^D, mNm^{-1}	γ^A, mNm^{-1}	γ^B, mNm^{-1}
Water	1.0	72.8	51.8	25.5	25.5
Glycerol	1.3	64.0	34.0	57.4	3.9
Formamide	1.1	58.0	39.0	39.6	2.3
α-Bromonaphthalene (ABN)	1.5	44.4	44.4	0.0	0.0
Di-iodomethane (DIM)	3.3	50.8	50.8	0.0	0.0

Table 2.3, Probe liquids used for surface energy measurement and their properties (van Oss et al., 1988; Yaws, 1999).

2.1 Solid phases

Ten solids were selected to represent a range of soil materials. Table 2.4 lists the solids, their source, original form, and density. Silica (SiO_2), calcite ($CaCO_3$), dolomite ($CaMg(CO_3)_2$), talc ($Mg_3Si_4O_{10}(OH)_2$, and graphite (C_4) represent pure mineral phases.

Quartz is the most abundant soil mineral and occurs in several forms in the environment including sandstones and sedimentary rocks as well as their weathering products, sand, silt and clay-sized individual particles (Miller and Gardiner, 1998). Silica was obtained in two forms. Quartz is a highly crystalline form of silica so not all silica sands are actually quartz. Quartz microscope slides (Quartz Scientific, Fairport Harbor, OH) were used for contact angle measurement. A graded foundry sand (U.S. Silica, Ottawa, IL) was used as particulate silica. In this study, when referring to contact angle measurements the sample is referred to as quartz, but in particulate measurements the sample is silica. Calcite is the most common secondary soil mineral and consists of calcium (the 5th most common element in soils) ionically bonded to carbonate in a regular repeating structure which causes the mineral to break into perfect rhomboids. This feature is useful for creating smooth surfaces because it is possible to cleave calcite along a single layer of molecules. The calcite samples were obtained from Ward's Natural Science (Rochester, NY) and were collected in Creel, Chihuahua, Mexico. Dolomite is very similar to calcite except some of the calcium ions are substituted by magnesium, the 8th most common soil element (Miller and Gardiner, 1998). Like calcite, dolomite is typically a sedimentary product of concentrated seawater and thus may occur naturally in layers with other materials such as shales and siltstones. The dolomite samples were obtained from Ward's Natural Science (Rochester, NY) and were collected in Rochester, NY. Talc is fairly common and has been cited as being hydrophobic in the literature (Anderson, 1986; Giese et al., 1991). Talc is a 2:1 layer clay consisting of two layers of tetrahedral silicate sandwiching an octahedral silicate layer that is substituted with magnesium, giving a charge neutral clay structure (Sposito, 1989). The talc samples were obtained from Ward's Natural Science (Rochester, NY) and originated in Balmat, NY as foliated, pebble size masses. Graphite is mineralized carbon and was chosen to represent the end point of soil material maturation and was obtained in natural form as pure foliated graphite from Ward's Natural Science (Rochester, NY). It is black in color with a greasy feel due to the fine layers of carbon sheets. Each carbon in graphite is bonded to four neighbors with three sigma bonds and one pi bond in hexagonal sheets. The pi electrons are believed to have a large influence on the properties of high carbon

content materials. This may be due to the fact that pi bonds are more polarizable than sigma bonds. The edges of the sheets may contain other functionalities.

Ann Arbor II sand is a humic containing field soil classified by the US Soil Service as Brookston series (Engel, 1977). Ann Arbor II sand is an example of a humic acid coated silica sand. It was collected at less than 1 meter depth. Total organic carbon is 0.55% (Weber et al., 1992). Lachine shale was obtained from Bell quarry in Alpena, MI. It is an upper Devonian black shale containing type II kerogen. Garfield shale is a type III kerogen shale from the Green River formation in Garfield County, Wyoming and is believed to contain a complex mixture of organic compounds held together with both pi and sigma bonds (McKay, 1984). Waynesburg coal is a humic, bituminous coal from the Waynesburg seam, West Virginia. Polytetrafluoroethylene (PTFE, trade named Teflon®, DuPont, Wilmington, DE) is a well characterized anthropomorphic solid. Contact angles measured on PTFE were expected to represent a non-water wetting extreme that is unlikely to occur in natural materials.

Ann Arbor II sand, Lachine shale, Garfield shale, and Waynesburg coal each represent organic carbon-containing soil materials with varying degrees of soil carbon maturation. Rather than extract the soil carbon, the rocks themselves containing both organic and inorganic solids were used. Although excellent methods exist to extract organic material from geological solids (Eglinton and Murphy, 1969; Goklen et al., 1984), these techniques could alter the surface functional groups of the material so the original wettability would not be preserved (Snoeyink and Weber, 1972). The density of the carbon-containing soil materials was determined using a pycnometer as outlined in ASTM standard D854-58 (1979). The mineral densities are published values based on pure materials.

Material	Source	Carbon Type	Density, g/cm^3
Teflon (PTFE)	DuPont, Wilmington, DE	Polytetrafluoroethylene	2.2[#]
Ann Arbor II	Local Sample	Humic coated sand	2.65
Lachine	Bell Quarry, Alpena, MI	Type II kerogen shale	2.52
Garfield	Ward's Natural Science, Rochester, NY	Type III kerogen oil shale	2.04
Waynesburg	Ward's Natural Science, Rochester, NY	Bituminous coal	1.52
Graphite	Fisher Scientific, Fair Lawn, NJ	Mineralized, covalent sheets	2.24
Talc	Ward's Natural Science, Rochester, NY	No carbon	2.69*
Dolomite	Ward's Natural Science, Rochester, NY	Mineralized, ionic structure	2.90*
Calcite	Ward's Natural Science, Rochester, NY	Mineralized, ionic structure	2.93*
Quartz	U.S. Silica, Ottawa, IL	No carbon	2.65

Table 2.4, Solid phase characteristics. *Density provided by Ward's Natural Science (Rochester, NY). [#]Density provided by DuPont (Wilmington, DE). The other densities in this study were determined using ASTM D854-58.

2.2 Preparation of particulate solids

Quartz sand and Ann Arbor II sand were sieved to produce sands of the desired size using ASTM standard sieves (copper finish, 9" rounds) and 20 minutes of shaking on a Rotap RS 29 machine (W.S. Tylor, Mentor, OH). Sieves were washed with copious amounts of de-ionized water, combed with a stiff nylon brush, rinsed with Milli-Q water, dried with paper towel and finally air dried over night to prevent contamination between materials. Rocks were processed into particulate samples by first crushing in a jaw-crushing machine. Between samples, the machine was cleaned with pressurized air to prevent contamination. Fine particles were created by crushing these particles further in a duel ring titanium shatterbox that was cleaned with pressurized air and water between samples. Soil materials were dry sieved as described above to the desired particle size distribution and stored in closed Nalgene bottles until use.

2.3 Preparation of particles for composition analysis

Particles for the FT-IR analysis must be 30 μm or smaller to reduce the effect of diffraction on the spectra and small particles are preferable for NMR and bulk elemental analysis. Particles less than 55 μm were selected by dry sieving. These particles were further shattered by placing them in a Wig-L-Bug grinding machine (Thermo Nicolet, Madison, WI) with a stainless steel 2 mL chamber and stainless steel shaker ball. Between each use, the shaker chamber was washed with methanol, rubbed with a Q-tip, washed with copious Milli-Q water and rubbed dry with lint free Kimwipes (Kimberly-Clarke, Roswell, GA). The shaking duration was approximately 2 minutes. The samples were then placed in a 10 mL glass vial and placed in a lab oven at approximately 100 °C for 24 hours to dry. After drying, they were placed in a desiccation chamber containing calcium silicate drying media until use. No further processing was required for bulk elemental or NMR analysis. For FT-IR, potassium bromide (KBr, spectroscopy grade, 99%+ purity, Sigma Aldrich, St. Louis, MO) was added as a neutral background material. The desiccated samples were combined with KBr to 0.5% by weight. This low fraction of sample was necessary to prevent saturation of the output spectra due to the fact that the soil materials had highly absorptive carbon contents. The samples were then placed in the Wig-L-Bug grinder for a second shaking to ensure that the KBr was appropriately sized and thoroughly mixed with the sample. After adding KBr, the samples were stored in 4 mL vials covered with foil in a covered 500 mL jar half filled with desiccation media until use. After use, they were discarded due to the likely accumulation of water at the surface.

2.4 Preparation of geoslides

Parent rock material was obtained in the form of geological hand samples and test chips. A water-cooled saw (Target Guardmatic, Husqvarna, Olatha, KS) was used to cut these pieces into 40 mm x 20 mm or smaller chips that could fit within the Axis-symmetric Drop Shape Analysis (ADSA) sample chamber. No cutting oil was used and the saw blade was cleaned with copious tap water between pieces to minimize contamination of the cut surfaces with foreign material. The chips were then polished using a wet lapping wheel (Model 18L, Highland Park Manufacturing, Hawthorne, CA).

400 μm silicon-carbide grit was used as an abrasive (AP-140, Mager Scientific, Dexter, MI). Surfaces with cracks or flaws were re-cut or discarded. The surfaces were then hand polished under running tap water with silica-carbide papers of 600, 800, 1000, and 2000 grit until the 2000 grit paper was not removing any more material. The papers were wrapped around Lexan blocks to ensure a flat grinding surface. The slides were washed in copious amounts of Milli-Q water and air dried. The laboratory relative humidity is estimated to have been between 59 and 71%, following the average humidity for Ann Arbor, MI. Once dried, they were brushed with a lint-free cloth to remove stray particles. The method for preparing the geoslides is similar to that in Botsaris and Glazman (1989). Calcite was not cut with a saw. Instead, it was cleaved using a chisel and hammer and then polished with silica carbide papers. Due to its softness, talc was broken by hand to an appropriate size and then polished with silica carbide papers as described above. Clean, cut slides were stored in closed egg cartons to protect them from dust and scratches. Once used, the slides were rinsed with methanol from a spray bottle, Milli-Q water from a spray bottle and then air dried. Once dry, they were re-polished from the 1000 grit stage to ensure a fresh surface, unimpacted by previous liquid contact.

2.5 Qualitative bottle test method

Bottle tests have proven useful for the estimation of contact angle (Dubey and Doe, 1993; Anckner and Powers, 1996). For those tests, wettability hysteresis was not considered. Bottle tests were conducted using particles 425-500 μm in size. A narrowly defined particle size was chosen to minimize the effects of pore shape and size on the fluid distributions. A 10 mL glass vial was filled halfway with particles. The particles were initially saturated with either PCE or 0.01 M NaCl aqueous solution. Oil-red-O dye (Alfa Aesar, Ward Hill, MA) was used to distinguish the PCE from the aqueous phase. After equilibration for twenty four hours, the excess fluid was drained from the surface of the solids and a second phase was carefully introduced. The distribution of fluids was then assessed. A digital camera was used to record the fluid distribution.

2.6 Sessile drop contact angle measurements

Sessile drop contact angles were measured using the Axis-Symmetric Drop Shape Analysis (ADSA) apparatus designed by Cheng et al. (1990). Slides were equilibrated in the receding fluid for at least seven days prior to a contact angle measurement as described in Section 2.7. After six days of equilibration, the pH was adjusted as described in Section 2.8. pH was re-adjusted on the day of measurement if necessary. After at least seven days equilibration, approximately 20 mL of equilibrated immersion phase was transferred from the 50 mL sample jar used for equilibration to an optical grade quartz sample holder, (Rame-Hart, Mountain Lakes, NJ) with dimensions of 40 mm x 45 mm x 30 mm. The sample was then quickly transferred from the equilibration jar to the ADSA chamber so that it was only momentarly not immersed in fluid. A 100 μm glass syringe fitted with a 21 gauge stainless steel needle (Hamilton Company, Reno, NV) was used to place a droplet on the geoslide. When the droplet was denser than the surrounding phase, the droplet was placed atop the slide. When the droplet was a lighter phase, a J-shaped needle was used to place it beneath the slide which was supported on two Teflon blocks. Because the geoslides have level but not necessarily parallel surfaces, a leveling stage beneath the sample chamber was then adjusted to find a visually level position where the droplet would not roll. The droplet was photographed within two minutes of placement. Three images were recorded for each of six to eight drops on each slide.

The ADSA (Cheng et al., 1990) was used to determine the contact angle from drop photographs. A M3Z Plan S microscope (Wild Leitz, Heerbrugg, Switzerland) was used to provide 16-40 times magnification of the drop. A digitized image of each sessile droplet profile was recorded with a CCD camera (4810-15, Cohu, San Diego, CA). The distance from the center of the visible three point contact line to the edge is determined at many locations around the drop. The shape of the drop and hence the interfacial tension and contact angle were calculated 20 times for each image to account for random differences in the curve fitting routine performed by the computer. Contact angles are reported through the aqueous phase unless otherwise specified.

Contact angles were collected for all the materials listed in Table 2.4, other than Ann Arbor II sand. Unfortunately, the wettability of Ann Arbor II sand could not be

measured by this method due to the surface roughness and chemical heterogeneity created when coating a slide with humic acid. The average contact angle is the average of all images collected for a given system. Contact angles are reported to the nearest tenth of a degree through the water phase, unless otherwise specified. The first phase listed in the description of a contact angle measurement indicates the immersion phase, in other words, the phase that recedes from the surface when a second fluid phase is introduced in the form of a drop. Thus, the designation "water-air" indicates that the geoslides were placed in the aqueous phase and a bubble of air was placed on the surface. This labeling convention will be used for all the fluid-liquid-solid systems.

2.7 Solid-liquid equilibration

The standard pre-equilibration time for the solid sample and liquid phases was one week. 50 mL glass sample jars with PTFE-lined lids were filled with 40 mL of the immersion phase. The solid was then submerged in the 50 mL jar which was filled with NAPL in the NAPL-water systems and NAPL-air systems and 0.01 M NaCl solution in the water-NAPL and water-air systems. When the droplet phase was NAPL, 1.8 mL of the NAPL phase was placed in a 2 mL gas chromatograph sample vial. The vial was left uncapped and gently immersed in the larger 50 mL jar containing the solid and the aqueous phase. The NAPL remained in the vial but the interface between the NAPL and aqueous phase allowed the equilibration of the two fluids. After the equilibration period, forceps were used to remove the vial of NAPL. The NAPL was then drawn with a syringe from the bottom of the vial to avoid mixing the phases in the drop. When the droplet phase was water, 5 mL was slowly pipetted into the 50 mL sample jar to float in contact with the NAPL after the solid had been completely submerged in the NAPL. Before NAPL-water measurements, the floating water was drawn off to a small beaker with a pipette. It was allowed to rest in the beaker for up to 30 minutes to allow any of the immersion phase that was taken up with the pipette to settle out. Then the droplet phase was drawn into a syringe.

On the sixth day of sample equilibration, the pH was measured with an Orion EA920 Expandable Ion Analyzer instrument using an Orion 8013 Ross probe (Orion Research, Boston, MA). The instrument was first calibrated with two standards (pH 4

and pH 7 or pH 7 and pH 10) that covered the range of desired final pH. The standards were purchased as liquid solutions (Fisher Scientific, Fair Lawn, NJ). The pH was calibrated to 0.01 pH units. pH values before adjustment varied from 3.5 to 8.5. The pH was adjusted by drop-wise addition of 0.1 M HCl or 0.1 M NaOH. Between the addition of acid or base drops, the jars were manually stirred using a clean 1 mL pipette tip to avoid disturbing the solid geoslide. The pH was adjusted to within 0.2 pH units of the desired value, which was 7.0, unless otherwise indicated. The pH was checked and adjusted further as necessary on the seventh day immediately before measuring the contact angle. The samples required varied amounts of acid and base addition due to their varied chemical nature and amount of solid surface area.

Additional samples were equilibrated for an 80 day period to determine if wettability changes would occur as a result of time-dependent properties of the surfaces. The pH was adjusted to the desired level on the sixth day. The pH was adjusted again on day 79. On the following day, the pH was fine tuned and the measurements taken.

2.8 Surface and interfacial tension determination

Surface and interfacial tension were determined with the ADSA pendant drop method. The quartz ADSA chamber was filled with the aqueous phase. A glass gas tight syringe was used to draw up 100 μL of drop fluid. The syringe needle was immersed in the fluid filled chamber. A flat-ended stainless steel needle (Hamilton Company, Reno, NV) was used to provide a sharp cutoff point for the drop. A drop was formed on the end of the needle and the camera was focused on the droplet. Approximately two minutes were allowed for the drop to cease moving before the photograph was taken. The image was processed by the ADSA software to produce a value of surface or interfacial tension.

To prepare the surface and interfacial tension samples, three 20 mL vials were each filled with 2g of soil sieved to less than 53 μm. 10 mL of PCE was added to two of the vials. One of those had 10 mL of Milli-Q added in addition. 10 mL of Milli-Q was added to the third vial. In designated vials, Oil red O dye (Alfa Aesar, Ward Hill, MA) was added to the PCE phase. The vials were capped with PTFE-sealed caps and rotated on a lab tumbler (Labquake Model 110, Lab Industries, Berkeley, CA) for 48 hours.

They were then allowed to settle for seven days which was sufficient to produce a clear supernatant phase. The surface tension of 9-16 drops from each of the two vials that contained Milli-Q was determined with the ADSA method. The syringe was flushed with methanol, 0.01 M HCl and 0.01M NaOH between samples. Then the supernatant liquid was drawn up and discarded three times to prevent cross contamination between samples. The surface tension of the vials containing Milli-Q only was measured to determine if Milli-Q solubilized surface active agents from the solid surface. The aqueous surface tension from the vials containing both PCE and Milli-Q was measured to determine if any surface-active components were transferred to the aqueous phase after being solubilized by the PCE phase.

Interfacial tension samples were created by pre-equilibrating 100 mL of PCE and 400 mL of Milli-Q water in a closed jar for 7 days. The ADSA sample chamber was then filled with the pre-equilibrated water. Drops of PCE from the vial containing PCE and soil only were then suspended in the chamber to determine if PCE solubilized surface-active agents. The interfacial tension between drops of water that had been equilibrated with both PCE and soil, and pre-equilibrated PCE was measured using a J-shaped needle to determine if surface-active components of the solids were solubilized by the PCE and transferred to the Milli-Q phase. The pH of the surface and interfacial tension samples was not measured because the small liquid volumes and high particle content made it difficult to get an accurate reading with the Orion probe.

2.9 Droplet equilibration

The equilibration time necessary to establish a sessile drop was assessed by taking time-series photographs of drops. The ADSA software was used to photograph the drop at ten second intervals. The photograph series was begun, and then the droplet was placed. The first few data points of the series, before the droplet was placed, are discarded by the ADSA software because no drop edges can be detected. Two systems were studied, water-PCE-quartz and water-PCE-Garfield shale systems. The systems were not pre-equilibrated for seven days prior to drop placement because this test was only concerned with the length of time necessary for physical equilibration of a sessile drop in the ADSA apparatus.

Figure 2.1 shows the stability of PCE drops placed on quartz immersed in the the aqueous phase over the course of two hours. Similarly, Figure 2.2 shows time lapse measurements of water-PCE systems on Garfield shale. The drops were photographed at specified intervals after placement. The straight lines on the graph are the average contact angle for each drop over the entire time span while the individual points are the instantaneous contact angle at each time point. The dynamic effects of drop placement appear to be very rapid and the three-phase contact line, the edge of the drop that is expanding over the surface, stopped moving before the drop image could be taken. Thus, it appears, from Figure 2.1, that at two minutes (120 seconds) the drops are not changing measurably. These contact angles differ from those presented for water-PCE systems because the fluid-fluid-solid systems were not pre-equilibrated for seven days. Without pre-equilibration, the dynamic effects of drop placement are expected to be increased because each fluid is sparingly soluble in the other. Also, the hydration of each surface site may be slightly different since there has not been sufficient time for the air at the surface to be solubilized into the water phase.

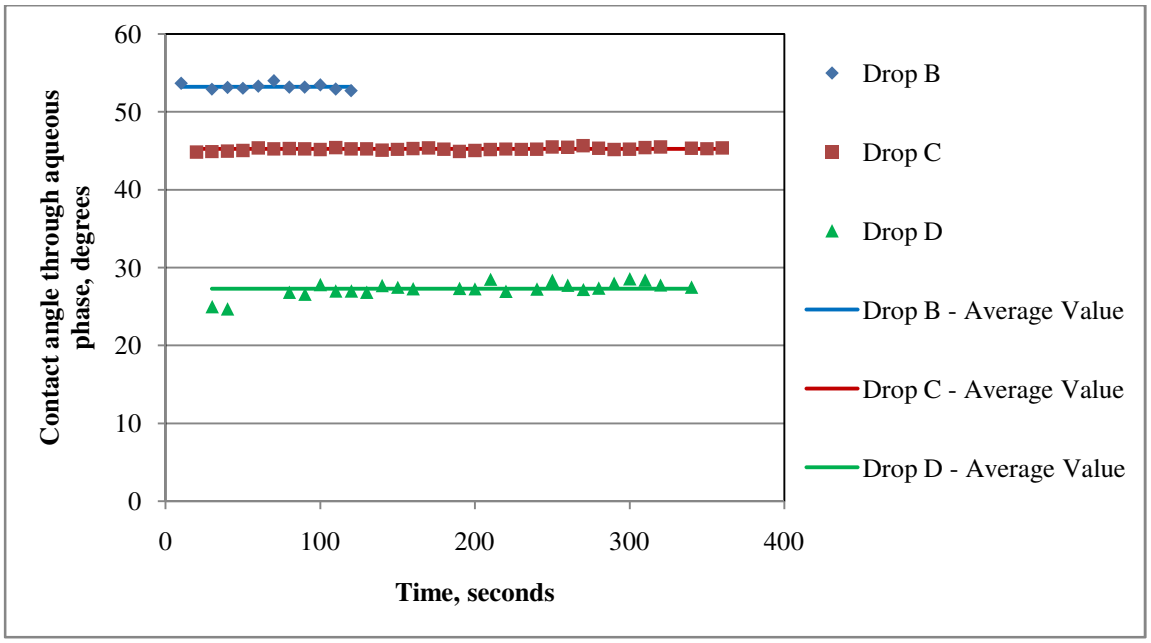

Figure 2.1, Time series of water-PCE contact angles on quartz.

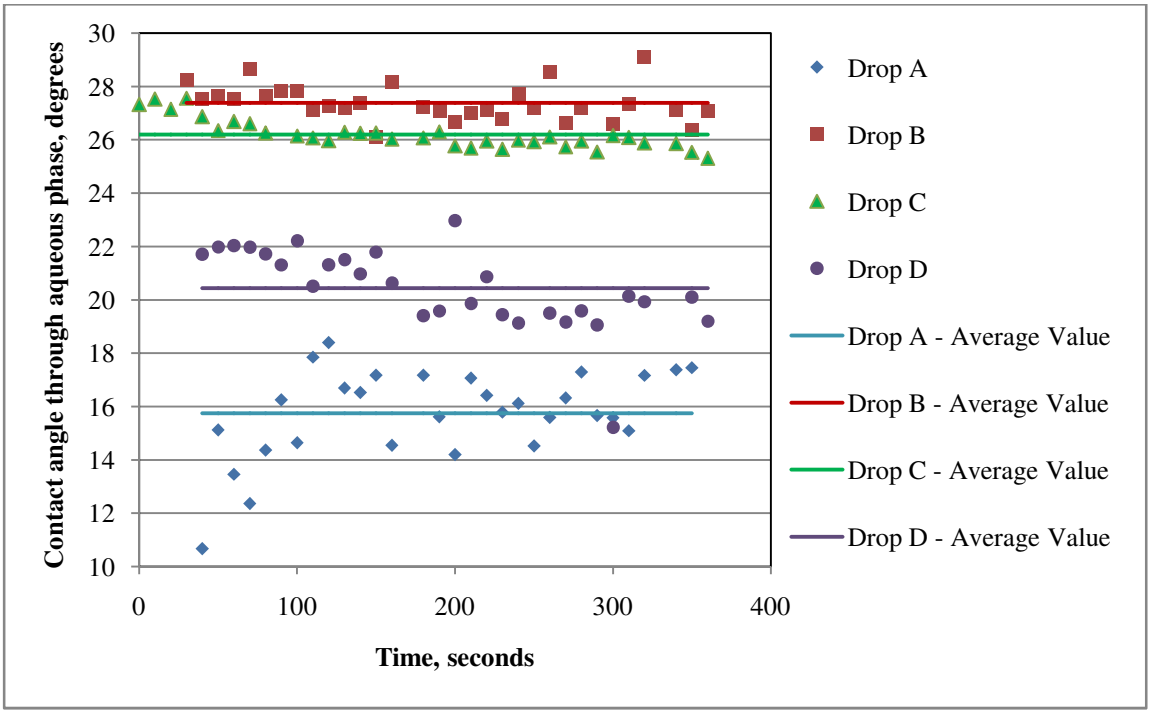

Figure 2.2, Time series water-PCE contact angles on Garfield shale.

2.10 Effects of roughness on wettability measurements

As described in Section 1.9, surface roughness can alter the observed contact angle by creating surfaces that are angled relative to the apparent slide surface. This, in turn, creates multiple configurations of the contacting fluid droplets and tends to exaggerate the contact angles toward the extremes of wetting or non-wetting. Table 2.5 compares the contact angle of water-PCE systems on quartz slides. The "scratched" sample is a microscope slide that was sanded with 600 and 2000 grit silica-carbide papers. After processing with the sanding papers under running water as described in Section 2.4, the scratched slides were cleaned in a chromic acid cleaning solution to produce a surface that was identically clean to the non-scratched quartz slides but had some additional roughness. The degree of roughness was not measured but the ridges are expected to be of similar amplitude and spacing to the roughness of the other materials since the silica carbide abrasive is harder than all the materials studied. The additional roughness gave the slides a cloudy appearance when viewed perpendicular to their surfaces but when viewed from the side the ridges could not be seen, even under the 10-16 times magnification of the ADSA camera. Roughness was not visible on the natural materials either. Four PCE droplet images were collected in an aqueous phase of pH 7.

The comparison slide, a clean quartz slide that was not roughened, was equilibrated in the same fluids.

Material	Water-PCE Contact Angle
Quartz slide	14.04° ± 0.34
Scratched slide	14.95° ± 0.14

Table 2.5, Water-PCE contact angles on smooth and rough quartz surfaces, measured through water.

These measurements suggest that additional roughness on the quartz slide had a negligible impact on the contact angle. The roughness created by the sanding process is likely small in amplitude and close spaced due to the processing with such fine grit sanding paper. Since the other materials include silicate minerals or are softer minerals than the quartz, it is reasonable to conclude that they will be similarly or less rough and thus, the roughness left by the polishing method appears to be insufficient to alter the contact angle appreciably.

2.11 Diffuse reflectance infrared Fourier transform spectroscopy (DRIFT)

To characterize the solid surface composition, Fourier Transform Infrared Spectroscopy analysis was performed using a Thermo-Nicolet 980 FT-IR system (Nicolet Instrument, Madison, WI) in the diffuse reflectance (DRIFT) mode. All measurements were compared to silica samples with a matching proportion of KBr. After leveling the sample chamber, each sample was purged with nitrogen gas to reduce absorbed water. Each spectrum was collected with 128 scans, at an aperture of 150 mm, and resolution of 4 cm^{-1}. Quantitative determination of the amount of each functional group present on the sample surface was not possible because each material differs in reflectivity, due to the fact that each contains a different amount and type of organic matter. For each material, a threshold absorbance of 14% was set below which peaks were considered noise. The largest 15 peaks were then selected and the most likely functional group identified. The composition of graphite cannot be measured by FT-IR due to its high reflectivity. Table 2.6 lists the wavenumber of functional groups often present in soil materials.

Functional Group		Wavenumber, cm^{-1}
Sp^2 carbon (unsaturated or halogenated)	$R\text{-}CH_x$	3100-3000
Sp^3 carbon (tetrahedral)	$R\text{-}CH_x$	3000-2800
Carboxylic acids, esters, aldehydes, ketones and amides	$R_2\text{-}C{=}O$	1600-1800
Alcohols	R-OH	3300-3600, sharp
Hydrogen bonding	R-OH	3300-3600, broad
Acids	R-OH	2400-3000, broad with medium intensity
Internal alkynes and nitriles	C-C and C-N	2200-2100
Carbonyl	$R_2\text{-}C{=}O$	1200-1300
Amines	N-H	3400, sharp
Aromatics	Ar	1500-1600
Water	H_2O	3300, 1645

Table 2.6, Typical infrared adsorption wavenumbers for organic functional groups. R refers to an unspecified group. Ar refers to aromatic structures (C_6H_6).

2.12 Carbon 13 nuclear magnetic resonance spectroscopy

Cross Polarized-Magic Angle Spinning Carbon 13 Nuclear Magnetic Resonance Imaging (CP-MAS ^{13}C NMR) analyses were completed for Garfield shale and Waynesburg coal by Dr. Francis P. Miknis (Western Research Institute, Laramie, WY) using a Chemagnetics 100/200 solid NMR spectrometer at 25 MHz with high power decoupling. Analyses were performed by visually identifying the peaks present. Table 2.7 lists the chemical shift locations for several common functional groups. Spectra for Ann Arbor II sand (Echols, 2000) and Lachine Shale (Johnson, 2000) were previously collected by the same laboratory. A usable spectrum for graphite could not be produced because graphite itself is conductive.

Functional Group		**ppm**
Carbonyl	R_2-C=O	210
Carboxyl	R-CO =O	178
Phenol	Ar=OH	154
Branched aromatic	Ar-C-C	130-140
Bridgehead aromatic	Ar-C-Ar	132
Protonated aromatic	Ar-CH	128
Oxy-methine	R_2-CH-O-R	60-70
Oxy-methylene	R-CH_2-O-R	50-60
Oxy-methyl	CH_3-O-R	40
Quaternary aliphatic	C	40
Functional Group		**ppm**
Methine	CH	39
Methylene (C_2)	C-CH_2-C	23
Methylene (C_2)	CH_2	30
Aliphatic methyl	$CH_3(CH_2)_x$	16
Aromatic methyl	CH_3Ar	20

Table 2.7, ^{13}C NMR chemical shifts for various functional groups, R refers to an unspecified group. Ar refers to aromatic structures (C_6H_6).

2.13 Bulk elemental composition

The bulk carbon, hydrogen, and nitrogen content of silica sand, Ann Arbor II sand, Lachine shale, Garfield shale, Waynesburg coal, and graphite materials was measured by a CHN-1000 (Leco Corporation, St. Joseph, MI). Tin capsules were used to deliver the soil materials to the furnace. The materials were used as crushed solids but the organic matter was not extracted from the mineral matter since, with the exception of Ann Arbor II sand, both were expected throughout the particles. This method of bulk elemental analysis could not distinguish the oxygen from organic matter from the oxygen of the mineral solid. Thus, to calculate molar ratios of the elements, the ash was assumed to be a dioxide soil mineral such as quartz. The elemental ratios were reported by the equipment as mass ratios and were later converted to molar ratios for comparison. The composition of talc, calcite, and dolomite was calculated from the molecular formula for each mineral.

2.14 Surface energy component analysis

The determination of solid free surface energies for each aquifer material utilized the method of van Oss et al. (1988a). This method requires the measurement of a sessile

drop contact angle for three probe liquids. The free energy components of each probe fluid must also be known. Two of the probe liquids must be polar and one non-polar. In this case, water, glycerol, and formamide served as polar liquids. Two non-polar liquids were used, α-bromonaphthalene (ABN) and di-iodomethane (DIM), to provide redundancy in the measurements. This was especially important for the less polar materials since the non-polar liquid tended to be very strongly spreading; thus, measurement of the contact angles by ADSA produces a larger error than in less spreading cases. The contact angle of the non-polar liquid determines the non-polar, or dispersion force for the calculation of free surface energy; consequently, it is critical to accurately measure a contact angle for a non-polar liquid.

The surface energy components were calculated from a system of three equations in the form of equation 1.12. For each solid, two to four sets of three equations were solved corresponding to the liquid systems of 1) water, glycerol, ABN 2) water, glycerol, DIM 3) water, formamide, ABN and 4) water, formamide, DIM. Table 2.3 lists the liquid surface energy components from the literature used for calculation of the solid properties. Ideally, surface energy values should be independent of the choice of fluid; thus, differences in the calculated values caused by the choice of probe fluids are assumed to result from different abilities to measure the contact angle accurately. However, several authors have discussed the fact that the choice of non-polar fluid influences the resulting γ_S^D value and suggest averaging the values from several systems to produce the most reasonable approximation of surface free energy (Janczuk and Zdziennicka, 1994; Chibowski et al., 2002; Granqvist et al., 2007). Consequently, the resulting γ_S^D, γ_S^A, and γ_S^B values from each system were averaged to produce the free surface energy component values assigned to each surface.

To solve the system of equations produced by the van Oss et al. method, Maple v10 (Waterloo Maple Inc.), an analytical mathematics software, was used. An example worksheet is given in Appendix D. The calculations were checked with SurfTen 4.3, a MathPad utility available online for the calculation of surface energy components from contact angle data (Della Volpe, 2004). The two methods were found to agree within 0.1 percent.

2.15 Statistical data treatments

Several standard statistical analyses were applied to the contact angle and surface free energy data. Error bars on measured values represent the 95% confidence interval. The 95% confidence interval is calculated as:

$$\bar{X} = 1.96\frac{sdev}{\sqrt{n}} \qquad \textbf{Eqn. 2.1}$$

The confidence interval depends on the sample size, n, and standard deviation, sdev (Toothaker, 1986). The narrower the confidence interval, the more reason there is to believe the mean measured value represents the true value for the system.

Two correlation parameters, Pearson and Spearman, are utilized. The Pearson correlation, also known as the product moment correlation, is a standardized measure of covariance between two data sets. The Pearson correlation describes the degree of linear correlation between sample values. The equation for calculating the Pearson correlation is:

$$\rho = \frac{\mathrm{cov}(X,Y)}{\sqrt{\mathrm{var}(X)\,\mathrm{var}(Y)}} \qquad \textbf{Eqn. 2.2}$$

where cov refers to the covariance of two data sets and var refers to the variance of a single data set. ρ must be between -1 and 1. A positive ρ indicates that X increases linearly with an increase in Y and a negative ρ indicates that X decreases linearly with an increase in Y. A value of ρ = 0 indicates that the two data sets are not linearly correlated. There are no definitive values for when a correlation is considered good, but the closer ρ is to -1 or 1, the stronger the relationship between the two variables. A second parameter, R^2, is presented on figures showing linear regressions. R^2 is the coefficient of determination and it describes what percent of variation in the dependent variable (the y axis on a scatter plot) is described by the linear fit to the independent variable (the x axis on a scatter plot). R^2 is numerically equal to the square of the Pearson correlation

coefficient. For these small data sets presented herein, an R^2 greater than 0.8 is considered a strong fit and suggests that the linear fit may be used predicatively.

Some data sets are non-linearly correlated so the value of ρ will be low, even though there is a visible trend to the data. Subsets within a larger data set can cause non-linear correlations. For this reason, the organic carbon-containing soil materials and mineral soil materials are analyzed separately in some cases. In addition to being limited to linear relationships between data sets, the Pearson correlation coefficient is also highly sensitive to outlier values. Because of this vulnerability in determining the degree of correlation, figures showing the actual data scatter plots are presented along with tables of correlation coefficients.

The Spearman correlation coefficient, ρ_s, indicates whether two data sets are monotonically related. The term monotonic simply means that there must be unique pairs of x and y data and hyperbolic or parabolic relationships are ruled out. The Spearman is essentially a Pearson correlation between the ranks of each data set. By using rank rather than actual values, the Spearman correlation is less sensitive to outlier points since the interval between points is uniform. Similar to the Pearson correlation, the Spearman correlation coefficient ranges from -1 to 1. One disadvantage of the Spearman correlation is that it indicates if the two data sets are correlated but it does not define the functional form of the relationship between the two data sets.

CHAPTER 3

WETTABILITY OF AQUIFER MATERIALS

3.0 Introduction

Few quantitative values of natural soil material wettability are available in the literature. Prior to the measurements described in this chapter, it was hypothesized that some of the organic carbon containing materials would be wet by the NAPL phase, given the information in the literature (Anderson, 1986). The objective of this chapter is to demonstrate that the presence of organic carbon constituents does not necessarily create a NAPL-wet surface. In three phase, liquid-liquid-solid systems, the immersion phase is shown to determine the wettability. A change in wettability is observed dependent on the order of fluid contact with the surface in some systems. The organic carbon-containing soil materials and one mineral, talc, are shown to have considerable wettability hysteresis. These results suggest that wettability in the vadose zone may be heterogeneous, depending on the fluid occupying the soil pore before the introduction of NAPLs to the system. However, in the saturated zone, the soil is likely to be water-wet unless surface-active components from wastes are sorbed to the natural soil surfaces.

3.1 Qualitative bottle tests

To assess the wettability of the PCE-water-solid systems listed in Table 3.1, qualitative bottle tests were conducted using the methodology described in Sections 2.2 and 2.5. Figure 3.1 shows pictures of the qualitative bottle tests with the interpretations given in Table 3.1. The label indicates the first liquid phase introduced to the bottle. The left side bottle in each image was initially filled with the aqueous phase and the right side bottle was initially filled with PCE. The PCE is dyed red with Oil-Red-O (Alfa Aesar, Ward Hill, MA) to differentiate between the PCE and aqueous phase. Although Jeong et al. (2002) showed that high (500 mg/L) concentrations of Oil-Red-O could alter the fluid

properties when the aqueous phase was saturated by the PCE, interfacial tension measurements presented in Section 3.7 show that the small amounts of Oil-Red-O added here do not significantly alter the interfacial tension between PCE and the aqueous phase. Each pair of bottles was filled with soil material to the same level, thus apparent differences between the left and right bottles in Figure 3.2 after liquid additions are the result of the liquids filling the pore space. Differentiation between water-wet and PCE-wet porous media was made by observing the location of the red PCE phase after 24 hours of equilibration. Previous researchers (Dubey and Doe, 1993) shook the bottles vigorously and then observed whether the particles settled to the bottom of the bottles. Since the materials used here have different densities (Table 2.4), they might be expected to settle differently on that basis instead of due to surface chemical differences. Accordingly, the bottles were not shaken so that the blobs and ganglia of PCE could be observed intact, similar to the method of Anckner and Powers (1996).

Material	**Water Immersion Wetting Liquid**	**PCE Immersion Wetting Liquid**
Ann Arbor II	Water	Water
Lachine Shale	Water	PCE
Garfield Shale	Water	PCE
Waynesburg Coal	Water	PCE
Graphite	Water	PCE
Talc	Water	PCE
Dolomite	Water	Intermediate
Calcite	Water	Intermediate
Silica	Water	Water

Table 3.1, Summary of qualitative bottle test results shown in Figure 3.1. Water indicates solids that appear to be water-wet. PCE indicates solids that appear to be NAPL-wet. Intermediate indicates solids where the wetting liquid is difficult to distinguish.

The first pair of bottles shown in Figure 3.1 is Ann Arbor II. The Ann Arbor II sand is clearly strongly water-wet. In the left bottle, a thin layer of red PCE is apparent above the soil. There do not appear to be any blobs of PCE within the soil pore space. The large blob of PCE observed in the Ann Arbor II bottle indicates that PCE is not entering the soil pores but rather descending (due to density differences) along the wall of the bottle where larger pores are available. The three organic carbon-containing

materials Lachine shale, Garfield shale, and Waynesburg coal are dark colored and it is difficult to actually see the red PCE phase. However, in these cases of these three materials, the left hand bottle shows a horizon of red PCE above the soil phase while the right hand bottle shows only clear aqueous phase above the soil phase. Therefore, it can be deduced that the PCE phase has entered the soil pores and the soil is PCE-wet when PCE is the first liquid to contact the Lachine, Garfield, and Waynesburg particles. Although there are equal amounts of graphite in the two bottles shown in Figure 3.1, picture E, the left bottle appears to contain a larger volume of graphite. The graphite particles are spread on the sides of the glass vial and on the surface of the water phase rather than immersed in the water phase, suggesting water repellency. When PCE initially contacts the graphite surface, the particles readily enter the PCE blob. Clear aqueous phase is apparent above the solid horizon in the right hand bottle; thus, graphite is PCE-wet when first immersed in PCE.

Talc, Figure 3.1, picture F, appears to be water-wet when water initially contacts the soil but PCE wet when PCE initially contacts the soil. This is in agreement with other reports in the literature which cite talc as a hydrophobic mineral (Mercer and Cohen, 1990) although these previous reports did not distinguish between talc that was initially immersed in PCE or water. Both dolomite and calcite (Figure 3.1, pictures G and H) behave similarly to the Ann Arbor soil despite their high carbon content. Even though they are sometimes cited as components of reservoirs that are oil-wet in petroleum engineering literature (Treiber, 1972; Anderson, 1986), PCE does not appear to enter the pore space when the aqueous phase contacts the dry soil first. It is difficult to determine which phase is the wetting phase when PCE contacts the dolomite and calcite surfaces first. A layer of red PCE is present above the soil layer and large blobs are seen at the edges of the bottle. However, close observation shows smaller blobs of PCE distributed through the materials giving them a pink color. This behavior was classified as symptomatic of intermediate wetting behavior.

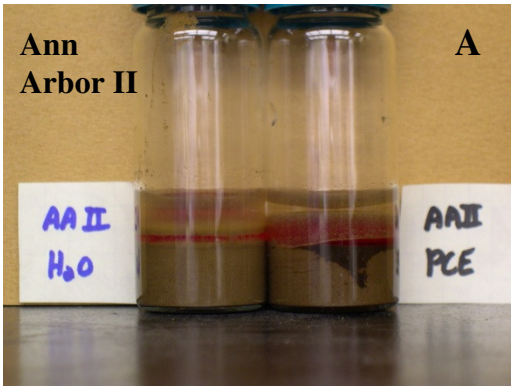
Ann
Arbor II
A
AA II
H2O
AAII
PCE

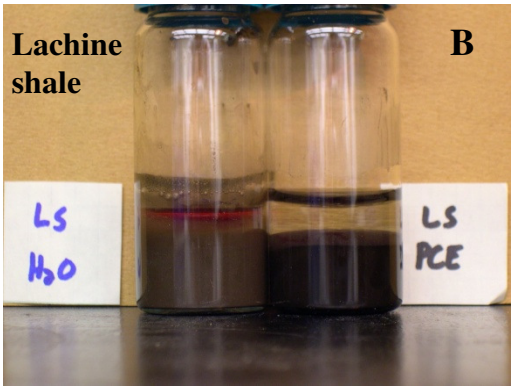
Lachine
shale
B
LS
H2O
LS
PCE

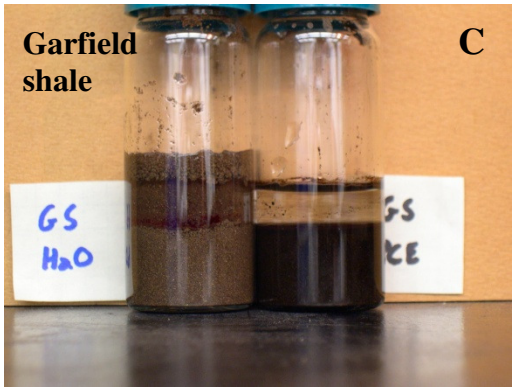
Garfield
shale
C
GS
H2O

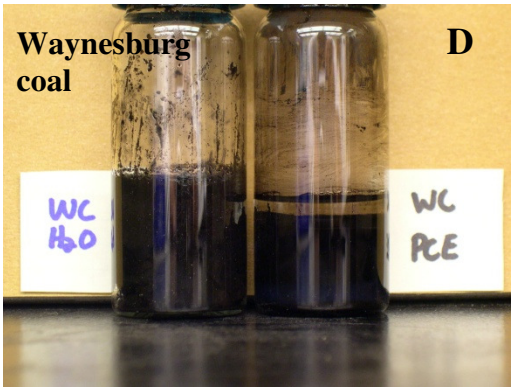
Waynesburg
coal
D
WC
H2O
WC
PCE

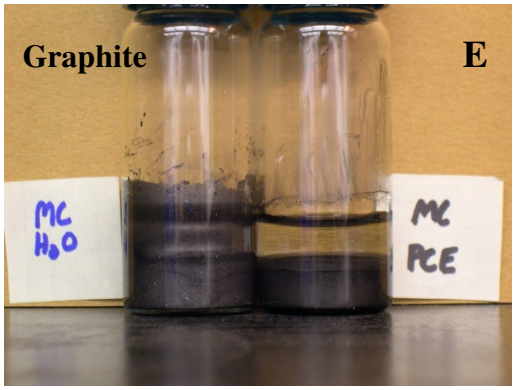
Graphite
E
MC
H2O
MC
PCE

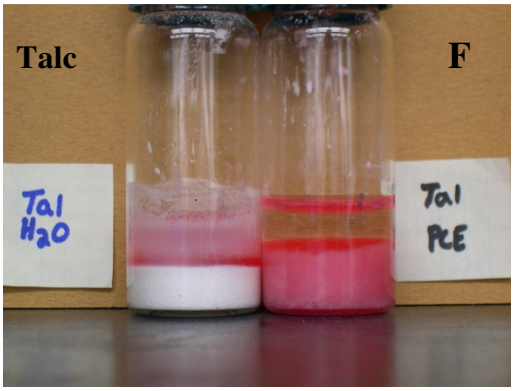
Talc
F
Tal
H2O
Tal
PCE

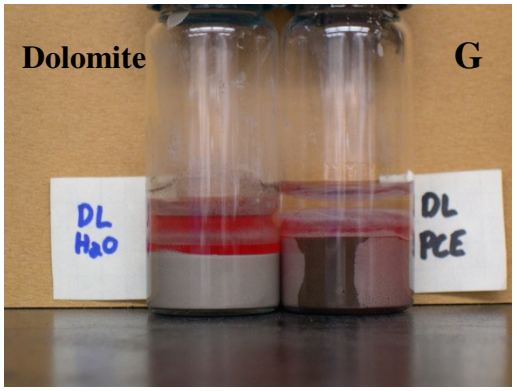
Dolomite
G
DL
H2O
DL
PCE

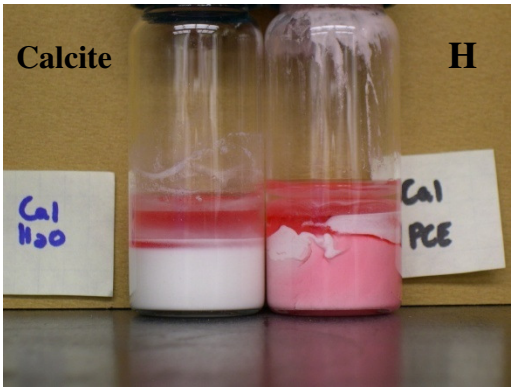
Calcite
H
Cal
H2O
Cal
PCE

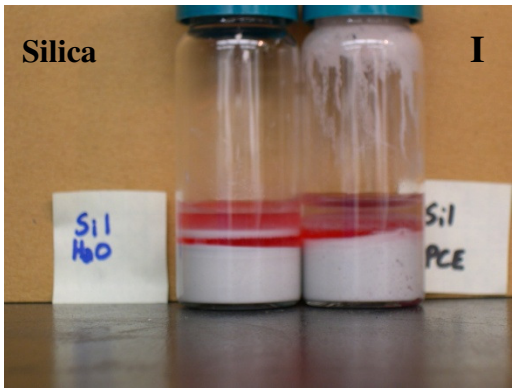

Figure 3.1, Qualitative bottle tests. PCE dyed red with Oil-Red-O. Left: water immersion. Right: PCE immersion.

Figure 3.2 shows comparative line-ups of soil equilibrated with aqueous phase before the introduction of PCE versus bottles of soil equilibrated with the PCE phase before addition of the aqueous phase. Figure 3.2 rows A and C, show the similarity between the mineral and organic materials when the particles are initially immersed in the aqueous phase. In the cases where the soil was initially immersed in water, the red PCE is not observed entering the soil pore space. When PCE is the initial fluid to contact the soil materials (rows B and D), the wettability varies among materials. It should be noted that the bottle test does not discriminate between pore shape and size effects, and surface chemical effects on the soil capillary behavior (Section 1.14). These soil materials were crushed to a uniform size range (425-500 μm) but the shape of individual soil grains varies. The silica and Ann Arbor II particles are round, smooth, and spherical. The Lachine shale and Garfield shale are sharply angular and platy. The talc and graphite are platy. Because the differences in particle shape can create differences in the pore size to pore throat ratio, a quantitative contact angle cannot be assigned to the materials based on the bottle test observations. However, the pore size differences between the soils are not likely to result in the wetting reversal observed between the two cases; thus the difference in behavior observed here likely results from wettability differences.

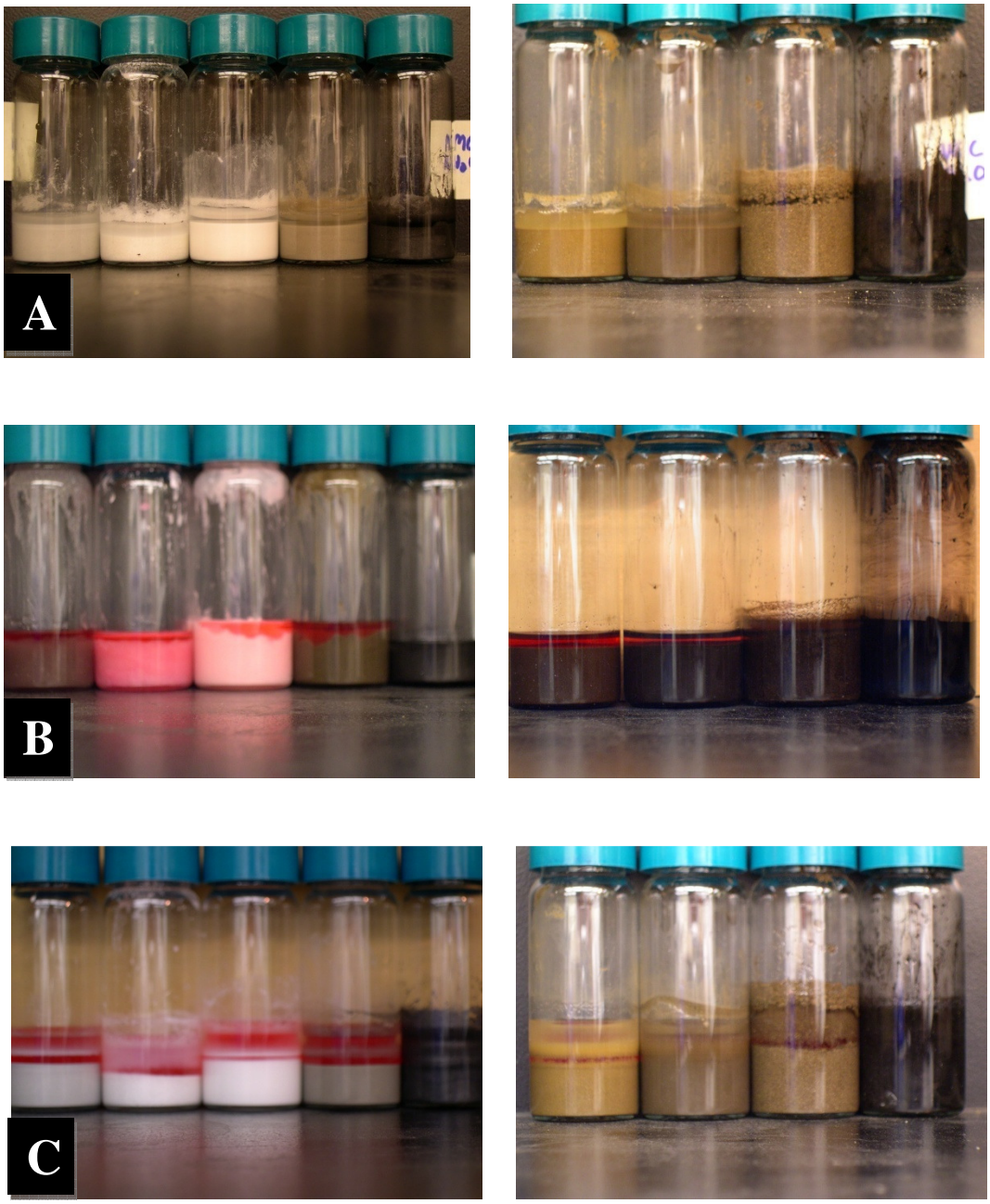
A
B
C

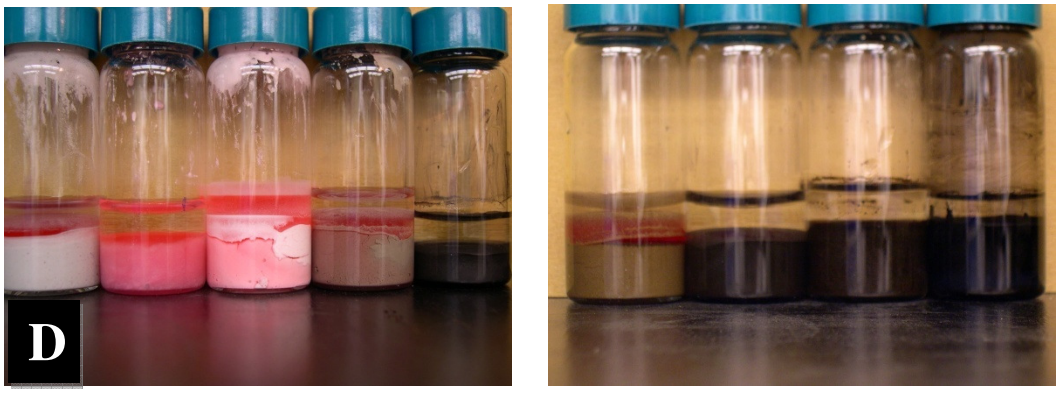

Figure 3.2, Bottle test comparative images. The left column includes mineral materials (from left to right) silica, talc, calcite, dolomite, graphite. The right column includes natural carbon-containing materials (from left to right) Ann Arbor II, Lachine shale, Garfield shale, Waynesburg coal. Row A) Two phase systems, dry soils immersed in aqueous phase. Row B) Two phase systems, dry soils immersed in PCE. Row C) Three phase systems, soils initially immersed in aqueous phase with PCE added second. Row D) Three phase systems, soils initially immersed in PCE with aqueous phase added second.

The bottle tests suggest the existence of wettability hysteresis in these systems. Wettability hysteresis, $\Delta\Theta$, defined here as the difference between the contact angle when the non-wetting phase is the droplet and when the non-wetting phase is the surrounding or immersion phase. Figure 3.3 illustrates how wettability hysteresis is different from "contact angle hysteresis". In contact angle hysteresis, the contact angle determined in advancing versus receding conditions is compared. To measure contact angle hysteresis, a droplet is first increased in size, causing the three phase contact line to move away from the drop center. The contact angle is measured and taken as the advancing contact angle. Then the droplet is withdrawn by applying suction to the syringe and a second contact angle, the receding angle, is measured. The receding contact angle is typically smaller, however, a reversal of wetting preference, a change in the sign of $\cos\Theta$, is not typical. In wettability hysteresis, the droplet and immersion fluids are switched between the two cases and in both cases the advancing contact angle is measured, but the magnitude of the contact angle varies with a possible change in the sign of $\cos\Theta$.

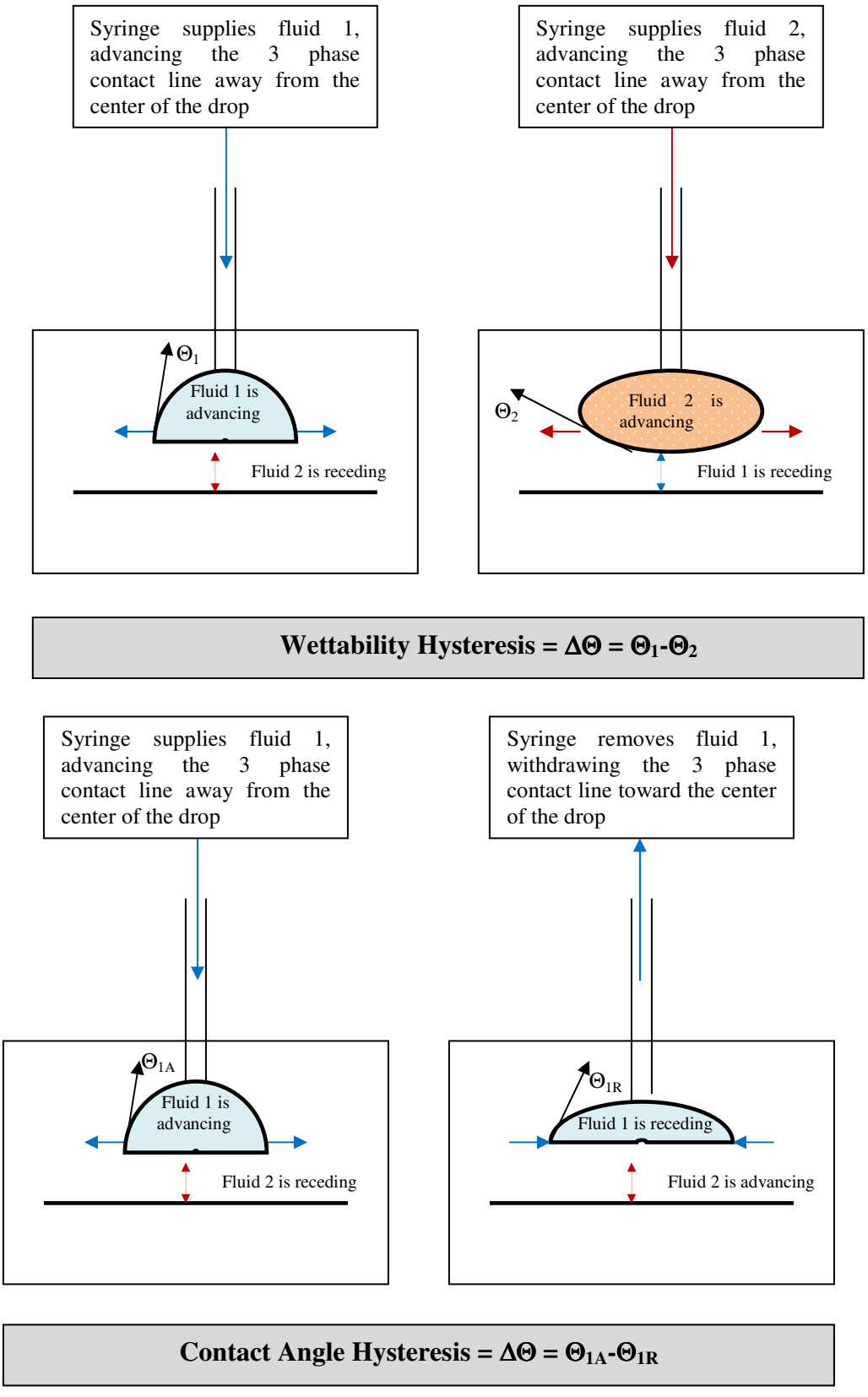

Figure 3.3, Comparison between wettability hysteresis and contact angle hysteresis.

3.2 Quantitative air-water-solid contact angles

While the bottle test results suggested the existence of wettability hysteresis, they cannot provide a quantitative measure of its magnitude. To confirm the bottle test observations with a quantitative measure of wettability, sessile drop contact angles were collected for air-water, PCE-water and all the solids listed in Table 2.4. Figure 3.4 shows contact angles for the air-water-solid systems at neutral pH, with the numerical values given in Table 3.2. The solids were prepared following the method described in Section 2.4. The contact angles were collected with the methods described in Sections 2.6 and 2.7. The first phase listed in the legend of Figure 3.4 indicates the immersion phase, in other words, the phase that recedes from the surface when a second fluid phase is introduced in the form of a drop. Contact angles are reported through the aqueous phase, unless otherwise specified. The error bars define the 95% confidence interval of the contact angle based on the spread in contact angle values determined for the collection of images taken for each system. The error bars are small in most cases.

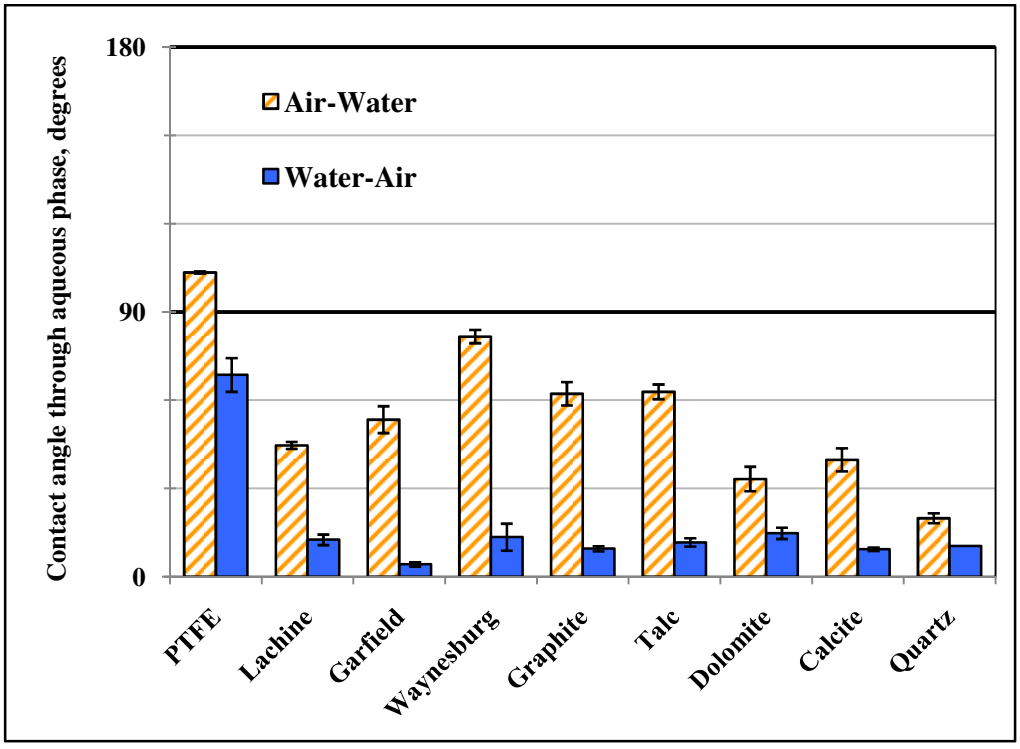

Figure 3.4, Air-water-solid system contact angles corresponding to the values in Table 3.2.

With the exception of polytetrafluoroethylene (PTFE), all the materials are strongly water-wet when initially immersed in the aqueous phase. This is consistent with the bottle test results shown in Figure 3.2. Even graphite is strongly water-wet, with a contact angle of 9.5°. For modeling purposes, contact angles less than 20° are generally considered the same as a contact angle of 0° because when calculating the capillary pressure, the cosine of the angle is taken and the difference between cosine of 0° and 20° is less than 10%. PTFE, has a water-air contact angle of 68.6° so it is considered intermediate-wetting. PTFE is one of the least wetting anthropomorphic materials but it is still water-wetting when immersed in the water phase. Thus, there probably are not many materials that naturally have a contact angle greater than 90° in water-air-solid systems.

Material	**Water-Air Contact Angle**	**Air-Water Contact Angle**	**ΔΘ**
PTFE	68.6 ± 5.7	103.4 ± 0.3	34.8
Lachine shale	12.6 ± 1.8	44.6 ± 1.2	32.1
Garfield shale	4.2 ± 0.7	53.4 ± 4.6	49.2
Waynesburg coal	13.4 ± 4.6	81.6 ± 2.3	68.2
Graphite	9.5 ± 0.9	62.2 ± 4.0	52.7
Talc	11.7 ± 1.4	62.9 ± 2.5	51.2
Dolomite	14.8 ± 1.9	33.2 ± 4.2	18.5
Calcite	9.4 ± 0.6	39.7 ± 3.9	30.4
Quartz	10.5 ± NA*	19.9 ± 1.7	9.5

Table 3.2, Air-water-solid system contact angles and wettability hysteresis. *NA=Not applicable because only one drop was measured on the silica surface. All measurements are given in degrees.

When water droplets are placed on air-dry surfaces, the contact angles are less than 90° through the water phase, denoting water-wetness. But the surfaces are less water-wet when air bubbles are placed on a surface immersed in water. In both cases, with the exception of PTFE, the materials are all water-wet. Quartz is the most water-wetting in this case, with a contact angle of 19.9°. Dolomite and calcite have similar contact angles that are slightly less water-wet than quartz. However, in the dry state there is significantly more variation between materials. The three organic carbon containing soil materials, Lachine shale, Garfield shale, and Waynesburg coal become less water-wetting in that order with contact angles through the aqueous phase ranging from 44.6° to 81.6°.

Neither graphite (62.2°) nor talc (62.9°) appears to be non water-wetting in an air-water system. Although these two materials are cited as being hydrophobic in the literature, (Mercer and Cohen, 1990) contact angles are not typically reported, suggesting that the term hydrophobic is applied to materials that are less strongly water-wet than quartz but that still have a contact angle smaller than 90° in air-water systems.

Significant wettability differences are apparent between the water immersion and air immersion cases, as shown by the values for wettability hysteresis, $\Delta\Theta$, given in Table 3.2. In the air-water-solid case, where water is contacting dry solids, quartz is the most water-wetting as shown in Figure 3.4. However, capillary pressure tests (Appendix C) show that the Ann Arbor II sand and silica coated with humic acids have no discernable differences in wetting behavior from pure quartz. Based on the results presented here, it appears that this system represents one end of the spectrum of wetting behavior in the subsurface.

3.3 Quantitative air-NAPL-solid contact angles

Table 3.3 lists the contact angles measured through the PCE phase for air bubbles placed on solids immersed in PCE. The contact angle through the PCE phase for air-PCE-solid systems appears to be very low for either wetting order. It ppears that there is no inherent impediment to PCE wetting the surfaces. The spreading of organic liquids preferentially over dry surfaces has been noted in the literature (Mercer and Cohen, 1990). Contact angles in the reverse case, drops of PCE placed on dry solids, could not be measured because they did not produce enough of an elevated drop profile to measure a contact angle by the ADSA method. Although the contact angle was not quantifiable it was visually less than 15° for air-PCE cases. A second complication with air-PCE-solid systems was that the measurement cell was not a sealed system so PCE vaporized from the surface changing the boundaries of the drop very rapidly. A closed container would be required to allow the drop to equilibrate with the surrounding air phase at a saturated vapor pressure.

Material	PCE-Air Contact Angle
Lachine shale	11.1± 1.4
Garfield shale	13.9± 1.0
Waynesburg coal	11.9 ± 2.4
Graphite	13.9 ± 1.7
Quartz	13.6 ± 1.4

Table 3.3, Contact angles measured through PCE for air bubbles placed on soil material surfaces immersed in PCE. All measurements are given in degrees measured through the PCE phase.

In both air-water and air-PCE systems, the surfaces are wet by the liquid phase, as opposed to air, regardless of which fluid contacts the solids first. When PCE encounters dry soil materials it will spread and enter the smallest dry soil pores. However, the vadose zone is not uniformly dry; some soil materials may have a water film at the surface and some pores may be filled with water prior to the introduction of solvent. In this experiment, the solids were open to the laboratory air before equilibration for contact angle measurement. Given the average relative humidity in Ann Arbor (59-71%), the soil materials were likely to have water vapor at the surface. It is not known how much humidity is necessary to develop a condensed water film sufficient to prevent PCE spreading. The next section explores the wettability of PCE-water-solid systems.

3.4 Quantitative NAPL-water-solid contact angles

Figure 3.5 shows the contact angles of PCE-water-solid systems. The systems were equilibrated for seven days and the pH was adjusted to neutral (7 ± 0.2), as described in Section 2.7. The wettability scale is sometimes divided into water-wetting, 0-60° measured through the water phase, intermediate wetting, 60-120°, and non water-wetting, 120-180°. For the case of immersion in water, PTFE is intermediate wetting with a contact angle of 73.7°. Lachine shale, Garfield shale, dolomite, calcite, and silica all have contact angles less that 20° so they can be viewed as completely water-wetting when water is the first liquid to contact the surface. With the exception of PTFE, water would preferentially occupy the smallest pores for all of these materials.

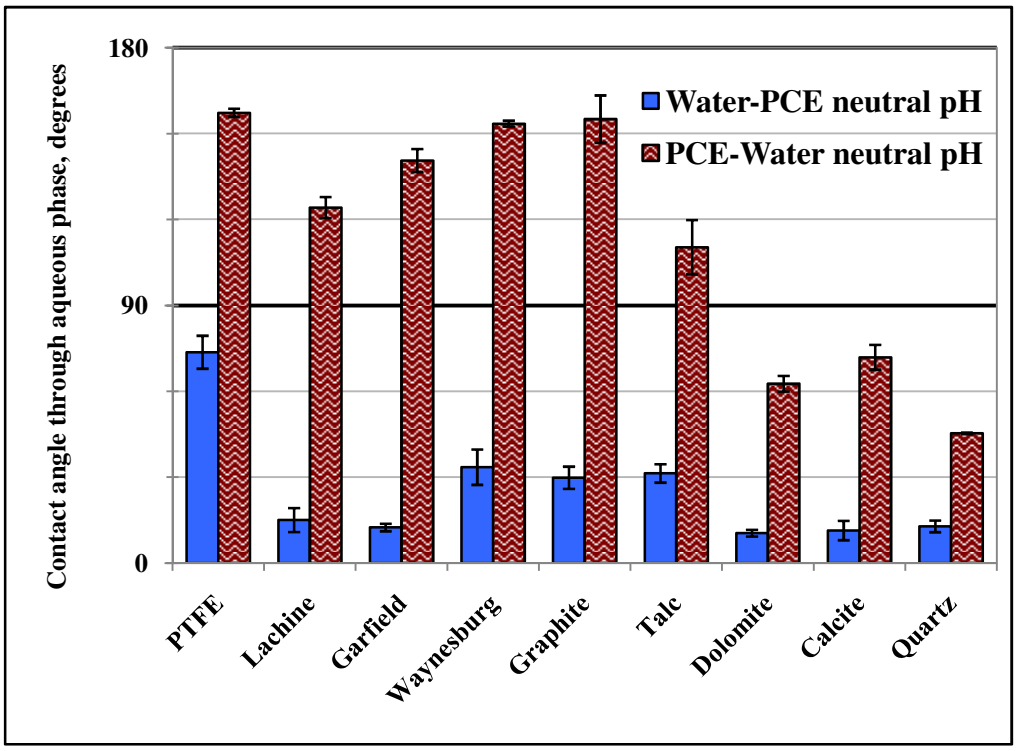

Figure 3.5, PCE-water-solid system contact angles corresponding to the values in Table 3.4. Aqueous phase pH controlled to 7 ± 0.2.

When the solids are immersed in PCE (patterned bars) there is significant difference in the water-solid contact angles. PTFE is PCE-wet, as expected. Similar to the results in the air-water-solid system, the contact angles for the organic carbon containing materials increase from weakly PCE-wet in the case of Lachine shale (124.2°) to strongly PCE-wet in the case of Waynesburg coal (153.5°). Graphite is strongly PCE-wet when immersed in the PCE phase. Talc is also PCE-wet in this situation, despite containing no organic carbon. Dolomite and calcite remain water-wet regardless of the wetting order; however, their contact angles indicate an intermediate-wetting state. Although the PCE-water-silica system is not strongly water-wet, it is still the most water-wetting of all nine systems studied. Once again, silica represents an endpoint of the range of wettability behavior for aquifer materials.

PCE-water-solid systems display more wettability hysteresis than air-water-solid systems. Svitova et al. (2002) also observed that air-water contact angles were not indicative of the trends in silicone oil-water contact angles. In their case, silica wafers coated with natural and anthropomorphic polymers displayed wettability reversals while

clean quartz wafers were always water-wet Table 3.4 shows that four materials have wettability hysteresis that exceeds 90°. However, quartz has a relatively small amount of hysteresis, only 32.5°. Small variability in quartz contact angles of 5-20º dependent on the measurement conditions has been shown in the literature (Iler, 1979; Barranco et al., 1997). Both of the minerals commonly believed to be hydrophobic, graphite and talc, are only non water-wetting when the immersion phase is PCE. PTFE, a substance known for its hydrophobicity, is water-wet if water contacts the surface first. From Table 3.4, it is apparent that it is not simply organic carbon content that makes soil materials have conditionally-dependent contact angles.

Material	**Water-PCE Contact Angle**	**PCE-Water Contact Angle**	**$\Delta\Theta$**
PTFE	73.7 ± 5.8	157.3 ± 1.4	83.6
Lachine shale	15.0 ± 4.2	124.2 ± 3.7	109.1
Garfield shale	12.4 ± 1.3	140.6 ± 4.0	128.2
Waynesburg coal	33.5 ± 6.2	153.5 ± 1.0	120.0
Graphite	29.8 ± 3.9	155.1 ± 8.3	125.3
Talc	31.3 ± 3.2	110.3 ± 9.5	79.0
Dolomite	10.5 ± 1.2	62.6 ± 2.8	52.2
Calcite	11.4 ± 3.4	71.9 ± 4.3	60.5
Quartz	12.8 ± 2.0	45.4 ± 0.3	32.5

Table 3.4, PCE-water-solid systems contact angles and wettability hysteresis. All measurements are given in degrees measured through the water phase.

CTET-water-solid system contact angles are shown in comparison to PCE-water-solid systems in Figure 3.6. Carbon tetrachloride (CTET) is a non-polar liquid with similar density, surface tension, interfacial tension, and dipole moment to PCE. (See Table 2.2 for specific values.) A CTET-water-quartz contact angle could not be measured because the water phase droplet was nearly completely spreading. CTET system contact angles are very similar to those for the PCE systems. These data demonstrate that the wettability hysteresis in PCE-water-solid systems is not limited to PCE but a property of other NAPL-water-solid systems as well. Table 3.5 lists the wettability hysteresis for CTET-water-solid systems. Again, there is large hysteresis for the organic carbon-containing soil materials and talc.

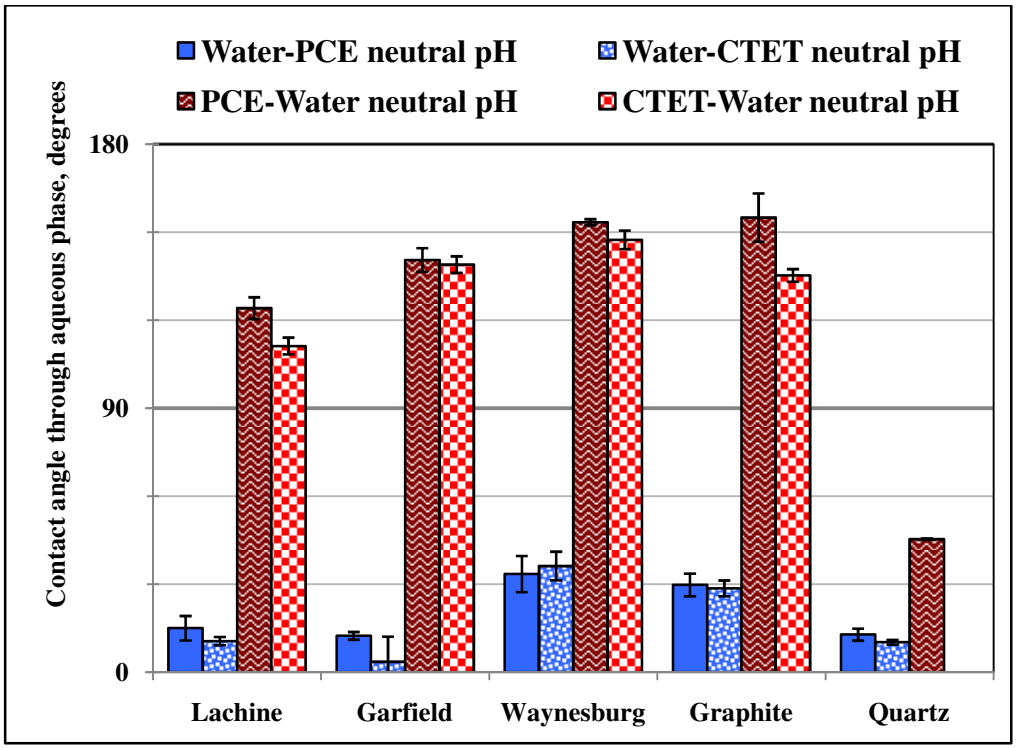

Figure 3.6, Comparison of contact angles in CTET-water-solid and PCE-water-solid systems.

Material	Water-CTET Contact Angle	CTET-Water Contact Angle	ΔΘ
Lachine shale	10.6 ± 1.4	111.3 ± 2.9	100.6
Garfield shale	3.6 ± 8.6	139.0 ± 2.8	135.4
Waynesburg coal	36.2 ± 4.9	147.5 ± 3.1	111.2
Graphite	28.6 ± 2.7	135.3 ± 2.2	106.7
Quartz	10.3 ± 0.8	NA*	NA*

Table 3.5, Wettability hysteresis in CTET-water-solid systems. *NA=Not measured, CTET-water-quartz contact angle could not be measured due to nearly complete spreading of the water phase. All measurements are given in degrees measured through the water phase.

Despite often being cited as hydrophobic in the literature (Anderson, 1986; Mercer and Cohen, 1990) it appears that the organic and mineralized carbon containing materials, as well as talc, appear to be water-wet under certain conditions. It is possible that the citations of NAPL-wet materials occurred in cases where the NAPL phase carried surface-active constituents which sorbed to the solid surfaces. The term hydrophobic solid also appears to be used to mean a surface that is not strongly water wet, similar to its use regarding water repellency. Mercer and Cohen (1990) cite several researchers who

found that dolomite and limestone (calcite) reservoirs could become NAPL-wet or fractionally NAPL-wet (patchy wetting of each phase) after contact with crude oil. The dolomite and calcite used for this study do not appear to be NAPL-wet under any conditions. In petroleum reservoir studies, it is likely that surface-active species such as resins and bitumens, the less soluble components of oils, are present in the fluids and sorbed to the reservoir solids, thus creating a non water-wet surface (Menon and Wasan, 1986; Buckley and Liu, 1998). The NAPLs in this study are pure phases. Several tests were performed to ensure that the wettability hysteresis observed in the systems described above were due to surface chemical differences as opposed to sorption processes.

3.5 Effect of equilibration fluid on wettability

Figure 3.7 shows the contact angles for slides that have been equilibrated in PCE, rinsed with 0.01M NaCl aqueous phase, and then immersed in fresh aqueous phase. The drop liquid is PCE. For comparison, the contact angles of PCE drops placed on surfaces equilibrated and immersed in the aqueous solution are shown as well. Although the water-PCE-solid system contact angles increased between 9.5° and 30.4° with equilibration in the PCE phase, they are still water-wet. A layer of PCE was not visible at the solid surface when the droplets were placed on the slides and photographed; however, it is possible that a PCE film is present even after rinsing with the aqueous phase.

The data presented in Table 3.3 showed that PCE was the preferential wetting phase on dry soil materials. Therefore, when the solids are immersed in the PCE phase for equilibration the PCE will enter the narrow valleys and micropores at the surface of the solid. When the solid is removed and rinsed with the aqueous phase most of the PCE will be removed by the water pressure but PCE may remain in some small surface pores. When a water drop contacts the surface it may then rest on a composite of bare surface and PCE-filled pores. Therefore, the PCE-filled pores will be less water-wetting than the solid alone, causing an increase in the contact angle.

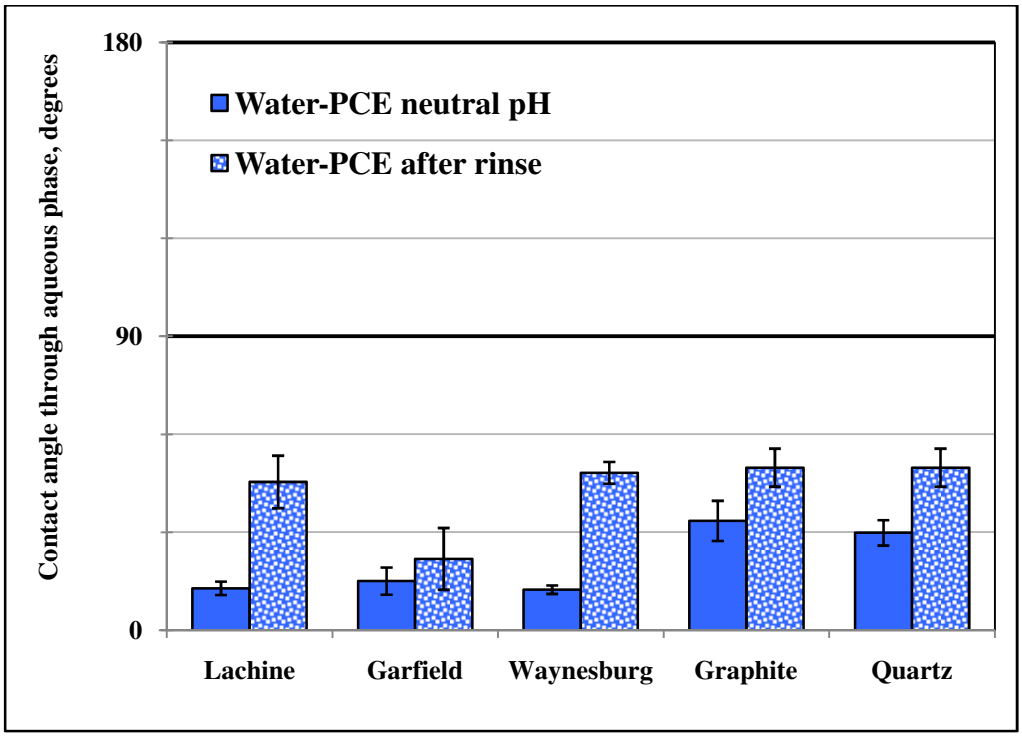

Figure 3.7, Contact angle of geoslides equilibrated in PCE and rinsed with aqueous solution measured through the aqueous phase.

A second possibility is that PCE is actually sorbed to the solid matrix. This is known to occur for organic solutes in water. Indeed, sorption of phenanthrene, a hydrophobic organic solute, to Lachine shale has been shown to be quite high compared to sorption to a humic acid coated sand (Huang and Weber, 1997). The K_{OC} value, the value of the partition constant for organic solutes partitioning to soil, for soil organic matter extracted from Lachine shale was 2812 L/g of organic carbon compared to 13.4 L/g of organic carbon for soil organic matter extracted from Chelsea soil. Partitioning coefficients for PCE in the literature vary. One estimate, for example, is that the Borden aquifer sand could sorb 185 µg/g (Ball and Roberts, 1991) if free phase PCE was present. The sorption of PCE to the surface of the solid could alter the solid-liquid interfacial tensions and the force balance that determines the contact angle. No specific tests were conducted to measure the degree of PCE sorption to the solids in PCE-water or water-PCE cases. However, in either water or PCE immersion, after a week of equilibration with free phase PCE in the jar, the aqueous phase was saturated with PCE. Thus, the

sorption of PCE to the soil materials is complete after seven days and not likely to cause the difference in contact angle between the two wetting order cases.

3.6 Effects of interfacial tension on wettability

Either of the preceding possibilities may explain the increase in water-PCE-solid contact angles when equilibration with PCE occurs before immersion in the aqueous phase. A third explanation for the increased contact angle when PCE first contacts the surface is that PCE is extracting soluble organic constituents from the surfaces of the solids. This would alter the interfacial tension between the PCE and aqueous phase, γ_{L1L2}. Equation 1.1 shows that when γ_{L1L2} is altered, the magnitude of the contact angle changes, although the change in interfacial tension will not actually cause a switch from water-wetting to NAPL-wetting or vice versa. PCE is typically used as a solvent because it solubilizes organic constituents on surfaces, leaving the surface clean. To check that surface-active agents were not being solubilized from the surface of the solids and affecting the liquid-liquid interfacial tension, three sets of powdered solids were equilibrated in contact with pure liquids. Section 2.8 describes how the samples were equilibrated. The resulting surface tensions are shown in Figure 3.8 and indicate that the surface tension of the aqueous phase does not vary after contact with the soil materials or with PCE which may have solubilized soil organic components. The error bars shown are 95% confidence intervals determined by measuring 9-16 drops for each material. For these measurements, the aqueous phase was Milli-Q purified water which had a surface tension of 72.6 mNm^{-1}, as shown in the first pair of bars in Figure 3.8. This is comparable to the literature value of 72.8 mNm^{-1} (Demond and Lindner, 1993; Hiemenz and Rajagapolan, 1997).

Figure 3.9 shows measured values of interfacial tension between PCE and water. The solid bars represent the interfacial tension between Milli-Q water that was equilibrated with PCE and soil materials, and PCE that was pre-equilibrated with Milli-Q as described in Section 2.8. A comparison of the solid bars shows that the system containing Garfield shale has the lowest interfacial tension. Garfield shale is classified as an oil shale so it is expected to have long-chain hydrocarbon groups and aromatic groups which may be soluble in the PCE phase. The solid bars of Figure 3.9 show that PCE

solubilized components from the surface of Garfield shale that partitioned into the aqueous phase and subsequently lowered the interfacial tension between the aqueous phase and a fresh PCE phase. The Garfield shale also lowers the interfacial tension between PCE that was equilibrated with the solid and Milli-Q that was pre-equilibrated with clean PCE. So, surface-active agents may be present at both the PCE and aqueous sides of the interface. Changes in the liquid-liquid interfacial tension may be a reason that Garfield shale and Lachine shale have different contact angles despite similar compositions.

The Ann Arbor II sand lowers the interfacial tension when Milli-Q that was equilibrated with PCE and soil materials is contacted by pre-equilibrated PCE (patterned solid bars in Figure 3.9). However, Ann Arbor II does not affect the water surface tension or the interfacial tension when the soil is equilibrated in PCE only (Figure 3.8 and patterned bars of Figure 3.9, respectively). When the Milli-Q equilibrated with the PCE and soil is removed and placed in contact with clean PCE, the surface-active agents are removed as well. Thus, they are likely to be amphiphilic molecules with a hydrophilic group that is stable in the aqueous phase side of the interface, both because these are the type of molecules that often influence interfacial tension, and because humic acids are typically large, complex molecules with many different functional groups.

It may be noted that the addition of Oil-Red-O dye only slightly alters the interfacial tension of PCE-water systems. This check on the interfacial tension following the addition of Oil-Red-O dye was necessary since Jeong et al. (2002) demonstrated that high concentrations of Oil-Red-O could significantly lower the interfacial tension between PCE and water. Figures 3.8 and 3.9 show that the addition of Oil-Red-O, which is only soluble in the organic liquid phase and not the aqueous phase, does not affect the surface tension of the aqueous phase or the interfacial tension between PCE and water enough to affect the wettability of the rock-liquid systems.

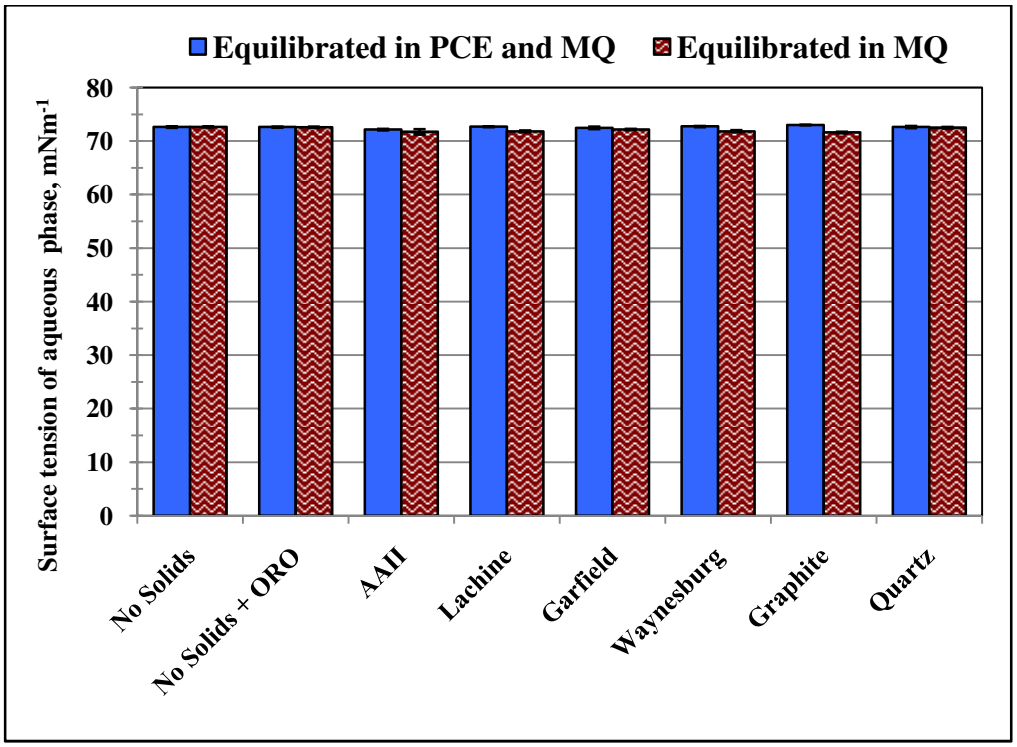

Figure 3.8, Surface tension of water following equilibration with soils, PCE, and Oil-Red-O dye (ORO).

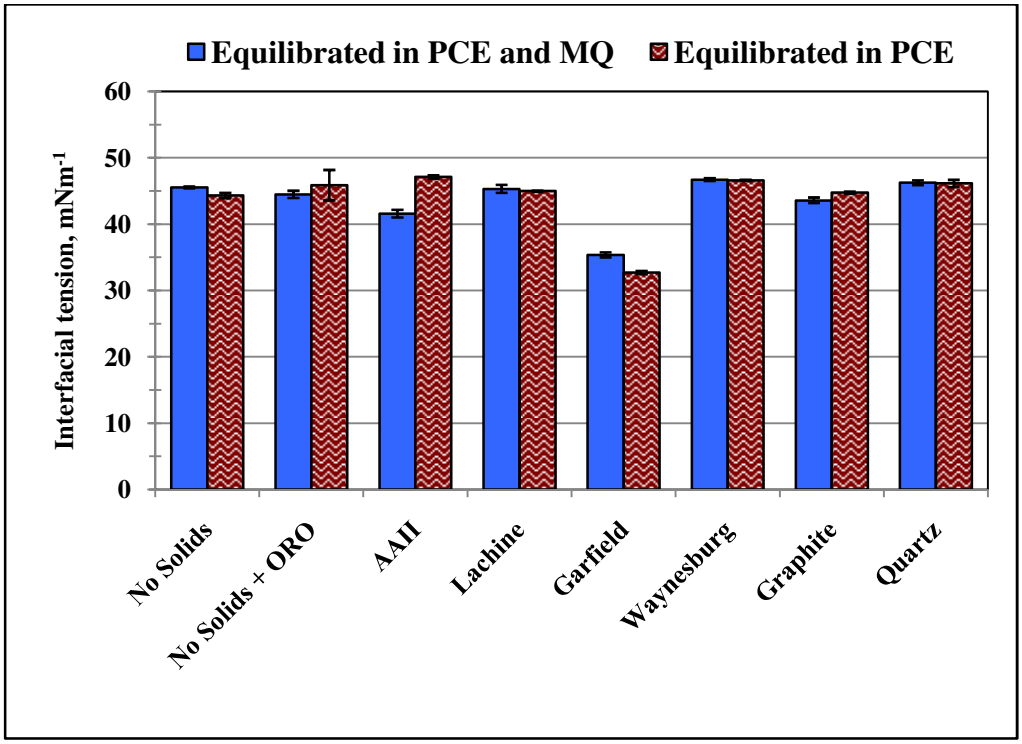

Figure 3.9, Interfacial tension of water and PCE following equilibration with soil materials, aqueous phase and Oil-Red-O dye.

3.7 Effects of immersion phase equilibration time on wettability

Figure 3.10 compares the contact angles of PCE-water-solid systems measured after extended equilibration to the contact angles obtained after the typical seven days of equilibration used for most of the systems in this study. In the extended equilibration measurements, the solid samples were equilibrated with the immersion phase for 80 days in a 50 mL jar that also contained 1.8 mL of the droplet phase. The droplet phase and immersion phase were in contact but the droplet phase was separated from the solid surface. Details of the equilibration process are given in Section 2.7. For the organic carbon containing materials, extending the length of equilibration does not significantly alter the contact angles in either the PCE-water or water–PCE systems. Given that the interfacial tension between the fluids is not likely to change based on the results discussed in Section 3.6, these results show that the solid-fluid interfacial tensions in these systems are stable over long times. The only system that shows significant difference after 80 days of equilibration is the quartz. Also, quartz is the only solid of the five examined in this test that is not PCE-wet after seven days. The increase of 22° in the quartz contact angle over the extended equilibration period may be due to the fact that, after 80 days of contact with the PCE, sufficient concentrations of impurities from PCE have sorbed to the polar quartz surface to cause a decrease in the solid surface energy, and hence an increase in the contact angle. Ball and Roberts (1991), among others, found that long equilibration times were necessary to achieve equilibrium between trace organic solutes and solids in a study of the sorption of organicss to Borden sand, often used as a model aquifer sand. In this case, the specific surface area of the geoslides is small relative to that of the porous medium used by Ball and Roberts which may be a factor in the observation that the system appears to be at equilibrium in less than seven days. Also, free phase NAPL is present in these systems whereas the organics were trace constituents of the aqueous phase in Ball and Robert's systems. Iler (1979) also showed that very small changes in the surface of quartz plates could dramatically alter the surface energy which, in turn, alters the surface-fluid interfacial tension and thus the contact angle.

Corey (1994) states that, even if initially wetted by oil, most porous media will eventually be wetted by water due to the adsorption of water at the surface over time. However, for the PCE-water-solid systems immersed in PCE, where the NAPL-wetting condition is not due to the sorption of organic constituents from an oil phase, the surfaces do not appear to revert to water-wetting over an extended time period. For the organic carbon materials, the small amount of impurities in the PCE may not cause a significant difference since the surfaces are already chemically heterogeneous and not uniformly polar. Also, since the organic carbon surfaces are less polar to begin with, they may not sorb polar impurities to the same extent as quartz. Finally, the natural carbon surfaces are likely to be more porous than the quartz. A comparison of specific surface area for silica soil and Lachine shale reveals that the Lachine shale has 400 times more surface area than the silica (12.3 m^2/g versus 0.03 m^2/g as measured by N_2 sorption by Huang (1997a)) so a higher solution concentration of surface-active agents would be needed to effect a change in percent coverage of the Lachine surface.

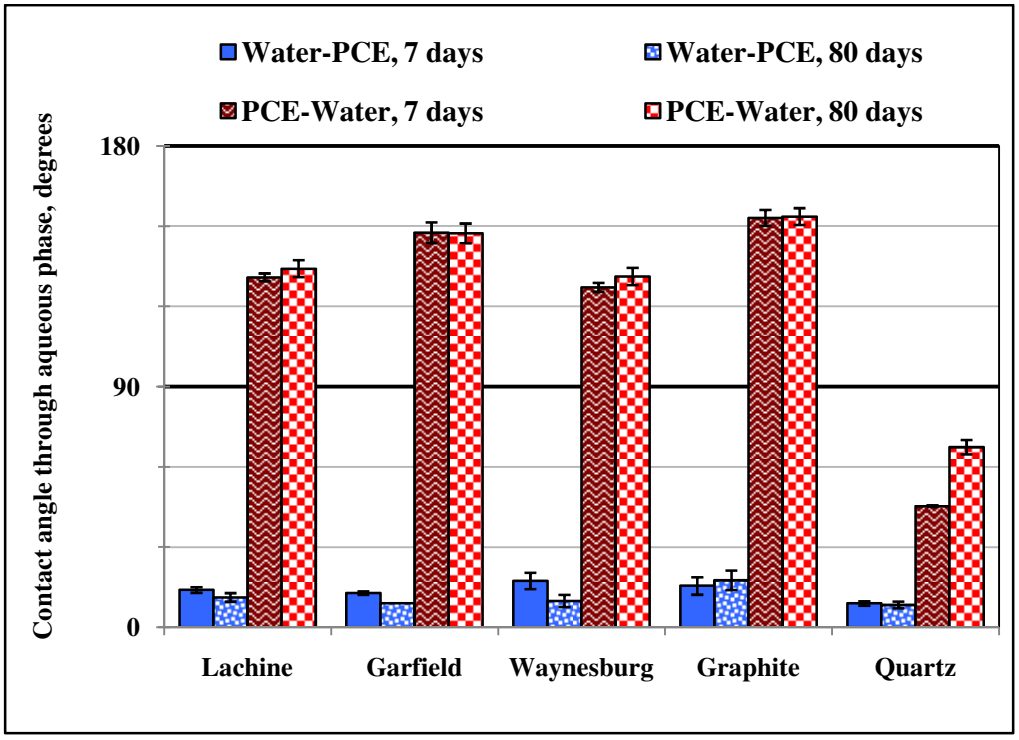

Figure 3.10, PCE-Water contact angles after an extended equilibration time.

Sections 3.5, 3.6, and 3.7 showed that wettability hysteresis is not due to the effects of sorption of the NAPL phase, liquid phase surface and interfacial tension changes, or the length of equilibration prior to measurement of the contact angle, respectively. An alternative hypothesis, that wettability hysteresis is caused by the presence of a persistent film of water when the solids are initially immersed in water preventing the non-aqueous droplet phase from interacting with the solid surface, is explored in Chapters 4 and 5.

3.8 Classification of soil materials based on wettability and degree of hysteresis

Based on the bottle tests and the contact angles measured in the water-air-solid and water-PCE-solid systems, it is possible to sort the experimental solids into several categories to describe both the contact angle and the degree of wettability hysteresis. Table 3.6 indicates the categories assigned to each of the solids examined by bottle tests and contact angle measurements. For this classification, the terms water-wet and NAPL-wet describe the wetting phase in NAPL-water systems. Thus, the classification must specify the surrounding phase since it will influence the wettability. Here it is given for non-polar NAPL immersion phases. Strongly water-wetting indicates contact angles measured through the water phase of less than 20°. Moderately water-wetting indicates contact angles between 20° and 60° and weakly water-wetting indicates contact angles between 60° and 90°, while weakly NAPL wetting indicates contact angle between 90° and 120°. Moderately NAPL-wetting describes contact angles between 120° and 150° and strongly NAPL-wetting contact angles are greater than 150°. Conditionally water-wet cases are those where the wettability switches from water-wet to non-water wet depending on the immersion phase and non-conditional wetting describes solids where the wetting phase is constant, regardless of the order of fluid contact with the soil materials. There were no materials non-conditionally NAPL-wet in NAPL-water-solid systems and it is likely that there are very few, if any, materials that fall into this category. It should be noted that the degree of wetting under one immersion fluid is not necessarily correlated to strong or weak wetting under another immersion fluid. A bottle test can be used to determine the wetting fluid and if there is wettability hysteresis, but a contact angle measurement is necessary to determine the degree of wetting.

Material	Wettability	Hysteresis
PTFE	Strongly NAPL-wet	Conditional
Lachine shale	Moderately NAPL-wet	Conditional
Garfield shale	Moderately NAPL	Conditional
Waynesburg coal	Moderately NAPL	Conditional
Graphite	Moderately NAPL	Conditional
Talc	Weakly NAPL-wet	Conditional
Dolomite	Weakly Water-wet	Non-conditional
Calcite	Weakly Water-wet	Non-conditional
Quartz	Moderately water-wet	Non-conditional

Table 3.6, Classification of solids based on wettability and degree of wettability hysteresis. The designation water-wet or NAPL-wet refers to the wettability of solids immersed in NAPL. Conditional and non-conditional refers to wettability hysteresis between NAPL-water and water-NAPL systems.

3.9 Summary and conclusions

The results shown in this chapter indicate that there are significant wettability differences between soil materials. In water-air-solid systems, all the materials are wet by the water phase regardless of the wetting order. In air-water systems, where the solids are dry before the introduction of a water droplet, they vary from strongly water-wetting in the case of quartz to intermediate-wetting in the case of talc and Waynesburg coal. In water-air systems, where the solids are immersed in the water phase, all the natural materials are strongly water-wet. Although often believed to be hydrophobic, the organic carbon containing materials are water-wet in water-NAPL systems, where they are immersed in water before contacting NAPL, as are all the mineral solids and PTFE. However, the Lachine shale, Garfield shale, Waynesburg coal, graphite, talc and PTFE show the reverse wettability in NAPL-water systems where they are immersed in the NAPL phase before the aqueous phase. This wetting reversal is apparent in qualitative bottle tests using porous media and in quantitative contact angles measured using polished geoslides. Quartz is not representative of the range of contact angles possible for natural soil materials or the degree of hysteresis between order of wetting conditions.

Surface-active components of the solids may be solubilized for Ann Arbor II and Garfield shale and slightly alter the interfacial tensions in the fluid-fluid-solid systems but they cannot explain the wettability hysteresis. The hysteresis is not due to

equilibration time, as the contact angles are practically unchanged between 7 and 80 days of equilibration. Also, carbon tetrachloride, another non-polar solvent, displays nearly identical wetting behavior as PCE, including wettability reversal with a switch in the order of fluid contact.

Given the wettability hysteresis observed for a range of aquifer materials, it is important to note that the correct contact angle to assume for capillary flow in the subsurface will depend not only on the type of soil material, but also on the fluid contact history. The contact angles shown in Figures 3.4 and 3.5 suggest that, in the vadose zone, it is possible to have both NAPL-wet and water-wet media. In the saturated zone, water-wet media is likely due to the pre-existing water phase. Van Dijke and Sorbie (2002) argue that these wetting behaviors are all thermodynamically possible, as well as media that is preferentially wet by the gas phase although that case was not observed with the combinations of solids and liquids chosen for this study. Typically, silica sand is used to measure capillary pressure curves and then the curves are scaled to produce variations in capillary behavior with changes in system properties, such as the reduction of the fluid-fluid interfacial tension due to surfactants. However, capillary pressure-saturation curves cannot be readily scaled from a water-wetting regime to predict a NAPL-wetting regime. Soil materials displaying wettability hysteresis will have even larger hysteresis in the capillary pressure-saturation curve because different pores will be filled depending on the fluid occupation history. This conclusion is consistent with Bauters et al. (2000) who examined the capillary pressure-saturation behavior of air-water systems in octadecyltrichlorasilane (OTS) coated sands and suggested that the contact angle was greater during imbibition into dry soils than during drainage from water saturated soils. Cary et al. (1994) also postulated that the failure of models to predict the redistribution of fluids in layered soils was due to the fact that many numerical transport codes do not consider the capillary pressure-saturation hysteresis, which may be partly due to wettability hysteresis. They attempted to modify a model to allow for some reversal of wetting order whereby water following oil into previously dry soils would encounter oil-wet solids and displace oil from the larger pores but leave oil trapped in isolated small pores. This resulted in a water phase with greater conductivity than that predicted from a non-hysteretic capillary pressure-saturation curve. Materials

that display conditional wettability have the potential to severely affect phase interconnectedness, resulting in greater formation of immobilized NAPL blobs that can only be removed under high flow/high pressure conditions or by dissolution. Remediation should take into account that the NAPL may be in the small soil pores in the vadose zone but in the large soil pores of the saturated zone.

Further investigation into the nature of aquifer solid surfaces is necessary to determine the unique physical or chemical causes of the wettability behavior observed. Chapter 4 investigates the chemical composition of the soil materials, specifically, the composition of their surface functional groups. Surface functional groups generate the forces between the solid and the liquid molecules that determine the wettability. Therefore, Chapter 5 examines the surface forces present in soil material systems to explain the complex wettability hysteresis behaviors observed.

CHAPTER 4

COMPOSITION OF AQUIFER MATERIALS

4.0 Introduction

The composition of soil solids is highly variable. Particles may be composed of minerals, carbon, or both. The carbon within the soil materials may be a separate phase as with humic materials or integrated into a solid matrix as in shales and coals. Regardless of the material, the interfacial forces that generate capillary forces are the result of the attraction or repulsion between functional groups at the surface of the materials and the fluids contacting the surface. This chapter presents composition data from three perspectives. Bulk elemental composition gives the percentage of elements in the soil particle. FT-IR is limited to the outermost 30 nm of the particle surface. NMR is limited to the outermost layer of molecules, truly the surface functional groups. ^{13}C NMR is also limited to bonds with carbon so it is specifically applied to the carbon containing materials. It is shown that the oxygen content of materials is a better indicator of contact angle than the carbon content. FT-IR and NMR are used to show that polar functionality decreases with material age and NAPL wetting.

4.1 Bulk elemental composition

The bulk elemental composition of the materials was determined by the method described in detail in Section 2.12. A powdered sample was loaded into a tin ampoule. The tin ampoule was flash ignited and the gases generated were used to determine the mass of each element, carbon, nitrogen, and hydrogen. The ash was assumed to be a dioxide mineral so that the approximate oxygen content could be determined. The composition of talc, calcite, and dolomite was not measured analytically since they are semi-crystalline solids. Their composition was calculated from the molar formulas for each material, ($Mg_3Si_4O_{10}(OH)_2$ for talc, $CaCO_3$ for calcite, and $CaMg(CO_3)_2$ for

dolomite). Table 4.1 lists the bulk elemental content on the basis of mass percent. Table 4.2 lists the bulk elemental composition on the basis of molar percent. Molar percent may be more appropriate for analysis of wettability because it is the contribution of forces from different molecules at the surface of the material that is expected to influence wettability, not strictly the mass of material.

Based on Table 4.2, an approximate formula for each organic carbon-containing material is CHO_4Si_2 for Lachine shale, $C_2H_2O_2Si$ for Garfield shale, and $C_{13}H_{11}O_2Si$ for Waynesburg coal. Thus, the ratio of carbon to mineral matter increases as the materials age. Table 4.2 gives the values of the molar oxygen to carbon and hydrogen to carbon ratios for each material. These ratios also decrease with material maturity. A Van Krevelen diagram for the organic carbon containing materials is shown in Figure 4.1. The most highly processed materials are closest to the origin. Graphite, appearing at the origin, has O/C and H/C ratios of nearly zero, in accordance with its structure as mineralized carbon. Lachine shale and Garfield shale are similar in hydrogen content but Garfield shale has twice the carbon of Lachine shale.

	Mass Percent			
Material	**% C**	**% H**	**% N**	**% Ash**
Lachine shale	9.08	0.84	0.37	89.72
Garfield shale	25.06	2.28	0.81	71.85
Waynesburg coal	68.31	4.74	1.44	25.52
Graphite	96.06	0.00	0.06	3.87
Talc*	0.00	0.53	0.00	49.38
Dolomite*	13.01	0.00	0.00	86.99
Calcite*	11.99	0.00	0.00	88.01
Silica	0.00	0.00	0.02	99.97

Table 4.1, Elemental content based on measured elemental mass in natural soil materials. *Determined by calculation from molecular formula.

Material	Mol Percent				Molar Ratios	
	% C	% H	% N	% O	O/C	H/C
Lachine shale	12.43	13.62	0.43	48.84	3.93	1.10
Garfield shale	26.13	28.30	0.72	29.80	1.14	1.08
Waynesburg coal	48.35	39.95	0.88	7.19	0.15	0.83
Graphite	97.55	0.04	0.05	1.57	0.02	0.00
Talc	0.00	9.52	0.00	57.14	NA	NA
Dolomite	20.00	0.00	0.00	60.00	3.00	NA
Calcite	20.00	0.00	0.00	60.00	3.0	NA
Silica	0.00	0.06	0.04	66.38	NA	NA

Table 4.2, Molar elemental content of natural soil materials calculated from the mass percentages shown in Table 4.1. NA refers to materials where carbon or hydrogen was absent.

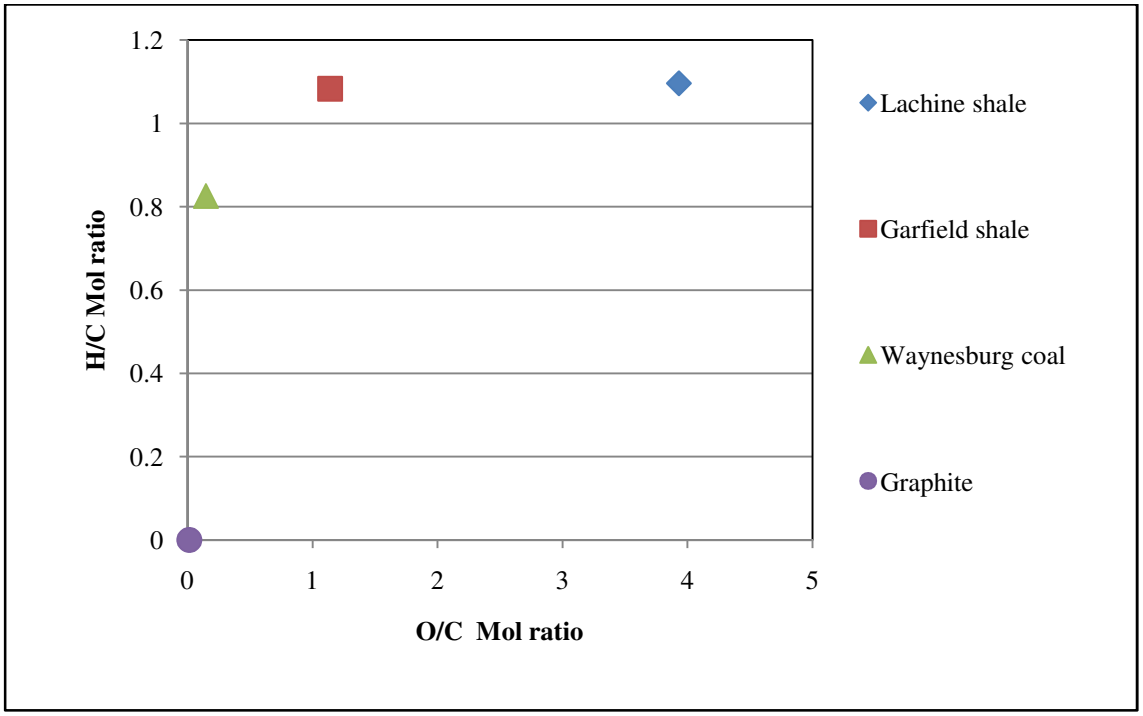

Figure 4.1, Van Krevelen depiction of organic carbon-containing natural soil materials.

4.2 Relationship between contact angle and carbon content

Many correlations between the contact angles, presented in Tables 3.2, 3.4, and 3.5, and bulk composition parameters, presented in Tables 4.1 and 4.2, were explored. It was previously believed that carbon content was correlated to NAPL wetting or water

repellency in solids (Anderson, 1986). Correlations were determined by plotting composition parameters versus contact angle data as shown in Figures 4.2–4.11. The Pearson correlation parameter, ρ, was calculated for each data set as described in Section 2.14. ρ indicates whether or not two parameters are linearly correlated. A positive ρ indicates that the contact angle increases with an increase in the composition parameter and a negative ρ indicates that the contact angle decreases with an increase in the composition parameter. The Pearson correlation was considered significant if it was greater than |0.5|. A line was fit to each data set. The coefficient of determination, R^2, which is given with each linear fit, is equal to ρ^2 and describes how well one data set explains the variation in a second set. Thus, an R^2 of 0.95 indicates that 95% of the variation in the y data set can be explained by the variation in the x data set. Where the ρ and R^2 show a strong correlation and the R^2 value is greater than 0.8, the equation for the linear fit may be suitable as a predictive tool. The Spearman correlation coefficient, ρ_s, is also given. The Spearman correlation is a Pearson correlation on the rank of each data point within the data set rather than the actual data value. The Spearman correlation does not indicate what order polynomial can be used as a predictive relationship between the two data sets but it can be used to determine if they are non-linearly correlated. When ρ_s is close to 1 or -1, it indicates that the two data sets are strongly monotonically correlated. A ρ_s greater than 0.5 or less than -0.5 was assumed to indicate a relationship between the two data sets whereby one can explain the trend in the other, although not necessarily linearly.

All materials, N=8			**Organics, N=4**			**Minerals, N=4**		
System	**ρ**	**ρ_s**	**System**	**ρ**	**ρ_s**	**System**	**ρ**	**ρ_s**
Air-water	0.65	0.43	Air-water	0.68	0.80	Air-water	-0.17	-0.11
Water-air	-0.07	-0.08	Water-air	0.16	0.00	Water-air	0.30	0.32
PCE-water	0.72	0.75	PCE-water	0.92	1.00	PCE-water	-0.23	-0.11
Water-PCE	0.61	0.30	Water-PCE	0.87	0.60	Water-PCE	-0.56	-0.21
			CTET-water	0.60	0.40			
			Water-CTET	0.82	0.60			

Table 4.3, Statistics describing the relationship between carbon mass % and contact angle. ρ is the Pearson (linear) correlation coefficient. ρs is the Spearman (rank) correlation coefficient.

The linear correlations in Sections 4.2 through 4.5 describe three data sets. "All materials" indicates the eight materials listed in Table 2.4, excluding PTFE, are included. "Organics" refers to those materials containing significant carbon of organic origin: Lachine shale, Garfield shale, Waynesburg coal, and graphite. "Minerals" refers to the crystalline solids: talc, calcite, dolomite, and quartz silica. The contact angle was analyzed in these groupings because the types of surfaces, and thus the surface forces likely to be present, are different for the organic and mineral groups. Thus, in some cases, the data subsets show a stronger correlation between composition and contact angle than the entire group of eight materials.

Table 4.3 and Figure 4.2 summarize the results of linear regressions between contact angle and carbon mass percentage. As described previously, the first fluid describing each system in Table 4.3 is the immersion phase while the second fluid listed is the droplet phase. The specific contact angle values and 95% confidence limits for air-water-solid systems, PCE-water-solid systems, and CTET-water-solid systems are given in Tables 3.2, 3.4, and 3.5 respectively. As Table 4.3 shows, when the dataset is limited to the organic materials, there is significant correlation (both ρ and ρ_s are high) between the contact angle and carbon mass percent for all cases except the case of air bubbles resting on the solids immersed in water. However, a linear correlation is not effective at predicting the contact angle except for the case of PCE-water-organic systems which has an R^2 of 0.85, as shown along with the form of the linear regression on Figure 4.3.

Figures 4.2 and 4.3 show the linear fits to the contact angle and carbon mass percent data sets across the set of eight natural materials and the organic carbon-containing soil materials only. Two of the four materials in the mineral data set, talc and quartz, have no carbon but very different contact angles, making a linear correlation to carbon content impossible. Also, the other two minerals, calcite and dolomite, contain carbon in ionically-bonded mineralized carbonate groups rather than covalently-bonded organic groups. The PCE-water-solid systems and CTET-water-solid systems are similar to one another but the PCE systems show more linearity. This is possibly due to the fact that there is generally less error in the PCE measurements because more drop images were collected.

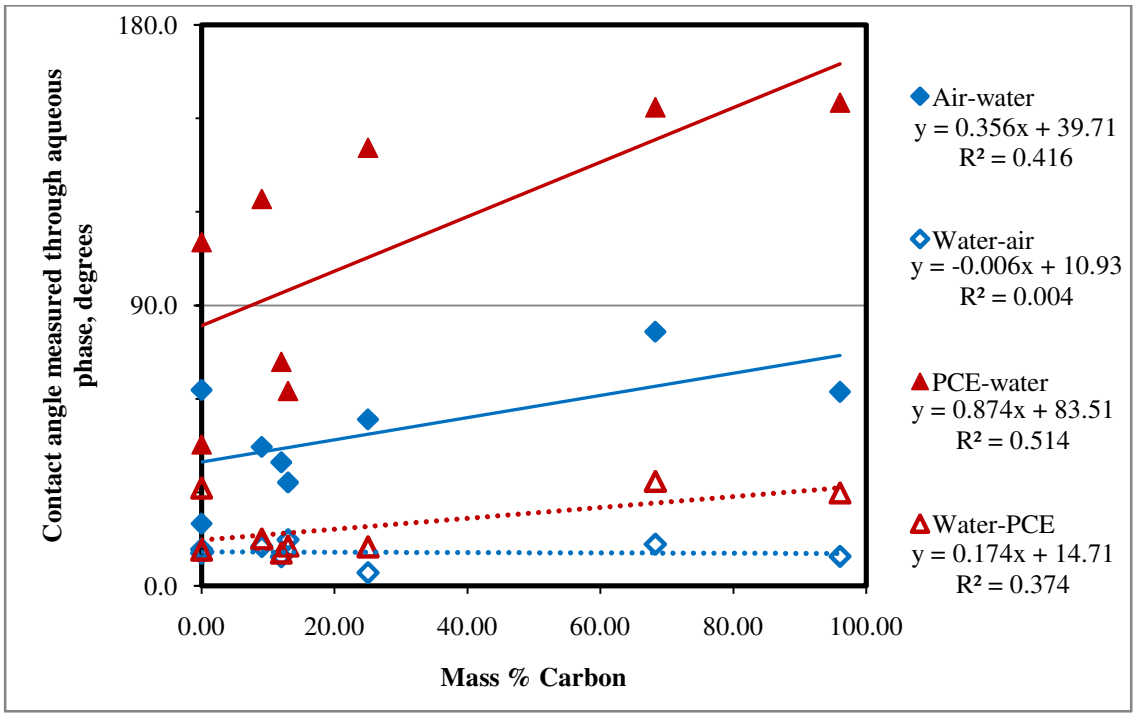

Figure 4.2, Linear correlations between carbon mass % and contact angle considering all eight natural soil materials.

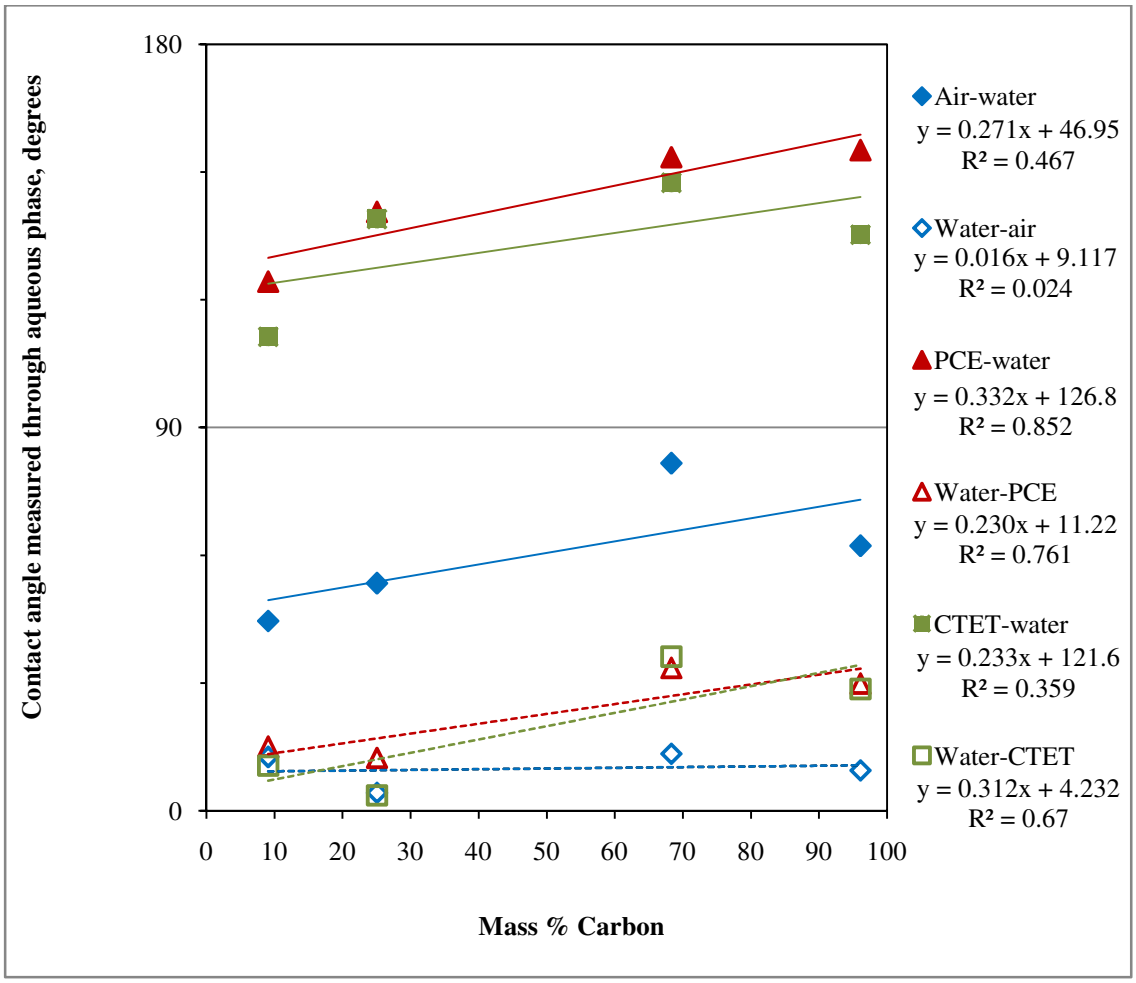

Figure 4.3, Linear correlations between carbon mass % and contact angle considering only organic carbon-containing soil materials.

Table 4.4, and Figures 4.4 and 4.5 describe the correlation between contact angle and carbon content on a percent molar scale considering all the materials and considering only the organic carbon-containing materials. In this case, there is a weak linear correlation for the complete data set and the organic subset in the NAPL-water-solid systems. The presence of carbon does not strongly indicate an increase in non-polar forces because carbon can occur in many types of functional groups, both polar and non-polar. Even though the mineral data set is small, it appears that the carbon indices are not good predictors of the contact angle for mineral soil materials. This is due to the fact that carbon is always associated with oxygen in the mineral soil materials so the amount of carbon does not indicate the amount of non-polar material. Also, the molar carbon content of calcite and dolomite is identical but those minerals have slightly different

contact angles, resulting in a less linear relationship between carbon content and contact angle.

All materials, N=8			Organics, N=4			Minerals, N=4		
System	**ρ**	**ρ_s**	**System**	**ρ**	**ρ_s**	**System**	**ρ**	**ρ_s**
Air-water	0.42	0.45	Air-water	0.46	0.80	Air-water	-0.16	0
Water-air	-0.12	-0.16	Water-air	0.02	0.00	Water-air	0.25	0
PCE-water	0.65	0.77	PCE-water	0.83	1.00	PCE-water	-0.22	0
Water-PCE	0.49	0.27	Water-PCE	0.72	0.60	Water-PCE	-0.57	-0.45
			CTET-water	0.44	0.40			
			Water-CTET	0.66	0.60			

Table 4.4, Statistics describing the relationship between carbon mol % and contact angle. ρ is the Pearson (linear) correlation coefficient. ρ_s is the Spearman (rank) correlation coefficient.

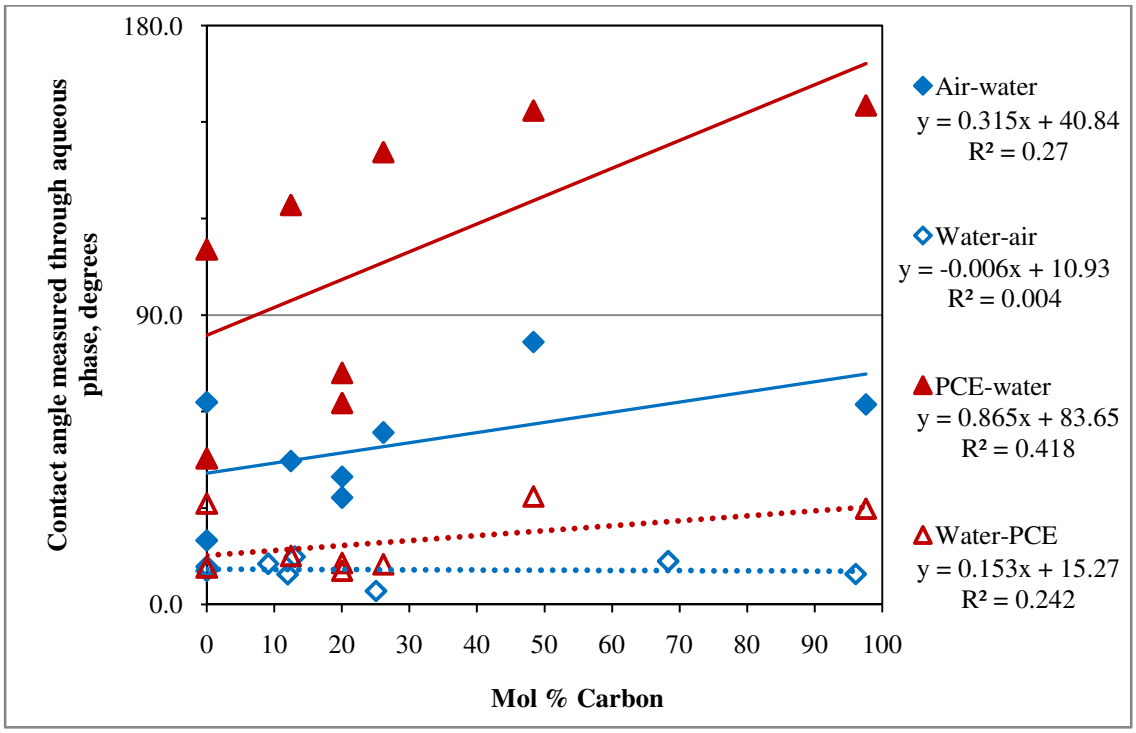

Figure 4.4, Linear correlations between carbon mol % and contact angle considering all eight natural soil materials.

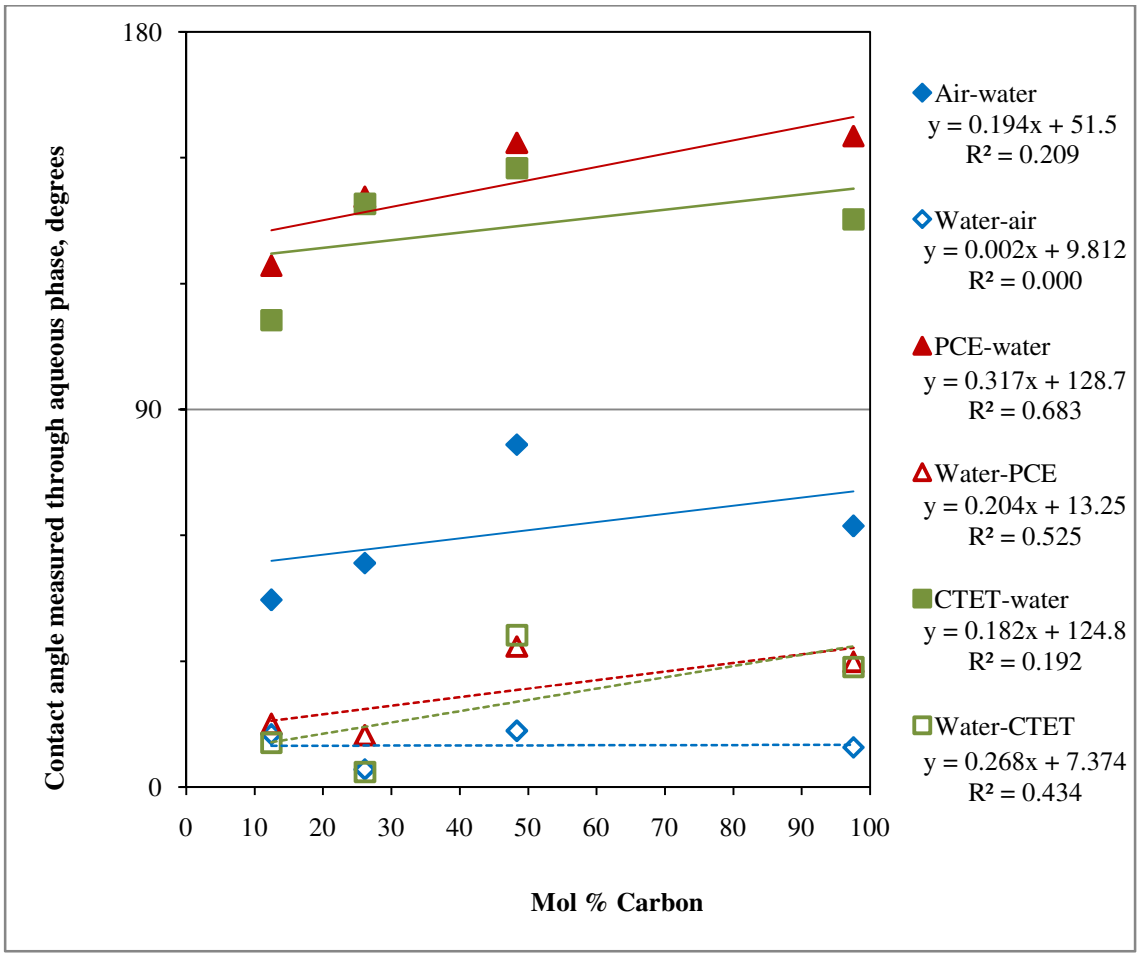

Figure 4.5, Linear correlations between carbon mol % considering only organic carbon-containing soil materials.

As shown in the Van Krevelen diagram (Figure 4.1), the hydrogen to carbon ratio (H/C) is used as a measure of soil maturity. Table 4.5 and Figure 4.6 show the correlation between H/C ratio and contact angle for the set of soil materials that contain both hydrogen and carbon, the organic carbon-containing materials. There is a weak negative linear correlation in the case of NAPL-water systems but the linear fit is not a good predictive model of contact angle. This may be partly the result of having only a very small change in H/C ratio over the range of materials studied.

Organics, N=4		
System	**ρ**	**ρ_s**
Air-water	-0.31	-0.80
Water-air	-0.06	0.00
PCE-water	-0.70	-1.00
Water-PCE	-0.65	-0.60
CTET-water	-0.26	-0.40
Water-CTET	-0.59	-0.60

Table 4.5, Statistics describing the relationship between H/C molar ratio and contact angle. ρ is the Pearson (linear) correlation coefficient. ρ_s is the Spearman (rank) correlation coefficient.

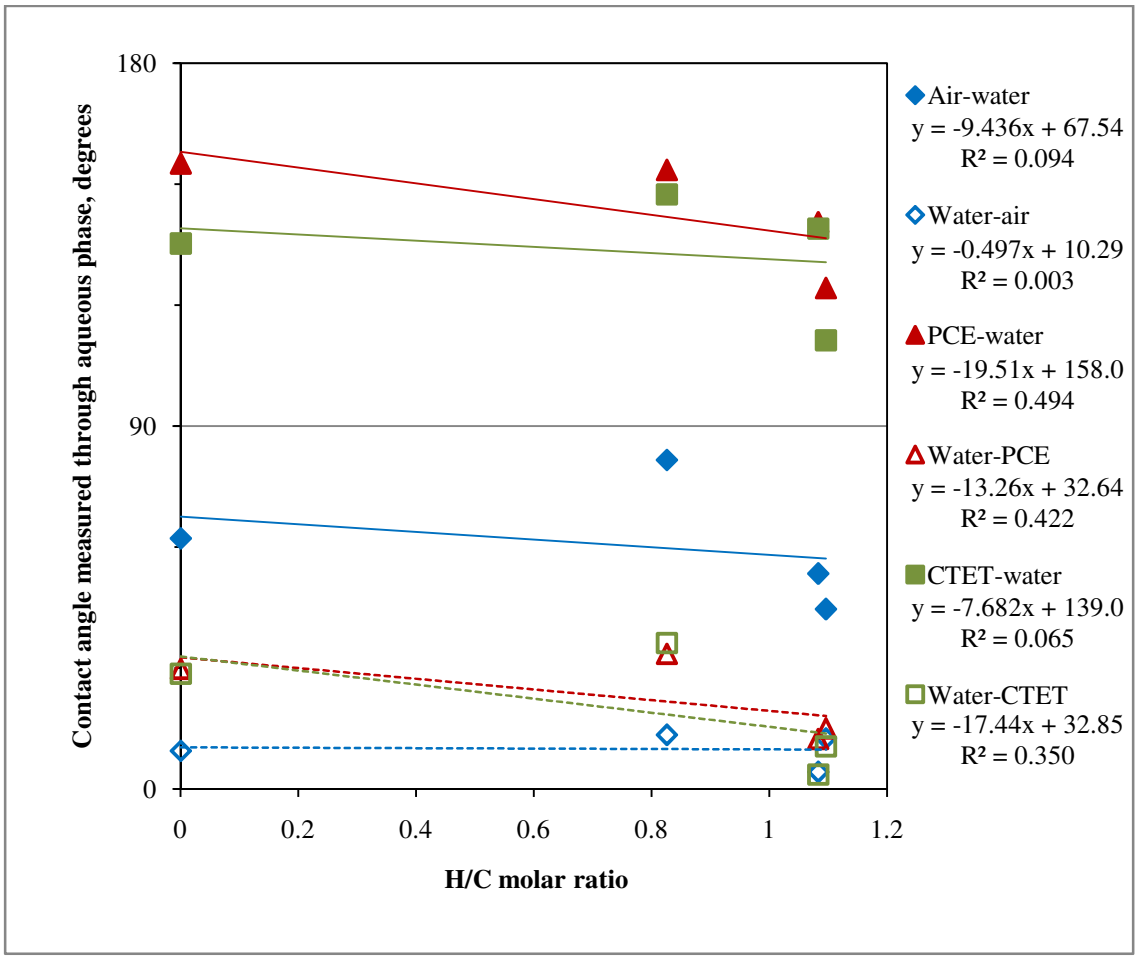

Figure 4.6, Linear correlations between H/C molar ratio and contact angle considering only organic carbon-containing soil materials.

4.3 Relationship between contact angle and oxygen content

Figures 4.7, 4.8, and 4.9 show the relationship between molar oxygen percentage and contact angles for the three data sets. Table 4.6 summarizes the statistics. In each case, the NAPL-water or air-water system contact angles show a stronger linear correlation with oxygen content than those for the water-NAPL and water-air systems. Particularly in the case of PCE-water-organic carbon-containing solid system, the linear fit is reasonable with an R^2 of 0.98, as shown on Figure 4.8. The linear fit for the air-water-mineral system is also adequate with an R^2 of 0.81 (Figure 4.9). For water-PCE-mineral systems, the regression is good with an R^2 of 0.88. The mineral only data sets (Table 4.6) generally show higher R^2 values for the correlation between oxygen content and contact angle, probably due to the fact that the percentage of oxygen is higher in the mineral materials and there is not a mix of polar and non-polar carbon containing groups in these materials. The mineral materials are grouped close to 60% oxygen. The slope of the water-PCE-mineral data set is positive because one sample, quartz, has a higher contact angle than the other materials, once again placing quartz at one end of the spectrum of aquifer materials. Lachine shale, near 10% oxygen content, is almost always slightly above the linear prediction line. This may be due to the fact that Lachine shale contains other mineral groups, such as pyrite, whose effect on wettability is unknown. Overall, oxygen content is a better predictor of contact angle than carbon content.

All materials, N=8			**Organics, N=4**			**Minerals, N=4**		
System	**ρ**	**ρ_s**	**System**	**ρ**	**ρ_s**	**System**	**ρ**	**ρ_s**
Air-water	-0.78	-0.80	Air-water	-0.80	-0.80	Air-water	-0.90	-0.95
Water-air	0.19	0.10	Water-air	-0.06	0.00	Water-air	-0.27	-0.32
PCE-water	-0.88	-0.99	PCE-water	-0.99	-1.00	PCE-water	-0.87	-0.95
Water-PCE	-0.54	-0.30	Water-PCE	-0.86	-0.60	Water-PCE	0.94	0.63
			CTET-water	-0.79	-0.40			
			Water-CTET	-0.59	-0.60			

Table 4.6, Statistics describing the relationship between oxygen mol % and contact angle. ρ is the Pearson (linear) correlation coefficient. ρ_s is the Spearman (rank) correlation coefficient.

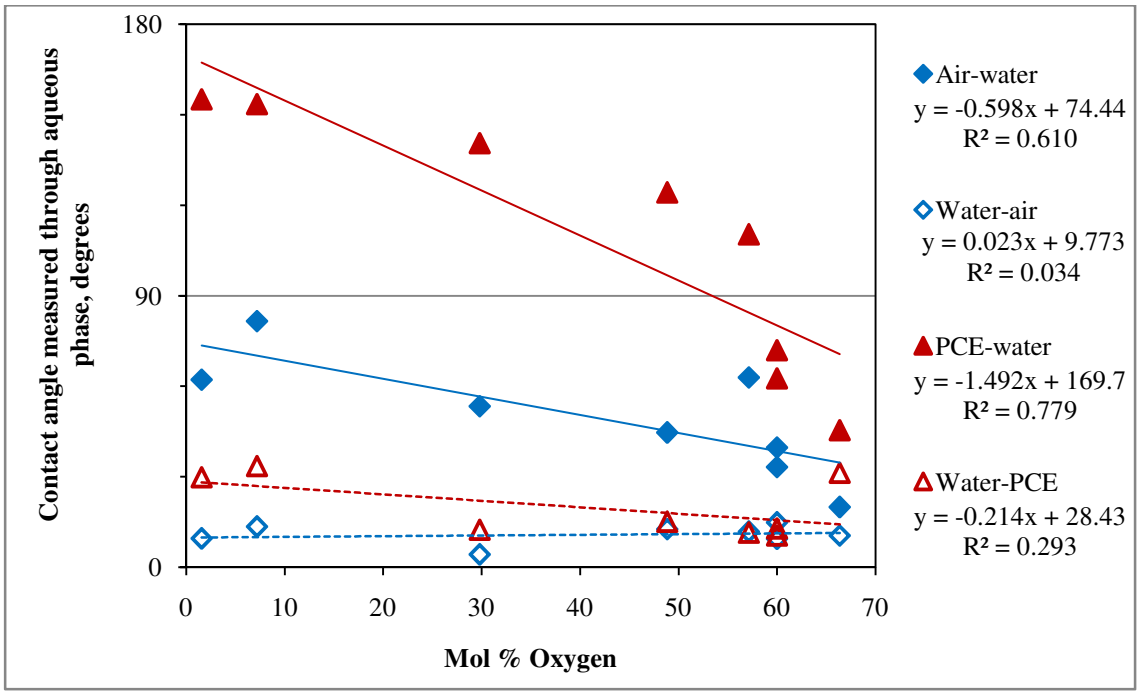

Figure 4.7, Linear correlations between oxygen mol % and contact angle considering all eight natural soil materials.

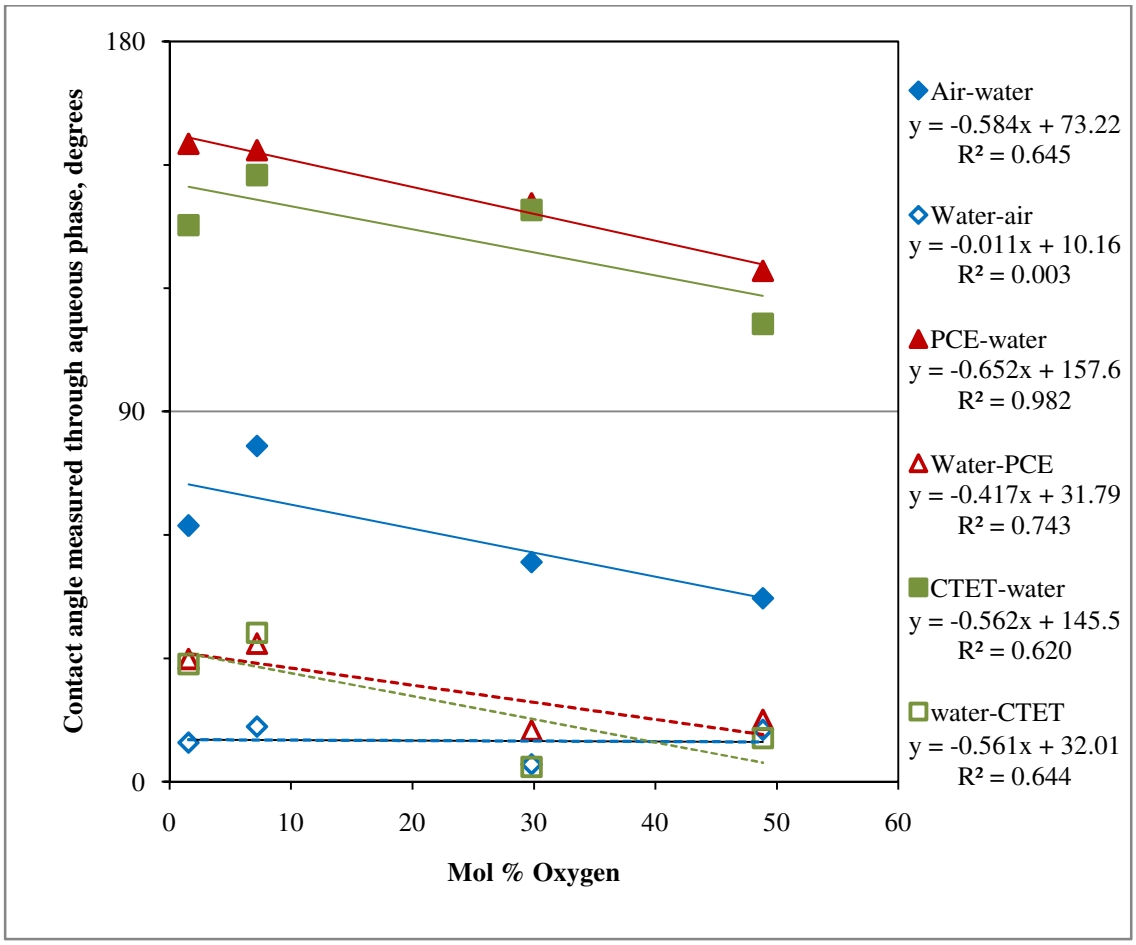

Figure 4.8, Linear correlations between oxygen mol % and contact angle considering only organic carbon-containing soil materials.

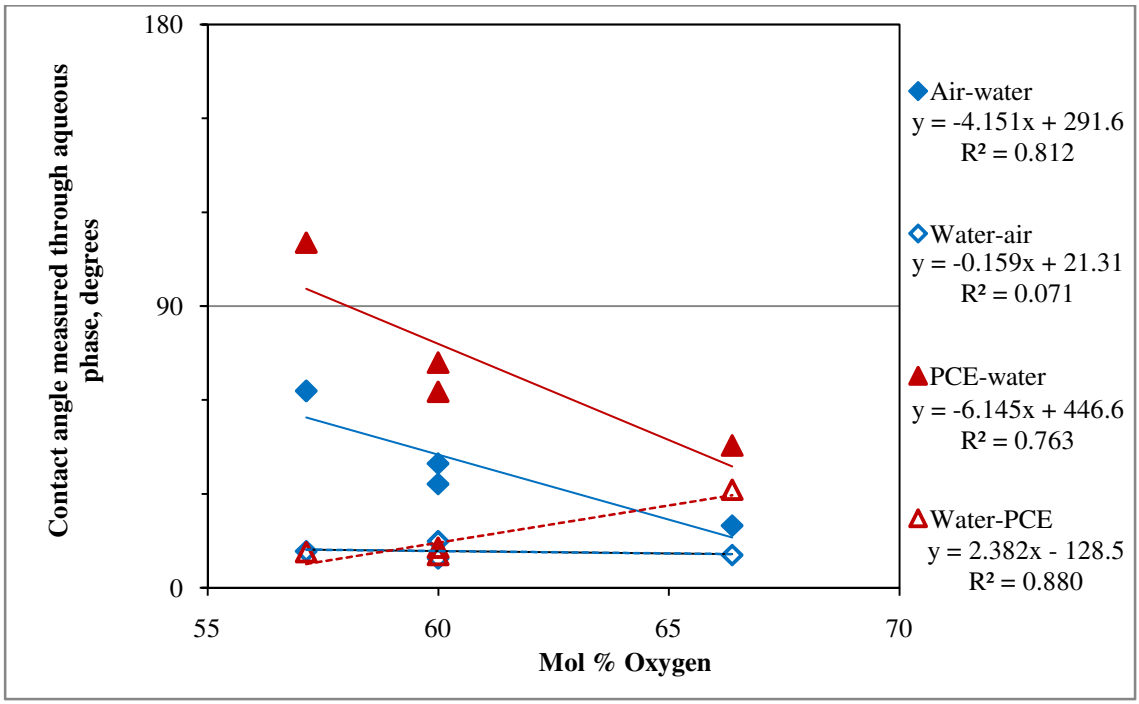

Figure 4.9, Linear correlations between contact angle and oxygen mol % considering only mineral soil materials.

Table 4.7 and Figures 4.10 and 4.11 describe the relationship between the oxygen to carbon ratio and contact angle. This table and these figures indicate that the oxygen to carbon ratio is the most consistently reliable metric of those studied for predicting the contact angle. With the exception of water-air systems where all the contact angles are strongly water-wet without enough variation to form the basis for any correlation, all the systems show a significant negative correlation between the oxygen to carbon molar ratio and the contact angle. Because only calcite and dolomite have both oxygen and carbon, a correlation was not attempted for mineral systems alone. The predictive relationship for PCE-water-organic system contact angle based on the O/C molar ratio (Figure 4.11) is quite strong, with an R^2 value of 0.96. The linear correlation for the CTET-water-organic systems also has a high R^2 value of 0.84. The slopes of these two regressions are very similar; thus, a reasonable estimate of the contact angle made by a water droplet against other organic carbon-containing aquifer materials immersed in the same non-polar chlorinated NAPL can be obtained by applying a factor of 7.77* O/C ratio plus approximatly 150.

Oxygen and carbon-containing materials, N=6			Organics, N=4		
System	**ρ**	**ρ_s**	**System**	**ρ**	**ρ_s**
Air-water	-0.83	-0.75	Air-water	-0.78	-0.80
Water-air	0.30	0.14	Water-air	0.20	0.00
PCE-water	-0.73	-0.81	PCE-water	-0.98	-1.00
Water-PCE	-0.79	-0.49	Water-PCE	-0.70	-0.60
			CTET-water	-0.92	-0.40
			Water-CTET	-0.62	-0.60

Table 4.7, Statistics describing the relationship between O/C molar ratio and contact angle. ρ is the Pearson (linear) correlation coefficient. ρ_s is the Spearman (rank) correlation coefficient.

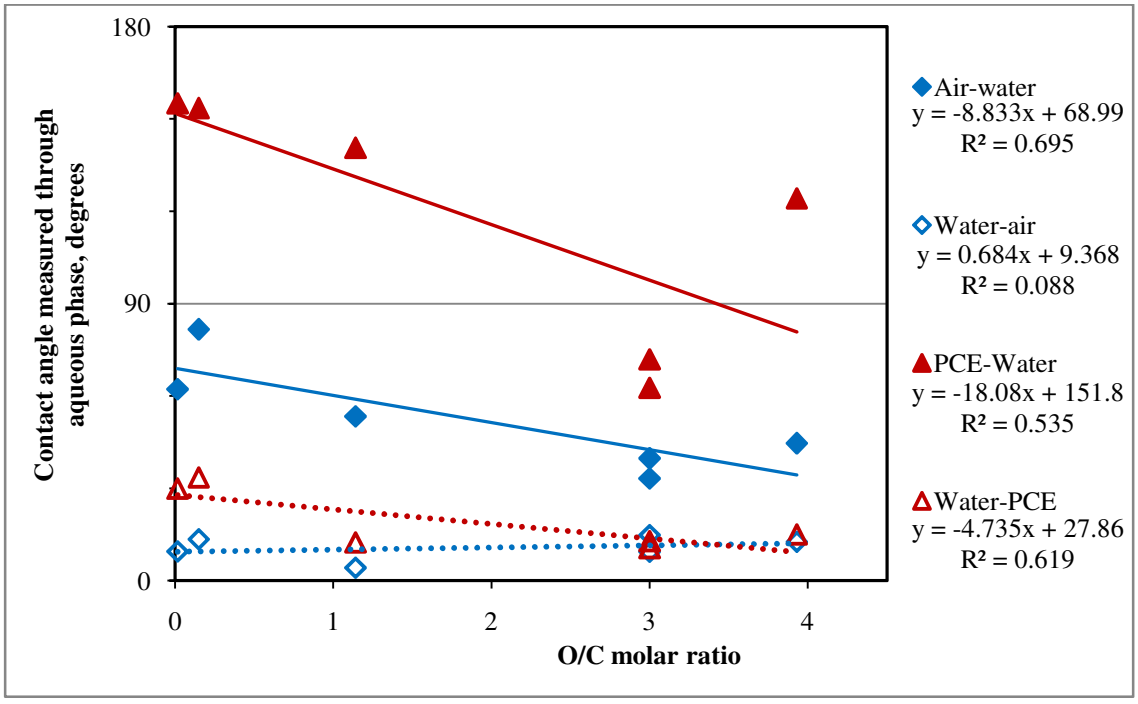

Figure 4.10, Linear correlations between O/C molar ratio and contact angle considering the six natural soil materials that contain both oxygen and carbon: Lachine shale, Garfield shale, Waynesburg coal, graphite, calcite, and dolomite.

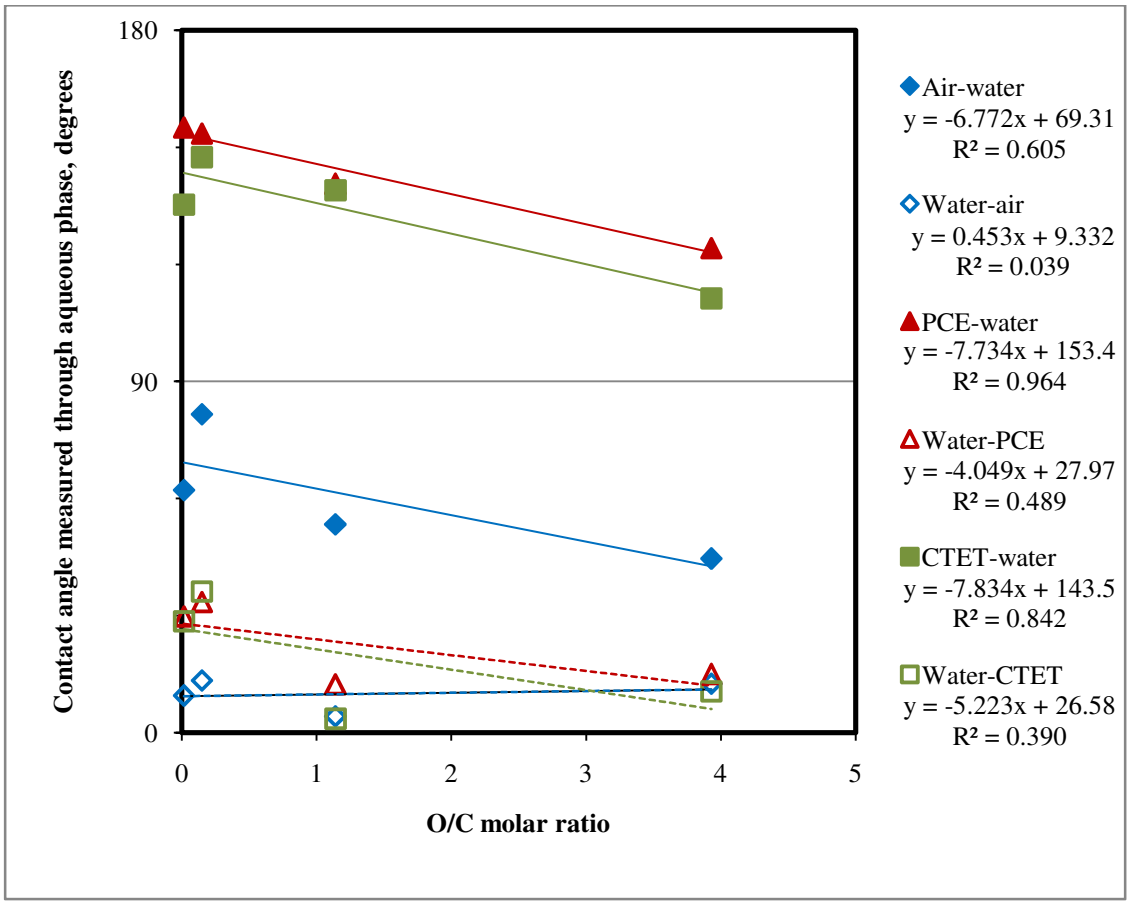

Figure 4.11, Linear correlations between O/C molar ratio and contact angle considering only organic carbon-containing soil materials.

It should be noted that linear predictions of contact angle based on composition should be limited to materials with compositions similar to the materials studied. It would be inadvisable to extrapolate beyond the range of compositions studied because the relationship between composition parameters and contact angle may not be linear at the extremes. Even with this limited data set, it is apparent that two materials with no carbon, quartz and talc, have very different contact angles. Also, because there are two known contact angles for each fluid system, one with water as the immersion phase and one with water as the droplet phase, the wetting history of the system must be known to determine which correlation is more appropriate. In other words, it must be known a priori which fluid is originally contacting the solid surface. Predictive relationships for wettability based on bulk composition are not available in the literature. Related work with self assembled monolayers (SAM's) has shown a strong correlation between surface composition and wettability whereby the chain length of the SAM directly influenced the

contact angle (Atre et al., 1995). The density of SAM chains on surfaces has been shown to affect wettability as well (Miranda et al., 1998). The location of oxygen groups within the alkyl tails of SAMs caused variability in contact angle (Laibinis et al. 1995), further evidence that it is not just the bulk elemental composition but also the organization of the surface atoms into functional groups that influences wettability.

4.4 Correlation of carbon content to wettability hysteresis

Wettability hysteresis, $\Delta\Theta$, can also be correlated to bulk composition parameters. In other words, the difference between the aqueous phase contact angle in non-water and water immersion cases changes with composition. This is analogous to the findings of Crawford et al. (1994) who showed that contact angle hysteresis, the difference between advancing and receding contact angles, in water-oil systems decreased as the rank of the coal increased. Tables 4.8, 4.9, and 4.10 show the linear (Pearson) and rank (Spearman) correlation coefficients between various carbon indices and $\Delta\Theta$. None of the carbon indices, molar percentage, mass percentage, or hydrogen to carbon molar ratio, are reliable indicators of wettability hysteresis. As discussed above, the carbon indices do not appear to be reliable indicators of the type of interactions possible at the surface of the solid material.

All materials, N=8			**Organics, N=4**			**Minerals, N=4**		
System	**ρ**	**ρ_s**	**System**	**ρ**	**ρ_s**	**System**	**ρ**	**ρ_s**
Air-water	0.53	0.60	Air-water	0.48	0.80	Air-water	-0.19	0.00
PCE-water	0.55	0.70	PCE-water	0.50	0.00	PCE-water	-0.01	0.00
			CTET-water	-0.21	1.00			

Table 4.8, Statistics describing the relationship between carbon mol % and wettability hysteresis. ρ is the Pearson (linear) correlation coefficient. ρ_s is the Spearman (rank) correlation coefficient.

All materials, N=8			Organics, N=4			Minerals, N=4		
System	ρ	ρ_s	System	ρ	ρ_s	System	ρ	ρ_s
Air-water	0.65	0.59	Air-water	0.68	0.80	Air-water	-0.21	-0.11
PCE-water	0.59	0.68	PCE-water	0.48	0.00	PCE-water	-0.02	-0.11
			CTET-water	-0.21	1.00			

Table 4.9, Statistics describing the relationship between carbon mass % and wettability hysteresis. ρ is the Pearson (linear) correlation coefficient. ρ_s is the Spearman (rank) correlation coefficient.

Organics, N=4		
System	ρ	ρ_s
Air-water	-0.31	-0.80
PCE-water	-0.38	0.00
CTET-water	0.33	-1.00

Table 4.10, Statistics describing the relationship between H/C molar ratio and wettability hysteresis. ρ is the Pearson (linear) correlation coefficient. ρ_s is the Spearman (rank) correlation coefficient.

4.5 Correlation of oxygen content to wettability hysteresis

Oxygen indices have a greater correlation with wettability hysteresis than carbon indices. Table 4.11 shows that the correlations between wettability hysteresis and molar oxygen percentage are negative, suggesting that increased oxygen content increases the water drop-solid interaction in NAPL-water cases, causing less difference between NAPL-water and water-NAPL cases when the oxygen content is high. Thus, the NAPL-water-solid contact angle decreases while the water-NAPL-solid contact angle changes only slightly, as shown in Figure 4.8. The linear correlations between oxygen content and contact angle for the four organic carbon-containing soil materials are not particularly strong. However, when placed in the context of all eight natural soil materials (Figure 4.12), it appears that there may be non-linear correlations between oxygen content and wettability hysteresis that could be applied to a large range of soil and liquid pairings. Table 4.11 also indicates high Spearman correlations for the set of all eight materials in both air-water and PCE-water systems.

The strong linear fits between oxygen molar content and wettability hysteresis in the case of mineral soil materials are shown in Figure 4.14. The correlation shows the

highest R^2 in the case of mineral soil materials. The trend of increasing wettability hysteresis with decreasing oxygen content is in agreement with the results reported by Crawford et al. (1994) that showed that contact angle hysteresis increased with increasing mineral content. The air-water systems are less responsive to changes in oxygen content. Due to the changes in surface charge and hydrogen bonding at the solid mineral-water interface, the contact angle may also be a function of aqueous solution pH. The contact angle measurements for these correlations were made at near neutral pH (7 ± 0.2). Appendix A presents some additional contact angle measurements which suggest that pH may have a minor influence mineral wettability.

All materials, N=8			**Organics, N=4**			**Minerals, N=4**		
System	**ρ**	**ρ_s**	**System**	**ρ**	**ρ_s**	**System**	**ρ**	**ρ_s**
Air-water	-0.80	-0.90	Air-water	-0.84	-0.80	Air-water	-0.86	-0.95
PCE-water	-0.78	-0.92	PCE-water	-0.61	0.00	PCE-water	-0.95	-0.95
			CTET-water	0.00	-1.00			

Table 4.11, Statistics describing the relationship between oxygen mol % and wettability hysteresis. ρ is the Pearson (linear) correlation coefficient. ρ_s is the Spearman (rank) correlation coefficient.

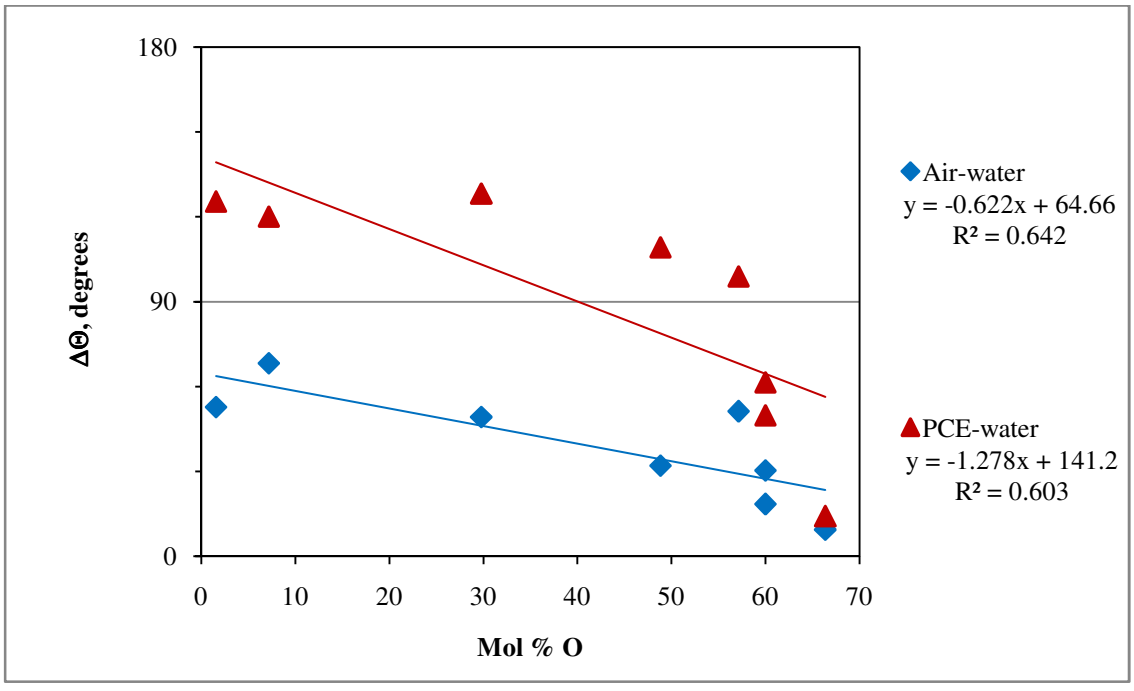

Figure 4.12, Linear correlations between oxygen mol % and wettability hysteresis considering all eight natural soil materials.

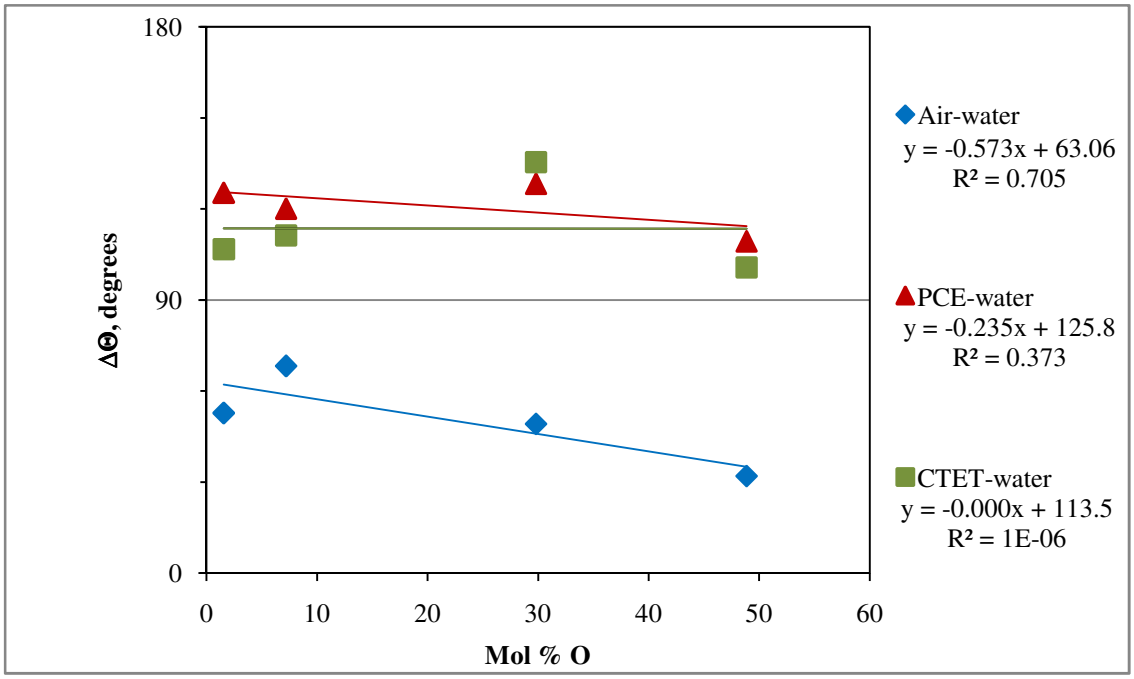

Figure 4.13, Linear correlations between oxygen mol % and wettability hysteresis considering only organic carbon-containing soil materials.

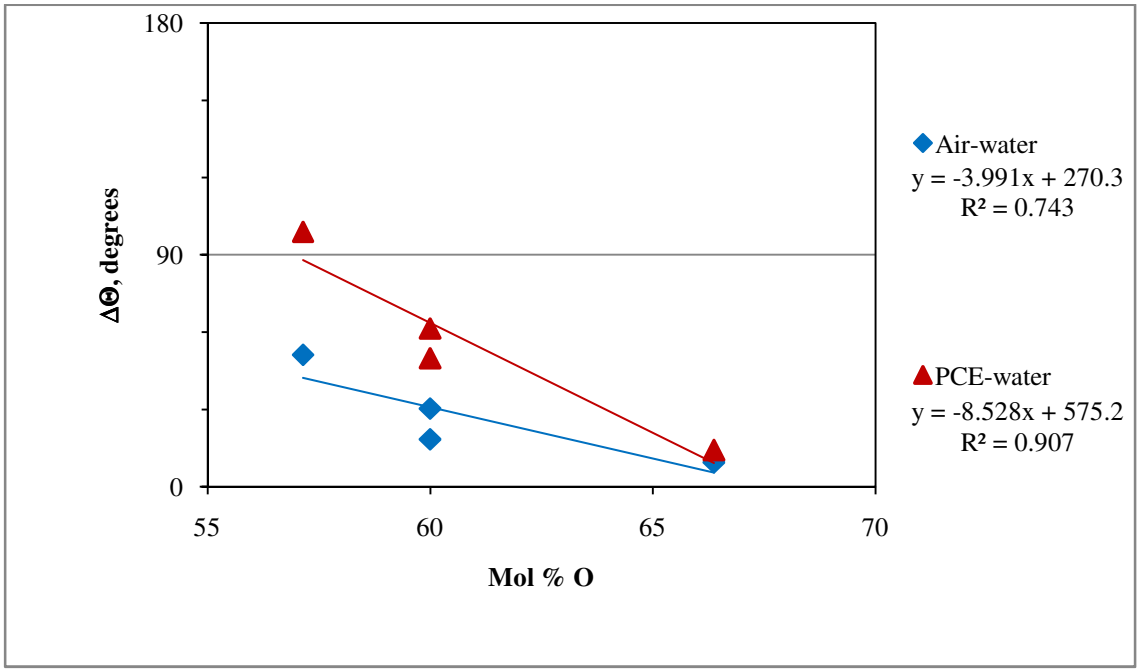

Figure 4.14, Linear correlations between oxygen mol % and wettability hysteresis considering only mineral soil materials.

Calcite and dolomite have the same percent oxygen, but in both PCE-water and air-water cases, there is greater wettability hysteresis in the calcite contact angles. This is likely because the substitution of magnesium into the crystal lattice of dolomite causes dolomite to be more electronegative than calcite (1.31 Pauling units for Mg versus 1.00 Pauling units for Ca) so dolomite has a greater tendency toward polar bonding and has smaller non-water immersion contact angles even though the water immersion contact angles are similar. This effect was predicted by Wright et al. (2001) who simulated the calcite and dolomite surfaces and predicted that dolomite would have a greater tendency to form hydrogen bonds with water than calcite. The wettability hysteresis of PCE-water-mineral systems can be estimated by the equation given on Figure 4.14 showing an R^2 of 0.91. In any of the correlations based on oxygen percent, calcite and dolomite plot very close to one another at 60% oxygen.

Wettability hysteresis is also negatively correlated with O/C molar ratio. As with the contact angle, the degree of correlation with wettability hysteresis for the oxygen molar content and the O/C molar ratio is about equal. Table 4.12 lists the correlation parameters for the correlations between $\Delta\Theta$ and the O/C ratio. All materials refers to only those that have both oxygen and carbon (i.e., it excludes talc and quartz). For both sets, the air-water systems are slightly more responsive to changes in the O/C molar ratio than the NAPL-water systems because of hydrogen bonding and surface charge. Crawford et al. (1994) reported the same effect with contact angle hysteresis. In the case of contact angle hysteresis, it was proposed that the higher the coal rank, and hence the lower the O/C molar ratio, the greater the chemical heterogeneity of the surface which promotes a difference in the advancing and receding contact angle because the advancing contact angle is believed to reflect the low energy sites (higher contact angle) and the receding contact angle is believed to represent the high energy sites, such as the more water wetting mineral sites.

All materials, N=6			Organics, N=4		
System	**ρ**	**ρ_s**	**System**	**ρ**	**ρ_s**
Air-water	-0.87	-0.64	Air-water	-0.88	-0.80
PCE-water	-0.75	-0.64	PCE-water	-0.80	0.00
			CTET-water	-0.31	-1.00

Table 4.12, Statistics describing the relationship between O/C molar ratio and wettability hysteresis. ρ is the Pearson (linear) correlation coefficient. ρ_s is the Spearman (rank) correlation coefficient. Here, all materials excludes talc and quartz.

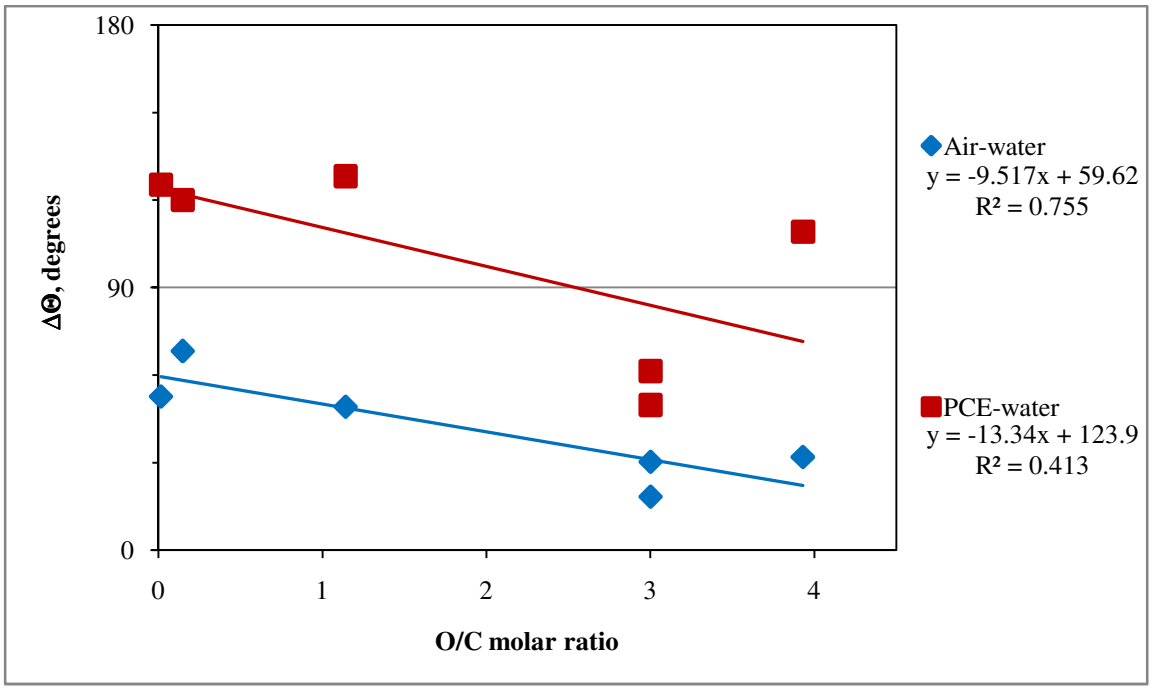

Figure 4.15, Linear correlations between O/C molar ratio and wettability hysteresis considering six natural soil materials.

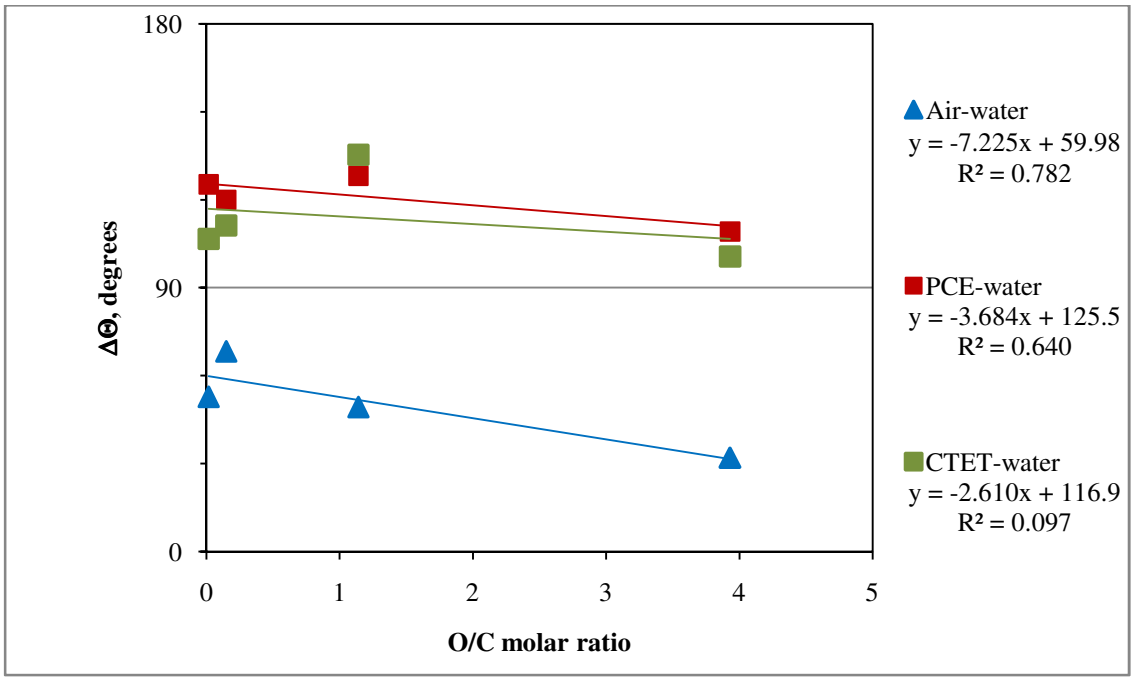

Figure 4.16, Linear correlations between O/C molar ratio and wettability hysteresis considering only organic carbon-containing soil materials.

The correlations discussed thus far are based on bulk composition measurements. One limitation of relating bulk elemental composition to contact angle behavior is that the interfacial forces between the solid and liquid phases at the surface (γ_{SL1} and γ_{SL2} in Equation 1.1) result from interactions between the liquid molecules and the surface functional groups, not the individual elemental species at the surface. So, an oxygen or carbon atom at the surface will have greater or lesser influence on wettability based on the atoms to which it is bonded. Thus, the remainder of Chapter 4 focuses on the composition of the eight natural soil materials from the perspective of surface functional groups rather than bulk individual elements.

4.6 Functional groups by FT-IR measurement

To characterize the solid surface composition, Fourier Transform Infrared Spectroscopy analysis was performed using a Thermo-Nicolet 980 FT-IR system (Nicolet Instrument, Madison, WI) in the diffuse reflectance (DRIFT) mode. Quantitative determination of the amount of each functional group present on the soil surfaces was not possible because each material differs in reflectivity, due to the fact that each contains a

different amount and type of organic matter. Details of the FT-IR method are presented in Section 2.11.

4.7 FT-IR spectra of organic carbon-containing soil materials

Figure 4.17 shows the spectra collected for the organic carbon-containing soil materials. Lachine shale contains potassium bromide, silicate, and hydrogen peaks at 1000, 1100 and 3600 cm^{-1} as expected. The potassium bromide peak is present in all the samples due to the mulling agent used to pack the sample in the DRIFT method. The 1100 cm^{-1} peak is also present in most of the materials due to the presence of silicates. The 3600 cm^{-1} peak is due to the hydrogen bonds between the surface and absorbed water. Prominent are branched alkane groups appearing at about 1450 cm^{-1}. This location indicates two to three methyl groups surrounding one carbon. Also prominent in the Lachine shale spectrum is the peak at 800 cm^{-1} which is indicative of long chains of four or more carbons. Like the other organic carbon-containing materials, there are several small peaks in the 1600-2000 cm^{-1} region. The one at 1600 cm^{-1} indicates ether, aldehyde, and ketone groups (R_2CO). These groups contribute to the polar forces at the surface. The peak at 1700 cm^{-1} is likely from substituted aromatic groups. In the Lachine shale, these two peaks appear about equal in intensity. Also present are two small peaks in the 2800-3000 cm^{-1} region indicating stretching vibrations from symmetric and asymmetric aliphatic and methyl carbon groups respectively (CH_2 and CH_3).

The Garfield shale spectrum is similar to that for the Lachine shale. The CH_2 and CH_3 deformations due to the presence of methyl groups at about 1450 cm^{-1} are stronger and more defined for the Garfield shale than for the Lachine shale. The peak near 1600 cm^{-1} is also larger than at 1700 cm^{-1}, indicating more aliphatics than substituted aromatics. The peaks at 2800 and 2900 cm^{-1} are also large, indicating that long chain hydrocarbon groups are an important feature of the Garfield shale surface, suggesting a less polar surface than the Lachine shale. A small peak at 2500 cm^{-1} shows the presence of aliphatic or aromatic alcohol groups.

The spectrum of Waynesburg coal has a significantly larger organic signature than those of the Lachine and Garfield shales, consistent with the higher carbon content determined by bulk elemental analysis. The combination of peaks at 1050, 1200, and

3600 cm^{-1} indicates that there is carbon to oxygen single bond stretching and phenolic groups. The significant peak near 1700 cm^{-1} suggests that substituted aromatic groups are a major component of the Waynesburg carbon. The peak at 1600 cm^{-1} is due to the presence of ether groups. The wide peak at 1300-1500 cm^{-1} is due to various alkane groups, including the methyl groups present in Lachine and Garfield shales. There are three peaks in the 2800 to 3100 cm^{-1} region, indicating the presence of saturated alkane groups in Lachine and Garfield shale as well as of some unsaturated CH_2 groups. Despite being a highly processed material, Waynesburg coal contains several types of functional groups. This is probably because the source material for coal is generally organic detritus in anaerobic aquatic environments. Thus, the biological processing of the material may be more limited before geological aging begins.

The spectrum of graphite is almost flat because it is highly reflective. However, the surface is expected to be almost exclusively alkane groups with some small inclusions of ethers and acid groups due to exposure to the atmosphere.

In general, Figure 4.17 shows that as the soil carbon becomes more mature, the mineral signatures (the peaks in the FT-IR spectrum due to the mineral components of the solid surface) and the presence of oxygen-containing groups, such as aromatic ethers, decline and there is a corresponding increase in tetrahedral-bonded carbon. In oil reservoir studies, the sorption of nitrogenous compounds has been implicated in wettability alteration (Buckley, 1998; Mercier, 1999; Standal 1999). However, none of the materials examined here show a significant presence of nitrogen-containing functional groups. This finding is consistent with the low nitrogen percentages observed in the elemental analysis given in Table 4.1 All the materials examined contain oxygen in the form of aliphatic alcohol groups in addition to the mineral signature. These groups may provide the polar forces that cause the surfaces to be water wet when initially contacted with a polar liquid like water.

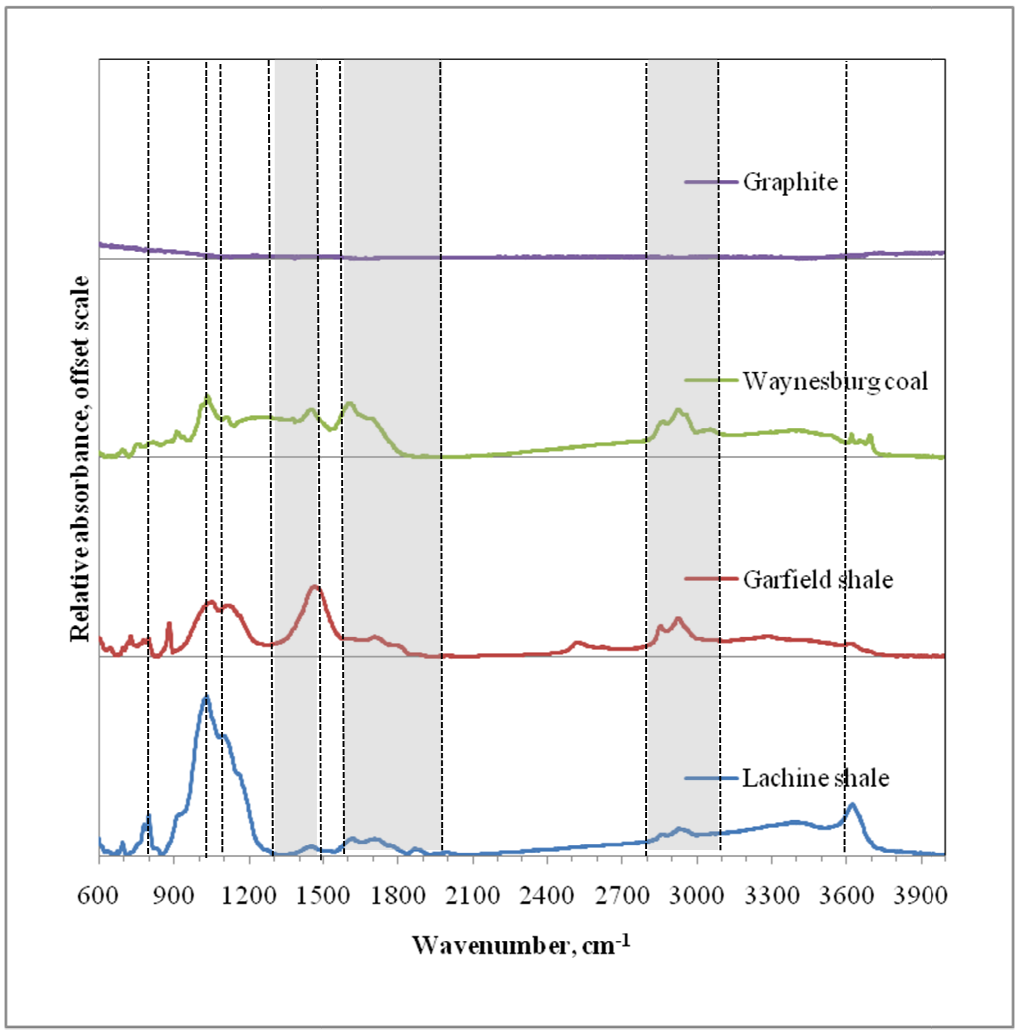

Figure 4.17, FT-IR spectra of organic carbon-containing soil materials. Dashed lines indicate peaks of interest. Shaded bars indicate regions where several peaks are grouped.

It has been proposed that for an air-dry surface to be water repellent, perhaps the surface functional groups must be dominated by straight-chain alkane (Ma'Shum et al., 1988), terminal methyl (Capriel et al., 1995), or unsubstituted aromatic groups. The data presented here (Table 3.2, Figures 3.4 and 4.17) suggest that, for air-water or NAPL-water cases, the surfaces containing these types of non-oxygenated carbon groups are not as strongly water-wet as the mineral surfaces, with the exception of talc which is also less water-wet but is a mineral. Quartz, with an abundance of hydroxyl groups, is strongly water-wet. For the water-air and water-NAPL cases, where the surface has been contacted by water prior to the non-aqueous phase, the surfaces are all water-wet, despite

the differences in composition. It appears that, in these cases, the mineral matter and the aliphatic alcohols, phenols, and ethers present cause a water film to be retained once a surface has contacted water, despite the presence of some non-oxygenated groups. Some aromatic groups containing oxygen are present in the highly processed shale and coal materials. However, the aromatic groups have low dipole moments. In addition, both unsaturated and saturated alkane groups (CH_2 and CH_3) are considered non-polar and are associated with the soil materials that can be organic wetting.

The spectrum for Ann Arbor II sand (Figure 4.18) shows numerous functional groups. Humic acids are characterized as amorphous molecules containing resistant components of plant materials such as lignin and aromatic complexes. There are peaks near 1700 and 3600 cm^{-1}, indicating the presence of substituted aromatics. The peak near 1600 cm^{-1} is one of the largest indicating that carbon to oxygen bonds, such as ethers, aldehydes, and ketones, are important in the humic acid. Also important to the humic acid are the alkane groups at 2800 and 2900 cm^{-1} and the alkane peak near 1400 cm^{-1}. The peak at 1100 cm^{-1} for silicates is high in Ann Arbor II sand because the sample was produced by crushing the soil grains which created many mineral surfaces that were previously in the interior of the grains. Because the fraction of organic material is so low in the Ann Arbor II sample, the potassium bromide peak at 1050 cm^{-1} is large. There is also hydrogen bonding indicted from sorbed water by a broad peak between 3000 and 3600 cm^{-1}. Figure 4.18 shows the spectra of several other humic acid sands for comparison. They all share the high silicate and potassium bromide peaks at 1100 and 1050 cm^{-1} respectively. Ann Arbor II sand appears to be higher in aromatics (1700 and 3600 cm^{-1}) and alkanes (2800 to 3100 cm^{-1}).

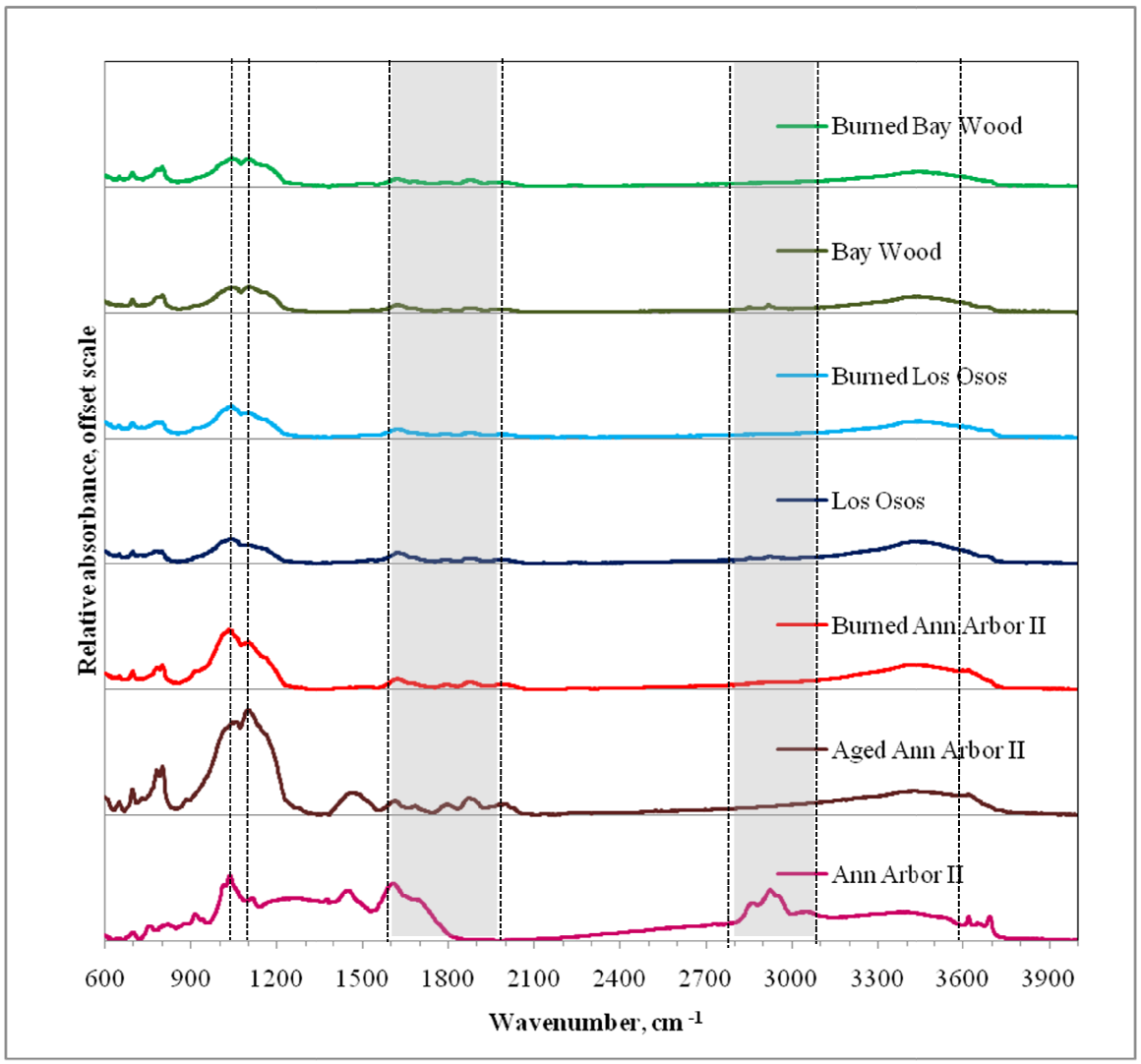

Figure 4.18, Comparison of Ann Arbor II sand FT-IR spectrum to several other humic sands. Dashed lines indicate peaks of interest. Shaded bars indicate regions where several peaks are grouped.

Capriel (1995) estimated a hydrophobicity index (HI) based on the ratio of alkanous carbon peaks to total carbon in FT-IR spectra. McKissock (2003) used a single aliphatic carbon FT-IR peak to correlate MED tests of water repellency to the composition of humic sands. Both were successful within a narrow range of materials. While these approaches may have some merit, they could be improved by standardizing the surface area of the sample and using a contact angle as the measure of wettability. The specific surface area of each solid powdered for FT-IR analysis was not measured so this type of quantitative analysis was not performed.

4.8 FT-IR spectra of mineral soil materials

The mineral spectra are given in Figure 4.19. Silica's spectrum contains a very large dual peak near 1000 cm^{-1}. The two tops of this peak represent potassium bromide and silicate minerals at 1050 and 1100 cm^{-1} respectively. They are large in this material because the organic groups are proportionally very minor. Like the carbon containing groups, silica contains peaks at 1450, 1600, 1700, and 3600 cm^{-1} for branched alkane stretching, carbon to oxygen double-bonded groups, substituted aromatics, and sorbed water; however in silica, they are very small. The breadth of the peak from 3100 to 3600 cm^{-1} is typical for DRIFT analysis where the sample is exposed to the atmosphere and can have numerous hydrogen bonds with water vapor. The organic group peaks are all minor, probably due to small amounts of sorbed material. Noticeably absent are peaks at 2800 and 2900 cm^{-1}, indicating a lack of alkanous carbon groups.

The talc spectrum is relatively bare. The only major peaks are at 1020 cm^{-1} for potassium bromide and at 3676 cm^{-1} which is the MgO_3 signature. Small peaks between 1600 to 1900 cm^{-1} indicate that there is a very minor presence of ether groups at the surface. Thus, for this material, it is likely that the representation as pure talc that was assumed in the elemental analysis is accurate.

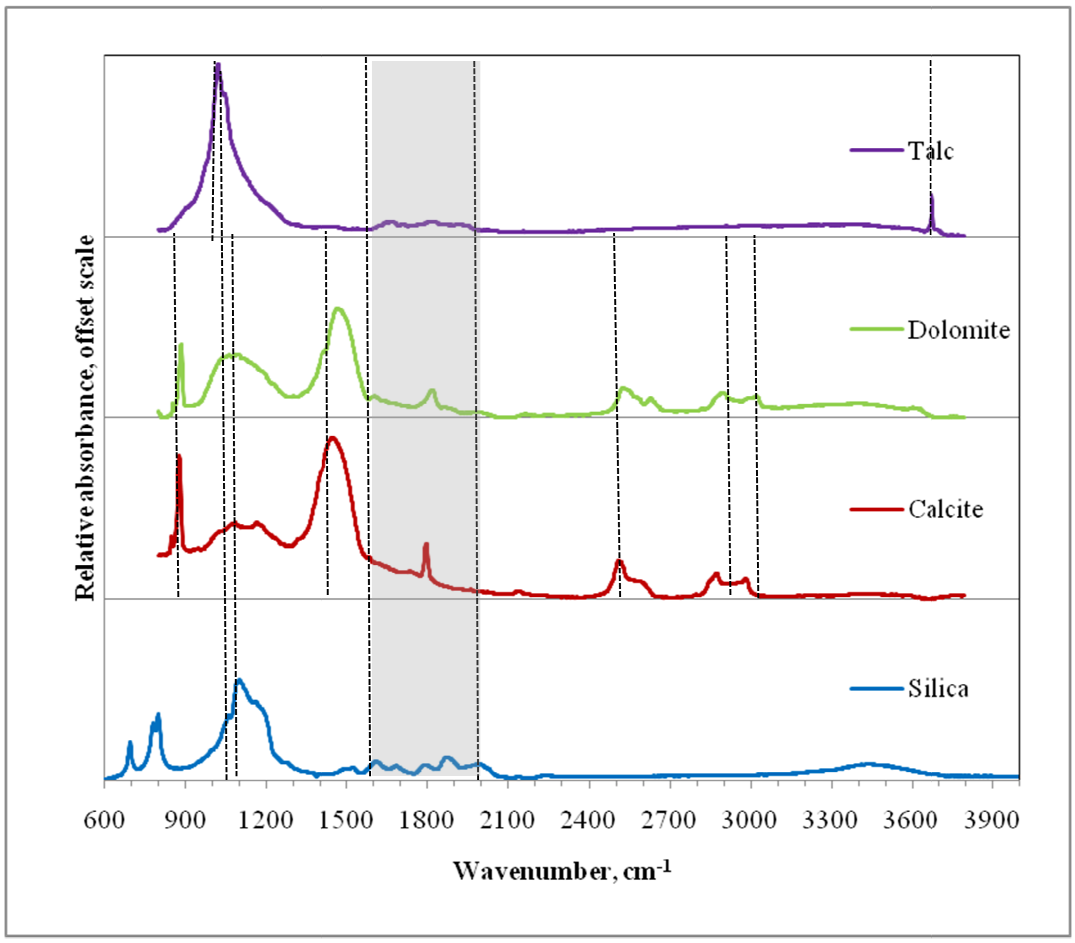

Figure 4.19, FT-IR spectra of mineral soil materials. Dashed lines indicate peaks of interest. Shaded bars indicate regions where several peaks are grouped.

Calcite and dolomite have similar spectra. Both feature large peaks at 878 and 1447 cm^{-1} due to the carbonate (CO_3) group. The peak at 1700 cm^{-1} for carbon to oxygen double bonds is present in both materials as well, although it is larger in calcite. These groups are probably due to the sorption of ester, aldehyde, and ketone groups (R-CO-R) which may be larger in calcite due to the fact that the calcium in calcite is slightly more electronegative than the magnesium in dolomite. Other groups present in both materials are alumnosilicates at 1100 cm^{-1}, alkane (CH) stretching at 2900 cm^{-1}, and hydroxyls at 2500 cm^{-1}. Dolomite has a small peak at 3676 cm^{-1} for MgO_3 groups because some of the Mg at the surface of the mineral complexed with oxygen after atmospheric exposure. Using atomistic simulation, Wright et al. (2001) showed that dolomite formed more hydrogen bonds between the carbonate groups and water at the surface than calcite. Based on the FT-IR analysis of these two materials, the contact angle, contact angle

hysteresis, and surface energy components are expected to be very similar although dolomite should be slightly more water wetting than calcite since it forms more hydrogen bonds with water, which appear in the FT-IR spectra as a broad rise between 3100 and 3600 cm^{-1}. Figures 3.4 and 3.5 show that dolomite is slightly more water-wetting than calcite in air-water and PCE-water systems, respectively. The correlations in Section 4.5 showed that wettability hysteresis is more strongly correlated with oxygen content for the subset of mineral soil materials than the group of all materials. The FT-IR spectra show that this may be partly due to the fact that the oxygen in these soil materials occurs as mineral species that are similar in polarizability. In contrast, in the carbon-containing soil materials, some oxygen is part of mineral dioxides but some is also bonded to organic molecules such as phenols which have a lower dipole moment and are, therefore, less polar.

4.9 FT-IR spectra of soil materials exposed to PCE

Figure 4.20 shows the FT-IR spectrum of silica and the FT-IR spectrum of silica that was previously exposed to pure PCE. The mineral signature of silica at 1100 cm^{-1} is increased after contact with PCE. Also, the broad peak at 3100 to 3600 cm^{-1} is slightly increased. This comparison suggests that contact with PCE removed surface impurities from the silica. The resulting surface has slightly more exposed mineral area and more sorbed water.

The equilibration of the Ann Arbor II sand with PCE resulted in the loss of some organic groups from the surface. This is consistent with the observations that PCE solubilized humic acid coatings from the surface of slides and that the interfacial tension between PCE and water decreased when the PCE was equilibrated with Ann Arbor II sand (Section 3.6). During filtering, some of the organic matter was apparently removed from the system, resulting in lower peaks in the alkanous regions of the spectrum, 2800-3100 cm^{-1} and 1500-2000 cm^{-1}. Similar to the case with silica, this removal leaves more exposed mineral and results in an increase in the silicate (1100 cm^{-1}) and sorbed water (3100-3600 cm^{-1}) peaks.

There is very little change in the Lachine shale and Waynesburg coal spectra following equilibration with PCE. This observation is consistent with the results

presented in Section 3.6 which showed that there was no change in the surface and interfacial tension of liquids equilibrated with these materials.

In Section 3.6, it was observed that PCE extracted surface-active constituents from the surface of Garfield shale. The increase in the silicate peak at 1100 cm^{-1} and the water sorption peak at 3100 to 3600 cm^{-1} seen in Figure 4.23 support this finding. There is also an increase in the peak at 1450 cm^{-1} for branched alkanes and in the peaks at 2800-3100 cm^{-1} indicating aliphatic and methyl carbons which may suggest some sorption of PCE at the surface or that some highly non-polar solubilized organic material is redeposited at the surface when PCE volatilizes.

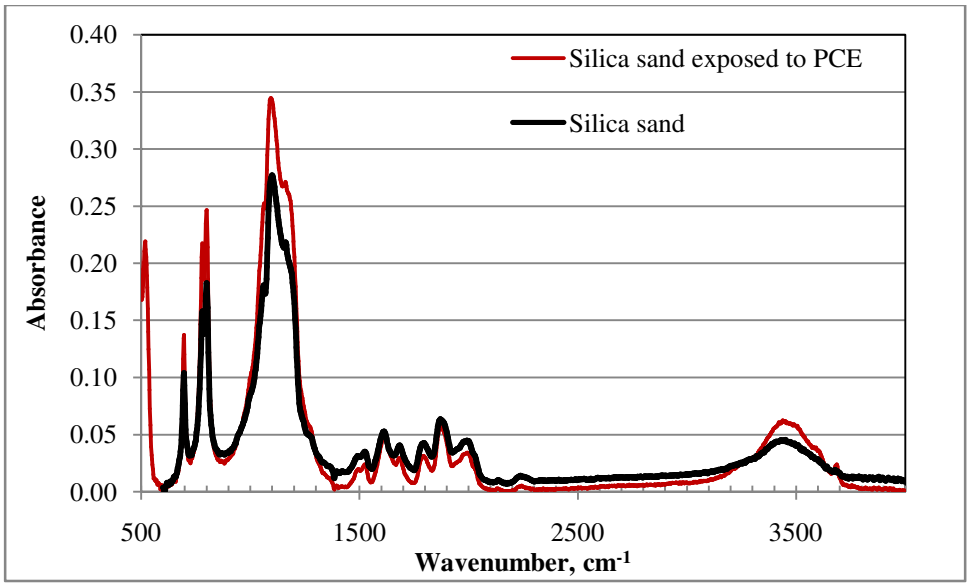

Figure 4.20, Comparison of FT-IR spectra for silica and silica exposed to PCE.

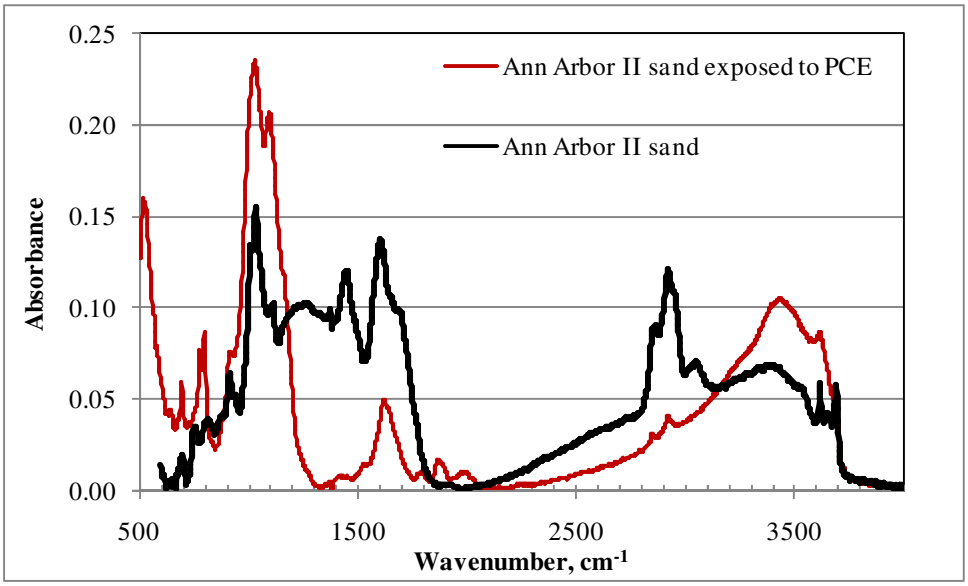

Figure 4.21, Comparison of FT-IR spectra for Ann Arbor II sand and Ann Arbor II sand exposed to PCE.

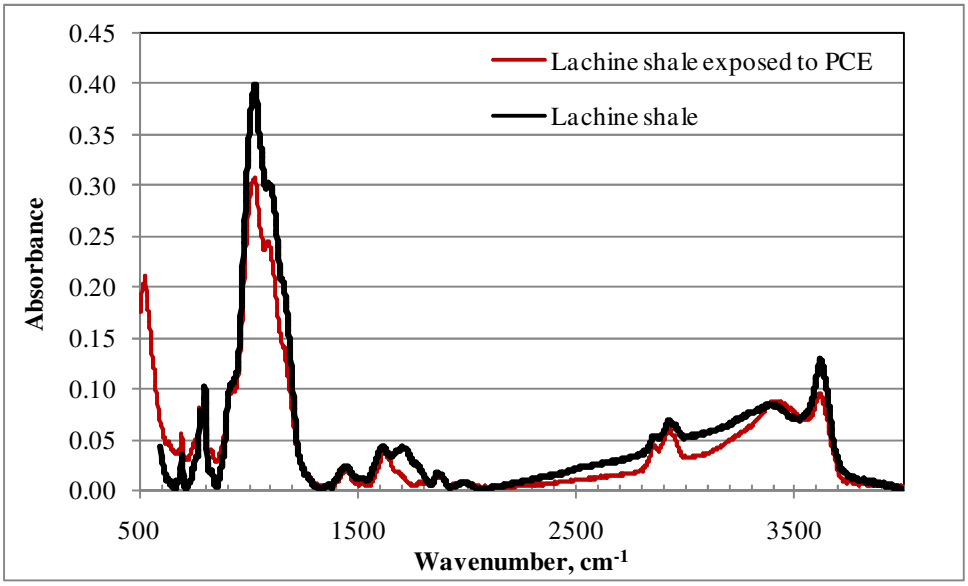

Figure 4.22, Comparison of FT-IR spectra for Lachine shale and Lachine shale exposed to PCE.

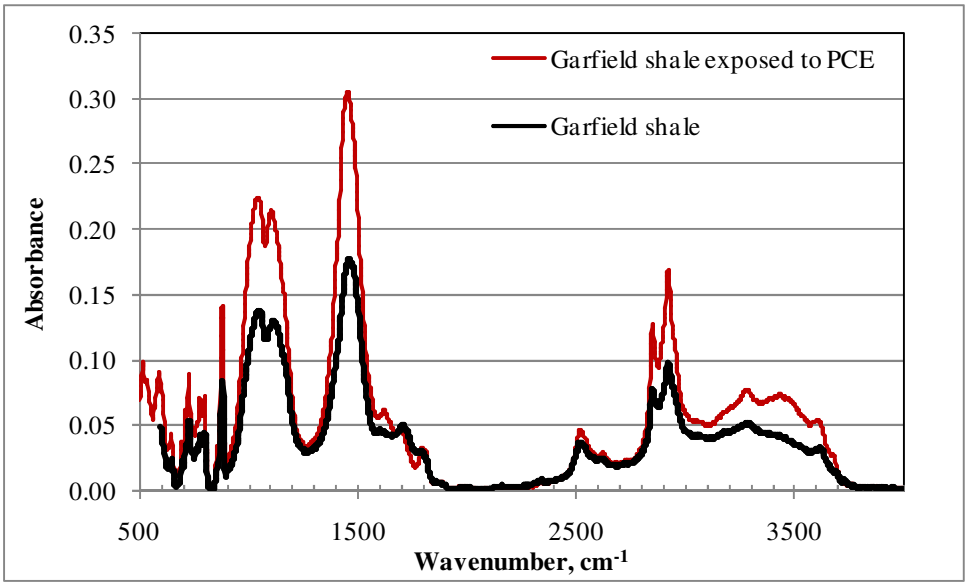

Figure 4.23, Comparison of FT-IR spectra for Garfield shale and Garfield shale exposed to PCE.

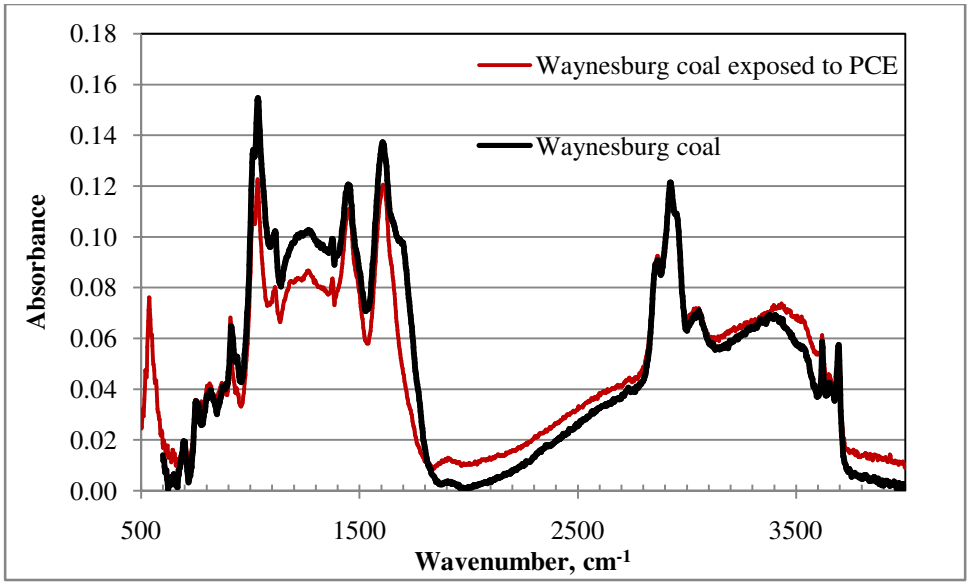

Figure 4.24, Comparison of FT-IR spectra for Waynesburg coal and Waynesburg coal exposed to PCE.

Figures 4.20 to 4.25 show that, although the relative strength of some peaks changes, there are no new peaks caused by the exposure to PCE. This may be due to the fact that PCE is quite volatile; after drying, there is not expected to be any PCE remaining at the surface. Some of the organic matter solubilized by the PCE during equilibration may leave the system when the PCE is removed by vacuum filtering but some may be redeposited on the surface as the PCE volatilizes. The critical implication

of this examination is that in the vadose zone, once the PCE has been removed by passive or active means (simple volatilization or engineered remediation), a minimal residual wettability effect is expected in soil materials exposed to PCE. This is in contrast to work by Roy et al. (1999) and Litvina et al. (2003) who observed that altered wettability areas remained present following remediation of crude oil spills. Two reasons that exposure to pure PCE might not produce this effect are: 1) the PCE used here does not contain any non-volatile impurities that remain after drying and thus permanently alter the surface and 2) the surface-functional groups of these mature materials are in a similar state when contacted by PCE or by air such that the surface-functional groups are already sharing electrons where necessary to minimize the number of incomplete bonds at the surface. In Roy's study, they found that the surface functional groups changed conformation after exposure to water because water provided the hydrogen bonds necessary to create neutral surface groups.

4.10 NMR spectra of carbon-containing soil materials

^{13}C NMR was selected as a composition analysis method due to the fact that it is very surface specific and yields a spectrum of carbon-bond types. Diffuse reflectance FT-IR, as a method, is handicapped by the fact that the absence of peaks is more definitive than the presence of peaks, because each peak can indicate more than one group.

Figure 4.25 shows the NMR spectrum of Ann Arbor II sand. This material is geologically young, containing relatively unprocessed organic precursor material. The three main peaks are carboxyl groups around 170 ppm, aromatic groups around 130 ppm, and methylated alkane and aromatic groups around 20 ppm. In addition, numerous small peaks around 70 ppm indicate that there are oxygenated methine groups. These peaks corroborate the FT-IR spectrum of Ann Arbor II which indicated a mix of aromatic, alkane, and oxygenated alkanes such as ethers. This material was water-wet under all circumstances in bottle tests. The Ann Arbor II sand showed a similar spectrum as the Ellerslie sand studied by Roy et al. (1999) and Litvina et al. (2003). NMR spectra of pristine Ellerslie and crude oil-contaminated Ellerslie soils were examined by NMR and

the hydrophobic soil was shown to have more aliphatic and carbohydrate-type groups (Litvina et al., 2003).

^{13}C NMR analysis showed that Lachine shale (Figure 4.26) contains predominantly aromatic (130 ppm) and alkane (39 ppm) groups. Carbonyl and carboxyl groups are definitely absent which implies that the small carbonyl peak on the FT-IR spectrum is probably a very minor component. The alkane groups may include oxygenated groups such as the ether, aldehyde, and ketone groups indicated by FT-IR. Compared to the Ann Arbor II sand, the Lachine shale has less diversity in functional group types. The selective diagenesis of organic materials results in this reduction of group types as only the more recalcitrant materials survive.

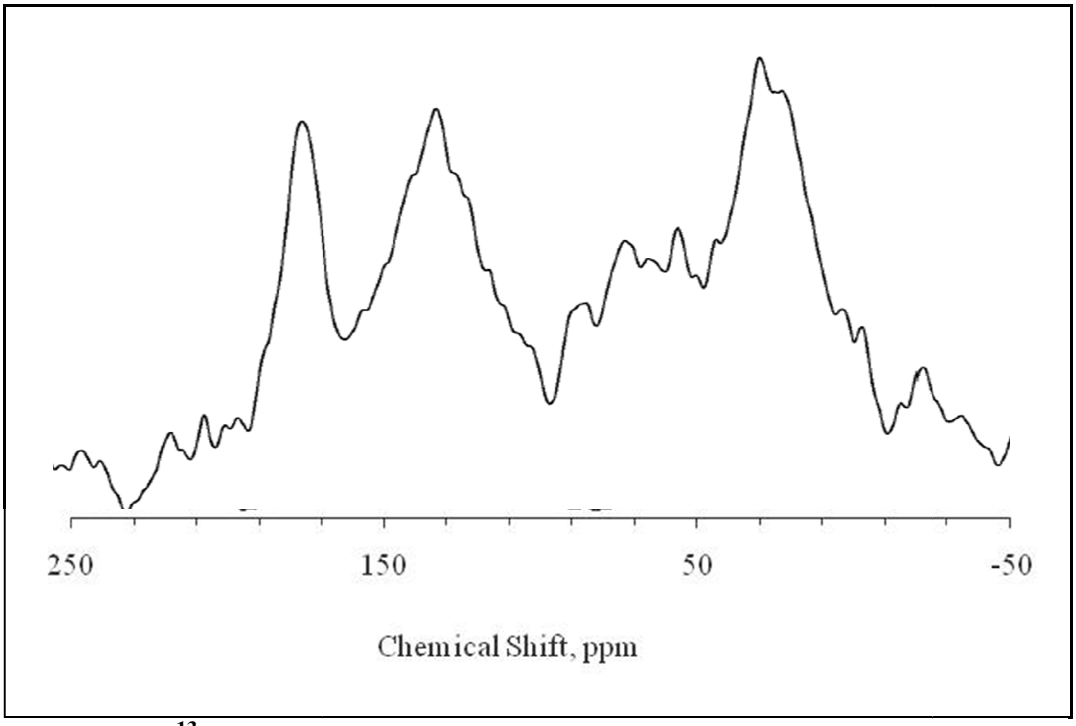

Figure 4.25, ^{13}C NMR spectrum of Ann Arbor II sand.

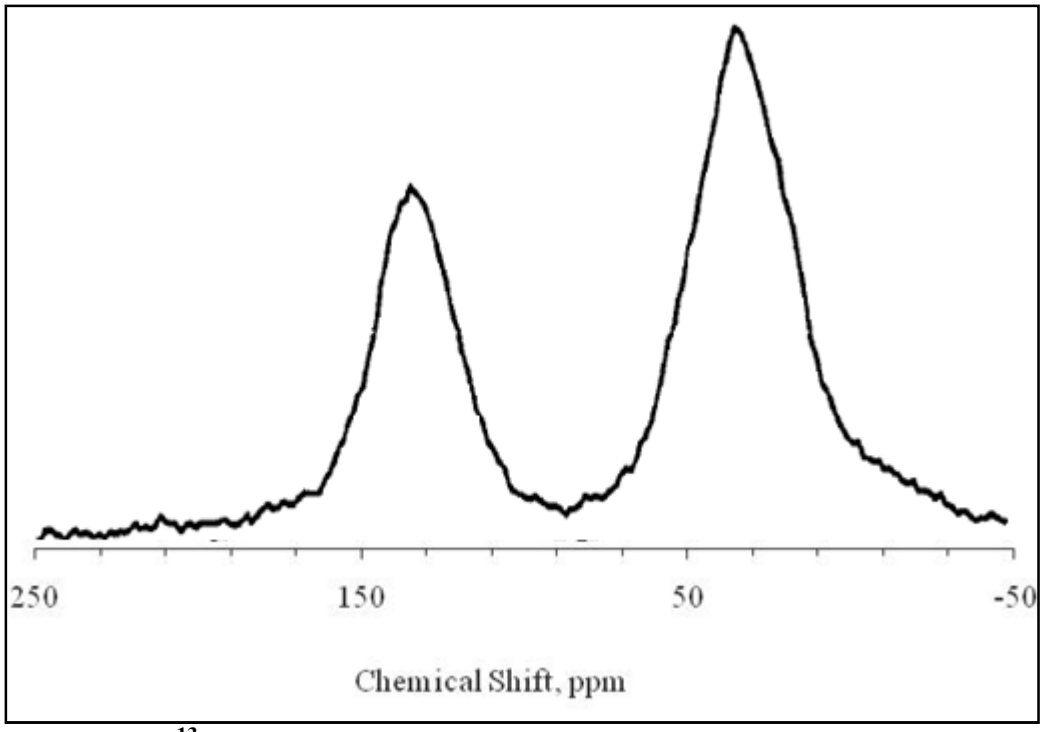

Figure 4.26, ^{13}C NMR spectrum of Lachine shale. (Spectrum provided by Johnson, 2000.)

The spectrum of Garfield shale, shown in Figure 4.27, shows a similar composition to that of Lachine shale, which is in agreement with the FT-IR analysis. The Garfield shale shows a similar profile with proportionately more aliphatic groups than aromatic. Also, the narrowing of the peak at 29 ppm suggests that Garfield shale has a dominance of methylene groups, while the composition of Lachine shale is more split between methyl and oxy-methyl groups, causing a broad peak. There is a small signal for phenolic aromatic groups which add some hydroxyl groups capable of inducing hydrogen bonding with the water phase, but the dipole moment of aromatics still tends to be small, so these oxygen-containing groups would be expected to be less polar than the oxygenated alkanes in the Lachine profile.

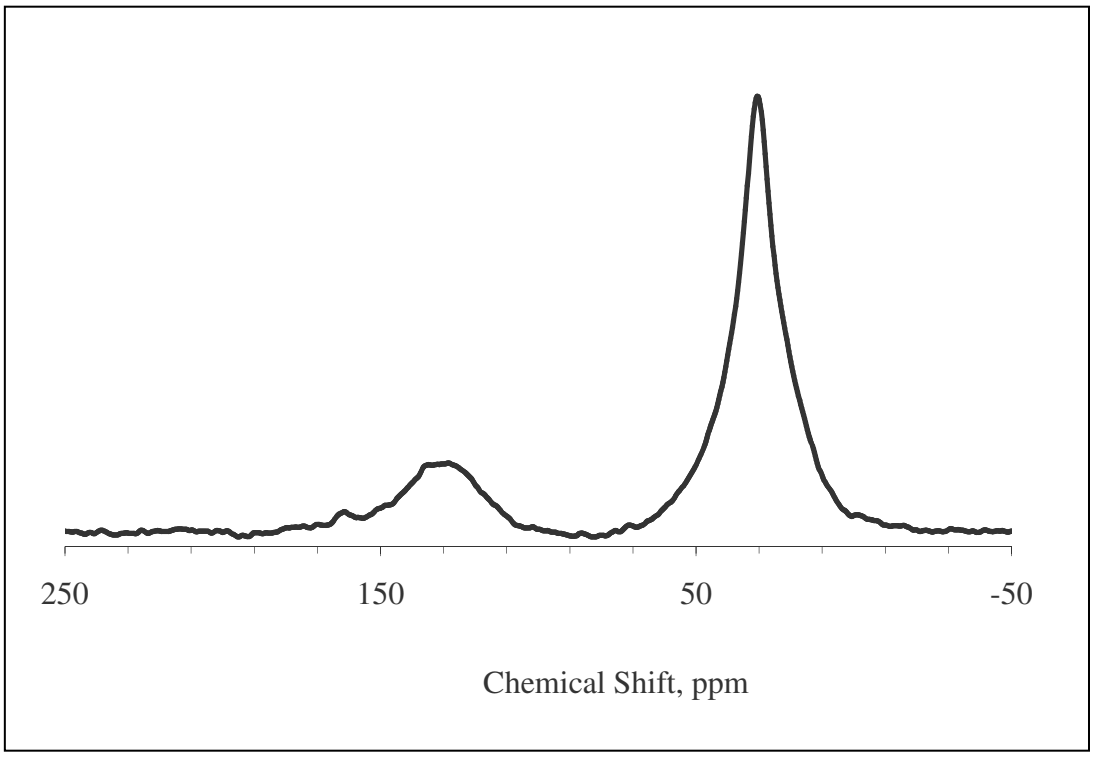

Figure 4.27, ^{13}C NMR spectrum of Garfield shale.

The Waynesburg coal spectrum is given in Figure 4.28. Waynesburg coal features the same two major peaks as the Lachine and Garfield shales; however, it has far more aromatic groups than alkanes. The Waynesburg coal also has a signature near 154 ppm for phenolic aromatics. This agrees with the FT-IR spectrum which showed substituted aromatics. These groups still have a small dipole moment even though they contain oxygen because the large six-carbon ring provides a large structure to spread the electrons away from the oxygen molecule. The region of the spectrum indicating alkanes (20-50 ppm) has two peaks which indicate the presence of both branched and straight chain methyl groups (R-CH_2 and R-CH). Again, branched and straight alkanes were visible on the FT-IR spectrum.

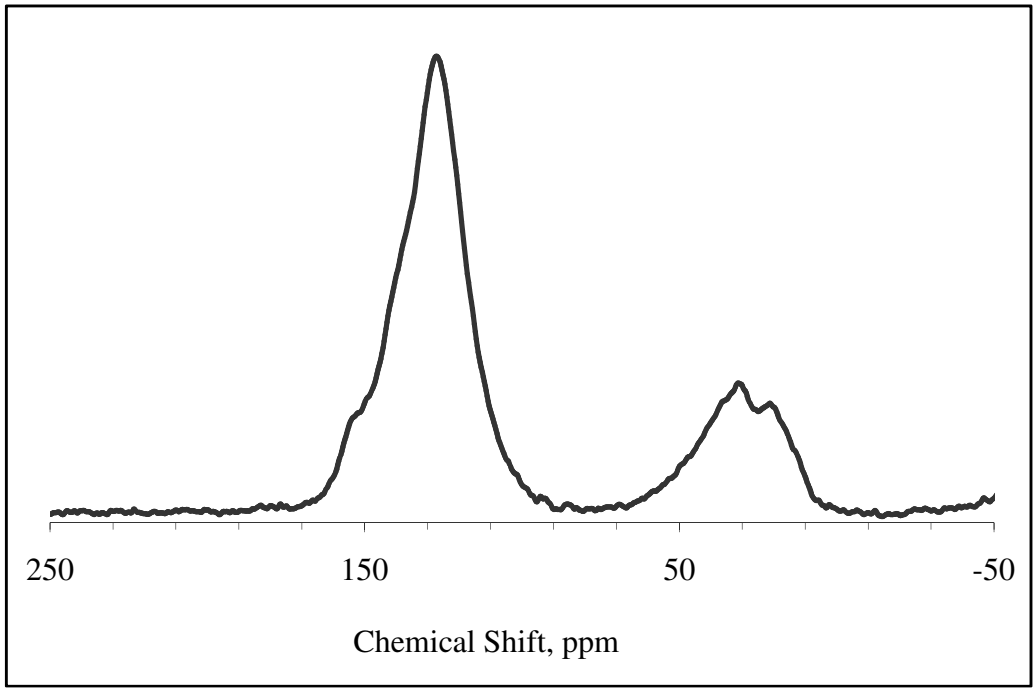

Figure 4.28, ^{13}C NMR spectrum of Waynesburg coal.

The four organic carbon-containing materials examined by ^{13}C NMR vary in both amount of soil carbon and geological maturity of that carbon. In contrast to bulk elemental analysis, the functional group information from FT-IR and NMR show that carbon and oxygen are bonded in functional groups of varying polarity. By examining the FT-IR and NMR spectra together, it is apparent that soil carbon becomes less diverse as the soil material is subjected to diagenesis. Comparing the organic carbon-containing soil material FT-IR spectra from Ann Arbor II sand to Waynesburg coal, there is a decrease in the alumnosilicate mineral peak at 1100 cm^{-1}, a decrease in the oxygenated alkane region of 1600 to 2000 cm^{-1}, and an increase in the alkane region at 2800-3100 cm^{-1}. Substituted aromatic groups, which are indicated by a peak at 1700 cm^{-1}, are more prominent in Ann Arbor II sand and Waynesburg coal than in Lachine and Garfield shales. NMR shows a more dramatic difference between Ann Arbor II sand and the other organic carbon-containing materials because the latter contain primarily two non-polar group peaks, aromatic groups and alkanes, while Ann Arbor II also contains a peak for polar oxygenated alkanes and several other minor polar group peaks. Although three of

the four organic carbon-containing materials measured by NMR have some phenolic groups present, the relative ratio of phenolic aromatic groups to other aromatic functionalities decreases as the materials mature toward the Waynesburg coal. Because of the attached hydroxyl group, phenolic groups are one of the more polar aromatic groups. Thus, the trend in bulk elemental composition that showed that oxygen content was highly correlated with contact angle, is reflected in the shift from a high proportion of oxygen-containing surface-functional groups in Ann Arbor II sand to a very low proportion of oxygen-containing surface-functional groups in the three organic carbon-containing materials, which are the least water wetting and have the most wettability hysteresis.

Tampy et al. (1998) showed that the type of carbon bonds in functional groups influences the wettability. CH groups are more water-wetting than CH_2 which, in turn, is more water-wetting than CH_3. Similarly, substituted aromatic groups, such as phenols, are more water-wetting than unsubstituted aromatics. Carbon to carbon double bonds are more wetting than saturated hydrocarbons, but it appears that, in the case of the solids examined here, aromatic groups, which do have many carbon pi bonds, are less water-wetting than substituted alkane groups. Thus, at equal carbon amounts (on a bulk molar percent basis), the Waynesburg coal would be expected to be less polar than the two shales because more of the Waynesburg carbon is in non-phenolic aromatic functional groups. The critical limitation to functional group measurement is that both FT-IR and NMR must be done on dry solids so the degree of hydrogen bonding when the water phase is present cannot be compared. A surface energy analysis is presented in Chapter 5 to compare the polar and non-polar components of the total surface energy directly, rather than inferring the forces present from the solid composition.

4.11 Summary and conclusions

The composition of the representative aquifer materials was analyzed by three methods, bulk elemental composition, FT-IR, and ^{13}C NMR. Scatterplots of the contact angle in air-water-solid and NAPL-water-solid systems versus five bulk elemental composition parameters (mass % carbon, mol % carbon, H/C molar ratio, mol % oxygen, and O/C molar ratio) were compared. It was apparent that the contact angle in water-air

and water-NAPL systems was not as strongly correlated with any bulk elemental composition parameter as the contact angle in air-water or NAPL-water systems. It is believed that when water is the immersion phase there is a film of water separating the drop from the surface. Thus, the composition of the surface is less important since the drop is resting on the water film instead of directly contacting the solid. However, mol % oxygen and O/C molar ratio had good linear correlations to air and NAPL immersion contact angles, as evidenced by high R^2 values. The degree of wettability hysteresis for air-water, PCE-water, and CTET-water cases was also correlated with mol % oxygen and O/C molar ratio.

The surface functional groups of the soil materials were analyzed using FT-IR and ^{13}C NMR. FT-IR showed that some carbon of the surface carbon is bound to polar oxygen, for example in the carbonate materials and Ann Arbor II sand. Thus, some of the carbon-containing groups are not completely non-polar. Also, the oxygen in the more mature organic carbon-containing materials is part of aromatic and long-chain hydrocarbon functionalities that are inherently less polar. Contact with PCE did not appear to dramatically alter the surfaces of the carbon containing materials. Once PCE volatilized from the surfaces, the surfaces show the same functional groups as the respective solids that are air-dry and have never contacted PCE. This indicates that PCE or impurities within the PCE, if present, are not sorbing to the solid surfaces rendering them PCE-wet. The surfaces may have different functional group conformations when immersed in the water phase, however, because the groups may re-conform to reduce the surface energy when water, which is highly ordered near surfaces, is present.

^{13}C NMR was conducted on four materials: Ann Arbor II sand, Lachine shale, Garfield shale, and Waynesburg coal. In addition to confirming the composition determined by FT-IR, NMR showed a progression in carbon bonds at the surface from oxygen-rich molecules in the case of Ann Arbor II, to aromatic groups in the case of Waynesburg coal. This follows the trend in wettability where Ann Arbor II is the most water-wet and Waynesburg coal is the least water-wet and most hysteretic of the materials studied. The bulk elemental and surface-functional group compositions indicate that, as the oxygen at the surface becomes bonded in larger and less polar

functional groups, the solids become less water-wet and have greater wettability hysteresis.

Chapter 5 presents surface free energy data to quantitatively illustrate how surface polarity affects the contact angle and the degree of wettability hysteresis. Surface free energy components can be used to quantitatively relate the polar and non-polar character of various surfaces. This method has been established for polymers and biological materials but had not been used widely on geologic materials because the surface energy of many minerals is too high to use commonly available liquids as surface probes. However, the materials selected for this study are relatively low energy compared to many oxide minerals. Based on the composition data, it is expected that the Waynesburg coal will have the lowest polar surface energy. The Garfield shale and Lachine shale are expected to be similar to each other in surface energy distribution. Among the minerals, quartz is expected to have the highest and most polar surface energy. Talc and graphite are expected to have lower polar components than the crystalline minerals. Calcite and dolomite will have similar surface energy, but dolomite should be slightly more polar than calcite.

CHAPTER 5

SURFACE ENERGY COMPONENTS OF AQUIFER MATERIALS

5.0 Introduction

It was previously believed that NAPLs would be the wetting fluids in systems containing organic carbon-containing soil materials. However, it has now been shown that, when the solids are immersed in water, pure non-polar NAPLs are unlikely to spread over the surfaces and the solids are always strongly water-wet. Thus, NAPLs in porous media saturated with water, such as the subsurface saturated zone, likely remain isolated in the largest soil pores and may easily become distributed into immobile blobs. A significant degree of wettability hysteresis is present for certain materials. Calcite, dolomite, and quartz are water-wet even if their surfaces have been initially immersed in the NAPL phase. However, Lachine shale, Garfield shale, Waynesburg coal, graphite, and talc are wet by the NAPL phase if the surface is immersed in the NAPL before being contacted by a water droplet. Chapter 4 examined the link between wettability and surface composition and showed that oxygen content is correlated to contact angle and the degree of wettability hysteresis.

One reason why oxygen atoms at the surface may influence wettability is that functional groups containing oxygen are highly polar. Water is also highly polar which creates a strong polar attraction between water and the polar surfaces that is not present when polar molecules do not populate the surface. The minerals are uniformly crystalline solids with regularly structured ionic bonds. As such, four forces are expected to be interacting at the water-mineral interface, Coulomb (permanent charges), Keesom (dipole-dipole), Debye (dipole-induced dipole), and London-van der Waals (induced dipole-induced dipole). At the NAPL-mineral interface only the Debye and London forces are expected. In contrast, the organic materials do contain some mineral matter

mixed with the organic matter so their surfaces are a mixture of organic and mineral functional groups. Therefore, in some locations the water-solid forces will be a combination of all four forces and, in others, only the Debye and London forces are expected to be present. The NAPL-solid interfaces will be characterized by a mix of London only and London plus Debye. This chapter will show that polar forces are indeed larger at the surface of the non-hysteretic materials. The relationship between free surface energy components, solid-liquid interfacial tensions, and contact angle will also be confirmed quantitatively.

5.1 Surface free energy of natural soil materials

The surface free energy of eight soil materials was calculated by the method of van Oss et al. (1988). As described in Chapter 2, contact angles were measured for each material in air-DIM, air-ABN, air-water, air-glycerol and air-formamide systems. The contact angle and surface energy components of the liquids were entered into the system of three equations described by van Oss (Equation 1.8) and the system was solved with MAPLE V.10 to find the values of the dispersion, acid, and base solid surface energy components, γ_S^D, γ_S^A, and γ_S^B respectively. The dispersion component of the surface free energy, γ_S^D, is entirely determined by the contact angle with a non-polar liquid. Two non-polar liquids were used and the calculated dispersion energy components were averaged. These surface energy component calculations were also repeated with Della Volpe's MathPad program SurfTen 4.3 (Della Volpe, 2004) to confirm the MAPLE calculation method and found to agree. Table 5.1 lists the contact angle values used in the calculation of solid surface free energies. Air-water contact angles were collected at near neutral pH (7 ± 0.20) because the protonation of the surface changes with solution pH and may affect the polar components of the surface free energy. Table 2.3 gives the liquid surface energy components used in the calculations.

	Polar Probe Liquids			Non-Polar Probe Liquids	
Material	**Water**	**Glycerol**	**Formamide**	**DIM**	**ABN**
Lachine shale	44.6	32.7	18.8	34.1	6.2
Garfield shale	53.4	55.1	37.8	32.3	14.0
Waynesburg coal	81.6	67.4	42.0	34.2	8.5
Graphite	62.2	54.2	32.9	20.1	8.2
Talc	62.9	47.3	DNM	35.0	14.9
Dolomite	33.2	27.9	DNM	31.3	12.2
Calcite	39.7	63.9	DNM	35.0	17.3
Quartz	19.9	29.6	47.6	44.2	21.7

Table 5.1, Contact angles for air-probe liquid-solid systems in degrees measured through the probe liquid droplet. DNM indicates that a contact angle for was not collected for that system. DIM is Di-iodomethane and ABN is α-bromonaphthalene.

Solids with a total surface energy less than about 100 mJm^{-2} are typically considered low energy surfaces. The energy components are given in units of mJm^{-2} which are mathematically equivalent to mNm^{-1} but are chosen to emphasize the fact that surface free energy is a measure of work. Table 5.2 lists the non-polar dispersion energy component (γ_S^D), the polar acid component (γ_S^A), and the polar base component (γ_S^B) determined from the contact angles presented in Table 5.1. The components listed are the average surface energy components determined from redundant calculations based on ABN and DIM as non-polar liquids and water, glycerol, and formamide as polar liquids. A table of the surface free energy values resulting from each system of three liquids is given in Appendix D. The total polar surface energy (γ_S^{AB}) was calculated from Equation 1.4. The total solid surface energy (γ_S) was calculated from Equation 1.3. The last column of Table 5.2 lists γ_S^D/γ_S which is the calculated ratio of dispersion energy (non-polar) to total surface energy. Table 5.2 shows that quartz has an unusually low dispersion energy component. Quartz does not have the highest total surface energy of the natural soil materials studied but it does have the highest polar surface energy caused by the strong acid mono-pole. However, the total surface energy of quartz is not out of the range of the other materials. The surface energy of quartz has been shown to vary dramatically in the literature depending on the surrounding conditions before measurement such as the temperature, humidity, and length of exposure to other liquids (Young and Bursh, 1960; Iler, 1979; DeRosa et al., 2003). In this case, the total surface

energy of the quartz is similar to previous observations for quartz microscope plates at room temperature (Janczuk and Zdziennicka, 1994) where it was observed that γ_S ranged from 57.2 to 67.9 mJm^{-2}. FT-IR had shown trace amounts of material sorbed from the atmosphere on the surface of quartz which would lower the surface energy from that expected for a freshly cleaved surface. The total surface energy of graphite and talc also fall close to other reported values (Chessick et al., 1960; Giese et al., 1991). For comparison, Siebold et al. (1997) found that the dispersion component of silica flours was 42 to 38.1 mJm^{-2} and, for a limestone, it was 39.1 mJm^{-2}. Chibowski and Perea-Carpio (2002) report silica dispersion components ranging from 28.5 to 48.4 mJm^{-2}. Giese et al. (1991) reported a dispersion energy component for talc of 31.5 mJm^{-2}. Table 5.2 also shows that the three non-hysteretic materials, calcite, dolomite, and quartz, have the lowest ratio of dispersion to total surface energy. Thus, it appears that a γ_S^D/γ_S of 70% or less indicates a material that is likely to be water wet under all circumstances. This ratio also implies that a material with more than 30% γ_S^{AB} is sufficiently polar to render the surface persistently water-wet.

	γ_S^D	γ_S^A	γ_S^B	γ_S^{AB}	γ_S	γ_S^D/γ_S
Lachine shale	43.3	24.1	1.8	13.3	56.6	0.8
Garfield shale	43.2	25.3	0.2	4.3	47.5	0.9
Waynesburg coal	42.8	2.2	1.0	2.9	45.7	0.9
Graphite	45.9	12.9	0.6	5.5	51.4	0.9
Talc	42.5	10.5	1.5	8.0	50.4	0.8
Dolomite	43.5	33.3	1.9	15.9	59.4	0.7
Calcite	42.2	58.8	0.8	14.1	56.3	0.7
Quartz	39.4	62.8	1.0	15.9	55.3	0.7

Table 5.2, Surface free energy components (in units of mJm^{-2}) of natural soil materials determined using the van Oss method (1988). γ_S^D is the dispersion (non-polar) component of the solid surface energy. γ_S^A is the acid solid surface energy component. γ_S^B is the base solid surface energy component. γ_S^{AB} is the total acid-base solid surface energy component. γ_S is the total solid surface energy. γ_S^D/γ_S is the ratio of non-polar to total solid surface energy.

Table 5.2 shows that the dispersion energy of the soil materials, γ_S^D, does not vary over a wide range but the polar acid and base components are highly variable. Thus, according to Equation 1.3, most of the variation in total solid surface energy for these materials is due to variation in the polar (acid and base) components. With the exception of Waynesburg coal, all of the surfaces are mono-polar, meaning they have significantly more γ_S^A than γ_S^B (few strong basic surfaces exist naturally). It has been noted by van Oss and co-workers (van Oss et al., 1988b) that most natural materials are mono-polar. It is because of the geometric nature of the acid-base interfacial energy (Equation 1.7) that some liquids have little interaction with the surface.

5.2 Correlation between surface free energy and composition

Table 5.3 is a matrix of Pearson correlation coefficients (ρ) between bulk molar composition of each material and each of the surface free energy components given in Table 5.2. For example, the first cell in the table shows $\rho = 0.77$ for the correlation between the calculated dispersion energy component of the eight surfaces and the measured bulk elemental molar carbon content of the surfaces. Studies utilizing surfactants, mono-layers of known materials, and polymers have used changes in surface energy components to explain why slight alterations in material composition can affect macroscale properties such as contact angle (van Oss et al., 1988a). In this case, the technique is applied to natural materials which have a larger variation in composition and may contain other atoms that could influence the surface energy components such as sulfur that are not accounted for in this analysis. The correlation statistics in Table 5.3 show that carbon, hydrogen, and nitrogen content are positively correlated to the dispersion energy of the surface and negatively correlated to the polar energy components. Oxygen content follows the reverse pattern, since an increase in oxygen generally increases the polar character of a surface.

	% C	% H	% N	% O
γ_S^D	0.77	0.05	0.09	-0.66
γ_S^A	-0.46	-0.59	-0.49	0.70
γ_S^B	-0.45	-0.27	-0.32	0.51
γ_S^{AB}	-0.56	-0.72	-0.65	0.85
γ_S	-0.35	-0.79	-0.69	0.70
γ_S^D/γ_S	0.59	0.73	0.66	-0.87

Table 5.3, Pearson correlation between the measured bulk molar composition of eight natural soil materials (given in Table 4.1) and the measured surface free energy components of those materials (given in Table 5.2). Each cell represents the correlation coefficient between the property indicated in the horizontal row header and the vertical column header.

Carbon in aquifer materials was expected to increase the dispersion content of the materials. Figure 5.1 shows that this is indeed true. The slope of the linear fit is strongly influenced by graphite which has an unusually high carbon content and also has the highest dispersion energy component. Also, the polar character of the surface depends on the surface functional groups rather than the presence of individual atoms since electrons are orbiting more than one atom and will be distributed differently in a phenol versus a carboxylic acid. Thus, the elemental composition cannot completely capture the surface energy trends, but it does reinforce the fact that oxygen is a source of polar character in soil materials.

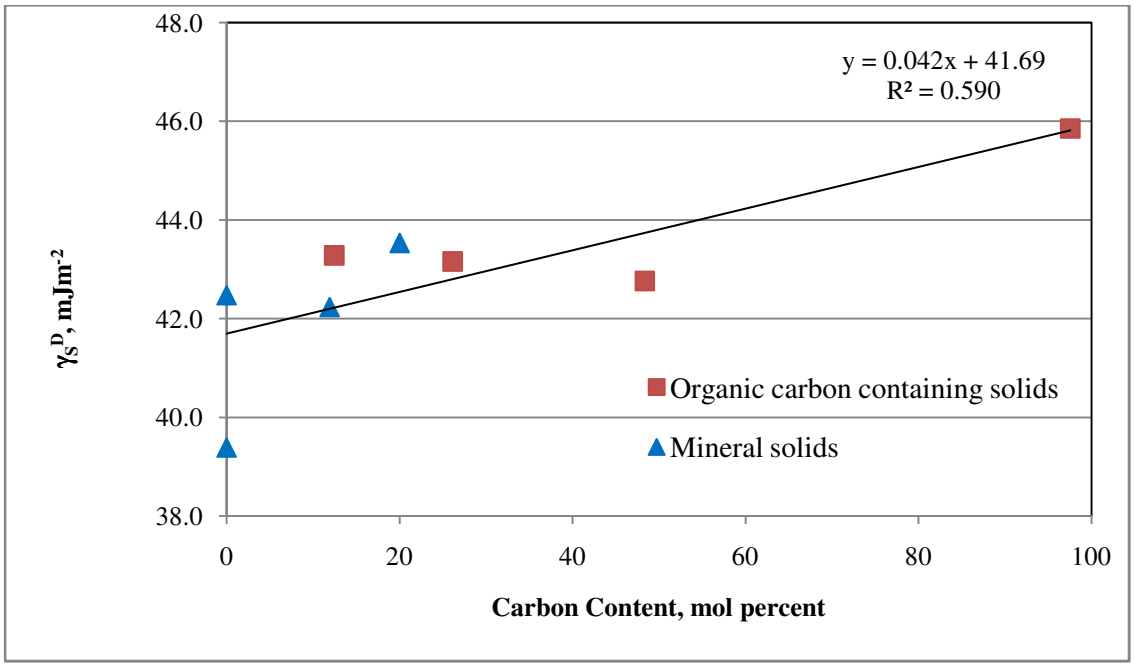

Figure 5.1, Correlation between solid dispersion energy component and carbon content, considering all eight natural soil materials.

Figure 5.2 shows the ratio of dispersion energy component to total surface energy of the eight soil materials as a function of oxygen content. This relationship is reasonably described by the linear fit given on the graph. The negative slope of the line indicates that, as the oxygen content of the surface increases, the non-polar component of the surface becomes a smaller proportion of the total surface energy, and the polar component increases. Given the range of material types, including both mineral and amorphous carbons, this linear fit is surprisingly good with an R^2 of 0.75.

Increasing the oxygen content of the solid increases the polar surface forces, as Figure 5.3 shows. This is expected but has not been directly shown in the literature for natural materials. Guy (1996) attributed differences in the wettability of coals to differences in polar surface energy based on the elemental oxygen content of the surface but did not determine the surface free energy components of the coals to test the hypothesis. This relationship is reasonably predictive, with an R^2 of 0.72 for the linear fit shown on the graph.

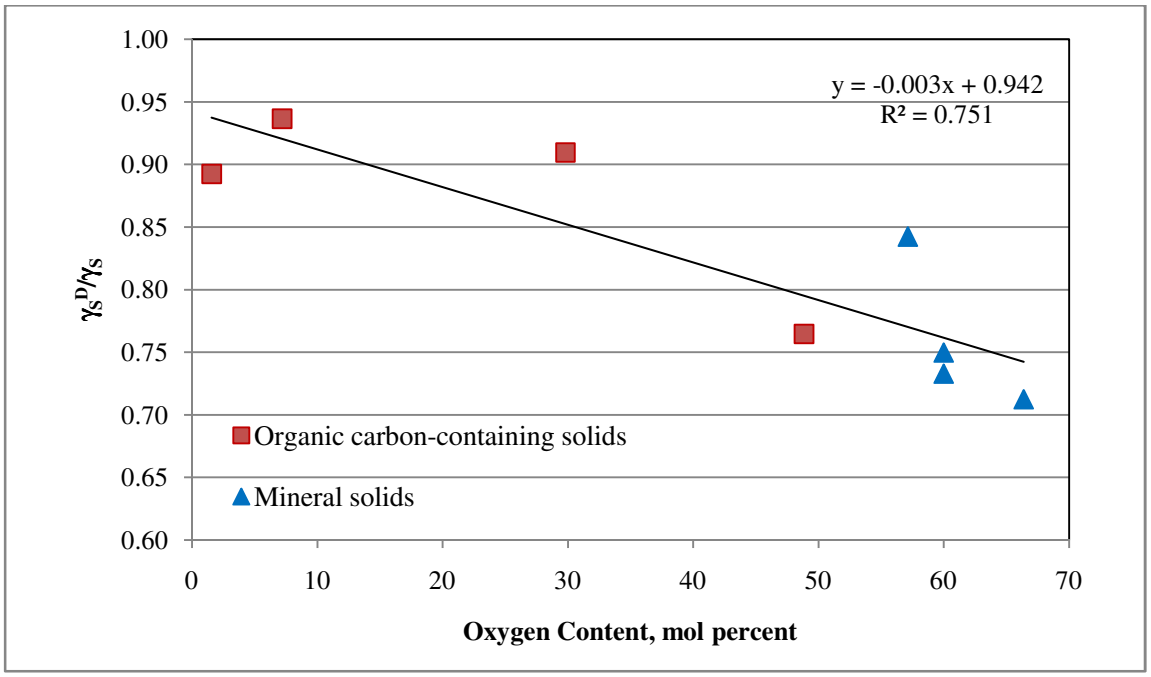

Figure 5.2, Correlation between the ratio of dispersion energy component to total surface energy and oxygen content, considering all eight natural soil materials.

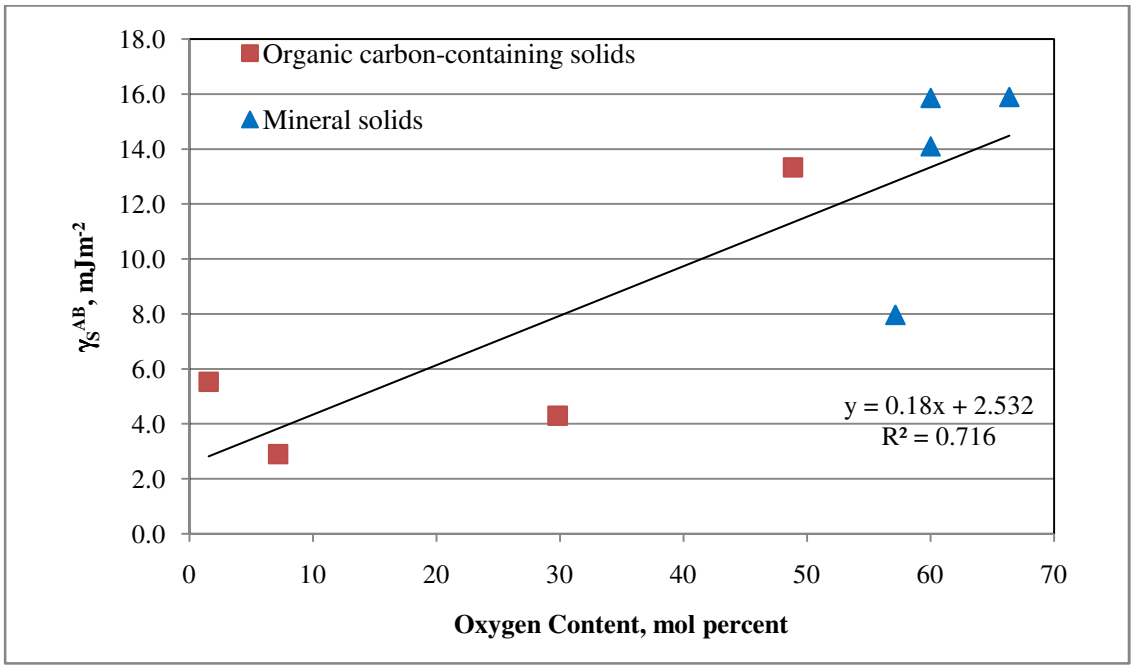

Figure 5.3, Correlation between oxygen content and solid acid-base energy component, considering all eight natural soil materials.

5.3 Traditional Zisman approach

Fox and Zisman (1954) showed that the relationship between liquid surface tension, σ_L and air-liquid contact angle for series of homologous liquids is linear. Zisman labeled the liquid surface tension, σ, at which cos(Θ) is equal to one the critical surface tension, σ_c, and described it as the maximum surface tension of a liquid that will spread completely over the surface. In other words, for any higher surface tension than the critical surface tension, a sessile droplet will form. This relationship has been proven useful for modeling series of liquids on low energy surfaces. However, based on the energy balance of the van Oss method, a more correct approach is to plot the square root of the liquid dispersion energy component, γ_L^D, versus cos(Θ). Equation 1.8 can be reduced for the interaction between an apolar liquid and apolar solid to give a form that predicts a linear relationship between cos(Θ) and $(\gamma_L^D)^{-1/2}$ for a given liquid:

$$\cos(\Theta) = 2(\gamma_S^D)^{1/2}(\gamma_L^D)^{-1/2} - 1 \qquad \textbf{Eqn. 5.1}$$

Although this form of the Zisman plot was suggested by Good (1992), it is not commonly used because it requires the assumption that there are no polar forces acting between the solid and liquid phases.

Figure 5.4 shows a traditional Zisman plot of the cosine of the air-NAPL contact angles versus the square root of the liquid surface tension, σ, (Table 2.3) for the solids that were found to have hysteretic wettability in Chapter 3 (Figures 3.3, 3.4 and 3.5; Lachine shale, Garfield shale, Waynesburg coal, graphite, and talc). Figure 5.5 shows the same treatment for the non-hysteretic solids (calcite, dolomite, and quartz). The fluids used were di-iodomethane (DIM), α-bromonaphthalene (ABN), formamide, glycerol, and water (Table 2.3). The surface tension of the probe liquids was given in Table 2.3. Table 5.4 shows the Pearson correlation between the two data series as well as the coefficient of determination of the linear fit. The solids shown in Figure 5.4 have the five highest γ_S^D/γ_S ratios of the eight solids, with greater than 70% of their total surface energy generated by dispersion forces.

The lines fitted to the contact angle data in Figure 5.4 converge and intersect the cos (Θ) =1 line near 45 mJm^{-2}. Previous researchers have pointed out that this value

appears common to many natural solids (Parekh and Aplan, 1978). Figure 3.4 showed that, in air-water systems, the least water-wet material is Waynesburg coal, followed by graphite and talc, then Garfield shale and lastly Lachine shale. The slope of the Zisman plot lines for the hysteretic solids follows this trend, with the least water-wetting material having the steepest slope. Therefore, the more non-wetting the material is, the greater the influence of the surface tension of the drop liquid on the contact angle.

Table 5.4 shows the calculated critical surface tension value, σ_C, value based on the linear fits to the contact angle data in Figures 5.4 and 5.5. Zisman expected that σ_C would be similar to γ_S^D if the solid was mostly a non-polar material. These values are not in exact agreement with the values of the solid dispersion energy components, γ_S^D, determined by the van Oss-Chaudhury-Good method (Table 5.2) but they are quite close. There is less than 10% difference between the two methods of estimating the solid dispersion component for the hysteretic solids, Lachine shale, Garfield shale, Waynesburg coal, graphite, and talc and less than 25% difference for calcite and dolomite. The slope shows that the Zisman method does not work well for silica, which is the most polar of the materials studied. There is a 0.7 Spearman (rank) correlation between the critical solid surface tension values predicted by the traditional Zisman approach applied to the hysteretic solids (Figure 5.4) and the measured solid dispersion energy component. The polar liquids, water and glycerol, significantly influence the slopes of the lines since they have higher surface tensions and also more polar interaction with the surface. Thus, they contribute polar forces that are not reflected in the simplified energy balance shown in Equation 5.1. One of the difficulties in constructing Figure 5.5 comes from the fact that, with higher solid surface energies, there are fewer non-polar liquids available that can form a sessile drop against the surface and the contact angles themselves were smaller, creating greater error in the measured values.

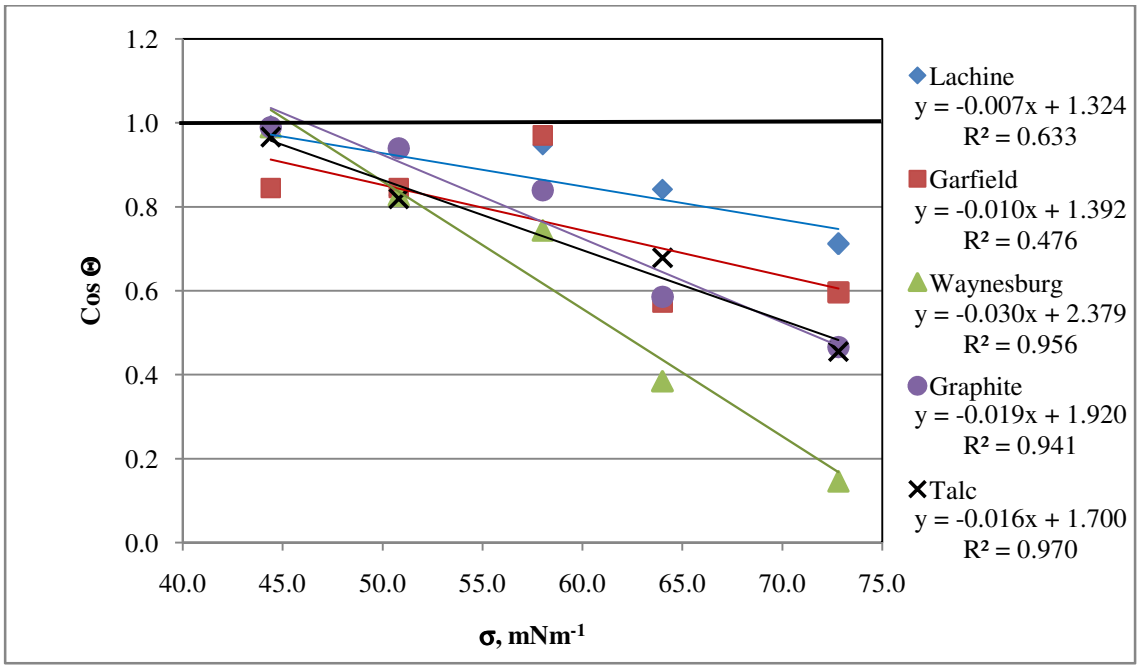

Figure 5.4, Traditional Zisman diagram of hysteretic soil materials.

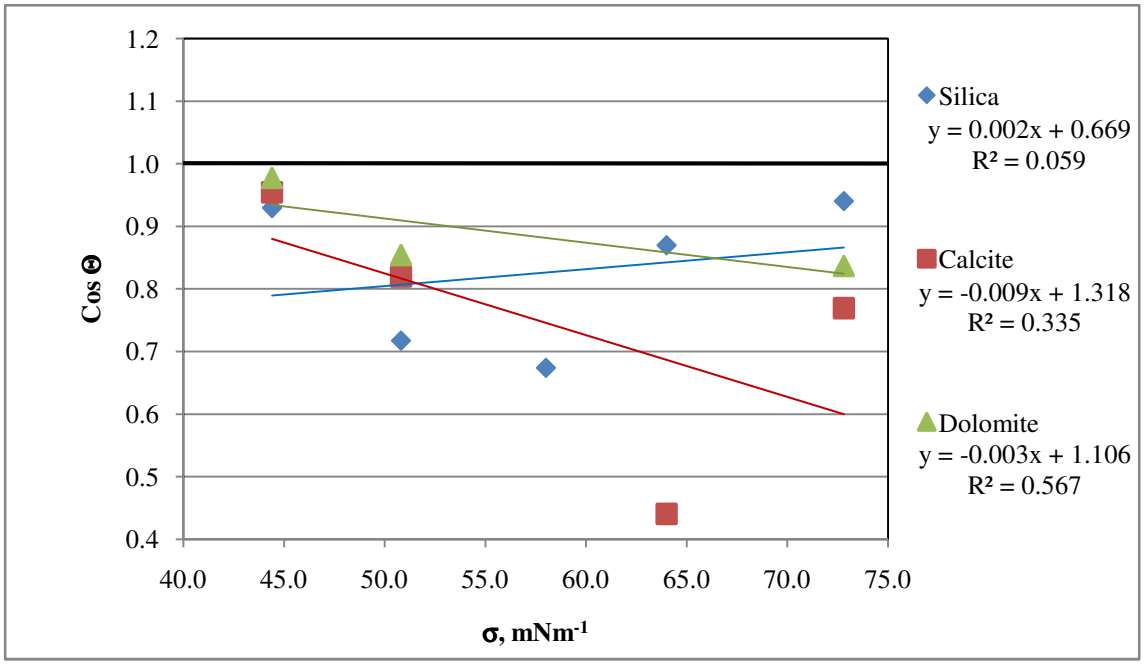

Figure 5.5, Traditional Zisman diagram of non-hysteretic soil materials.

Material	ρ	R^2	σc, mNm^{-1}
Lachine shale	0.79	0.63	46.3
Garfield shale	0.93	0.48	39.2
Waynesburg coal	0.98	0.96	46.0
Graphite	0.99	0.94	48.4
Talc	0.98	0.97	43.8
Dolomite	0.73	0.57	35.3
Calcite	0.66	0.34	35.3
Quartz	-0.25	0.06	165.5

Table 5.4, Linear correlation statistics and predicted critical interfacial tension, σ_C, from the traditional Zisman plots of all eight natural soil materials (Figures 5.4 and 5.5).

Plotting the same contact angle data versus the square root of the liquid surface energy dispersion component, γ_L^D, produces Figures 5.6 and 5.7. This method does not effectively improve the Zisman plot although several features remain consistent. The trend in the slope of the linear fits to the hysteretic soil materials, shown in Figure 5.6, is the same. Lachine shale, with the most water-wetting dry surface, again has the smallest slope and Waynesburg coal, which is the most water repellent, has the largest slope. This pattern is strongly defined by the air-water and air-glycerol contact angles which plot to the left side of the figure due to the low dispersion component of these two liquids.

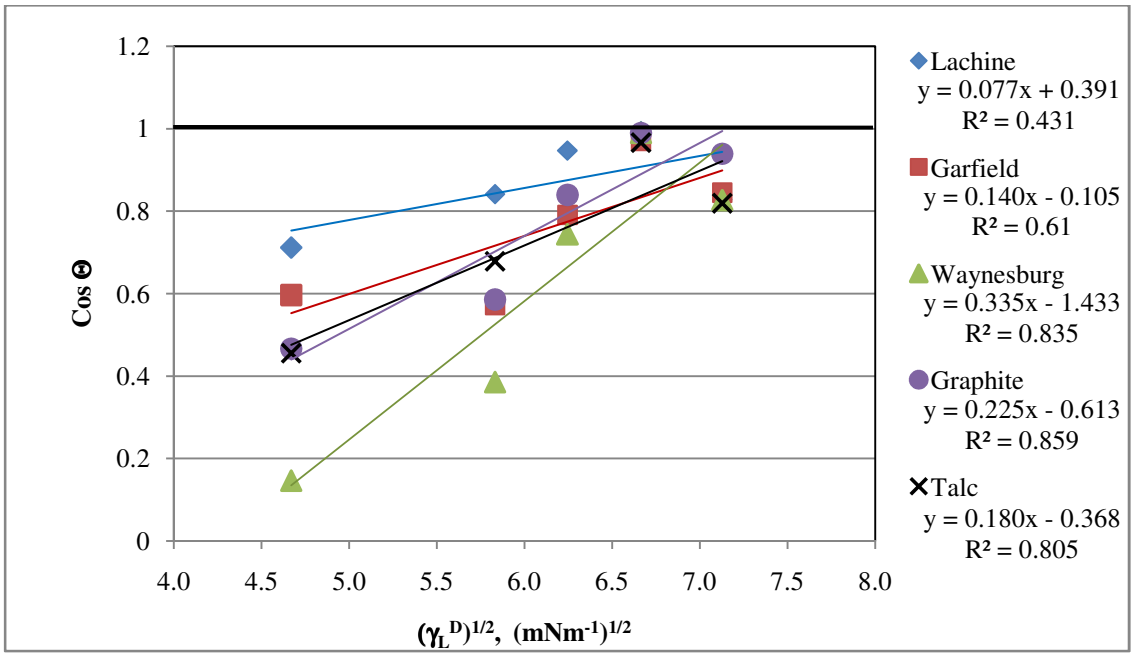

Figure 5.6, Alternate Zisman diagram of hysteretic soil materials accounting for the segregation of surface energy into components.

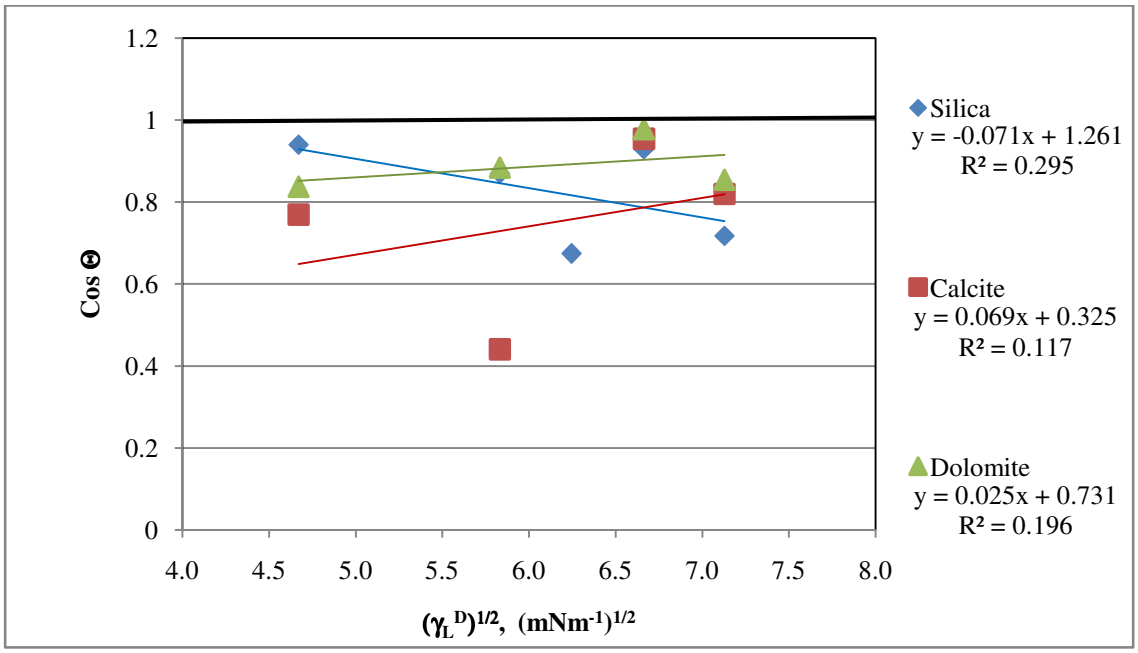

Figure 5.7, Alternate Zisman diagram of non-hysteretic soil materials accounting for the segregation of surface energy into components.

Table 5.5 shows the critical surface dispersion component as determined by extending the line fitted to the data for each solid through the line where cos(Θ)=1. The solid dispersion component is considerably overestimated with this approach. Like the

traditional Zisman approach, polar liquids, water and glycerol were used. However, in the traditional approach, the total energy of each material is used. The traditional Zisman approach gives a total liquid surface tension below which a liquid would be expected to totally spread over the surface. The value of γ_C determined by this alternate approach is the γ_L^D above which a liquid would be expected to spread over the surface. This is logical because most solvent liquids are highly non-polar and their dispersion component is large compared to polar liquids like water and glycerol. Thus, water, which has a γ_L^D of 21.8 mNm^{-1}, will bead up on most solids while PCE, which has a γ_L^D equal to its total liquid surface tension, γ_L, of 31.74 mNm^{-1} spreads on most surfaces. If a Zisman diagram is to be used as a tool for estimating the contact angle of an unknown liquid against a solid or determining whether the liquid will spread on a dry solid, the traditional approach is recommended.

	ρ	R^2	γc, mNm^{-1}
Lachine shale	0.80	0.43	62.6
Garfield shale	0.94	0.61	62.3
Waynesburg coal	0.99	0.84	52.8
Graphite	0.99	0.86	51.4
Talc	0.98	0.81	57.8
Dolomite	0.75	0.20	108.6
Calcite	0.68	0.12	368.8
Quartz	-0.22	0.30	13.5

Table 5.5, Linear correlation statistics and predicted critical interfacial tension from the alternate Zisman plots of all eight natural soil materials (Figures 5.6 and 5.7).

5.4 Application of the Zisman approach to two-liquid systems

Several researchers have attempted to apply the Zisman approach to three-phase systems composed of two liquids and one solid (Hamilton, 1971; Schultz, 1977; Guy et al., 1996). Most notably, Guy et al. (1996) measured the contact angle of eight organic liquids on five coal samples immersed in water. The cosines of the water-NAPL contact angles were plotted against liquid-water interfacial tension to produce a modified Zisman

plot for a three-phase system. In their case, the materials were always water-wet, but for each solid there was a particular liquid interfacial tension below which the contact angle was the same for all liquids. They called this value the critical interfacial tension, γ_C. The more polar the solid material was, the higher the value of γ_C.

NAPL-water contact angles were measured for PCE, CTET, TCE, and TCA systems. No clear trends were observable when cos(Θ) was plotted versus interfacial tension; however, Figure 5.8 shows that an alternate Zisman style plot using the surface tension of each liquid (Tables 2.2 and 2.3) produces linear fits. The difference between Figure 5.6 and Figure 5.8 is that in Figure 5.6, the contact angles were measured for air-liquid pairings where the liquids varied in polarity but in Figure 5.8 the contact angles are fluid-water and the fluids are either non-polar NAPLs or air. The four carbon-containing natural materials are non-water wet in NAPL-water systems so they plot below the cos(Θ) = 1 line. The surface tension at which the contact angle would become water wetting is given as γ_C in Table 5.6. The slope of the Garfield shale and Waynesburg coal plots cause the intersection with the cos (Θ) axis to occur at a value greater than 72.8 mNm^{-1}. If, in this case, γ_C is interpreted as the maximum surface tension of a liquid that can be displaced by the water drop allowing a contact angle through the water drop of less than 90°, then there is no liquid that can be displaced by the water phase against these two solids. Garfield shale and Waynesburg coal have the smallest total surface energy of the materials studied, and more importantly, the smallest polar surface energy component, γ_S^{AB}. In fact, the values of γ_C for NAPL-water systems from Table 5.6 rank in the same order as the γ_S^{AB} values presented in Table 5.2: quartz > Lachine shale > graphite > Garfield shale > Waynesburg coal.

The ranking of γ_C for NAPL-water systems with the polar surface energy component adds to the evidence that it is the proportion of polar surface forces that cause wetting differences, not the amount of carbon at the solid surface. Once the surface is immersed in the NAPL phase, the approaching water droplet is subject to only van der Waals attractions and the non-polar Keesom and Debye forces. The decay length of hydrogen bonds (a special kind of Keesom force) is much shorter than the van der Waals

forces. Thus, the surface must have a polar character to interact with the water phase across the NAPL film.

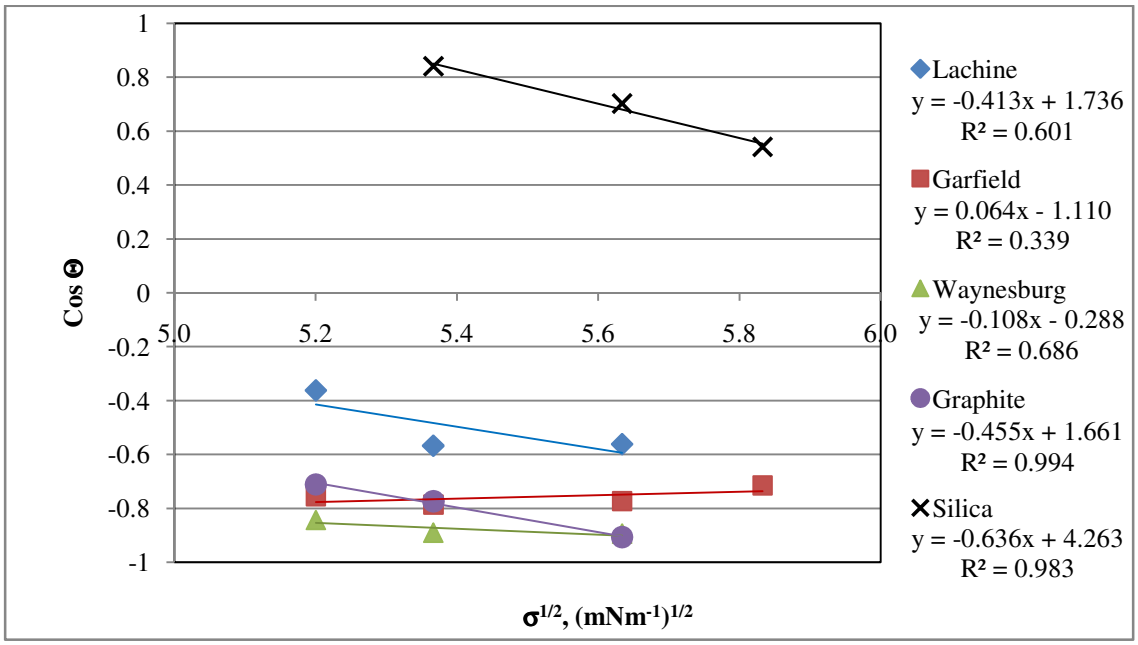

Figure 5.8, Application of the modified two-liquid Zisman approach to NAPL-water contact angle and NAPL surface tension.

	Material	ρ	R^2	γ_c, mNm^{-1}
NAPL-Water	**Lachine shale**	0.77	0.60	17.67
	Garfield shale	-0.59	0.34	NA*
	Waynesburg coal	0.83	0.69	NA*
	Graphite	0.99	0.99	13.33
	Quartz	1.00	0.98	44.93
Water-NAPL	**Lachine shale**	0.02	0.31	7.72
	Garfield shale	-0.15	0.79	20.66
	Waynesburg coal	-1.00	0.66	18.74
	Graphite	-0.99	0.86	19.82
	Quartz	-0.01	0.53	17.16

Table 5.6, Linear correlation statistics and predicted critical interfacial tension from the modified two-liquid Zisman approach (Figures 5.8 and 5.9). NA* Due to the slope of the linear fits, a γ_c could not be calculated for these materials.

Water-NAPL systems are shown in Figure 5.9. Contact angles were collected in water-air, water-DIM, water-ABN, water-PCE, and water-CTET systems for the carbon-containing soil materials and quartz (Table 3.4, 3.5, and 5.1). Water-air systems are included in Figure 5.9 because a water film is believed to separate the air bubble from the surface in the same way as it is believed to separate a NAPL drop from the surface. Talc is also shown even though only two points were collected because Figure 3.4 showed talc and graphite to have nearly identical wetting behavior. It is apparent from Figure 5.9 that they have very similar wetting behavior with respect to liquid surface tension as well. Table 5.6 lists the values of γ_C found from the intersection of the fitted lines with the $\cos(\Theta) = 1$ line.

Figures 3.3 and 3.4 indicated that, once immersed in water, all the solids studied are water-wet. The composition data in Figures 4.2-4.16 showed that the contact angle and degree of hysteresis in dry systems and NAPL-water systems could be correlated to surface composition, but the water-NAPL contact angle was not correlated to any composition parameter. Because water-NAPL contact angles show only a small variation from material to material, it was supposed that a water film separates the surface from the NAPL droplet. The water film is believed to be less than 10 angstroms in thickness (Hirasaki, 1991; Israelachvili, 1992). So the contact angle is believed to be essentially that formed by a NAPL resting on water rather than on the solid. Because the liquids considered in this study are all non-polar, the dispersion component of water, γ_W^D, would be expected to be the value of the critical interfacial tension, γ_C.

The fact that all of the water immersion cases in Figures 3.4, 3.5, and 3.5 were water-wet, regardless of the droplet phase or the solid composition suggests that, when the solid is immersed in water prior to the placement of a drop on the surface, a water film remains between the drop and the surface. Figure 5.9 supports this hypothesis. The lowest surface energy point is for water-air systems which draws all the lines to the water-air surface tension dispersion component, γ_W^D, of 21.8 mJm^{-2}. The Garfield and quartz plots, consisting of five data points each, suggest that the surface tension trend lines would converge to this point even if the water-air system was not included. Since the NAPLs are non-polar, only the non-polar, dispersion, component of the water surface is indicated. In other words, if Equation 5.1 was applied to a water surface interacting

with non-polar liquids the contact angles predicted would match those of the water-NAPL systems.

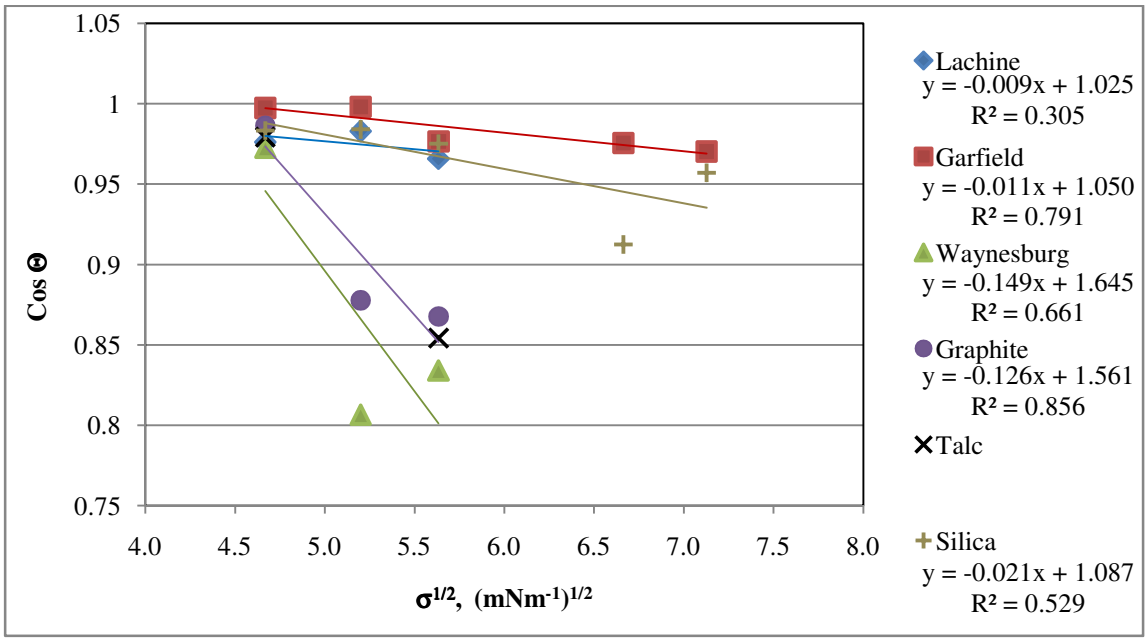

Figure 5.9, Application of the modified two-liquid Zisman approach to water-NAPL contact angle and NAPL surface tension.

5.5 Correlation between individual surface energy components and contact angle

The Zisman approach attempts to estimate an energy paramenter, γ_C, from contact angle data. The previous sections have shown that the Zisman approach can be successfully applied to analyze the magnitude of the contact angle of one fluid versus another on the same surface. Also, the Zisman approach offers proof that a water film prevents NAPLs from actual contact with the surface in water-NAPL systems. In both the single liquid systems (air-water-solid) and the two-liquid systems (NAPL-water-solid), the solid surface components determined using the van Oss-Good-Chaudhury method supported the conclusions drawn from the Zisman diagrams. This section will attempt to directly correlate the contact angle data from NAPL-water-solid systems with the calculated surface energy components to evaluate whether the surface energy components can be used in a predictive fashion. Air-water, air-glycerol, air-formamide, air-DIM, and air-ABN were used to calculate the surface energy components while air-water, PCE-water, CTET-water, TCA-water, and TCE-water-solid systems were used to

evaluate the correlation between surface energy components and contact angle in NAPL-water systems.

Figures 5.10 and 5.11 show the total polar surface energy component, γ_S^{AB}, for each of the eight materials studied versus the contact angle of NAPL-water systems. Since the air-water system is used in the calculation of surface energy components, that system shows a strong correlation. The air-water system is included in this analysis because it is an example of a system (like the NAPL-water cases) where there is not expected to be a water film preventing contact between the drop and the solid. Table 5.7 lists the Pearson correlation coefficient, ρ, and the coefficient of determination of the linear fit shown on the graph, R^2. Because the relationship between γ_S^{AB} and contact angle appears to be less linear at high γ_S^{AB} values, it is not recommended that the linear regressions be used for surfaces where more than 25% of the total surface free energy is due to polar forces such as the non-hysteretic materials, calcite, dolomite, and quartz examined here. An easy determination of hysteretic wetting could be made with a bottle test or a qualitative contact angle observation and then, if the material demonstrates wettability hysteresis, a contact angle for similar organic liquids can be estimated from the linear regressions given in Figure 5.10.

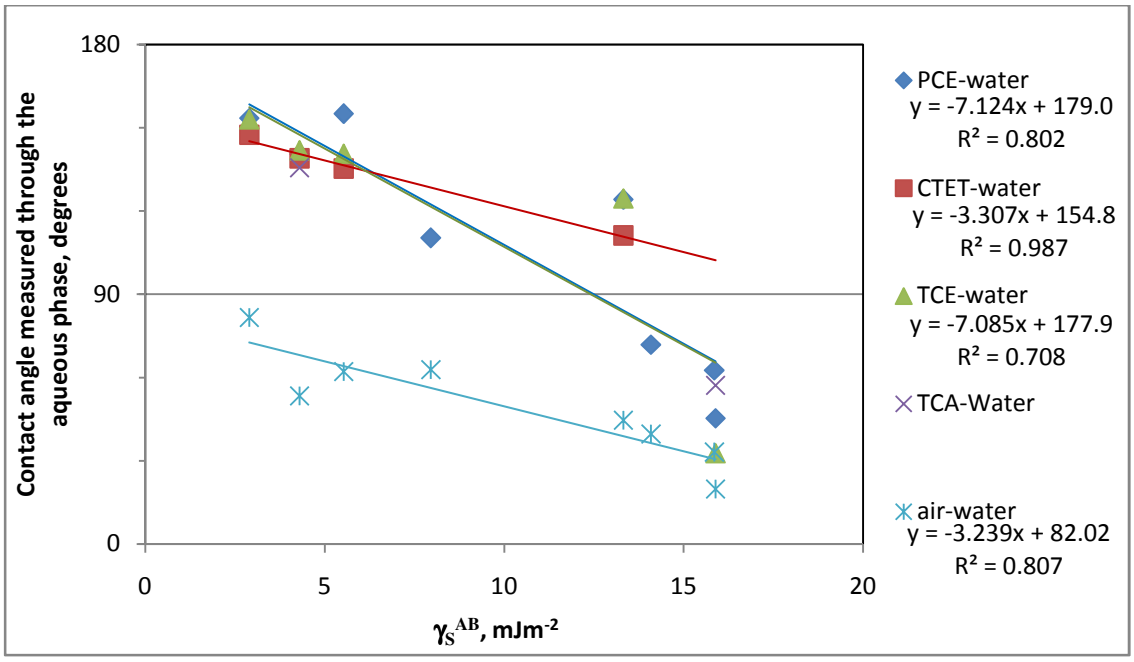

Figure 5.10, Linear correlations between solid acid-base surface energy component, γ_S^{AB}, and NAPL-water contact angle.

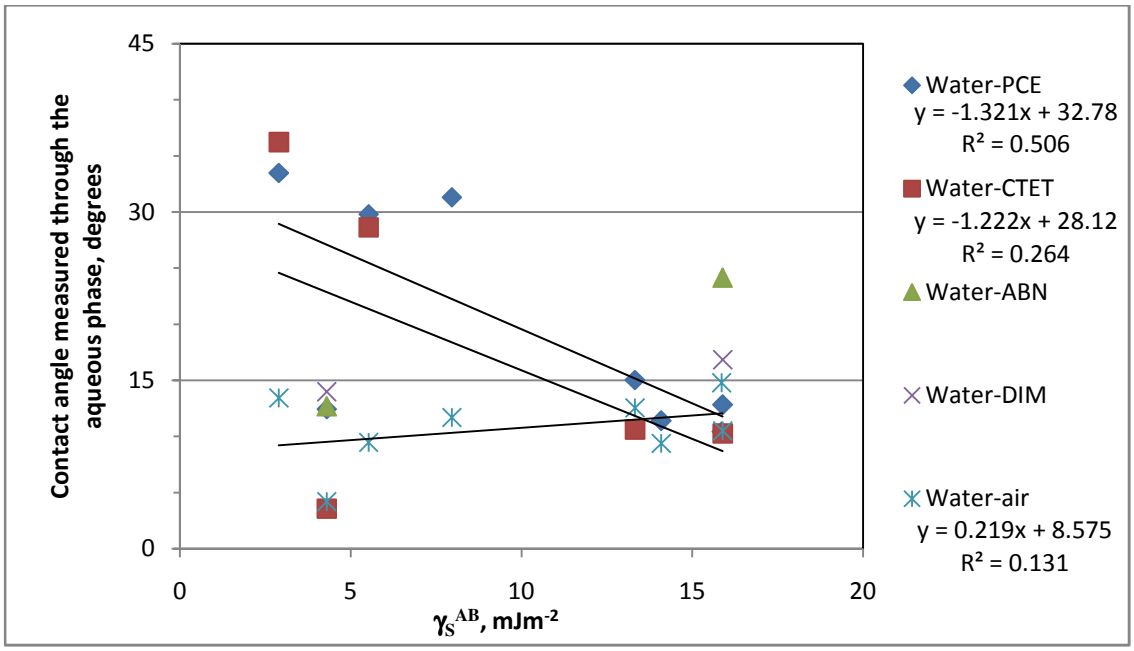

Figure 5.11, Linear correlations between solid acid-base surface energy component, γ_S^{AB}, and water-NAPL contact angle.

The linear fits between γ_S^{AB} and the contact angle for water-NAPL cases (Figure 5.11) show a low R^2, indicating there is not a reliable correlation between the two variables. This is not surprising, given the results of Section 5.4 which suggested that the water-NAPL systems consist of a NAPL drop resting on a water film so the spreading of the NAPL drop would depend on the interaction between it and the water phase, not between it and the solid. The fact that water-DIM and water-ABN contact angles are not correlated to the polar surface energy of the solids, γ_S^{AB}, even though air-DIM and air-ABN systems were used to determine these values, adds to the evidence that the NAPL is not interacting with the solid surface.

γ_S^{AB} and NAPL-Water contact angle (Figure 5.10)				γ_S^{AB} and Water-NAPL contact angle (Figure 5.11)			
System	**N**	**R^2**	**ρ**	**System**	**N**	**R^2**	**ρ**
PCE-Water	8	0.80	-0.90	**Water-PCE**	8	0.51	-0.71
CTET-Water	4	0.99	-0.99	**Water-CTET**	5	0.26	-0.51
TCE-Water	5	0.71	-0.84	**Water-TCE**	**Not Measured**		
Air-Water	8	0.81	-0.81	**Water-Air**	8	0.13	0.36

Table 5.7, Statistics describing the linear correlation between solid acid-base surface energy component, γ_S^{AB}, and contact angle.

Figure 5.12 shows the correlation between the ratio of surface dispersion forces to total surface forces, γ_S^D/γ_S, and the contact angle for NAPL-water systems. This parameter was expected to work well as a predictive tool in NAPL-water systems because the less polar the surface, the closer the surface force balance fits Equation 5.1. γ_S^D/γ_S works well to predict contact angle for a surface whose interaction is made up of 75% dispersion forces or more for totally non-polar liquids such as PCE and CTET. It appears that the lower the NAPL-water interfacial tension, the less polar the system can be before the relationship becomes non-linear. This is analogous to the use of critical interfacial tension plateaus in the three-phase Zisman approach of Guy et al. (1996). More soil materials in the 65% to 75% dispersion force range could be used to define the drop-off point more clearly. Table 5.8 gives the statistical measures of correlation for both the NAPL-water and water-NAPL systems. Similar to the case of the relationship between γ_S^{AB} and water-NAPL contact angles (Figure 5.11), the fraction of dispersion energy does not correlate well with the contact angle in these systems (Figure 5.13). In both cases, the poor correlation is probably due to the lack of interaction with the actual solid surface.

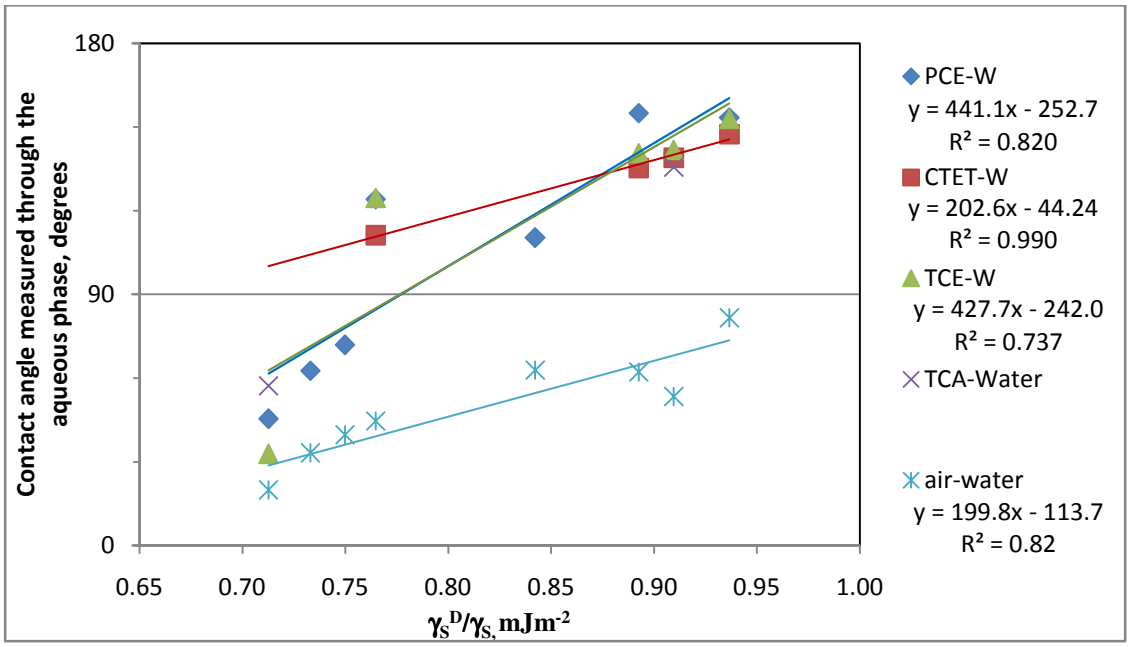

Figure 5.12, Linear correlations between the ratio of solid dispersion energy component to total solid surface energy, γ_S^D/γ_S, and NAPL-water contact.

γ_S^D/γ_S and NAPL-Water contact angle (Figure 5.12)				γ_S^D/γ_S and Water-NAPL contact angle (Figure 5.13)			
System	**N**	**R^2**	**ρ**	**System**	**N**	**R^2**	**ρ**
PCE-Water	8	0.82	0.91	**Water-PCE**	8	0.49	0.80
CTET-Water	4	0.99	1.00	**Water-CTET**	5	0.27	0.52
TCE-Water	5	0.74	0.86	**Water-TCE**	**Not Measured**		
Air-Water	8	0.82	0.91	**Water-Air**	8	0.11	-0.33

Table 5.8, Statistics describing the linear correlations between the ratio of solid dispersion energy component to total solid surface energy, γ_S^D/γ_S, and contact angle.

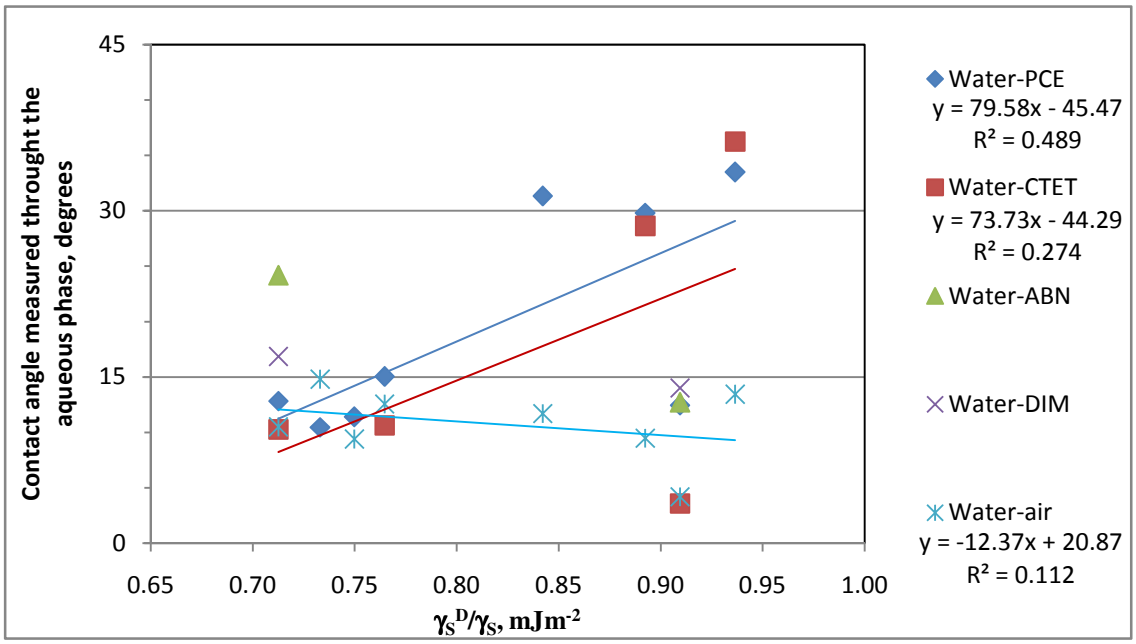

Figure 5.13, Linear correlations between the ratio of solid dispersion energy component to total solid surface energy, γ_S^D/γ_S, and water-NAPL contact.

5.6 Use of solid-droplet interfacial energy to predict contact angle

Table 5.9 lists the regression parameters for linear fits between the contact angles and the solid-NAPL interfacial energy, γ_{SL1}, and the solid-water interfacial energy, γ_{SL2}, in NAPL-water-solid systems (Figure 5.14). These data series show a somewhat linear correlation with contact angle but the R^2 values are still low. As the interfacial energy between the solid and the NAPL or air phase increases, the solid actually becomes water-wetting, perhaps because the weaker attraction between the surrounding NAPL and the solid allows the water drop to approach the solid surface. This results in stronger polar interactions between the drop and the solid, causing the drop to spread. Figure 5.15 shows the relationship between γ_{SL1} and water-NAPL contact angles. Linear fits are not shown since, as expected, the NAPL-solid interaction has little relationship to water-NAPL contact angle where a water film separates the NAPL drop from the actual solid surface. Table 5.9 also includes statistics for linear fits of the correlation between solid-water interfacial energy, γ_{SL2}, and contact angle in water immersion cases. A plot of these data showed a large scatter about the linear fit lines so it is not shown here.

Correlation between γ_{SL1} and NAPL-water Contact Angle (Figure 5.14)			
System	**N**	**R^2**	**ρ**
PCE-Water	8	0.56	-0.75
CTET-Water	4	0.95	-0.97
TCE-Water	5	0.40	-0.63
Air-Water	8	0.66	–0.82

Correlation between γ_{SL1} and Water-NAPL Contact Angle (Figure 5.15)				Correlation between γ_{SL2} and Water-NAPL Contact Angle (Not shown)			
System	**N**	**R^2**	**ρ**	**System**	**N**	**R^2**	**ρ**
Water-PCE	8	0.01	0.09	**Water-PCE**	8	0.74	0.86
Water-CTET	5	0.03	-0.16	**Water-CTET**	5	0.64	-0.16
Water-TCE	**Not Measured**			**Water-TCE**	**Not Measured**		
Water-Air	8	0.00	-0.03	**Water-Air**	8	0.05	-0.23

Table 5.9, Statistics for linear correlations between solid-liquid interfacial energies and water-NAPL-solid system contact angles, by liquid pairs.

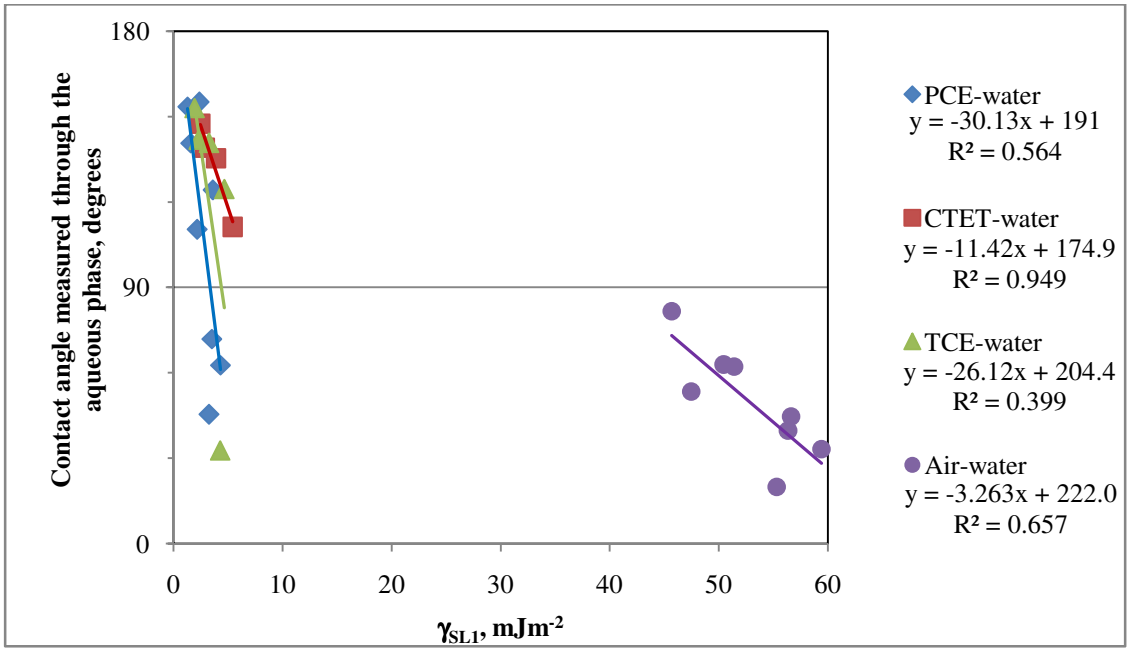

Figure 5.14, Linear correlations between solid-NAPL interfacial energy, γ_{SL1}, and NAPL-water contact angle.

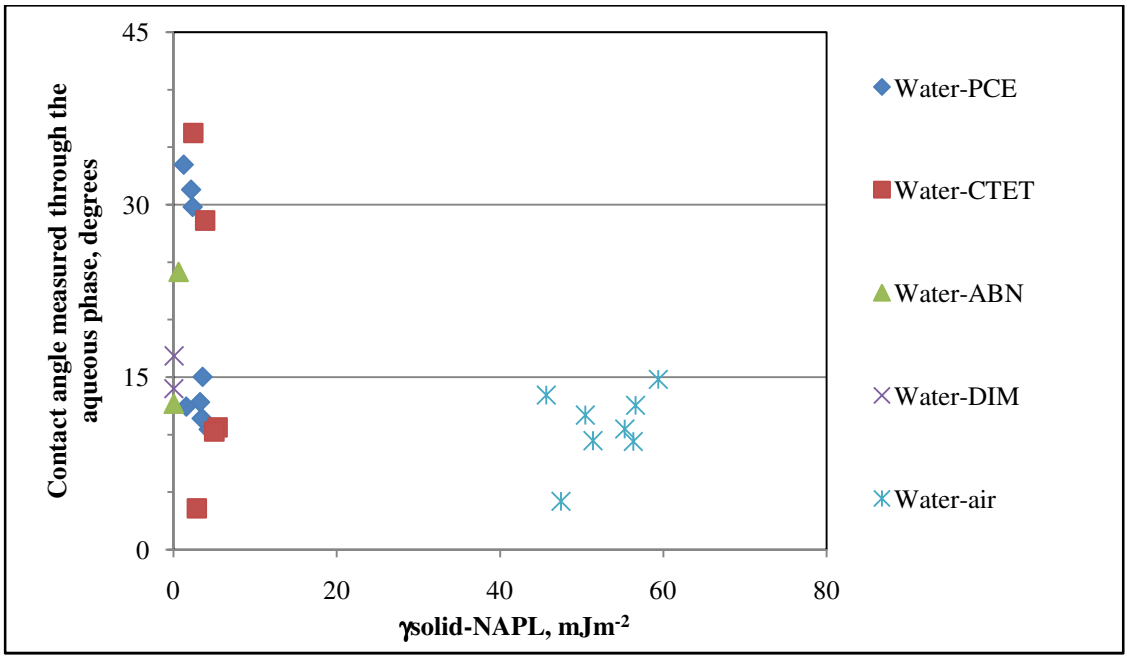

Figure 5.15, Linear correlations between solid-NAPL interfacial energy, γ_{SL1}, and water-NAPL contact angle.

In a NAPL-water system, the Young equation describes a balance between the NAPL-solid forces and the NAPL-water drop forces. Each of these forces is a sum of polar and non-polar force components. The statistics summarized in Table 5.10 suggest that the dispersion component of the solid-NAPL interfacial energy, γ_{SL1}^{D}, is not correlated to NAPL-water contact angles. Section 5.5 already showed that polar forces, generated by the solid's oxygen content, influence the wettability more than dispersion forces so these results corroborate previous observations.

System	N	R^2	ρ
PCE-Water	8	0.44	0.66
CTET-Water	4	0.00	-0.04
TCE-Water	5	0.62	0.79
Air-Water	8	0.27	0.52

Table 5.10, Statistics for linear correlations between the dispersion component of the solid-NAPL interfacial energy, γ_{SL1}^{D}, and contact angle, by liquid.

The acid-base or polar interactions between the surface and liquids are expected to be well correlated to contact angle because it has already been shown in Sections 4.3

and 4.5 that the oxygen content of the surface is definitively linked to wettability and wettability hysteresis. Table 5.11 lists the statistics for the correlations between the contact angle and the polar component of the solid surface tension, γ_S^{AB}, in water-NAPL-solid systems. Figure 5.16 shows the variation in NAPL-water contact angle as a function of the polar component of the interfacial tension between the solid and NAPL phase, γ_{SL1}^{AB}. As the polar interaction between the NAPL and solid increases, the contact angle decreases, resulting from the increase in the polar interaction between the solid and water.

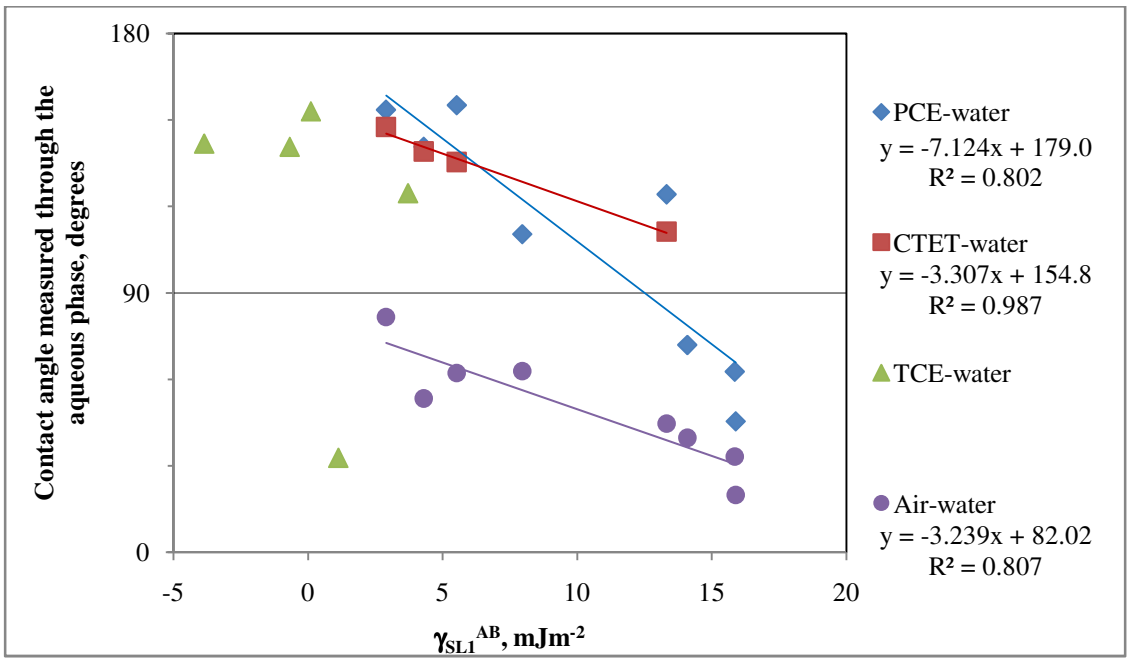

Figure 5.16, Linear correlations between the acid-base component of the solid-NAPL interfacial energy, γ_{SL1}^{AB}, and NAPL-water contact angle.

Correlations between γ_{SL1}^{AB} and NAPL-water contact angle (Figure 5.16)			
System	**N**	**R^2**	**ρ**
PCE-Water	8	0.80	-0.90
CTET-Water	4	0.99	-0.99
Air-Water	8	0.81	-0.90
Correlations between γ_{SL1}^{AB} and Water-NAPL contact angle (Not shown)			
System	**N**	**R^2**	**ρ**
Water-PCE	8	0.51	-0.71
Water-CTET	4	0.26	-0.51
Water-Air	8	0.13	0.36

Table 5.11, Statistics for linear correlation between the acid-base component of the interfacial energy between the solid and NAPL phases and water-NAPL-solid contact angles, by liquid pairs.

5.7 Use of solid-droplet interfacial energy accounting for the surrounding liquid phase to predict contact angle

Figure 5.17 and Table 5.12 describe the total interaction between each soil material and water given the presence of a surrounding NAPL phase, $\gamma_{SL2,L1}$. In this case, the air-water systems, with contact angles less than 90°, control the slope of the linear regressions. Also, moving from the lower left corner to the upper right corner, the materials progress from the least to most water repellent. Table 5.12 and Figure 5.18 show that the water-NAPL system contact angles cannot be predicted from the interaction between the surface and NAPL phase, even accounting for the intervening water phase. This observation is consistent with the previous observations that the solid surface properties, such as composition or surface energy components, have little influence on water-NAPL systems. Accounting for the surrounding phase does not dramtically improve the linear correlation between interfacial energy and contact angle for NAPL-water-solid systems relative to the results ignoring this phase (Section 5.6).

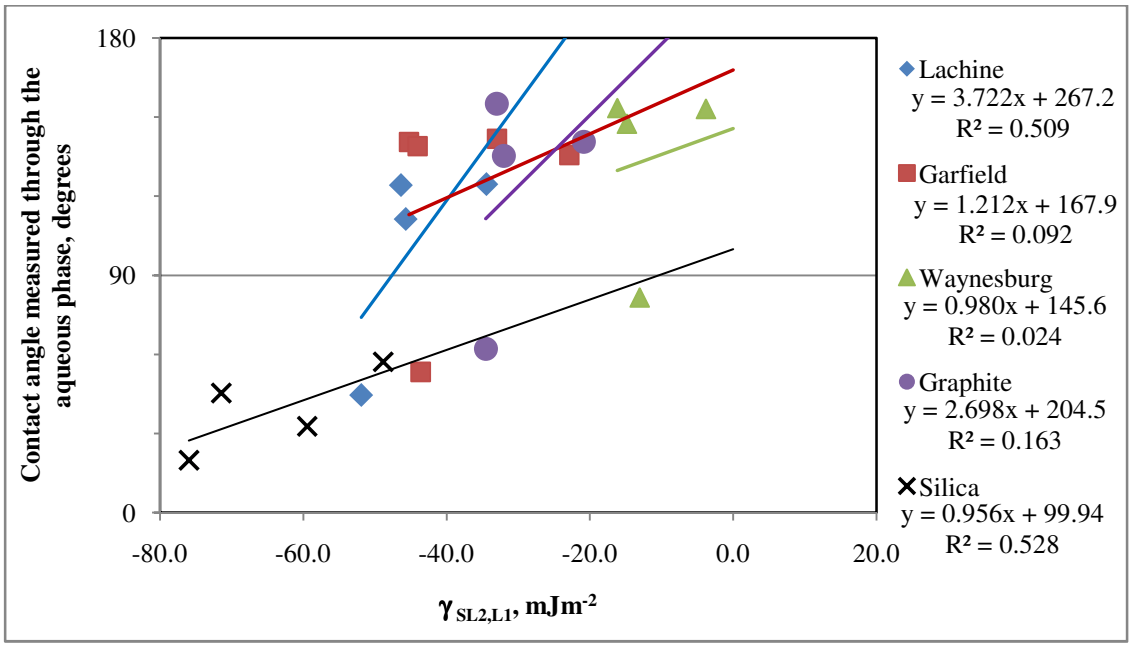

Figure 5.17, Linear correlations between solid-water drop interfacial energy given the presence of the surrounding NAPL phase, $\gamma_{SL2,L1}$, and NAPL-water contact angle.

$\gamma_{SL2,L1}$ and NAPL-Water systems (Figure 5.17)				$\gamma_{SL1,L2}$ and Water-NAPL systems (Figure 5.18)			
System	**N**	**R^2**	**ρ**	**System**	**N**	**R^2**	**ρ**
Lachine shale	4	0.51	0.71	**Lachine shale**	4	0.01	-0.09
Garfield shale	5	0.09	0.30	**Garfield shale**	5	0.22	-0.47
Waynesburg coal	4	0.02	0.16	**Waynesburg coal**	4	0.99	1.00
Graphite	4	0.16	0.40	**Graphite**	4	0.96	0.98
Quartz	4	0.53	0.73	**Quartz**	4	0.12	-0.34

Table 5.12, Statistics for linear correlations between solid drop interfacial energy given the presence of the surrounding phase, $\gamma_{SL2,L1}$ and $\gamma_{SL1,L2}$, and NAPL-water-solid system contact angles.

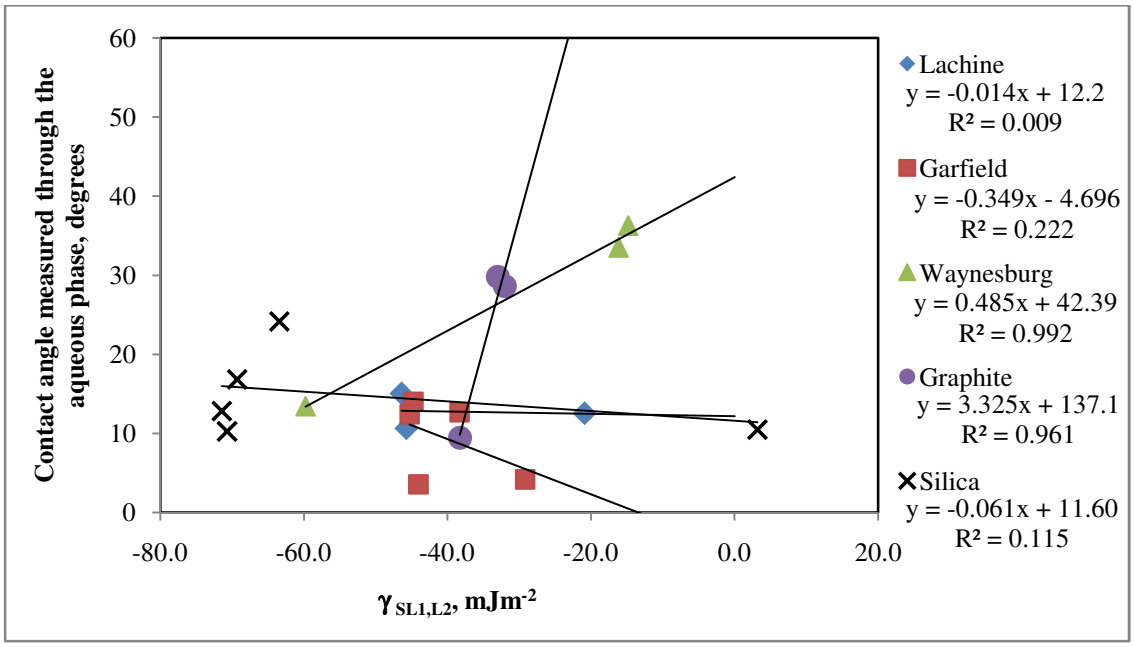

Figure 5.18, Linear correlations between solid-NAPL interfacial energy given the presence of the surrounding water phase, $\gamma_{SL1,L2}$, and water-NAPL contact angle.

Figure 5.19 shows the correlation between two-liquid phase interfacial energy and the behavior of individual NAPL-water systems for a variety of soil materials. $\gamma_{SL2,L1}$ is the solid-water drop interfacial tension given the presence of a surrounding NAPL phase. In the air-water system, this parameter is an excellent predictor of contact angle and $\gamma_{SL2,L1}$ could be used to estimate a contact angle in a system where the surface energy of the solid was known (for example from inverse gas chromatography measurements on a fine grained soil sample), but a suitable contact angle could not be measured. The linear fit may work well for PCE-water systems as well. Caution is advised in the CTET and TCE systems because there are fewer data points to support a linear model. The slope of the PCE and TCE curves is very similar and all the data sets point to the fact that as the force between the solid and water, $\gamma_{SL2,L1}$, increases, that is as it approaches -72.8 mJm^{-2}, the material becomes more water wetting. The correlation statistics for these series are given in Table 5.13.

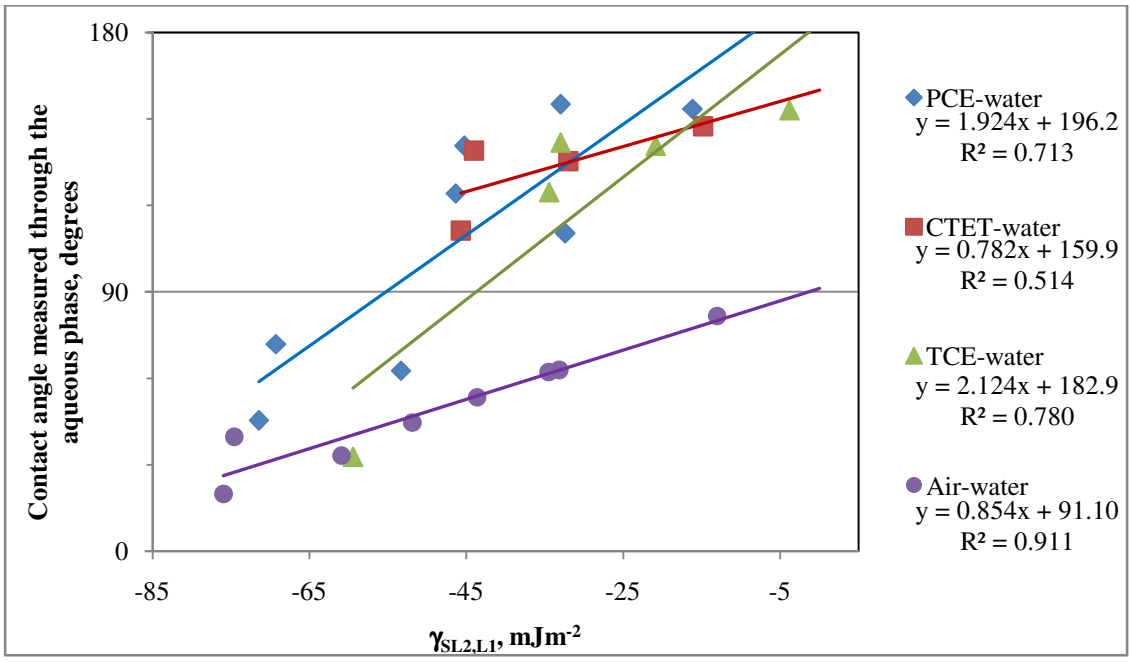

Figure 5.19, Linear correlations between solid-water interfacial energy, $\gamma_{SL2,L1}$, given the presence of the surrounding NAPL phase and NAPL-water contact angle.

Correlation between $\gamma_{SL2,L1}$ and NAPL-water contact angle (Figure 5.19)			
System	**N**	**R^2**	**ρ**
PCE-Water	8	0.71	0.84
CTET-Water	4	0.51	0.72
TCE-Water	5	0.78	0.82
Air-Water	8	0.91	0.95

Table 5.13, Statistics for linear correlations between solid-water interfacial energies accounting for the surrounding NAPL phase and NAPL-water contact angles.

Figure 5.20 shows the correlation between contact angle and the dispersion interaction between the solid and water drop, given the surrounding NAPL phase, $\gamma_{SL2,L1}^{D}$, for NAPL-water systems. The linear correlation parameters are given in Table 5.14. While the contact angles are strongly correlated to $\gamma_{SL2,L1}^{D}$, the linear fits are determined by the low surface tension of the air-water systems. It is unlikely that more liquids with high contact angles would provide a better correlation since it's already been shown that the oxygen content and polar forces control wettability rather than the carbon content and dispersion forces.

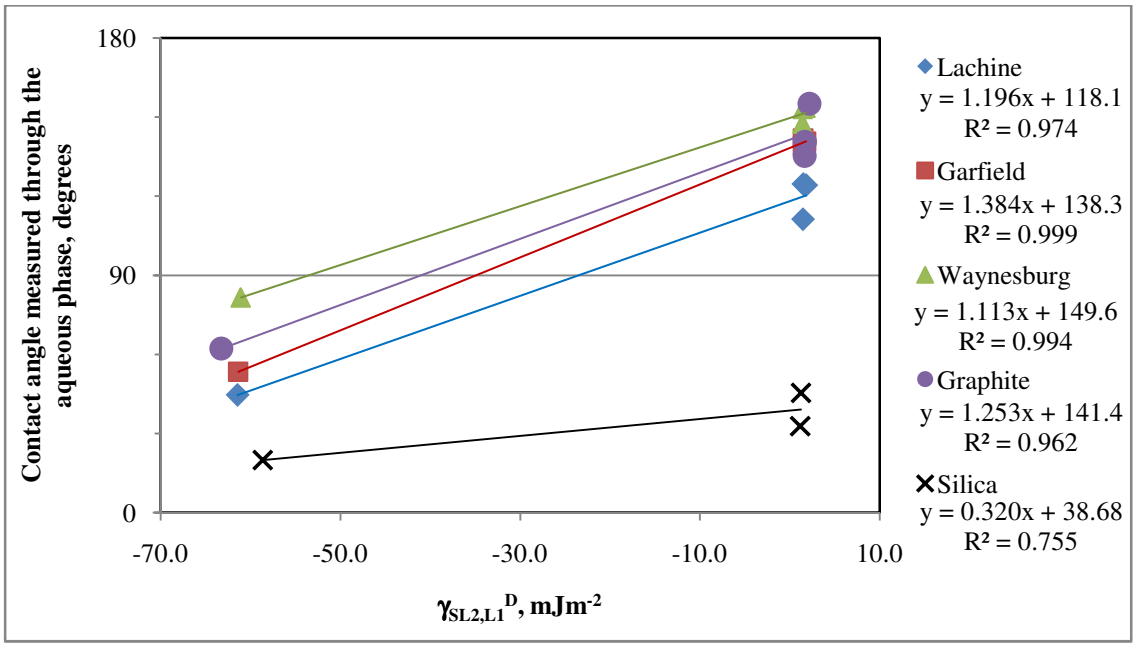

Figure 5.20, Linear correlations between the dispersion component of the solid-water drop interfacial energy, given the presence of a surrounding NAPL phase, $\gamma_{SL2,L1}^{D}$, and NAPL-water contact angle.

γ_{SL2}^{D} and NAPL-Water contact angle, (Figure 5.20)			
System	**N**	**R^2**	**ρ**
Lachine shale	4	0.97	0.99
Garfield shale	5	1.00	0.65
Waynesburg coal	4	0.99	1.00
Graphite	4	0.96	0.98
Quartz	3	0.76	0.00

Table 5.14, Statistics for linear correlations between the dispersion component of the solid-water drop interfacial energy, given the presence of a surrounding NAPL phase, $\gamma_{SL2,L1}^{D}$, and NAPL-water contact angle.

Figure 5.21 shows the dominating effect of polar forces on the contact angle as well. As the polar interaction between the solid and the water phase accounting for the NAPL phase, $\gamma_{SL2,L1}^{AB}$, increases in absolute magnitude, the solid becomes more water-wet. TCE-water behavior is not predicted as well as the behavior of the less polar liquids,

PCE and CTET, because the Quartz-TCE-water system contact angle is water-wetting. Being slightly polar, TCE interacts more with the water phase and the polar components of the surface. The corresponding water-NAPL contact angle system statistics are given in Table 5.15 but the data are not shown graphically. The linear fits are not as good, with R^2 less than 0.75.

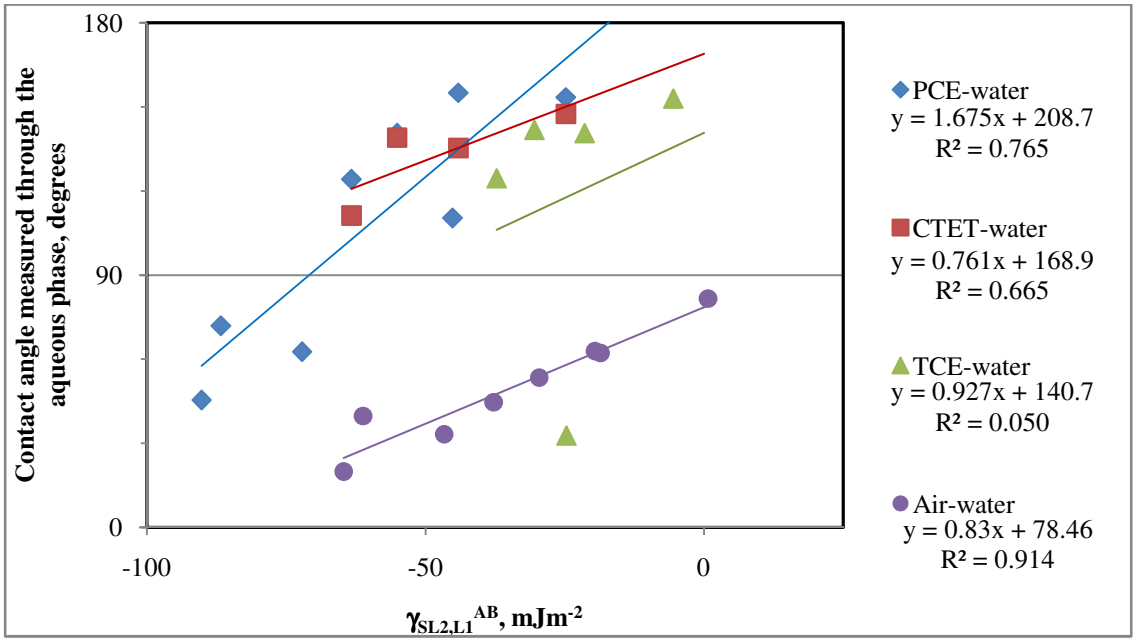

Figure 5.21, Linear correlations between the acid-base component of the solid-water interfacial energy given the presence of the surrounding NAPL phase, $\gamma_{SL2,L1}^{AB}$, and NAPL-water contact angle.

Correlations between $\gamma_{SL2,L1}^{AB}$ and NAPL-water contact angle (Figure 5.21)			
System	**N**	**R^2**	**ρ**
PCE-Water	8	0.77	0.88
CTET-Water	5	0.67	0.82
TCE-Water	5	0.05	0.22
Air-Water	8	0.91	0.96
Correlations between $\gamma_{SL2,L1}^{AB}$ and Water-NAPL contact angle (Not shown)			
System	**N**	**R^2**	**ρ**
Water-PCE	8	0.65	-0.80
Water-CTET	4	0.53	-0.73
Water-TCE	**Not Measured**		
Water-Air	8	0.06	-0.25

Table 5.15, Statistics for linear correlation between the acid-base component of the interfacial energy between the solid and NAPL phases and water-NAPL-solid contact angles, by liquid pairs.

5.8 Correlation between surface free energy and wettability hysteresis

Figure 5.22 shows that the wettability hysteresis increases as the percentage of surface forces due to dispersion increases. That is, as the solid becomes more non-polar, the NAPL-water contact angle becomes more non-water wetting, but the water-NAPL contact angle does not change significantly. This is yet further evidence that the water-NAPL system does not depend on the solid properties. It also explains why the most polar materials, calcite, dolomite, and quartz, have the least wettability hysteresis. Table 5.16 gives the correlation parameters for wettability hysteresis versus surface energy properties.

Crawford et al. (1994) showed that contact angle hysteresis, the difference between the advancing and receding contact angle, increased as the mineral content of the surface increased. Crawford et al. suggested that, as the mineral content of the surface increases, the surface heterogeneity increases, causing a greater difference in contact angle between the advancing and receding cases. In the case of contact angle hysteresis, the advancing angle represents a drop enlarging and causing the surrounding phase to

recede. Crawford et al.'s samples were coals which are typically on the high end of carbon content for natural soil materials, with carbon to oxygen ratios of 5 or greater; so the only sample in this data set that is similar is Waynesburg coal. Crawford concluded that the advancing contact angle is determined by the oxygen functionalities of the coal carbon while the receding contact angle is due to the oxygen functionalities of the coal mineral matter. The same group of researchers also showed in Guy et al. (1996) that the hysteresis in critical interfacial tension between the advancing and receding cases increased as the carbon to oxygen ratio increased. In other words, increasing the carbon or non-polar character of the surface increases the critical interfacial tension of advancing drops more than the critical interfacial tension for receding drops. Here, as mineral content increases, the wettability hysteresis decreases, which is analogous to Guy' findings. The relationship between contact angle hysteresis and wettability hystereis is still unkown.

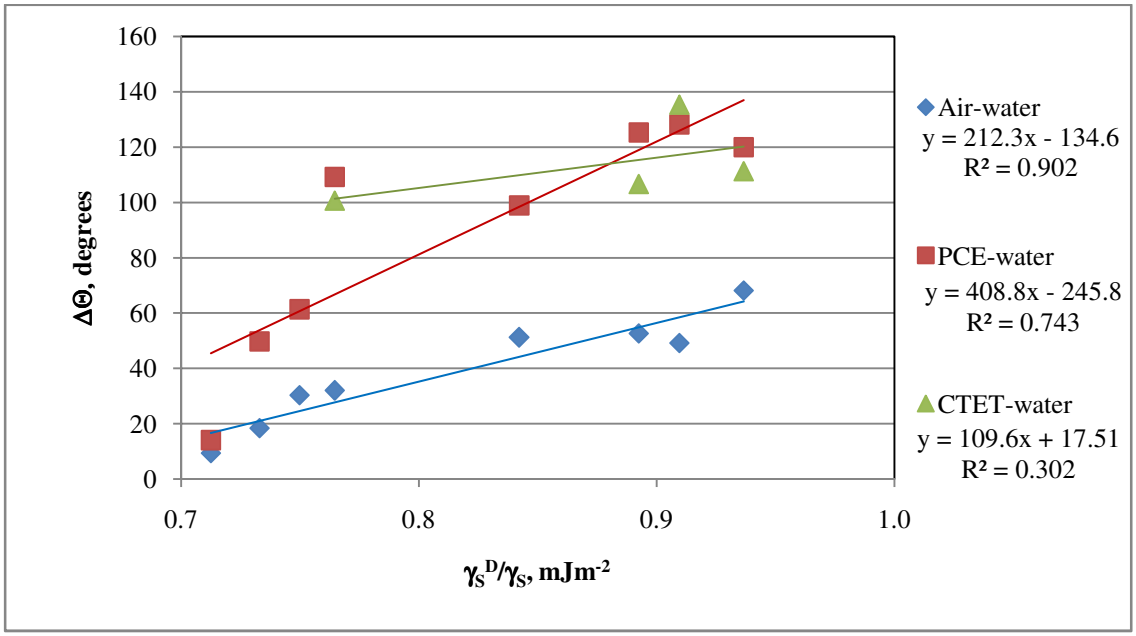

Figure 5.22, Linear correlations between the ratio of solid dispersion energy component to total solid surface energy, γ_S^D/γ_S and wettability hysteresis.

System		N	R^2	ρ
$\Delta\Theta_{Air\text{-}water}$	Correlation between the ratio of dispersion to total solid surface energy, γ_S^D/γ_S, and wettability hysteresis (Figure 5.22)	8	0.90	0.95
$\Delta\Theta_{PCE\text{-}water}$		8	0.74	0.86
$\Delta\Theta_{CTET\text{-}water}$		4	0.30	0.55
$\Delta\Theta_{Air\text{-}water}$	Correlation between polar solid surface energy component, γ_S^{AB}, and wettability hysteresis (Figure 5.23)	8	0.90	-0.95
$\Delta\Theta_{PCE\text{-}water}$		8	0.72	-0.85
$\Delta\Theta_{CTET\text{-}water}$		4	0.32	-0.57
$\Delta\Theta_{Air\text{-}water}$	Correlation between total solid surface energy, γ_S, and wettability hysteresis (Figure 5.24)	8	0.75	-0.87
$\Delta\Theta_{PCE\text{-}water}$		8	0.47	-0.69
$\Delta\Theta_{CTET\text{-}water}$		4	0.40	-0.63

Table 5.16, Statistics for linear correlations between surface free energy components and wettability hysteresis.

Figures 5.23 and 5.24 show similar trends to Figure 5.22. Figure 5.23 shows the variation in wettability hysteresis with polar surface energy component, γ_S^{AB}. As expected, increasing the polar surface energy decreases the wettability hysteresis. As the surface becomes more polar, the water-solid interactions become more dominant and the NAPL-water contact angle becomes closer to that in the water-NAPL case which, in both cases, is essentially the contact angle of a non-polar solvent resting on a highly polar surface, the mineral in NAPL-water systems and the water film in water-NAPL systems. It appears that the acid–base (polar) surface energy component is a very good predictor of wettability hysteresis.

Figure 5.24 shows that the total surface energy is somewhat correlated to wettability hysteresis. However, since the total surface energy encompasses both the non-polar (dispersion) and polar (acid-base) energies, which show opposing trends with respect to wettability hysteresis, the total surface energy is not as good an indicator of wettability hysteresis as the acid-base surface energy component.

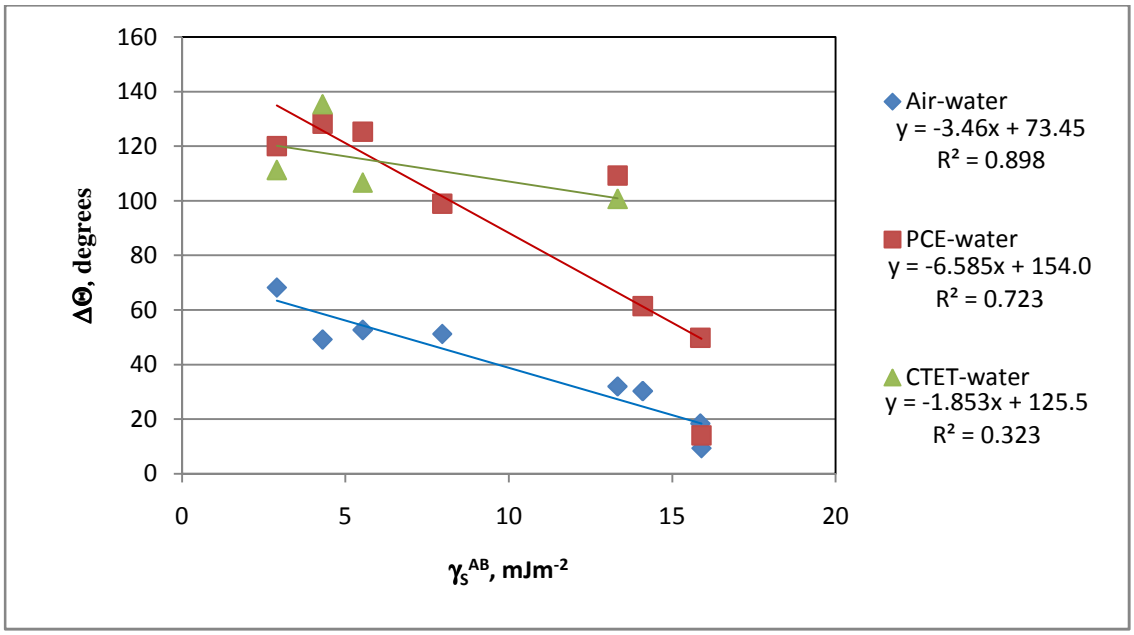

Figure 5.23, Linear correlations between the acid-base component of the solid-NAPL interfacial energy, γ_S^{AB}, and wettability hysteresis for all eight natural soil materials.

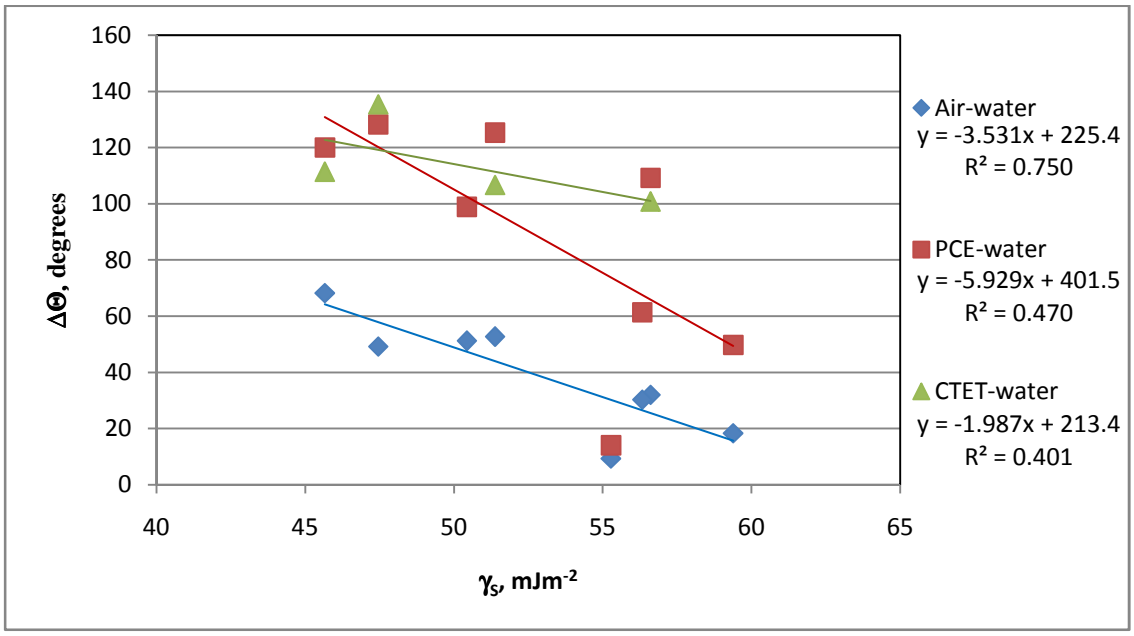

Figure 5.24, Linear correlations between solid surface energy, γ_S, and wettability hysteresis for all eight natural soil materials.

Given the linear fits shown in Figures 5.22 through 5.24, there appears to be several reliable methods to estimate the wettability hysteresis of a solid. Based on a single air-water contact angle value, the polar surface energy component can be estimated

using the regression presented in Figure 5.10. Using the estimated polar surface energy, the wettability hysteresis can then be estimated from Figure 5.23. The air-water system likely represents the lower bound of polar liquid wettability hysteresis because water has the greater polar character of any liquid and, therefore, the strongest interaction with the polar component of the surface. One limitation is that all the soil materials studied here are acidic monopoles. If the polar liquid is also a highly acidic monopole or if the surface is highly basic, the unknown system may not necessarily follow the trend of the air-water system. Rubber, latex, some fungi, and human skin are some natural basic monopoles. The PCE-water line can be used as an estimate of the behavior of a non-polar liquid system. As the liquid NAPL phase becomes more polar, the wettability hysteresis at any given solid surface energy characteristic is expected to fall within these bounds. Regression lines could be created for additional liquids to allow for more precision. For example, extending the CTET-water system line could provide a better estimate of the hysteresis expected with higher polarity solids because the single carbon CTET is even less polarizable than the double carbon bonded PCE and is, therefore, expected to have greater water contact angles and higher hysteresis in systems with more polar solids.

If the contact angle on the soil material is not known, the soil material composition can be used to estimate wettability hysteresis. The carbon or oxygen molar content can be compared with Figure 5.3 or 5.1 to estimate a value of γ_S^{AB} or γ_S^D/γ_S. These values can then be used in conjunction with Figures 5.22 and 5.23 to obtain an estimate of wettability hysteresis. Again, the air-water system describes the lower bound of wettability hysteresis and the PCE-water line is representative of a completely non-polar system.

5.9 Summary and conclusions

Calculations of surface free energies for aquifer materials show that these solids vary in polar and total surface energies. As the solids become more mineral in nature, the surface becomes more polar. The composition analysis presented in Sections 4.2 through 4.5 suggested this, but a quantitative description of the forces present at each soil material surface could not be determined from composition alone. Figures 5.1 through 5.3 show that surface energy components are linearly correlated to soil material composition.

The Zisman and modified Zisman approaches can be reliably applied to predict the dispersion character of highly non-polar surfaces, but the Zisman approach does not seem to be applicable to solids that have more than 25% polar character. However, the Zisman approach requires several contact angles of homologous liquids. Application of the modified Zisman approach to two-liquid phase water-NAPL systems shows that the critical solid surface tension γ_c is equal to the γ_W^D of water, 21.8 mJm^{-2}. This is evidence that a water film separates the NAPL from the surface, preventing NAPL-solid interaction. It offers an explanation as to why most water-NAPL contact angles are very similar, despite large variations in solid composition. Studies using surfactants show a wider range of water-NAPL contact angles, including NAPL wetting conditions, because the surfactants can disrupt the water film (Hiemenz and Rajagopalan, 1997; Lin et al., 2000).

The correlation of the surface free energy components and the contact angles of NAPLs shows that surface free energy components can be used to predict contact angles for an untested liquid in air-water and NAPL-water systems. The polar energy component, γ_S^{AB}, or the ratio of dispersion to total surface energy, γ_S^D/γ_S can be correlated to contact angles in air-water and NAPL-water systems but not to contact angles in water-NAPL systems. This once again shows that the surface energy properties, and thus the surface composition, have little bearing on water-NAPL system wettability. In the absence of surfactants that sorb to aquifer materials and alter their wettability, it appears the saturated zone will be water-wet regardless of the solid composition.

Once the surface energy components of the soil material are known, these can be combined with the surface energy components of the liquid to estimate the force between each solid-liquid pair. The intervening third phase, the surrounding liquid, can also be factored into the interaction. Again, the polar force, or the ratio of dispersion to total force, is the important parameter for predicting the contact angle. A ratio of 25% polar character or less is necessary to use γ_S^D/γ_S. Carbon content had already been shown to be an unreliable predictor of contact angle in Section 4.2. In this chapter, it is shown that this is likely because the total van der Waals interaction, γ_S^D, which is correlated to

carbon content (Table 5.2), is not a reliable predictor of contact angle. Again, the contact angles in water-NAPL systems are not well correlated with surface properties.

Finally, wettability hysteresis is strongly correlated with the polar surface energy component. Because the contact angles in water-NAPL systems are essentially the contact angle of a NAPL droplet resting on the water surface, rather than on the solid surface, wettability hysteresis decreases as the solid becomes more polar. Two methods were presented to estimate wettability hysteresis for similar acidic monopolar surfaces based on a single contact angle or the composition of the soil material. If an air-water contact angle is known for the material, this can be used to estimate the polar surface energy component and then that value can be used to estimate wettability hysteresis. Alternatively, the solid composition can be used to estimate the polar surface energy component which, in turn, can be used to estimate the wettability hysteresis.

CHAPTER 6

CONCLUSIONS AND RECOMMENDATIONS FOR FURTHER STUDY

6.0 Overview

Multiphase flow in the subsurface depends on the interfacial forces between soil solids and the liquid phases. The interfacial forces arising from the molecular interactions across the soil-liquid and liquid-liquid phase boundaries determine which liquid preferentially spreads over the solid. However, the solid-liquid interfacial tensions are not known for many natural systems. It has been suspected that heterogeneous soil composition might contribute to the wettability heterogeneity and differences in fluid distribution across field sites, yet this relationship heretofore is somewhat anecdotal rather than rigorously examined.

The wettability of several air-liquid-solid and liquid-liquid-solid systems was systematically examined in Chapter 3. The liquid phases included water, PCE, and CTET. The soil materials ranged from minerals such as quartz, calcite, dolomite, and talc to amorphous carbon-based materials such as Lachine shale, Garfield shale, Waynesburg coal, and graphite. They also varied in geological maturity.

It was shown that there is significant difference between the contact angle of soil materials immersed in the water phase, as they would be in the subsurface saturated zone, and soil materials immersed in the NAPL phase, as they may be in the vadose zone. This difference in contact angle, which depends on the order of fluid contact with the surface, was given the term wettability hysteresis. The assumption that contact angles are similar to quartz for all materials in the saturated zone appears accurate since all the solids examined here were water-wet if immersed in water. However, solids immersed in the NAPL phases or air dry displayed a greater variability in contact angle. The length of equilibration time between the soil materials and the immersion liquid did not affect the contact angle. The wettability hysteresis did not appear to be due to equilibration times,

as lengthening the equilibration to 80 days did not affect the contact angle. The soil materials themselves did not strongly alter the surface or interfacial tension of the liquid phases, although such an impact can only explain slight differences in contact angle and cannot explain wettability hysteresis since wetting or non-wetting character is determined by the difference between the solid-liquid interactions.

The composition of the solids was analyzed to determine if the wettability of soil materials varied systematically with composition. The contact angle in water immersion cases was independent of solid composition, but in air-dry and NAPL immersion cases, the composition of the solid was strongly correlated to the contact angle. The NAPL-water contact angles were most strongly correlated to oxygen indices (molar oxygen content and O/C molar ratio) and only weakly correlated to carbon-based indices. This suggests that it is the polar surface interactions that govern contact angle. The degree of wettability hysteresis was also better correlated with oxygen indices than carbon indices reinforcing the hypothesis that the polar character of surfaces determines their wettability, not the non-polar content. This concept is logical because non-polar interactions are present between all materials, over longer separation distances than polar interactions, while polar interactions only occur when each material has a monopole opposing that of the other phase. Since the NAPL-water contact angles measured here decreased with increasing solid oxygen content but water-NAPL contact angles were relatively similar across all soil material compositions, the hysteresis decreased with increasing solid oxygen content. As the solid becomes more polar, through higher oxygen content, the difference between the NAPL-solid interaction, determining the NAPL-water contact angle, and the NAPL-water film interaction, determining the contact angle in water-NAPL systems, is reduced. Essentially, as the surface is oxygenated it can form more hydrogen bonds with liquids at the surface. Thus, the NAPL-water contact angle on oxygenated surfaces is more water wetting.

Surface functional groups were analyzed by FT-IR and NMR to examine the carbon and oxygen functional groups at the solid surfaces. The carbon-based soil materials decreased in polar functional groups from Lachine shale to graphite in both the FT-IR and NMR spectra. A detailed examination of the functional groups did not reveal any particular functional group associated with water- or NAPL-wetting behavior.

However, in general, the oxygen found in the least water-wetting materials was associated with large aromatic or long chain hydrocarbon groups that are less polarizable. Methyl type groups were more common in the soil carbon of the less water-wetting and more hysteretic materials. Although two minerals examined here, calcite and dolomite, contain significant carbon, it is ionically bonded to oxygen so the surfaces remained water wet in all cases. Talc is a highly hysteretic mineral with similar wettability to graphite even though it contains no carbon. Bulk composition or functional group analysis alone then cannot truly explain the magnitude of the NAPL-water contact angles or the degree of wettability hysteresis.

The goal of the surface energy component analysis presented in Chapter 5 was to determine what component controls the contact angle since it did not appear to be a specific type of functional group. Surface energy components were calculated and shown to correlate well to soil material composition. It was suggested from the wettability hysteresis and composition data that the mechanism of wettability hysteresis may be the formation of a persistent water film that separates the NAPL from the solid in water immersion cases so that the composition of the soil material does not influence wettability in these cases, while the contact angle in air-dry and NAPL immersion systems is determined by the surface composition of the solid. It was shown that contact angles in water immersion cases are not, in fact, generated by interactions between the NAPL phase and the solid. Applying the Zisman approach to estimate the dispersion component of the solid in water-NAPL cases showed that the surface presented to the drop had approximately the same dispersion energy as water, suggesting that a water film is present between the surface and the NAPL droplet. Correlations of the NAPL-water contact angle with solid surface energy and solid-liquid interaction energies showed that, in every system examined here, the polar (acid-base) energy component was the best predictor of contact angle, followed by the ratio of dispersion to total surface energy. The soil materials displaying wettability hysteresis were those with greater than 70% dispersion energy component.

Wettability hysteresis was also shown to be strongly correlated to the surface energy components. The NAPL-water contact angle, and hence wettability hysteresis, decreased with increasing solid polarity. Wettability hysteresis is a different

phenomenon from contact angle hysteresis. In the former case, a drop of each fluid is brought in contact with the surface while the second fluid must recede to allow the drop to form a stable interface. So, in wettability hysteresis, the three-phase contact line is always moving over a surface that has not yet contacted the droplet phase. In the latter case, a droplet is brought in contact with a surface and then withdrawn such that the three-phase line of contact must move over area previously contacted by the droplet. The air-water-solid system provides a lower bound on wettability hysteresis while the PCE-water-solid system provides an upper bound since PCE is completely non-polar. Two methods to predict wettability hysteresis without necessitating numerous contact angle measurements were presented. If the oxygen composition of the solid is known, it can be used to estimate the contact angle directly, or it can be used to estimate the polar surface free energy component, which can then be used to estimate a contact angle. If an air-water contact angle is known, it can be used to estimate the polar surface free energy component and that can be used to estimate wettability hysteresis in another liquid system.

6.1 Implications

The assumption that the capillary behavior of natural materials in the saturated zone is similar to that of quartz systems is probably a good assumption when there are no surfactants present. This is because this research indicates that a persistent water film separates the solid from the pure NAPL phase, regardless of the solid composition. Thus, when surface-active species are absent, particle size, porosity, and tortuosity variations may be more important parameters for determining the liquid distribution in the saturated zone than solid composition.

Near the surface or in the vadose zone, air-dry carbon-containing natural solids are more water repellent than the minerals studied, with the exception of talc, but they are still water wet. Thus, water will occupy the smallest soil pores regardless of the system composition when there are no NAPLs present. However, when NAPLs contact dry soil they will fill the smallest soil pores. NAPL in the vadose zone is likely to have a highly heterogeneous fluid distribution because the solid surface energy components, which vary with soil composition, directly determine the contact angle when NAPL encounters

air dry solids. When water floods the vadose zone after a NAPL has contacted dry soils, there may be a higher residual saturation of NAPL because the pendular regions of water filling the crevices between soil grains may be smaller and the blobs of NAPL filling the central pore spaces may be larger than expected based on water-NAPL systems. From a modeling standpoint, it is now clear that a single contact angle or capillary pressure-saturation curve cannot fully describe the interfacial behavior of the vadose and saturated zones because the wettability will depend on multiple factors including the composition of the solids and the the presence or absence of soil pore water. However, the contact angle in the vadose zone and the degree of hysteresis between the vadose zone and saturated zone may now be estimated from soil material composition if the system history is known.

The assumption of water wetting in all water immersion systems is not necessarily a reliable assumption for real organic waste liquid or petroleum sites, where the liquids are likely to contain surface active species. These compounds have been shown to be capable of reversing wettability from the native state in both NAPL-water and water-NAPL systems (Denekas et al., 1959; Powers and Tamblin, 1995; Buckley et al., 1998). The influence of surfactants in a water-NAPL-solid system may very well depend on the composition and surface energy components of the solids because surfactant molecules can alter or even disrupt the water film. Surfactant systems are possibly more sensitive to equilibration time as well. Thus, the water-NAPL contact angle in surfactant systems, which are more representative of the conditions at waste liquid sites, may not be independent of the solid phase. Wettability hysteresis effects may also be more complex when surface-active species are present.

6.2 Ongoing research needs

The NAPLs used in this study were highly non-polar. Many of the linear regressions shown in Chapter 5 could be improved by measuring the contact angle of additional fluids, including NAPLs that are more polar than PCE and CTET, on the natural soil materials. Furthermore, the natural solids used here were all acidic monopoles so additional measurements using some basic solids might reveal different trends. pH may be an important system variable determining the acidity or basicity of the

measured surface free energy components since the protonation of many solid surfaces is pH dependent. For this study, a dry solid was defined as one that had been dried exposed to the laboratory atmosphere, thus the water content at the surface was low but not zero. However, surfaces in the vadose zone experience varying humidity levels. An investigation into the water content and water film thickness of vadose zone soil materials would aid in determining whether the degree of humidity influences wettability hysteresis. Important and unexplored system parameters regarding the effects of humidty on wettability include the thickness and variability of surface water films, the reversibility of NAPL or water wetting once established in porous media, and the influence of the level of soil humidification on the water film and water-NAPL wetting behavior. Also, naturally occurring porous media have internal porosity that provides a location for water to condense, the occurrence of which was likely reduced by the relatively smooth rock faces used in this study.

As described above, most NAPL samples from actual waste sites are expected to include surface active components. In addition, extracellular material from soil micro-organisms, colloidal soils, and nano-sized particles may disrupt the surface water film stability even when soil materials are immersed in the saturated zone. Theoretically the van Oss-Chaudhury-Good model can be extended to three-phase systems with the surface energy components calculated from solids immersed in any phase, not only air and water; however, this approach has not been utilized for natural materials. One limitation is the availability of probe phases with appropriate surface tensions to form sessile drops. A second approach could be to invert the van Oss-Good-Chaudhury approach to investigate the surface energy components of fluids from real waste sites or surfactant containing model phases. This might be accomplished by measuring contact angles of one liquid against three solids of known surface energy components. Comparisons between the interfacial activity of different solutes and surfaces could then be made. Using this approach, the change in aqueous phase surface energy components due to alterations in properties that may affect the water film such as pH, ionic strength, and redox condition can be examined.

Finally, the soil materials in this study were created from cut rock faces of model materials present in soils. This limited the quantitative analysis to hard carbon materials

such as shales rather than humic materials. Humic materials may act in similar ways as surfactants to influence the water film separating NAPLs from the surface in water-NAPL systems because they add many functional groups to the surface. The van Oss-Chaudhury-Good model has been applied to capillary rise measurements in powders and sands successfully (Siebold et al., 1997) and could conceivably be applied to humic sands utilizing capillary pressure curves or capillary rise experiments.

In conclusion, wettability heterogeneity in the subsurface is likely and can be partially explained by the presence of wettability hysteresis, a previously unacknowledged variation in contact angle depending on the condition of the surface before contact with a NAPL. Wettability and wettability hysteresis vary with soil material composition because changing the solid composition alters the solid-liquid interfacial tensions, and hence, the force balance that determines wettability and multiphase flow. The systems included in this study were based on smooth, flat, solid phases and pure liquid phases. The approaches used to assess the model systems could be expanded to examine the role of the solids in wettability determination in real field multiphase systems.

APPENDIX A

EFFECTS OF IONIC STRENGTH AND pH ON WETTABILITY

A.0 Introduction

Water phase conditions such as ionic strength, pH and redox state may affect the contact angle, particularly in water-NAPL systems. Ionic strength affects the thickness of the electrostatic double layer surrounding soil particles in solution. This, in turn, affects the extent to which electrostatic forces can attract water molecules to the surface and displace the NAPL molecules. For example, Svitova et al. (2002) found that potassium chloride did not strongly affect the wettability of three surfaces in oil-water systems but calcium chloride did change the zeta potential values of the surfaces and hence the wettability. In a study using carbon tetrachloride and trichloroethylene drops immersed in water, Barranco et al. (1997) demonstrated that increasing ionic strength caused quartz slides to become slightly more water-wet as the quartz-water interfacial tension decreased. Alkane-water contact angles on metal surfaces have also been shown to be dependent on ionic strength (Davis et al., 2003). When surfactants are present, the ionic strength can impact the alteration of interfacial tension and surface sorption thereby affecting the contact angle (Serrano-Saldana et al., 2004). Van Oss (1993) has suggested that the Coloumb forces contributing to the surface free energy can be considered a separate component from the polar forces described by γ_S^{AB}. Since neither the NAPL phases nor the air phase possess permanently charged groups, this component was neglected from all surface energy treatments in Chapter 5, but could become important if charged solutes were active in the liquid phases.

The charge of a mineral surface varies with pH as surface groups dissociate in contact with the aqueous phase. When immersed in the water phase, there is a particular pH that will provide the correct amount of hydrogen ions to balance the positive and negative sites. This neutral point is termed the isoelectric point (IEP). For quartz (and

silica sand) the IEP is near a pH of 2 (Parks and de Bruyn, 1962). Thus, below pH 2 the surface is positively charged and above pH 2 it is negatively charged due to the dissociation of the surface hydroxyls. Isoelectric points reported for coals are in the pH range of 5-6 (Orumwense, 1998). pH dependent contact angles have been demonstrated in the literature (Zhou et al., 1998; Fuerstenau and Colic, 1999; Gribanova et al., 2000). Ward et al. (1999) studied the thickness of the aqueous film separating a hydrocarbon drop from a quartz slide and found that it varied with pH. Barranco et al. (1997) showed that for carbon tetrachloride and trichloroethylene drops immersed in aqueous solution, the contact angle peaked at pH 2. Although the range of contact angle values in Barranco's study was very narrow, it can be concluded that the quartz was very slightly less water wet at its IEP.

All water-NAPL and water-air systems in Chapters 3, 4, and 5 were exposed to the atmosphere during contact angle measurement, and thus highly oxidized. The pH in the experiments described in Chapters 3-5 was maintained between 6.8 and 7.2 except for NAPL receding cases where the water drop pH was not measured but before equilibration the water phase was neutral. The ionic strength of the systems was controlled by the use of 0.01 M NaCl as the aqueous phase. When the pH was adjusted, the lowest concentration HCl or NaOH solution possible was used to maintain the ionic strength although the final ionic strength was not measured for confirmation.

A.1 Methods

The effect of ionic strength on contact angle was investigated by comparing the contact angle of PCE drops resting against quartz surfaces immersed in aqueous phases of 10^{-4} to 2 M NaCl. As described in Section 2.7, the systems were equilibrated for 7 days prior to measurement. The pH was not adjusted because addition of acid or base solution would affect the ionic strength of the systems, but the pH was recorded.

Contact angles were measured as a function of pH to investigate the effect of pH on wettability. For these measurements, water-PCE-quartz systems were equilibrated as described in Section 2.7. On the sixth day of equilibration, the pH was adjusted to the desired value using HCl and NaOH solutions between 1 and 10^{-2} M as needed. The ionic strength alterations were not recorded.

A.2 Effects of ionic strength on wettability

Figure A.1 shows the contact angle of water-PCE systems versus sodium chloride concentration. There is no clear trend with ionic strength until the effects of pH are simultaneously considered. For these systems the pH was not controlled which is different from the study of Barranco et al. (1997). It was noted that at a given ionic strength, the system with a lower pH produced a higher, less water wetting, contact angle. This is expected because at lower pH, the solid is closer to the IEP value of quartz, pH 2, and thus more neutrally charged. The data set is broken into two series, pH 7.3 to 7.9 and pH 7.9 to 8.9. From Figure A.1, it appears that ionic strength has a minor effect of quartz wettability, in all cases quartz remains strongly water-wet, but no quantitative relationship can be determined because the effect of pH was not simultaneously controlled.

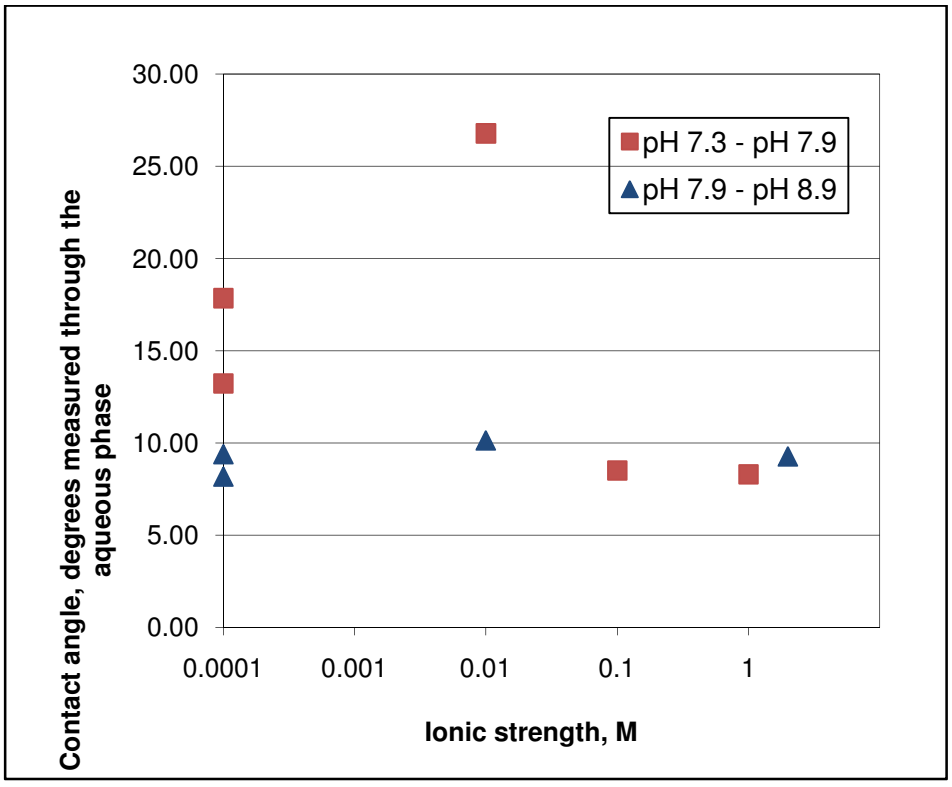

Figure A.1, Effect of NaCl concentration on water-PCE-quartz contact angle.

A.3 Effect of pH on wettability

Figure A.2 below shows the contact angles collected for PCE drop, water immersion systems as a function of the aqueous phase pH. The maximum contact angle is expected to occur near the isoelectric pH. Similar behavior has been observed by Orumwense (1998) for a series of coals in contact with oils. Figure A.2 appears inconclusive. One complicating factor is that the ionic strength was not controlled or recorded and the two factors, pH and ionic strength cannot be separated. Thus, two samples may have different contact angles at a similar pH. This is the same problem observed with the examination of ionic strength in Section A.2.

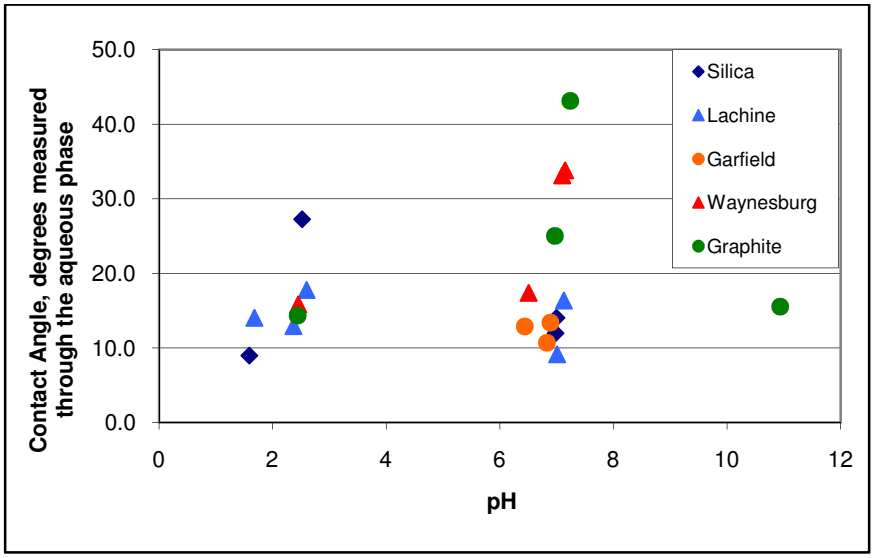

Figure A.2, PCE-water contact angles as a function of pH.

A.4 Conclusions and recommendations for future study

Although both pH and ionic strength are believed to influence contact angle values, the preliminary experiments shown here indicate that this effect is secondary to wettability hysteresis when solutes such as surface-active agents are absent. It is believed that pH and ionic strength must both be controlled to isolate trends in contact angle behavior. As shown in Chapters 3 and 5, the surface itself has little effect on the water receding contact angle when surfactants are not present but if pH and ionic strength influence the thickness of the surface water film, they may alter the level of interaction between NAPL drops and the surface in water immersion cases. Analogous experiments

in air-water or NAPL-water experiments may have different variations in contact angle as a function of pH and ionic strength. Finally, the effects of pH and ionic strength also may be more dramatic when other solutes are present in the liquid phases. Future experiments that may yield more conclusive results should measure the pH and ionic strength simultaneously.

APPENDIX B

RELATIONSHIP BETWEEN ZETA POTENTIAL AND WETTABILITY

B.0 Zeta potential

Zeta potential is defined as the electrical charge at the edge of the Stern layer. So strictly speaking, it is not the electrical charge of the solid surface itself. It is however the electrical potential experienced by a drop that approaches the surface. Both pH and ionic strength influence the zeta potential value of surfaces. Thus, using zeta potential as a descriptor of the aqueous phase condition may be a viable method to correlate the effects of aqueous phase fluid properties on wettability rather than deciding it from the individual effects of ionic strength and pH.

Zeta potential has been extensively correlated to suspended particle stability in the literature. For example, Fuerstenau et al. (1983) have presented a relationship between zeta potential and collector efficiency in the flotation of mineral ores. The relationship between zeta potential and polymer wettability was considered by Welzel et al. (2002) who observed changes in the speciation of the solid interface but did not observe contact angle differences. Drzymala found that zeta potential and surface charge were not singularly related to wettability. Wu et al. (2001) showed that the surface speciation of carbon and carbide solids could be linked to zeta potential measurements. Dubey and Doe (1993) showed that the pH at which the wettability of sands in contact with crude oil and brine switched from oil to water wetting was correlated to zeta potential. It has also been recognized that zeta potential effects are an additional component in the total solid surface energy by van Oss (1993).

B.1 Methods

A ZetaProbe (Colloidal Dynamics, Warwick, RI) was used to determine the isoelectric point and zeta potential curve for Ann Arbor II sand, Lachine shale, Garfield shale, Waynesburg coal, graphite, and silica. Six grams of dry soil that had been ground

to a size of less than 53 μm was placed in a 600 mL glass bottle. 0.01 M NaCl solution was then added until the total mass was 200g, producing a 3% (by mass) solution of particles. A PTFE coated magnet was used to stir the solution. Garfield shale, Waynesburg coal, and graphite particles tended to remain at the surface so the bottles of these systems were also shaken to force the particles into suspension. The pH of each bottle was adjusted to 9 using dropwise addition of 1 M NaOH. The bottles were then capped and mixed once daily for a week so that the surfaces and solution could equilibrate.

The ZetaProbe pH electrode was calibrated between each measurement. The electro-acoustic probe was calibrated monthly. On the seventh day of particle-fluid equilibration, the sample was poured into a clean ZetaProbe sample chamber. The samples were mixed at 175 rotations per minute throughout the measurement. The pH probe and two automatic pipetters were placed in the sample through the lid of the sample chamber. 0.5 M HCl was used as the titrant. The samples were titrated from the equilibrated high pH to about 1.7. The ZetaProbe automatically added small increments of acid allowing two minutes of equilibration between each aliquot, until the desired pH step was reached. At least 20 points were taken on each curve. For each data point on a sample curve, the signal given by a NaCl solution of the same conductivity was subtracted to remove the electrolyte background signal.

For zeta potential measurements after contact with PCE, soil particles sieved to less than 53 μm were placed in 40 mL jars with Teflon caps. 30 mL of PCE was allowed to equilibrate with the soil for one week. The soil particles were separated from the PCE using a vacuum filter. The filter cake was allowed to dry in a fume hood over night. The air dried particles were then suspended at 3% (by mass) ratio in 0.01 M NaCl solution. The suspensions were given at least 24 hours to re-equilibrate before measuring the zeta potential as described above.

B.2 Determination of zeta potential and isoelectric point

Figure B.1, A-F shows the zeta potential curves collected for each material. The solid symbols are the zeta potential of soil particles suspended in a 0.01M NaCl aqueous solution. The open symbols are particles equilibrated in PCE, separated by vacuum

filtering, and re-suspended in 0.01M NaCl aqueous solution. A single representative curve is displayed for each material and equilibration fluid although at least three were collected. Table B.1 shows the isoelectric points determined for each case. One difficulty in collecting the zeta potential of natural soil materials by the electrical acoustic method is that the dielectric constant of the material is required as input for the measurement. The dielectric constant is used to determine the expected vibration of the particles. It was estimated based on information provided in the operating manual for the Zetaprobe. Also, the density and size of the particles are necessary input values. The density of the particles is shown on Table 2.4. The particles were assumed to be spheres less than 30 μm in diameter, but in reality, the shale, coal and graphite particles are highly angular so 30 μm only describes the smallest radius. As the ionic strength increases, particle aggregation may also increase due to the compression of the water layer at the solid surface, so the effective particle size changes. The chamber was mixed at a high speed to provide sheer forces to reduce aggregation, but it was still observed that the effective particle size increased as more titrant was added and pH decreased.

Material	**Water Equilibrated pH of IEP**	**PCE Equilibrated pH of IEP**
Silica	1.7	1.9
Ann Arbor II	1.8	DNM
Lachine Shale	2.0	3.1
Garfield Shale	6.7	5.6
Waynesburg Coal	6.6	6.6
Graphite	> 11.2	6.6

Table B.1, Isoelectric pH of soil materials in 0.01 M NaCl aqueous solution. DNM = Did Not Measure.

From Table B.1 it is evident that the humic based soil and the Lachine shale will have similar electrostatic contributions to the total solid surface energy as quartz. This is not surprising given that these soil materials have a large silica component. The Garfield shale consistently gave an isoelectric point between 6.5 and 6.9. Although the estimated IEP for the Waynesburg coal is 6.6, numerous repeat evaluations were necessary, as this

material responded more slowly than the others to the addition of acid or base. The pH of Waynesburg samples was often significantly lowered after equilibration which may be due to the high surface area of the particles, as they appeared more porous than the other materials. The coal also very likely contains non-silicate mineral oxides that influence the pH through dissolution. Once the Waynesburg coal suspension had been equilibrated at low pH, if it was then brought to a higher pH the solution appeard cloudy and dark yellow. At neutral pH, it was very slightly yellow. Graphite was slightly positively charged over the entire pH range considered. It may become negatively charged at pH values higher than eleven but it was not possible to test this range without raising the electrolyte concentration so high that the background signal swamped the sample signal. The positive charge measured was very slight. This may be due to the fact that graphite is electrically conductive and therefore not expected to produce a large electro-acoustic response which is necessary for measurement with the ZetaProbe equipment. The pH values listed in Table B.1 were used as the IEPs for contact angle measurements in Section B.3.

PCE presence did have some effect on the IEPs but the measurements do not show a consistent trend. For silica, Ann Arbor II sand, and Lachine shale, the presence of PCE appeared to slightly reduce the negative zeta potential measured above the IEP. The IEP was slightly elevated when PCE is present. This may be due to a blocking of negatively-charged surface sites so that the surface became neutral at a lower hydrogen ion concentration (higher pH). For Garfield shale, the presence of PCE reduces the magnitude of the zeta potential and slightly lowers the IEP. The zeta potential curve is very similar for Waynesburg with and without exposure to PCE. In the case of these two higher carbon materials, the blockage of surface sites by PCE may be less pronounced since the charged sites are expected to cover a lower percentage of the surface. The graphite particles have an increased zeta potential signal after PCE exposure. In the case of graphite the may occur because PCE itself gives an electro-acoustic signal but the graphite particles give very little signal due to their conductivity. For the other materials, the relative proportion of the PCE signal to the particle signal is probably small. This electro-acoustical zeta potential method does not show a consistent loss of surface charge after contact with PCE. This probably indicates that the PCE was removed during the

vacuum filtration step and the soil material surfaces after exposure to PCE are not all that different from the dry soil materials suspended in water directly.

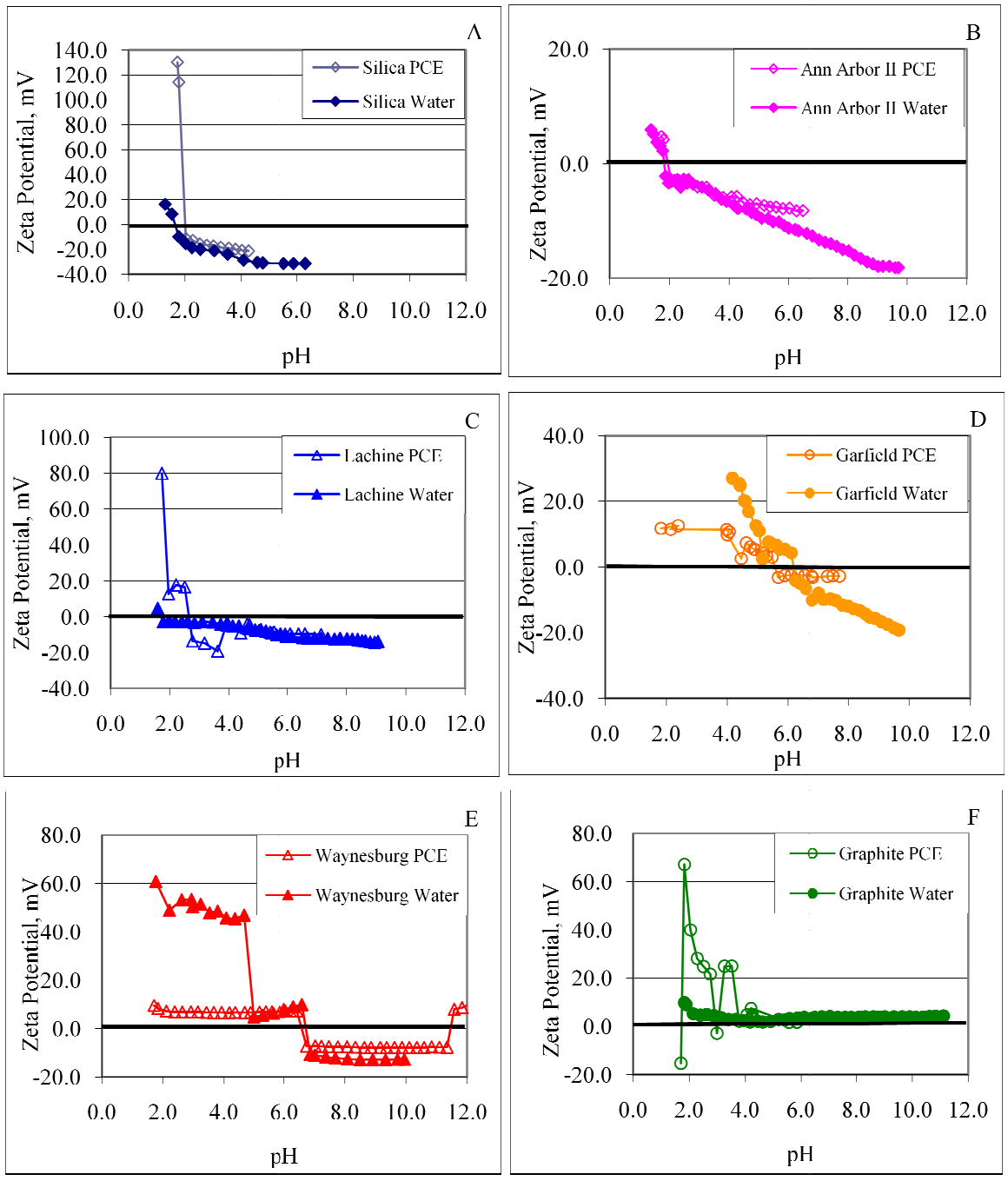

Figure B.1, Zeta potential of A) Silica Sand, B) Ann Arbor II Sand, C) Lachine Shale, D) Garfield Shale, E) Waynesburg Coal, F) Graphite.

B.3 Relationship between zeta potential and wettability

Figure B.2 shows the water receding, PCE advancing contact angle at pH 7 (solid symbols) versus the contact angle at the IEP of each material (open symbols). The contact angle is higher at pH 7, when the surfaces are more charged. For Waynesburg coal and Graphite, the change in contact angle between pH 7 and the IEP is dramatic and may be related to the small fraction of hydroxyl mineral sites at the surface. Even slight changes in pH may be enough to change the proportion of protonated hydroxyl sites. It is unclear, however, why the soil materials are more water wet at the IEP than at pH 7. One possibility is that the ionic strength of the solutions is higher at the IEP because 0.1 M HCl and 0.1M NaOH have been added to adjust the pH. The addition of electrolyte typically increases the interfacial tension between the aqueous and organic phases and may exaggerate the contact angle, making the surfaces appear more water-wet. Figure B.2 suggests that it is the change in hydrogen bonding caused by the changing nature of the surface at variable pH and ionic strength.

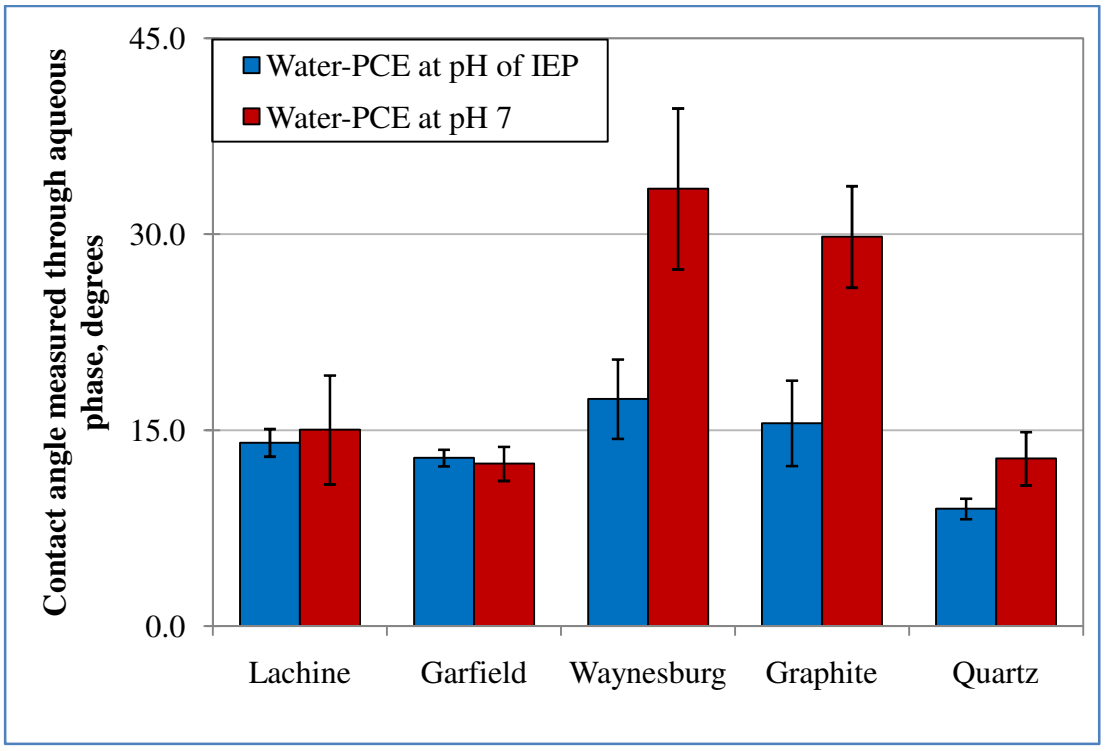

Figure B.2, Water-PCE contact angles at pH 7 and the isoelectric pH of each material.

Figure B.3 shows that there is a zeta potential of maximum organic wetting, although this may not be at the IEP. It was expected that there would be a parabolic trend to the contact angles as a function of zeta potential based on the results reported by Orumwense (1998). The zeta potential values assigned to the x-axis of the graph were determined by measuring the contact angle at a single pH and then matching that pH to a zeta potential titration plot such as those in Figure B.1. The pH of the contact angle systems was adjusted from neutral to the desired pH manually, rather than by a titration from high pH so the ionic strength and direction of approach of the systems do not necessarily match, a source of difference in the zeta potential values. The particle systems have a significantly higher surface area than the contact angle systems so much more acid or base is needed to satisfy the surface hydroxyl groups when adjusting the pH and a higher ionic strength may result. There is a significant change in contact angle, as much as 28.8° in the case of graphite, depending on the aqueous solution pH. Contact angles at more pH values are necessary to truly define the curves. Also, if the zeta potential data were re-assessed accounting for particle size variation, angularity, and the more precise dielectric constants, the curves may shift to align with a maximum contact angle at a zeta potential equal to zero.

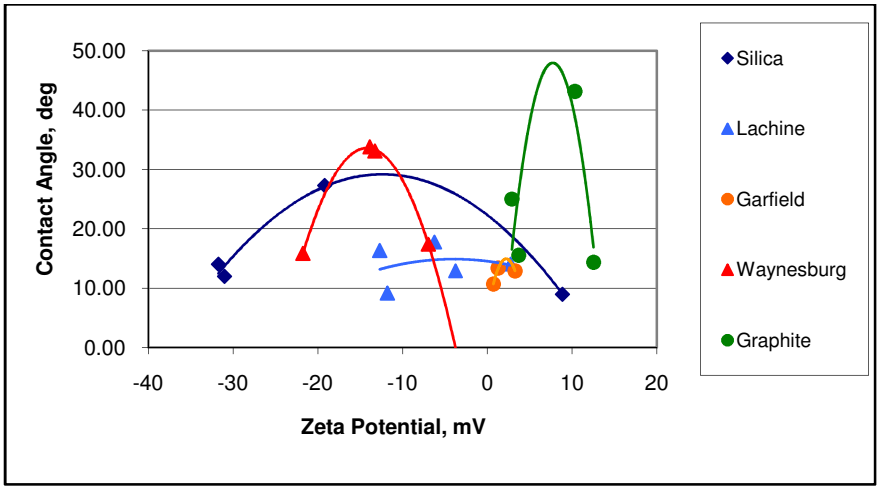

Figure B.3, Water receding, PCE advancing contact angles for each material as a function of zeta potential.

B.4 Conclusions and recommendations for future work

The zeta potential of surfaces immersed in water may influence wettability but the trends from the exploratory experiments presented here were not consistent. More pH values above and below the expected isoelectric point are necessary to better define the contact angle versus zeta potential curves. One possible way to isolate ionic strength and pH effects may be to equilibrate the contact angle geoslide in the same container as the particles for zeta potential measurement. The dielectric constant and particle radius of the samples must be better defined to improve the electro-acoustical method. Particle aggregation should be prevented and a test of zeta potential versus mixing speed might help determine a more optimal mixing speed than the one used, 175 rpm. A lower concentration of particles would also help reduce aggregation effects although it does reduce the electro-acoustic signal as well. Finally, the ZetaProbe could be used to examine the effect of ionic strength as well by titrating an electrolyte solution instead of adjusting pH.

APPENDIX C

USE OF CAPILLARY METHODS TO ASSESS WETTABILITY

C.0 Introduction

Capillary pressure-saturation curves are give the relationship between the degree of saturation of the soil pores and capillary pressure. Typically, the saturation scale is the water phase saturation. Leverett (1941) reported that the pressure in one material could be scaled to another material. Section 1.12 describes the use of capillary pressure methods to determine the wettability of soils.

C.1 Methods

Capillary pressure – saturation curves were collected for water-air and water-PCE systems. Capillary pressure-saturation measurements were made following the method of Lord (1999). A custom designed rapid Tempe cell (Salehzadeh and Demond, 1999) was packed with dry soil material. A stainless steel frit was used to support the bottom of the cell followed by a water-wet membrane. The empty cell weight was recorded. The soil material was added in three layers. Each layer was tamped down lightly with a glass stopper and the surface was scored with a small spatula between additions. The dry soil was weighed in the cell. A stainless frit was also used on the top of the cell. The cell was closed and attached to a dry CO_2 source. CO_2 was allowed to flow through the cell in both the forward and reverse directions for about five minutes each. Approximately 300 mL of aqueous solution was then allowed to flow through the cell from the bottom (water wet membrane end) up. The aqueous solution was 0.01 M NaCl that had been pre-equilibrated with the soil and PCE (for water-PCE systems) for at least seven days. The flushing was stopped when the cell was completely saturated. The saturated cell was weighed and the weights before and after saturating the cell were used to determine the porosity. The water outlet line was attached to a 1 m long, 3.3 mm inner diameter glass

tube that measured effluent volume. A valve at the capillary tube was closed. The opposite end of the cell was removed and the level of the soil smoothed. For water-PCE systems, a PCE-wet membrane was soaked in a small dish of pre-equilibrated PCE. It was then carefully placed on the surface of the soil without trapping air bubbles beneath. A stainless frit was soaked in the dish of PCE then placed atop the membrane. The top of the cell was dried with a tissue and then replaced on the PCE end of the cell and sealed. A syringe was used to fill the port at the PCE end of the cell with PCE. The remaining PCE was placed in a glass reservoir and attached to the cell. The top of the reservoir was attached to an activated carbon VOC trap and left open to the atmosphere. For water-air systems, the top was replaced and a pressurized air line was attached. The pressurized air was passed over a water bath before reaching the cell to prevent evaporation losses at the inlet of the cell.

The inlet reservoir or pressure was set to a level so that the initial offset between the outlet tube, center of the cell, and reservoir was near zero and the applied air pressure was zero. The outlet valve was opened and water flowed through the cell until equilibrium was reached. The outlet tube was read at two hour intervals. If the change in the water level was less than 2 mm in two hours then the reservoir height was measured, recorded along with the outlet level, and the reservoir was raised (or lowered for imbibition) or the air pressure at the inlet was increased. The curves began with primary drainage of the water phase.

The molarity of an ethanol droplet (MED) test was performed following the procedure first described by King (1981) as a rapid method to assess the water repellency of soil materials. The theory behind the method is that there is a maximum interfacial tension between the ethanol droplet and air that will allow imbibition. In other words, the meniscus must be sufficiently curved to allow imbibition of the droplet. Ethanol solutions were prepared in 20 mL vials using Milli-Q purified water and ethyl alcohol (Aldrich, 95+% purity, St. Louis, MO) in 0.2 (± 0.02 M) increments from 0 to 5 M. Soil materials were sieved to less than 1 mm and air dried. The soil was then placed in a straight sided dish approximately 55 mm in diameter by 10 mm deep. A straightedge was dragged across the surface to create a smooth platform to support the droplets. A Pasteur pipette was used to place approximately 40 µl of solution on the surface. Individual

droplets were placed on the surface rather than dropped from the pipette to prevent additional gravitational forces from distorting the results. A stopwatch was started as the drop contacted the surface and the time until the peak of the drop became level with the soil surface was recorded. In accordance with King (1981), the lowest molarity at which the drop penetrates in less than 10 seconds was considered the molarity of an ethanol droplet (MED) value for that soil material.

C.2 Air-water capillary pressure – saturation curves

Figures C.1 through C.4 show the water-air capillary pressure-saturation curves of four samples. AAII refers to the humic acid sand, Ann Arbor II. Sulfuric acid and peroxide were used to strip the humic acid from this sand to produce a second material with identical morphology. This sand is labeled as stripped and a small microscope was used to confirm that the particles had similar size and shape but appeared to be pure quartz with little organic matter at the surface. The coated material was created by soaking the stripped soil in a humic acid standard solution purchased from the international humic society. By alternately raising and lowering the pH, the material was coated onto the soil to provide a second humic acid coated sand. Lachine refers to Lachine shale particles that were sieved and reconstituted to have a matching particle size distribution as the sands. The Leverett scaling factor (LSF) was computed as:

$$LSF = \sqrt{\frac{(\kappa/\eta)}{\gamma}} \qquad \text{Eqn. C.1}$$

Where κ is the Kozeny Carman conductivity, γ is the water surface tension or PCE-water interfacial tension measured with a DuNouy tensiometer, and η is the porosity. These values are given in Table C.1.

System	pH	γ, mN/m	η	Mean particle size (μm)	Carmen Kozeny κ	Leverett scaling factor
PCE-Water AAII Soil (B)	7.42	35.17	0.367	340	79.2	0.418
PCE-Water AAII Soil (A)	7.53	35.17	0.388	340	100.2	0.457
PCE-Water Stripped Soil (B)	7.18	43.68	0.356	316	60.4	0.298
PCE-Water Stripped Soil (A)	7.60	43.68	0.389	316	87.5	0.343
PCE-Water Coated Soil (A)	7.44	39.78	0.371	316	71.6	0.349
Air-Water AAII Soil (C)	7.10	73.33	0.383	340	94.8	0.221
Air-Water AAII Soil (B)	7.60	73.33	0.348	340	63.7	0.191
Air-Water AAII Soil (A)	7.30	73.33	0.391	340	103.5	0.230
Air-Water Stripped Soil (B)	7.25	72.87	0.366	316	67.7	0.187
Air-Water Stripped Soil (C)	7.31	72.87	0.384	316	82.8	0.201
Air-Water Coated (A)	7.41	64.03	0.387	316	85.6	0.232
Lachine Air-Water B	7.75	72.622	0.439	349	181.9	0.280
Lachine Air Water C	7.51	71.16	0.452	349	208.1	0.302
Lachine PCE Water C	7.05	43.6	0.458	349	221.3	0.504

Table C.1, Characteristics of capillary pressure-saturation curves and Leverett scaling factors.

The air entry pressure, the point in the capillary pressure curve where the saturation begins to decrease rapidly, is very similar across all four materials at about 5 cm H_2O. Figures C.2 through C.4 show each material as compared to the stripped soil. The capillary pressure is slightly higher in the Ann Arbor II sand and Lachine shale as compared to the stripped sand. For the Ann Arbor II sand, the humic acid may create micropores. In the case of the Lachine shale, the particles are highly angular and could not be packed to the same porosity. The coated sand is almost indistinguishable from the stripped sand. Water is very clearly the wetting phase in all four systems. The lack of coincidence is perhaps due to the fact that the materials are not physically similar, a condition for satisfactory scaling.

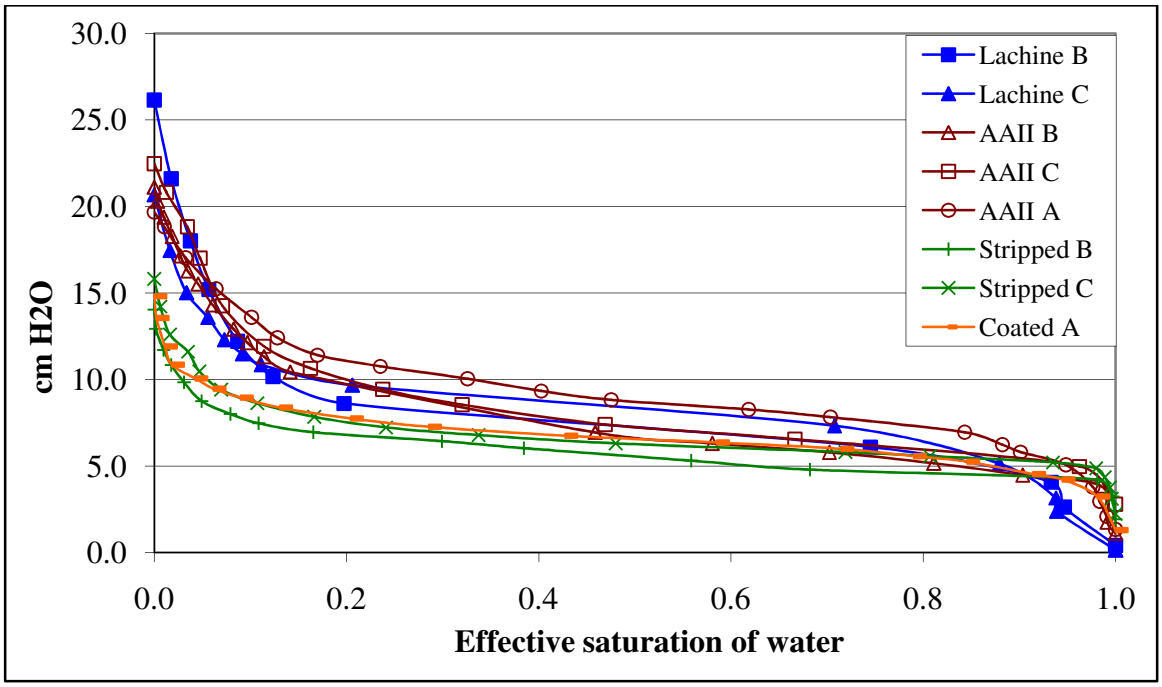

Figure C.1, Comparison of scaled water-air capillary pressure curves for several materials where AAII refers to Ann Arbor II natural humic acid sand, stripped is AAII sand after acid treatment, coated is stripped AAII sand with a commercial humic acid coating. The letters (A, B, C) denote repeat measurements of the same size and material sample.

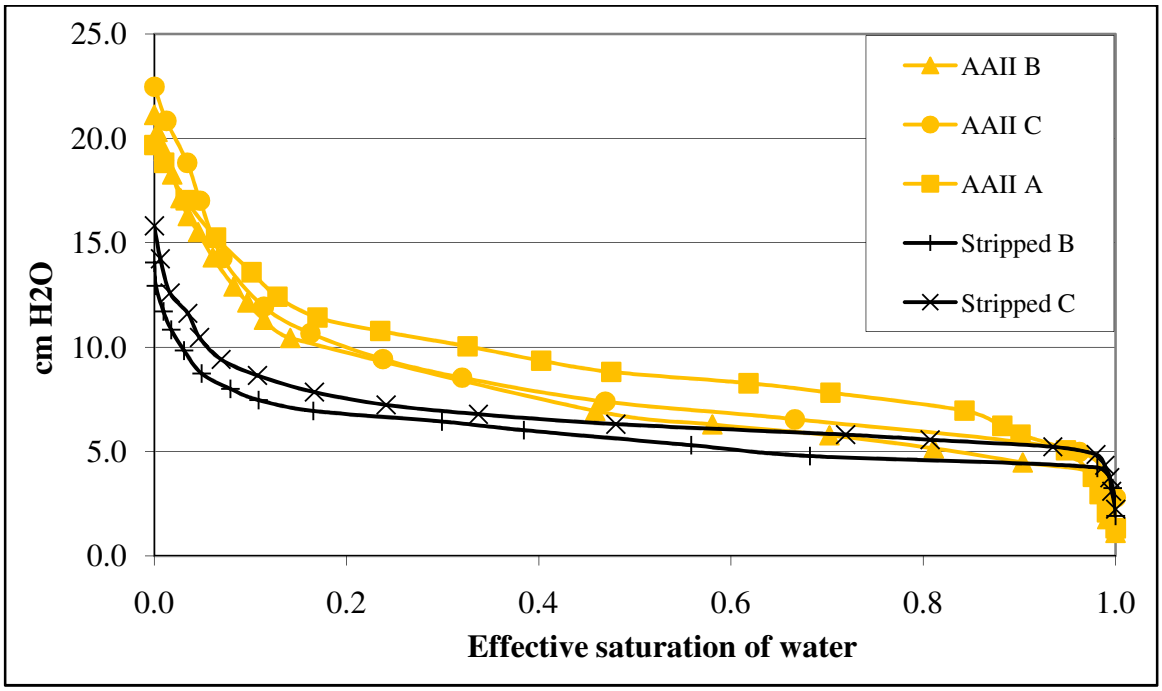

Figure C.2, Scaled water-air capillary pressure curves where stripped refers to Ann Arbor II sand acid treatment. The letters (A, B, C) denote repeat measurements of the same size and material sample.

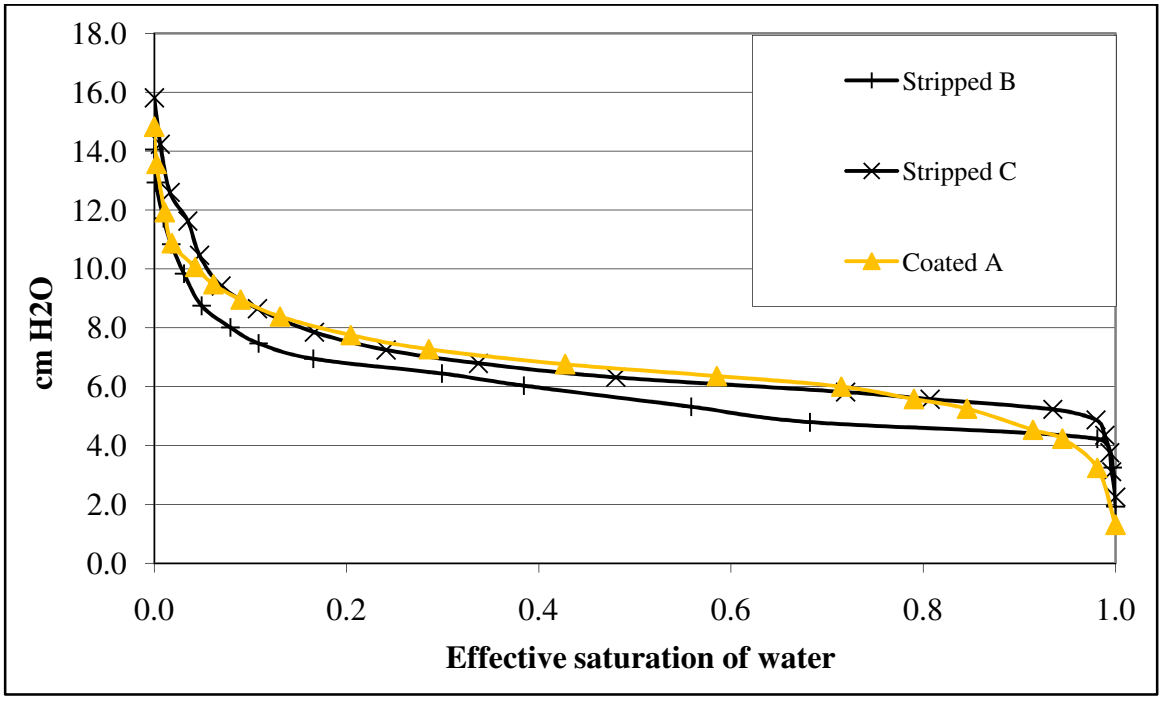

Figure C.3, Scaled water-air capillary pressure curves for humic coated sand where stripped refers to Ann Arbor II sand after an acid treatment and coated is stripped sand treated with a comercial humic acid. The letters (A, B, C) denote repeat measurements of the same size and material sample.

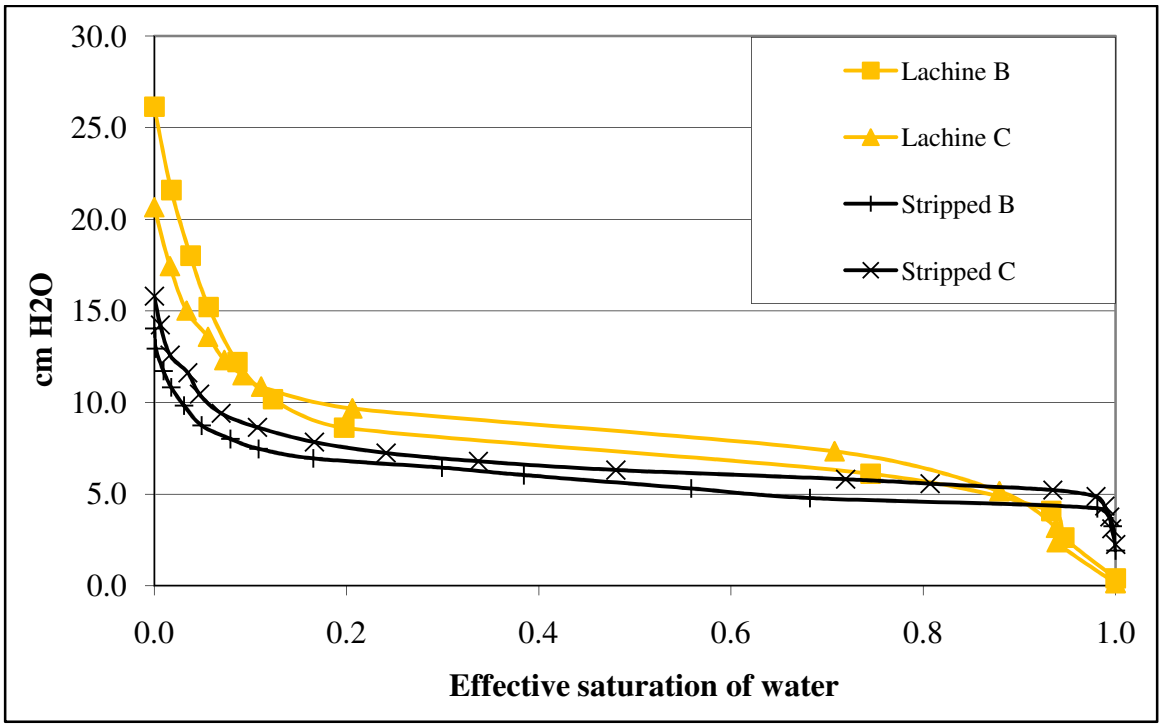

Figure C.4, Scaled water-air capillary pressure curves for Lachine shale compared to Ann Arbor II sand stripped by acid treatment.

C.3 Water-PCE capillary pressure – saturation curves

Figures C.5 through C.8 show the capillary pressure – saturation curves for water-PCE systems of four natural materials, again scaled to compare to the stripped sand characteristics. Water is the wetting fluid, as expected, based on the contact angles shown in Figure 3.5, since water is the receding or draining phase. There is little difference in the scaled PCE entry value from material to material. The coated sand has the lowest lower capillary pressure at a given saturation. PCE may dissolve the artificial humic acid coating as it contacts the coated solids. Also, the roughness of the coated particles could be greater than the Ann Arbor II sand itself which might disrupt the water film and allow more interaction between the solid surfaces and the PCE phase. It was initially believed that the Lachine shale would be significantly less water wetting than the stripped or humic material due to the maturity of the Lachine organic kerogen. However, as Figure C.8 shows, there is no discernable difference between the shale and the stripped material which agrees with the water-PCE contact angles on flat solids for Lachine and quartz presented in Figure 3.5. The water film that was shown to be persistent for water receding systems in Chapter 5 is also likely present in porous media.

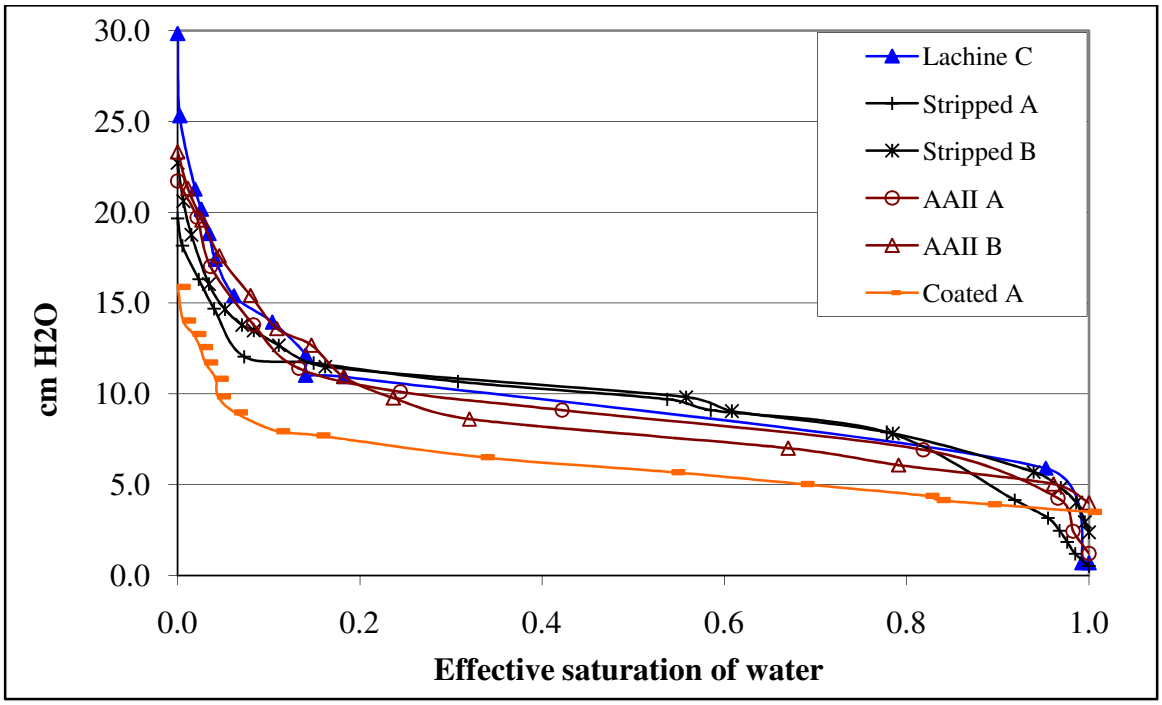

Figure C.5, Comparison of scaled water-PCE capillary pressure curves for several materials where AAII refers to Ann Arbor II natural humic acid sand, stripped is AAII sand after acid treatment, coated is stripped AAII sand with a commercial humic acid coating. The letters (A, B, C) denote repeat measurements of the same size and material sample.

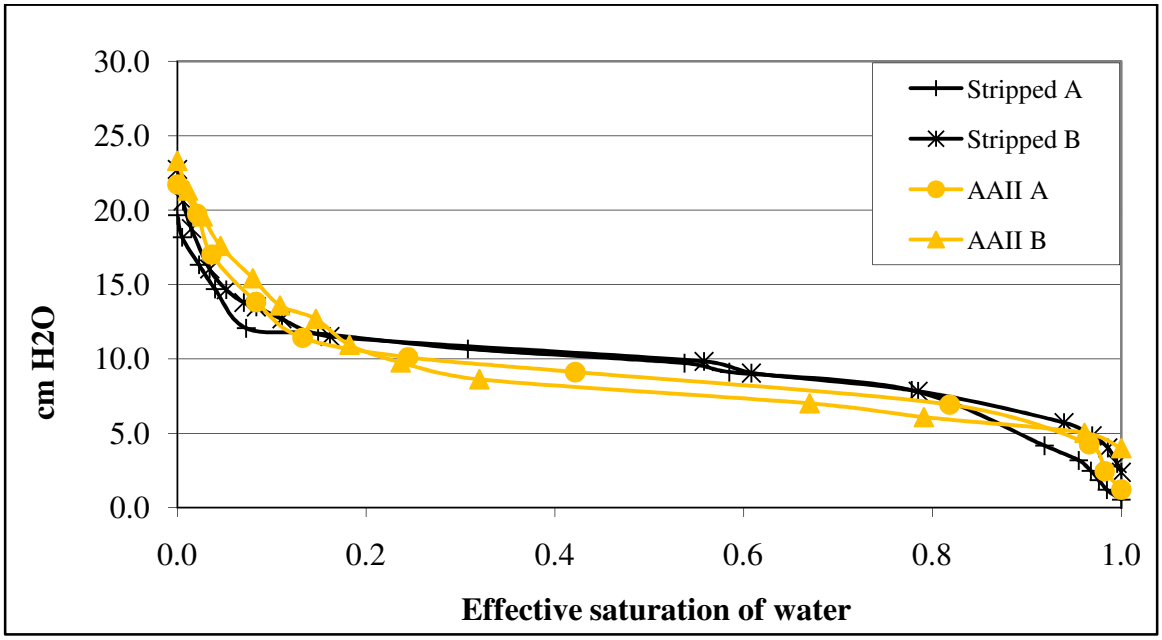

Figure C.6, Scaled water-PCE capillary pressure curves for Ann Arbor II sand where stripped refers to Ann Arbor II sand acid treatment. The letters (A, B, C) denote repeat measurements of the same size and material sample.

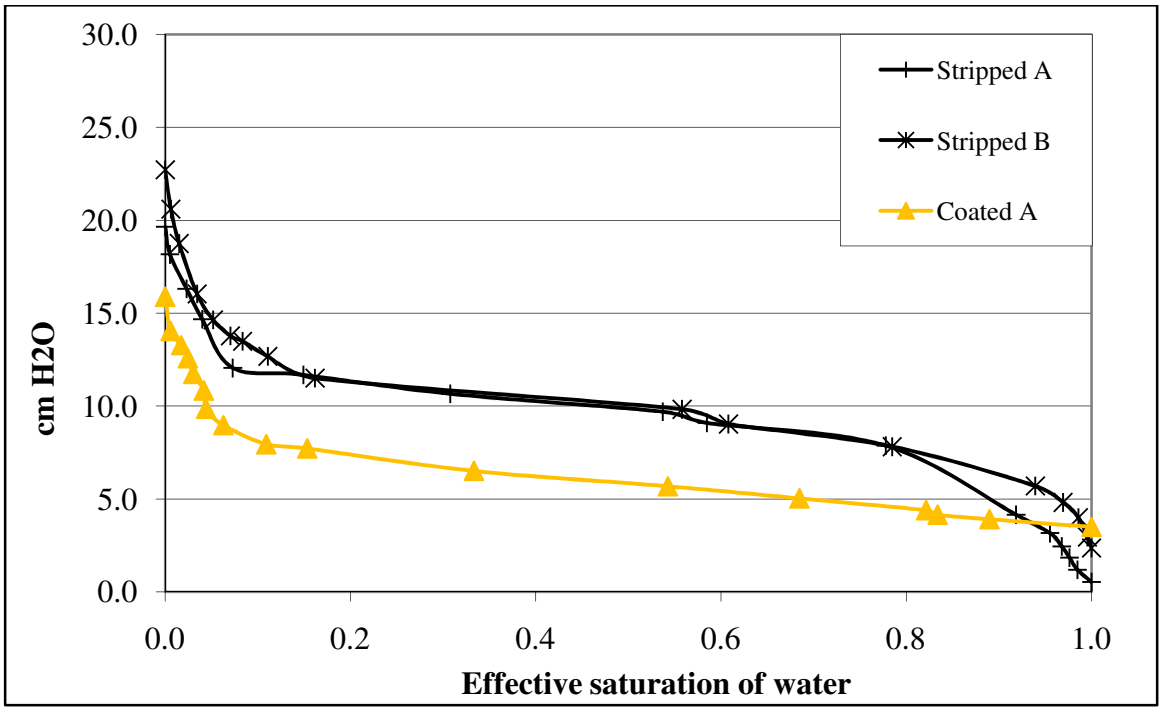

Figure C.7, Scaled water-PCE capillary pressure curves for a humic coated sand where stripped refers to Ann Arbor II sand after an acid treatment and coated is stripped sand treated with a comercial humic acid. The letters (A, B, C) denote repeat measurements of the same size and material sample.

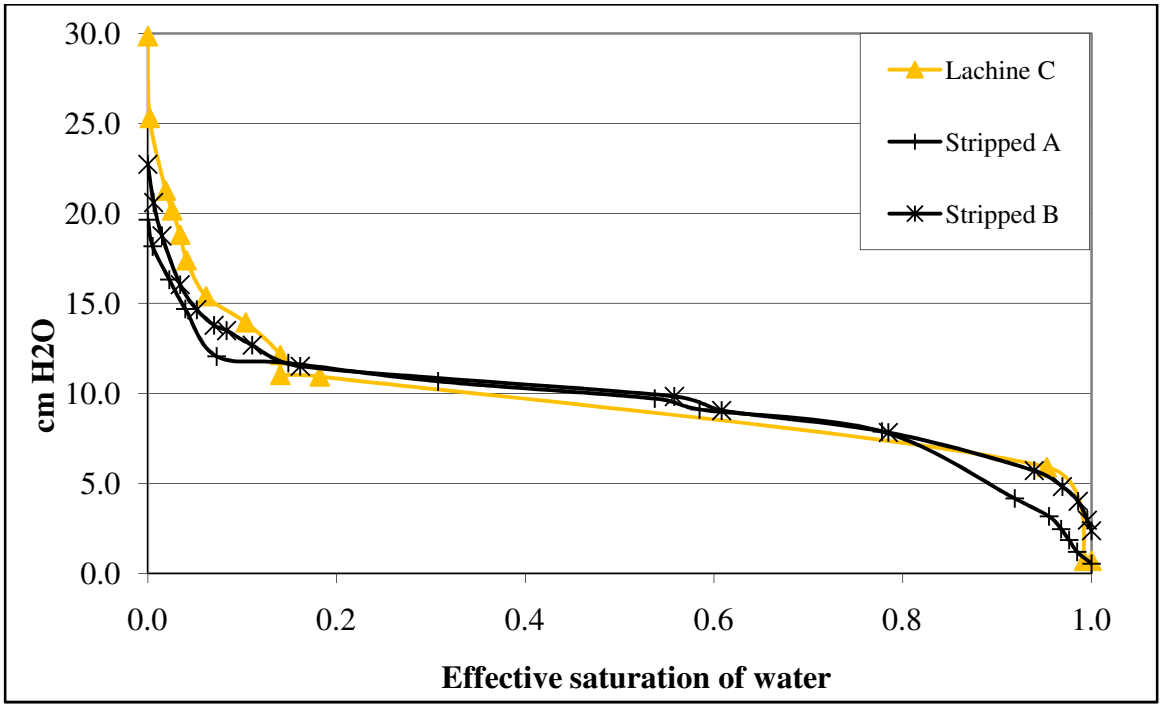

Figure C.8, Scaled water-PCE capillary pressure curves for Lachine shale compared to Ann Arbor II sand stripped by acid treatment. The letters (A, B, C) denote repeat measurements of the same size and material sample.

C.4 Capillary pressure – saturation curves for organic soil materials

Figures C.10 and C.11 compare the capillary pressure-saturation curves for three organic carbon-containing soil materials with that of silica. For these capillary pressure – saturation curves the particle size distribution was constrained to 425 – 500 μm. This narrow region was chosen to limit the pore size distribution with the goal of creating a very sharp PCE entry point. Also, it was hoped that a narrow particle size range would help reduce the differences due to particle size and shape. However, the Lachine and Garfield shales are very angular and, as shown in Table C.2, have a very high porosity even when packed to a maximum density. Waynesburg coal had a higher porosity still, which is probably due to internal porosity in the coal particles. The systems were scaled as described in Section C.2 to match the silica sample. Table C.1 lists both the scaled and unscaled entry pressures for water. Garfield shale is the most difficult for PCE to enter, followed by Waynesburg coal and then Lachine shale. This pattern is probably the result of a combination of the pore size and wettability differences in the materials. In the water-PCE contact angles presented on Figure 3.5, Waynesburg was the least water-wet followed by Lachine and then Garfield. The shale particles are angular and Garfield has a larger porosity than Lachine. Without porosimetry studies, it is unclear whether Garfield is less tightly packed or has more internal pores than Lachine. Also, repeat measurements of capillary pressure could help determine if the curves are truly reflective of a physical phenomenon.

Figure C.10 shows curves that are not scaled for effective saturation or for porosity or interfacial tension. From this figure, the residual saturation of water can be seen as the point where increases in capillary pressure cannot displace any more water from the pores. This is the point where the water phase becomes isolated distinct blobs. The residual saturations are given in Table C.2 and they follow the order expected based on contact angles given in Figure 3.5. So, for the most PCE-wet material, Waynesburg coal, the water phase becomes dissociated at high water saturation and PCE enters the smallest pores.

Solid material	Porosity	Solid density, g/cm^3	Entry pressure, cm H_20	Scaled entry pressure, cm H_2O	Residual water saturation
Silica	0.37	2.65	17.8	17.8	0.14
Lachine shale	0.53	2.52	15.3	18.2	0.32
Garfield shale	0.59	2.04	23.4	29.5	0.41
Waynesburg coal	0.76	1.51	16	22.9	0.55

Table C.2, Comparison of PCE-water capillary pressure curve features.

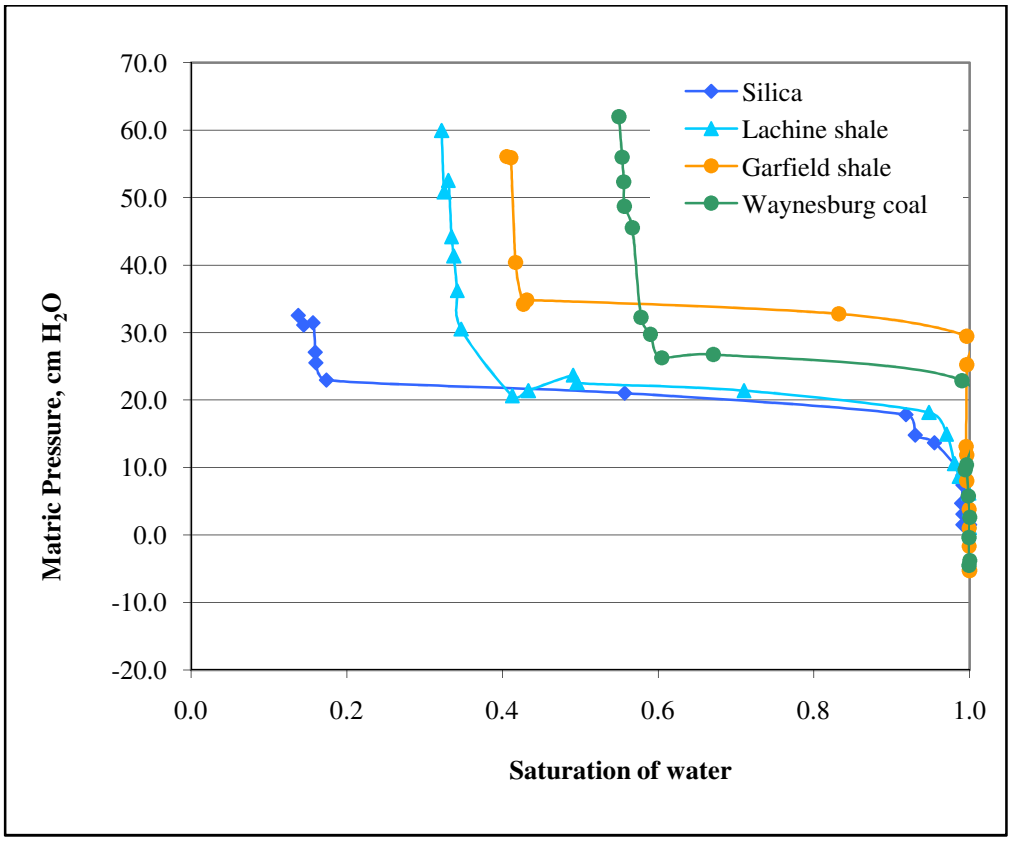

Figure C.10, water-PCE capillary pressure curves for four materials, unscaled.

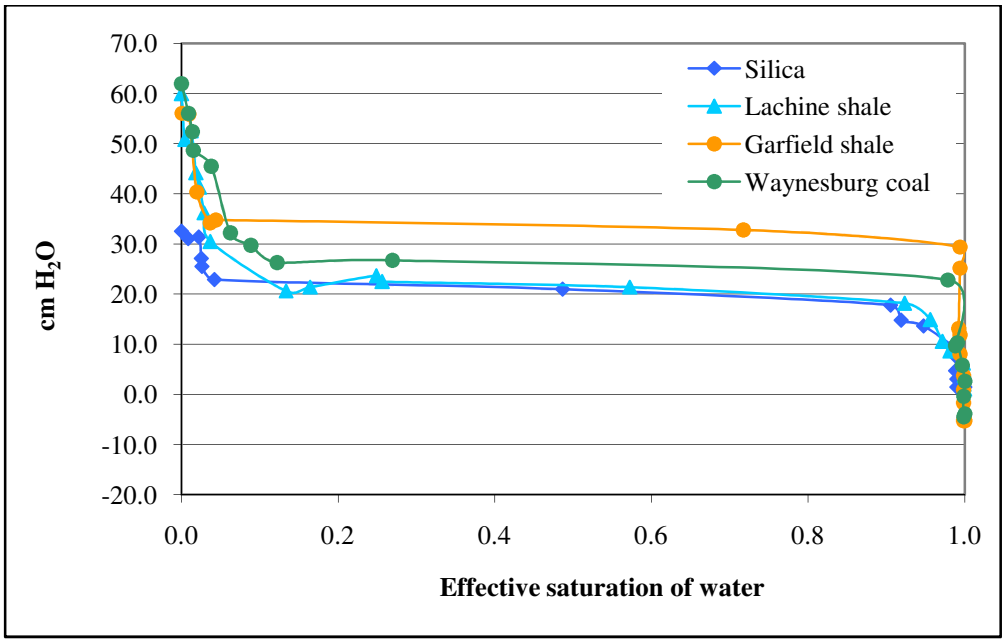

Figure C.11, Water-PCE capillary pressure curves for four materials.

C.5 MED tests

Table C.3 shows the MED values for the soil materials studied as well as contact angles recorded for air-water, PCE-Water systems on geoslides at neutral pH. The MED value is the minimum molarity of an ethanol droplet that imbibes into the dry soil material in less than 10 seconds. The MED test shows no correlation to contact angle. Soil particle size and pore shape are not controlled in King's method (1981) but should affect the outcome since the test is actually measuring the entry of a liquid into a three dimensional pore and not the spread over a smooth surface. Because a meniscus will form across a pore, the fluid may enter before the contact angle is zero. Also, the volume and height of the droplet shrinks as the ethanol concentration increases so the pressure head above a pore is not the same at each concentration. For field purposes, where the objective of the MED test is to rapidly compare the wetting behavior of soils in-situ, it may be adequate. However, the MED value seems to be a poor indicator of the contact angle in air-water systems and cannot be extended to infer the contact angle in organic-water systems. Doerr (1998) found that MED values could be categorized to predict contact angles for a series of similar soils. In this study however, the shape of each soil

particle varies from platy and angular (shale) to rounded and uniform (silica) so it is very likely that the pore tortuosity varies as well.

Solid	Air-Water Contact Angle, degrees	PCE-Water Contact Angle, degrees	MED, M
Silica	10.5	45.4	0.0
Lachine Shale	44.6	130.9	0.0
Garfield Shale	53.4	147.6	4.5
Waynesburg Coal	81.6	127.1	6
Graphite	62.2	153.1	0.5

Table C.3, MED values for selected soil materials.

C.6 Conclusions and recommendations for future study

Capillary methods allow the examination of the effects of wettability in the actual porous media. However, when comparing multiple materials, some sort of scaling is necessary to account for porosity and tortuosity differences. The experiments with humic sands and organic carbon-containing aquifer materials were all limited by the fact that both wettability and pore morphology differences were present. Coatings of extracted organic material may be one way to standardize the pore morphology for comparing different materials; however extraction and redeposition often alters the organic material so the wettability of the coated material may not be representative of the natural material. However, the results herein are consistent with the water-air and water-PCE contact angles presented in Figures 3.3 and 3.5 and all the materials appeared similarly water-wet. Also, the residual saturation of water-PCE-solid systems ranks in order with the PCE–water contact angle. The more PCE wetting the material is, the higher the water saturation at which the water phase becomes immobilized. PCE receding tests or water imbibition tests are needed to help determine if the wettability hysteresis observed in sessile drop contact angles occurs in porous media. The MED test, which does not separate the surface tension from the pore morphology effects, does not seem to be a very reliable test of wettability. Employing particles with similar morphology may improve the results.

APPENDIX D

DETERMINATION OF SOLID SURFACE ENERGY COMPONENTS

D.0 Example calculation of quartz solid surface energy components

The MAPLE worksheet used to calculate the solid surface energy components of quartz is shown in Figure D.1. This calculation used water, glycerol, and DIM as the probe liquids.

```
> gw := 72.8; gwd := 21.8; gwa := 25.5; gwb := 25.5; gg := 64.0; ggd :
  = 34.0; gga := 57.4; ggb := 3.92; gf := 58; gfd := 39; gfa := 39.6;
  gfb := 2.28; gdi := 50.8; gdia := 0; gdib := 0; gdid := 50.8;
  galf := 44.4; galfa := 0; galfb := 0; galfd := 44.4; qw := 0.35;
  qdi := .77; qg := .52; qf := .825541; qalf := .38;
```

$$gw := 72.8$$

$$gwd := 21.8$$

$$gwa := 25.5$$

$$gwb := 25.5$$

$$gg := 64.0$$

$$ggd := 34.0$$

$$gga := 57.4$$

$$ggb := 3.92$$

$$gf := 58$$

$$gfd := 39$$

$$gfa := 39.6$$

$$gfb := 2.28$$

$$gdi := 50.8$$

$$gdia := 0$$

$$gdib := 0$$

$$gdid := 50.8$$

$$galf := 44.4$$

$$galfa := 0$$

$$galfb := 0$$

$$galfd := 44.4$$

$$qw := 0.35$$

$$qdi := 0.77$$

$$qg := 0.52$$

$$qf := 0.825541$$

$$qalf := 0.38$$

```
> eqn1 := 2 · (sqrt(gsd · gwd) + sqrt(gsa · gwb) + sqrt(gsb · gwa))
      − gw · (1 + cos(qw));
```

$$eqn1 := 9.338094024\sqrt{gsd} + 10.09950494\sqrt{gsa} + 10.09950494\sqrt{gsb} - 141.1863335$$

```
> eqn2 := 2 · (sqrt(gsd · ggd) + sqrt(gsa · ggb) + sqrt(gsb · gga))
      − gg · (1 + cos(qg));
```

$$eqn2 := 11.66190379\sqrt{gsd} + 3.959797974\sqrt{gsa} + 15.15255754\sqrt{gsb} - 119.5404275$$

```
> eqn3 := 2 · (sqrt(gsd · gdid) + sqrt(gsa · gdib) + sqrt(gsb · gdia))
      − gdi · (1 + cos(qdi));
```

$$eqn3 := 14.25482374\sqrt{gsd} - 87.2698620$$

```
> solve(eqn3 = 0, gsd);
```

$$37.4804568$$

```
> gsd := %;
```

$$gsd := 37.4804568$$

```
> solve(eqn1 = 0, gsa);
```

$$69.20500445 - 16.63790906\sqrt{gsb} + gsb$$

```
>
> gsa := %;
```

$$gsa := 69.20500445 - 16.63790906\sqrt{gsb} + gsb$$

```
> solve(eqn2 = 0, gsb);
```

$$1.84503953$$

```
> subs(gsb = %, gsa = %% );
```

$$48.45040068 = 48.4504006$$

```
> gsa := %;
```

$$gsa := 48.45040068 = 48.4504006$$

```
>
>
```

Figure D.1, MAPLE worksheet for the calculation of surface energy components.

	Free Surface Energy Component	ABN + Water + Glycerol	DIM + Water + Glycerol	ABN + Water + Formamide	DIM + Water + Formamide	Average
Lachine Shale	γ_S^D	44.14	42.43	44.14	42.43	43.29
	γ_S^A	22.86	23.13	25.22	25.11	24.08
	γ_S^B	2.00	2.27	1.38	1.72	1.84
Garfield Shale	γ_S^D	43.09	43.23	43.09	43.23	43.16
	γ_S^A	27.17	27.14	23.07	23.70	25.27
	γ_S^B	0.05	0.05	0.31	0.32	0.18
Waynesburg Coal	γ_S^D	43.92	42.38	43.92	42.38	43.15
	γ_S^A	3.50	3.59	0.77	0.77	2.16
	γ_S^B	0.07	0.12	1.85	1.85	0.97
Graphite	γ_S^D	43.95	47.76	43.95	47.76	45.86
	γ_S^A	14.83	14.38	11.19	11.35	12.94
	γ_S^B	0.35	0.15	1.20	0.66	0.59
Talc	γ_S^D	42.92	42.03	DNM	DNM	42.48
	γ_S^A	10.44	10.53	DNM	DNM	10.49
	γ_S^B	1.45	1.57	DNM	DNM	1.51
Dolomite	γ_S^D	43.40	43.66	DNM	DNM	43.53
	γ_S^A	33.28	33.23	DNM	DNM	33.26
	γ_S^B	1.91	1.87	DNM	DNM	1.89
Calcite	γ_S^D	42.42	42.05	DNM	DNM	42.24
	γ_S^A	58.71	58.80	DNM	DNM	58.76
	γ_S^B	0.86	0.83	DNM	DNM	0.85
Quartz	γ_S^D	41.32	37.46	41.32	37.46	39.39
	γ_S^A	47.53	48.43	77.86	77.37	62.80
	γ_S^B	1.32	1.87	0.61	0.22	1.01

Table D.1, Resulting surface free energy components, in mNm^{-1}, depending on probe liquids. Formamide contact angles were not measured for talc, dolomite, and calcite.

BIBLIOGRAPHY

ASTM Standard D854-48, *Standard Test Method for Specific Gravity of Soils*; American Society for Testing and Materials: West Conshohocken, PA, 1979.

ASTM Standard D422-63, *Standard Test Method for Particle Size Analysis of Soils*; American Society for Testing and Materials: West Conshohocken, PA 1990.

Adamson, A. W.; Gast, A. P., *Physical Chemistry of Surfaces*. Sixth Edition; John Wiley: New York, 1997; p 784.

Aiken, M., Wershaw, MacCarthy, *Humic Substances in Soil, Sediment and Water, Geochemistry, Isolation and Characterization*. John Wiley & Sons: New York, 1985.

Akhlaq, M. S., Characterization of the Isolated Wetting Crude Oil Components with Infrared Spectroscopy. *Journal of Petroleum Science and Engineering* **1999,** *22*, 229-235.

Anckner, W. H. J.; Powers, S. E., Relating Wettability of Contaminated Sands to NAPL Composition. In *NAPLs in the Subsurface Environment: Assessment and Remediation*, Reddi, L. N., Ed. ASCE: New York, NY, 1996; pp 502-512.

Anderson, W. G., Wettability Literature Survey-Part 2: Wettability Measurement. *Journal of Petroleum Technology* **1986,** *38*, (12), 1246-1262.

Austad, T.; Standnes, D. C., Spontaneous Imbibition of Water into Oil-Wet Carbonates. *Journal of Petroleum Science and Engineering* **2003,** *39*, (3-4), 363-376.

Bachmann, J.; Horton, R.; Van Der Ploeg, R. R.; Woche, S., Modified Sessile Drop Method of Assessing Initial Soil-Water Contact Angle of Sandy Soil. *Soil Sci. Soc. Amer.* **2000,** *64*, (March-April), 564-567.

Bahrani, B.; Mansell, R. S.; Hammond, L. C., Using Infiltration of Heptane and Water into Soil Columns to Determine Soil-Water Contact Angles. *Soil Sci. Soc. Amer. Proc.* **1973,** *37*, 532-534.

Ball, W. P.; Roberts, P. V., Long Term Sorption of Halogenated Organic Chemicals by Aquifer Material. 1. Equilibrium. *Environmental Science & Technology* **1991,** *25*, (7), 1223-1237.

Barranco, F. T.; Dawson, H. E.; Christener, J. M.; Honeyman, B. D., Influence of Aqueous pH and Ionic Strength on the Wettability of Quartz in the Presence of Dense Non-Aqueous-Phase Liquids. *Environmental Science & Technology* **1997,** *31*, (3), 676-681.

Bartell, F. E.; Osterhof, H. J., Adhesion Tension Pressure of Displacement Method. *unknown* **1933**, 543-552.

Bauters, T. W. J., Steenhuis, T.S., DiCarlo, D.A., Nieber, J.L., Dekker, L.W., Ritsema, C.J., Parlange, J.-Y., Haverkamp, R., Physics of Water Repellent Soils. *Journal of Hydrology* **2000,** *231-232*, 233-243.

Bisdom, E. B. A.; Dekker, L. W.; Schoute, J. F. T., Water Repellency of Sieve Fractions from Sandy Soils and Relationships with Organic Material and Soil Structure. *Geoderma* **1993,** *56*, (1-4), 105-118.

Botsaris, G. D.; Glazman, Y. M., *Interfacial Phenomena in Coal Technology*. Marcel Dekker Inc.: New York, 1989.

Bouska, V., *Geochemistry of Coal*. Elsevier Scientific Publishing Company: New York, 1981; Vol. 1, p 284.

Bradford, S. A.; Leij, F., J., Fractional Wettability Effects on Two-and Three-Fluid Capillary Pressure-Saturation Relations. *Journal of Contaminant Hydrology* **1995,** *20*, 89-109.

Bradford, S. A.; Phelan, T. J.; Abriola, L. M., Dissolution of Residual Tetrachloroethylene in Fractional Wettability Porous Media: Correlation Development and Application. *Journal of Contaminant Hydrology* **2000,** *45*, 35-61.

Bradford, S. A.; Vendlinski, R. A.; Abriola, L. M., The Entrapment and Long-Term Dissolution of Tetrachloroethylene in Fractional Wettability Porous Media. *Water Resources Research* **1999,** *25*, (10), 2955-2964.

Brown, R. J. S.; Neustadter, E. L., The Wettability of Oil/Water/Silica Systems with Reference to Oil Recovery. *Journal of Canadian Petroleum Technology* **1980,** *19*, 1773-1780.

Buckley, J. S., Effective Wettability of Minerals Exposed to Crude Oil. *Current Opinion in Colloid and Interface Science* **2001,** *6*, 191-196.

Buckley, J. S.; Liu, Y.; Monsterfleet, S., Mechanisms of Wetting Alteration by Crude Oils. *SPE Journal* **1998**, 54-60.

Buczko, U.; Bens, O.; Fischer, H.; Huttl, R. F., Water Repellency in Sandy Luvisols Under Different Forest Transformation Stages in Northeast Germany. *Geoderma* **2002,** *109*, 1-18.

Capriel, P.; Beck, T.; Borchert, H.; Gronholz, J.; Zachmann, G., Hydrophobicity of the Organic Matter in Arable Soils. *Soil. Biol. Biochem* **1995,** *27*, (11), 1453-1458.

Cary, J. W.; Simmons, C. S.; McBride, J. F., Infiltration and Redistribution of Organic Liquids in Layered Porous Media. *Soil Sci. Soc. Amer. J.* **1994,** *58*, 704-711.

Chatzis, I.; Morrow, N. R.; T., L. H., Magnitude and Detailed Structure of Residual Oil Saturation. *Society of Petroleum Engineers* **1983**, (April 1993), 311-326.

Cheng, P. W. P. Automation of Axissymetric Drop Shape Analysis Using Digital Image Processing. Ph.D., University of Toronto, Toronto, Ontario, 1990.

Chessick, J. J.; Zettlemoyer, A. C.; Yu, Y.-F., Free Energies, Heats and Entropies of Wetting of Graphite. *Journal of Physical Chemistry* **1960,** *64*, (5), 530-531.

Chibowski, E.; Perea-Carpio, R., Problems of Contact Angle and Solid Surface Free Energy Determination. *Advances in Colloid and Interface Science* **2002,** *98*, (2), 245-264.

Combes, R.; Robin, M.; Blavier, G.; Aidan, M.; Degreve, F., Visualization of Imbibition in Porous Media by Environmental Scanning Electron Microscopy: Application to Reservoir Rocks. *Journal of Petroleum Science and Engineering* **1998,** *20*, 133-139.

Commission on Geosciences, Environment and Resources, *Alternatives for Groundwater Cleanup*. National Academies Press: 1994.

Corey, A. T., *Mechanics of Immiscible Fluids in Porous Media*. 3rd ed.; Water Resources Pub.: Highlands Ranch,CO, 1994.

Crawford, R. J.; Guy, D. W.; Mainwaring, D. E., The Influence of Coal Rank and Mineral Matter Content on Contact-Angle Hysteresis. *Fuel* **1994,** *73*, (5), 742-746.

Daughney, C. J., Sorption of Crude Oil from a Non-Aqueous Phase onto Silica: The Influence of Aqueous pH and Wetting Sequence. *Organic Geochemistry* **2000,** *31*, 147-158.

Davis, A. N.; Morton, S. A.; Counce, R. M.; DePaoli, D. W.; Hu, M. Z.-C., Ionic Strength Effects on Hexadecane Contact Angles on a Gold-Coated Glass Surface in Ionic Surfactant Solutions. *Colloids and Surfaces A: Physicochemical and Engineering Aspects* **2003,** *221*, (1), 69-80.

DeBano, L. F., Water Repellency in Soils: A Historical Overview. J*ournal of Hydrology* **2000,** *231-232*, 4-32.
DeBano, L. F.; Mann, L. D.; Hamilton, D. A., Translocation of Hydrophobic Substances into Soil by Burning Organic Litter. *Soil Science Society of America Proceedings* **1970,** *34*, (1), 130.

Della Volpe, C. SurfTen 4.3. http://devolmac.ing.unitn.it:8080/ (May 25).

Demond, A. H.; Lindner, A. S., Estimation of Interfacial Tension between Organic Liquids and Eater. *Environmental Science & Technology* **1993,** *27*, (12), 2318-2330.

Denekas, M. O.; Mattax, C. C.; Davis, G. T., Effects of Crude Oil Components on Rock Wettability. *Petroleum Transactions* **1959,** *216*, 330-333.

DeRosa, R. L.; P.A., S.; J.E., S., Hydrophilic Nature of Silicate Glass Surfaces as a Function of Exposure Condition. *Journal of Non-Crystalline Solids* **2003,** *331*, (1), 32-40.

Doerr, S. H., On Standardizing the 'Water Drop Penetration Time' and the 'Molarity of an Ethanol Droplet' Techniques to Classify Soil Hydrophobicity: A Case Study Using Medium Textured Soils. *Earth Surface Processes and Landforms* **1998,** *23*, 663-668.

Domenico, P. A.; Schwartz, F. W., *Physical and Chemical Hydrogeology*. 2nd ed.; John Wiley & Sons Inc.: New York, 1998; p 506.

Dubey, S. T.; Doe, P. H., Base Number and Wetting Properties of Crude Oils. *SPE Reservoir Engineering* **1993**, 195-200.

Dullien, F. A. L., *Porous Media Fluid Transport and Pore Structure*. 2nd ed.; Academic Press, Inc.: New York, 1992.

Dupré, A., *Théorie Mécanique de la Chaleur*. Gauthier-Villars, Paris, 1869.

Dwarakanath, V.; Jackson, R. E.; Pope, G. A., Influence of Wettability on the Recovery of NAPLs from Alluvium. *Environmental Science & Technology* **2002,** *26*, (2), 227-231.

Echols, R. T., NMR data for Humic Acid Soil. In personal communication to Ryder, J. L., Ann Arbor, MI, 2000.

Eglinton, G.; Murphy, M. T. J., *Organic Geochemistry, Methods and Results*. 1969.

Engel, R. J.; Stroesenreuther, N. W., *Soil Survey of Washtenaw County, Michigan. United States.* Soil Conservation Service: Washington, DC, 1977.

Ethington, E. F. *Interfacial Contact Angle Measurements of Water, Mercury, and 20 Organic Liquids on Quartz, Calcite, Biotite, and Ca-Montmorillonite Substrates*; USGS-OFR-90-409; Department of the Interior: 1990; p 18.

Fowkes, F. M., Attractive Forces at Interfaces. *Industrial and Engineering Chemistry* **1964,** *56*, (12), 40.

Fox, H. W.; Zisman, W. A., The Spreading of Liquids on Low-Energy Surfaces .3. Hydrocarbon Surfaces. *Journal of Colloid Science* **1952,** *7*, (4), 428-442.

Franco, C. M. M.; Clarke, P. J.; Tate, M. E.; Oades, J. M., Hydrophobic Properties and Chemical Characterization of Natural Water Repellent Materials in Australian Sands. *Journal of Hydrology* **2000,** *231-232*, 47-58.

Fuerstenau, D. W.; Colic, M., Self-Association and Reverse Hemi-Micelle Formation at Solid-Water Interfaces in Dilute Surfactant Solutions. *Colloids and Surfaces A* **1999,** *146*, 33-47.

Fuerstenau, D. W.; Rosenbaum, J. M.; Laskowski, J., Effect of Surface Functional Groups on the Flotation of Coal. *Colloids and Surfaces* **1983,** *8*, 153-174.

Gatenby, W. A.; Marsden, S. S., Some Wettability Characteristics of Synthetic Porous Media. *Prod. Monthly* **1957,** *22*, 5.

Gerin, P. A.; Dufrene, Y. F., Native Surface Structure of Natural Soil Particles Determined by Combining Atomic Force Microscopy and X-ray Photoelectron Spectroscopy. *Colloids and Surfaces B: Biointerfaces* **2003,** *28*, 295-305.

Giese, R. F.; Costanzo, P. M.; van Oss, C. J., The Surface Free-Energies of Talc and Pyrophyllite. *Physics and Chemistry of Minerals* **1991,** *17*, (7), 611-616.

Giovannini, G.; Lucchesi, S., Modifications Induced in Soil Physico-Chemical Parameters by Experimental Fires at Different Intensities. *Soil Science* **1997,** *162*, (7), 479-496.

Goklen, K. E.; Stoecker, T. J.; Baddour, R. F., A Method for Isolation of Kerogen from Green River Oil Shale. *Ind. Eng. Chem. Prod. Res. Dev.* **1984,** *23*, 308-311.

González, G. In *The Adsorption of Asphaltenes and Resins onto Quartz and Feldspar*, Intersociety Energy Conversion Engineering Conference, Washington, D.C., 1986; American Chemical Society: Washington, D.C., 1986; pp 245-258.

Good, R. J., Contact Angle, Wetting, and Adhesion: a Critical Review. *Journal of Adhesion Science and Technology* **1992,** *6*, (12), 1269-1302.

Gosiewska, A.; Drelich, J.; Laskowski, J. S.; Pawlik, M., Mineral Matter Distribution on Coal Surfaces and Its Effect on Coal Wettability. *Journal of Colloid and Interface Science* **2002,** *247*, 107-116.

Gribanova, E. V.; Zhukov, A. N.; Antonyuk , I. E.; Benndorf, C.; Baskova, E. N., Effect of Acidity of Aqueous Solutions on the Wettability of Diamond, Graphite and Pyrocarbon Surfaces. *Diamond and Related Materials* **2000,** *9*, 1-6.

Guy, D. W.; Crawford, R. J.; Mainwaring, D. E., The Wetting Behavior of Several Organic Liquids in Water on Coal Surfaces. *Fuel* **1996,** *75*, (2), 238-242.

Haberhauer, G.; Gerzabek, M. H., Drift and Transmission FT-IR Spectroscopy of Forest Soils: an Approach to Determine Decomposition Processes of Forest Litter. *Vibrational Spectroscopy* **1999,** *19*, 413-417.

Hair, M. L.; Hertl, W., Adsorption on Hydroxylated Silica Surfaces. *Journal of Physical Chemistry* **1969,** *73*, (12), 4269.

Hajnos, M.; Sokolowska, Z.; Jozefaciuk, G.; Swieboda, R. In *Influence of Surface Coverage by Humic Acids on Wettability of Kaolin*, 17th World Congress of Soil Science, Bangkok, Thailand, August 12-21, 2002; Bangkok, Thailand, 2002.

Hamilton, W. C., A Technique for the Characterization of Hydrophilic Solid Surfaces. *Journal of Colloid and Interface science* **1971,** *40*, (2), 219-222.

Hatcher, P. G.; Breger, I. A.; Maciel, G. E.; Szeverenyi, N. M., Geochemistry of Humin. In *Humic Substances in Soil, Sediment and Water, Geochemistry, Isolation and Characterization*, Aiken, M., Wershaw, MacCarthy, Ed. John Wiley & Sons: New York, 1985.

Hiemenz, P., C.; Rajagopalan, R., *Principles of Colloid and Surface Chemistry*. Third ed.; Marcel Dekker, Inc.: New York, 1997.

Hillel, D., *Environmental Soil Physics*. Academic Press: New York, 1998.

Hirasaki, G. J., Wettability: Fundamentals and Surface Forces. *SPE Formation Evaluation* **1991**, 217-225.

Horsely, R. M.; H.G., S., Principles of Coal Flotation. *Fuel* **1951,** *30*, 54-63.

Hsu, H.-L. Determination of Interfacial Tension and Contact Angle of Dense Non-Aqueous Phase Liquid Waste Mixtures. Ph.D. dissertation. University of Michigan, Ann Arbor, 2005.

Hsu, H. L.; Demond, A. H., Influence of Organic Acid and Organic Base Interactions on

Interfacial Properties in NAPL-Water Systems. *Environ. Sci. Technol.* **2007,** *41*, (3), 897-902.

Huang, W. Sorption and Desorption by Soils and Sediments: Effects of Sorbent Heterogeneity. Ph.D. dissertation, University of Michigan, Ann Arbor, 1997.
Huang, W.; Weber, W. J., A Distributed Reactivity Model for Sorption by Soils and Sediments. 10. Relationships between Desorption, Hysteresis, and the Chemical Characteristics of Organic Domains. *Environ. Sci. Technol.* **1997,** *31*, (9), 2562-2569.

Huethorst, J. A. M.; Leenaars, A. F. M., A New Method for Determining the Contact Angle of a Liquid Against Solid Spherical Particles. *Colloids and Surfaces* **1990,** *50*, 101-111.

Hunt, J. R.; Sitar, N.; Udell, K. S., Nonaqueous Phase Liquid Transport and Cleanup 2. Experimental Studies. *Water Resources Research* **1988,** *24*, (8), 1259-1269.

Iler, R. K., *The Chemistry of Silica*. John Wiley & Sons: New York, 1979; p 835.

Israelachvili, J. N., *Intermolecular and Surface Forces*. 2nd ed.; Academic Press: New York, NY, 1992.

Janczuk, B.; Zdziennicka, A., A Study on the Components of Surface Free Energy of Quartz from Contact Angle Measurements. *Journal of Materials Science* **1994,** *29*, 3559-3564.

Jaramillo, D. F.; Dekker, L. W.; Ritsema, C. J.; Hendrickx, J. M. H., Occurrence of Soil Water Repellency in Arid and Humid Climates. J*ournal of Hydrology* **2000,** *231-232*, 105-111.

Jeong, S.-W.; Wood, A. L.; Lee, T. R., Effects of Pure and Dyed PCE on Physical and Interfacial Properties of Remedial Solutions. *Journal of Hazardous Materials* **2002,** *B59*, 125-135.

Johnson, M. D. Phenanthrene sorption/desorption mechanisms and rapid prediction of long-term desorption rates using superheated water. Ph.D. dissertation, University of Michigan, Ann Arbor, MI, 2000.

Johnson, M. D.; Walter J. Weber, J., Rapid Prediction of Long-Term Rates of Contaminant Desorption from Soils and Sediments. *Environmental Science & Technology* **2001,** *35*, (2), 427-433.

Jouany, C., Surface Free-Energy Components of Clay-Synthetic Humic-Acid Complexes from Contact-Angle Measurements. *Clays and Clay Minerals* **1991,** *39*, (1), 43-49.

Karnok, K. A.; Rowland, E. J.; Tan, K. H., High pH Treatments and the Alleviation of Soil Hydrophobicity on Golf Greens. *Agronomy Journal* **1993,** *85*, 983-986.

Kia, S. F., Modeling the Retention of Organic Contaminants in Porous Media of Uniform Spherical Particles. *Water Research* **1988,** *22*, (10), 1301-1309.

Killops, S. D.; Killops, V. J., *An Introduction to Organic Geochemistry*. 1 ed.; John Wiley & Sons, Inc.: New York, 1993; p 265.

King, P. M., Comparison of Methods for Measuring Severity of Water Repellence of Sandy Soils and Assessment of Some Factors the Affect its Measurement. *Aust. J. Soil Res.* **1981,** *19*, 275-85.

Kramer, G.; Somasundaran, P., Conformational Behavior of Polyelectrolyte Complexes at the Solid/Liquid Interface. *Langmuir* **2002,** *18*, (24), 9357-9361.

Lagerge, S.; Keh, E.; Partyka, S.; Lindheimer, M., On the Behavior of Nonionic Surfactants at the n-Heptane/Silica Gel Interface: Influence of the Presence of Interfacial Water Inferred from Adsorption Isotherms and Calorimetric Data. *Journal of Colloid and Interface Science* **2000,** *227*, (2), 412-420.

Laibinis, P. E.; Bain, C. D.; Nuzzo, R. G.; Whitesides, G. M., Structure and Wetting Properties of ω-Alkoxy-n-alkanethiolate Monolayers on Gold and Silver. *Journal of Physical Chemistry* **1995,** *99*, 7663-7676.

Leverett, M. C., Capillary Behavior in Porous Solids. *Petroleum Technology* **1940**, 152-169.

Lin, C.-K.; Hwang, C.-C.; Uen, W.-Y., A Nonlinear Rupture Theory of Thin Liquid Films with Soluble Surfactant. *Journal of Colloid and Interface science* **2000,** *231*, 379-393.

Littke, R., *Lecture Notes in Earth Sciences*. Springer-Verlag: New York, 1993; p 216.

Litvina, M.; Todoruk, T. R.; Langford, C. H., Composition and Structure of Agents Responsible for Development of Water Repellency in Soils following Oil Contamination. *Environmental Science & Technology* **2003,** *38*, 2883-2888.

Lopez-Ramon, M. V.; Stoeckli, F.; Moreno-Castilla, C.; Carrasco-Marin, F., On the Characterization of Acidic and Basic Surface Sites on Carbons by Various Techniques. *Carbon* **1999,** *37*, 1215-1221.

Lord, D. L. Influence of Organic Acid and Base Solution Chemistry on Interfacial and Transport Properties of Mixed Wastes in the Subsurface. Ph.D. dissertation, University of Michigan, Ann Arbor, 1999.

Lord, D. L.; Buckley, J. S., An AFM Study of the Morphological Features that Affect

Wetting at Crude Oil-Water-Mica Interfaces. *Colloids and Surfaces A: Physicochemical and Engineering Aspects* **2002,** *206*, (1), 531-546.

Ma'Shum, M.; Farmer, V. C., Origin and Assessment of Water Repellency of a Sandy South Australian Soil. *Australian Journal of Soil Research* **1985,** *23*, (4), 623-626.
Ma'Shum, M.; Tate, M. E.; Jones, G. P.; Oades, J. M., Extraction and Characterization of Water-Repellent Materials from Australian Soils. *Journal of Soil Science* **1988,** *39*, 99-110.

McBride, M. B., *Environmental Chemistry of Soils*. Oxford University Press, Inc.: New York, 1994; p 406.

McCaffery, F. G.; Mungan, N., Contact Angle and Interfacial Tension Studies of Some Hydrocarbon-Water-Solid Systems. *The Journal of Canadian Petroleum Technology* **1970**, 185-196.

McKay, J. F., A Discussion of the Chemical Structure of the Organic Matter in Green River Oil Shale. *Energy Sources* **1984,** *7*, (3), 257-271.

McKissock, J.; Gilkes, R. J.; van Bronswijk, W., The Relationship of Soil Water Repellency to Aliphatic C and Kaolin Measured Using DRIFT. *Australian Journal of Soil Research* **2003,** *41*, 251-265.

Menon, V. B.; Wasan, D. T., Particle-Fluid Interactions with Application to Solid Stabilized Emulsions, Part I. The Effect of Asphaltene Adsorption. *Colloids and Surfaces A* **1986,** *19*, 89-105.

Mercer, J. W.; Cohen, R. M.; Matthews, J., *DNAPL Site Evaluation*. C.K. Smoley: Boca Raton, FL, 1993.

Mercier, F.; Toulhoat, N.; Potocek, V.; Trocellier, P., The Role of Nitrogen and Sulphur Bearing Compounds in the Wettability of Oil Reservoir Rocks: an Approach with Nuclear Microanalysis and Other Related Surface Techniques. *Nuclear Instruments and Methods in Physics Research B* **1999,** *152*, 122-128.

Miller, R. W.; Gardiner, D. T., *Soils in Our Environment*. 8th ed.; Prentice Hall: Upper Saddle River, NJ, 1998; p 736.

Miranda, P. B.; Pflumio, V.; Saijo, H.; Shen, Y. R., Surfactant Monolayers at Solid-Liquid Interfaces: Conformation and Interaction. *Thin Solid Films* **1998**, 327-329.

Miyamoto, S.; Bristol, A.; Gould, W. L., Wettability of Coal-Mine Spoils in Northwestern New Mexico. *Soil Science* **1976,** *123*, (4), 258-263.

Mohal, B. R.; Chandler, S., A New Technique to Determine Wettability of Powders-Imbibition Time Measurements. *Colloids and Surfaces* **1986,** *21*, 193-203.

Morrow, N. R., The Effects of Surface Roughness on Contact Angle with Special Reference to Petroleum Recovery. *Journal of Canadian Petroleum Technology* **1975**, (October-December), 42-53.

Morrow, N. R.; Chatzis, I.; Taber, J. J., Entrapment and Mobilization of Residual Oil in Bead Packs. *SPE Reservoir Engineering* **1988,** *3*, (3), 927-934.

Morrow, N. R.; Cram, P. J.; McCaffery, F. G., Displacement Studies in Dolomite With Wettability Control by Octanoic Acid. *Society of Petroleum Engineers* **1973,** *13*, (4), 221-232.

Nguyen, H. V., Nieber, J.L., Oduro, P., Ritsema, C.J., Dekker, L.W., Steenhuis, T.S., Modeling Solute Transport in Water Repellent Soil. *Journal of Hydrology* **1999,** *215*, 188-201.

Orumwense, O., F., Estimation of the Wettability of Coal from Contact Angles Using Coagulants and Flocculants. *Fuel* **1998,** *77*, (9/10), 1107-1111.

Parekh, B. K.; Aplan, F. F., The Critical Surface Tension of Wetting of Coal. In *Recent Development in Separation Science*, Li., N. N., Ed. CRC Press: West Palm Beach, FL, 1978; pp 107-113.

Parks, G. A.; de Bruyn, P. C., The Zero Point of Charge of Oxides. *The Journal of Physical Chemistry* **1962,** *66*, 967-973.

Perwuelz, A.; Novais De Olivera, T.; Caze, C., Study of Wetting at the Silicone Oil/Water/Fibre Interface. *Colloids and Surfaces A* **1999,** *147*, 317-329.

Poulenard, J.; Michel, J. C.; Bartoli, F.; Portal, J. M.; Podwojewski, P., Water Repellency of Volcanic Ash Soils from Ecuadorian Paramo: Effect of Water Content and Characteristics of Hydrophobic Organic Matter. *European Journal of Soil Science* **2004,** *55*, (3), 487-496.

Powers, S. E. Dissolution of Nonaqueous Phase Liquids in Saturated Subsurface Systems. Ph.D. dissertation, University of Michigan, Ann Arbor, 1992.

Powers, S. E.; Tamblin, M. E., Wettability of Porous Media after Exposure to Synthetic Gasolines. *Journal of Contaminant Hydrology* **1995,** *19*, 105-125.

Pratt, L. M.; Comer, J. B.; Brassell, S., C. In *Geochemistry of Organic Matter in Sediments and Sedimentary Rocks*, SEPM Short Course 27, 1992, 1992; 1992.

Riddick, J. A.; Bunger, W. B.; Sakano, T. K., *Organic Solvents Physical Properties and Methods of Purification*. John Wiley & Sons: New York, 1986; p 1325.

Riley, R. G.; Zachara, J. M.; Wobber, F. J. *Chemical Contaminants on DOE Lands and Selection of Contaminant Mixtures for Subsurface Science Research*; DOE/ER-0547T; Pacific Northwest Laboratory: April 1992, 1992; p 77.

Rixey, W. G.; Fuerstenau, D. W., The Young Equation and the Effect of Surfactants on the Wettability of Minerals. *Colloids and Surfaces* **1994,** *88*, 75-89.

Robichaud, P. R.; Hungerford, R. D., Water Repellency by Laboratory Burning of Four Northern Rocky Mountain Forest Soils. *Journal of Hydrology* **2000,** *231*, 207-219.

Roehl, P. O.; Choquette, P. W., Perspectives on World-Class Carbonate Petroleum Reservoirs. *AAPG Bulletin-American Association of Petroleum Geologists* **1985,** *69*, (1), 148-148.

Rouxhet, P. G.; Doren, A.; Dewez, J. L.; Heuschling, O., Chemical Composition and Physico-Chemical Properties of Polymer Surfaces. *Progress in Organic Coatings* **1993,** *22*, 327-344.

Roy, J. L. Soil Water Repellency at Old Crude Oil Spill Sites. Ph.D. dissertation, University of Alberta, Edmonton, 1999.

Roy, J. L.; McGill, W. B., Characterization of Disaggregated Nonwettable Surface Soils Found at Old Crude Oil Spill Sites. *Canadian Journal of Soil Science* **1998,** *78*, (2), 331-344.

Roy, J. L.; McGill, W. B., Flexible Conformation in Organic Matter Coatings: An Hypothesis about Soil Water Repellency. *Canadian Journal of Soil Science* **2000,** *80*, (1), 143-152.

Salathiel, R. A., Oil Recovery by Surface Film Drainage. *Journal of Petroleum Technology* **1973**, (255), 1216-1224.

Salehzadeh, A.; Demond, A. H., Pressure Cell for Measuring Capillary Pressure Relationships of Contaminated Sands. *Journal of Environmental Engineering* **1999**, 385-388.

Savage, S. M.; Martin, J. P.; Letey, J., Contribution of Some Soil Fungi to Natural and Heat-Induced Water Repellency in Sand. *Soil Sci. Soc. Amer. Proc.* **1969,** *33*, 405-409.

Schultz, J.; Tsutsumi, K.; Donnet, J.-B., Surface Properties of High Energy Solids 1. Determination of the Dispersive Component of the Surface Free Energy of Mica and Its Energy of Adhesion to Water and n-Alkanes. *Journal of Colloid and Interface Science* **1977,** *59*, (2), 272-276.

Schwille, F., *Dense Chlorinated Solvents in Porous and Fractured Media-Model*

Experiments. Lewis Publishers: Chelsea, MI, 1988.

Serrano Saldaña, E.; Ortiz, A. D.; Aguilar, H. P.; Straus, I. K.; González, F. R., Wettability of Solid/Brine/n – Dodecane Systems: Experimental Study of the Effects of Ionic Strength and Surfactant Concentration. *Colloids and Surfaces A: Physicochemical and Engineering Aspects* **2004,** *241*, 343-349.

Siebold, A.; Walliser, A.; Nardin, M.; Oppliger, M.; Schultz, J., Capillary Rise for the Thermodynamic Characterization of Solid Particle Surface. *Journal of Colloid and Interface Science* **1997,** *186*, 60-70.

Snoeyink, V. L.; Weber, W. J. J., Surface Functional Groups on Carbon and Silica. In *Progress in Surface and Membrane Science*, Danielli, J. F.; Rosenberd, M. D.; Cadenhead, D. A., Eds. Academic Press: New York, 1972; Vol. 5, pp 63-113.

Somasundaran, P.; Zhang, L.; Fuerstenau, D. W., The Effect of Environment, Oxidation and Dissolved Metal Species on the Chemistry of Coal Floatation. *International Journal of Mineral Processing* **2000,** *58*, 85-97.

Sparks, B. D.; Kotlyar, L. S.; O'Carroll, J. B.; Chung, K. H., Athabasca Oil Sands: Effect of Organic Coated Solids on Bitumen Recovery and Quality. *Journal of Petroleum Science and Engineering* **2003,** *39*, 417-430.

Sparks, D. L., *Environmental Soil Chemistry*. Academic Press, Inc.: New York, 1995.

Sposito, G., *The Chemistry of Soils*. Oxford University Press: New York, 1989; p 277.

Standal, S.; Haavik, J.; Blokhus, A. M.; Skauge, A., Effect of Polar Organic Components on Wettability as Studied by Adsorption and Contact Angles. *Journal of Petroleum Science and Engineering* **1999,** *24*, 131-144.

Svitova, T.; Theodoly, O.; Christiano, S.; Hill, R. M.; Radke, C. J., Wetting Behavior of Silicone Oils on Solid Substrates Immersed in Aqueous Electrolyte Solutions. *Langmuir* **2002,** *18*, 6821-6829.

Tampy, G. K.; Prudich, M. E.; Savage, R. L.; Williams, R. R., Free-Energy Changes and Hydrogen-Bonding in the Wetting of Coals. *Energy & Fuels* **1988,** *2*, (6), 787-793.

Toledo, P. G.; Araujo, Y. C.; Leon, V., Wettability of Oil Producing Reservoir Rocks as Determined from X-ray Photoelectron Spectroscopy. *Journal of Colloid and interface science* **1996,** *183*, 301-308.

Toothaker, L. E., *Introductory Statistics for the Behavioral Sciences*. McGraw-Hill, Inc.:

New York, 1986; p 606.

Treiber, L. E.; Archer, D. L.; Owens, W. W., Laboratory Evaluation of Wettability of 50 Oil-Producing Reservoirs. *Society of Petroleum Engineers Journal* **1972,** *12*, (6), 531-540.
U.S. Department of Health and Human Services, Report. on Carcinogens. http://ntp.niehs.nih.gov/ntp/roc/toc11.html (June 26).
Ustohal, P.; Stauffer, F.; Dracos, T., Measurement and Modeling of Hydraulic Characteristics of Unsaturated Porous Media with Mixed Wettability. *Journal of Contaminant Hydrology* **1998,** *33*, (1-2), 5-37.

van Dijke, M. I. J.; Sorbie, K. S., The Relation Between Interfacial Tensions and Wettability in Three-Phase Systems: Consequences for Pore Occupancy and Relative Permeability. *Journal of Petroleum Science and Engineering* **2002,** *33*, 39-48.

van Oss, C. J., Acid-Base Interfacial Interactions in Aqueous Media. *Colloids and Surfaces A: Physicochemical and Engineering Aspects* **1993,** *78*, (1), 1-49.

van Oss, C. J.; Chaudhury, M. K.; Good, R. J., Interfacial Lifshitz-van der Waals and Polar Interactions in Macroscopic Systems. *Chemical Review* **1988a,** *88*, 927-941.

van Oss, C. J.; Good, R. J.; Chaudhury, M. K., Additive and Nonadditive Surface-Tension Components and the Interpretation of Contact Angles. *Langmuir* **1988b,** *4*, 884-891.

van Oss, C. J.; Wu, W.; Docoslis, A.; Giese, R. F., The Interfacial Tension with Water and the Lewis Acid-Base Surface Tension Parameters of Polar Organic Liquids Derived from Their Aqueous Solubilities. *Colloids and Surfaces B: Biointerfaces* **2001,** *20*, 87-91.

Wallis, M. G.; Horne, D. J.; Palmer, A. S., Water Repellency in a New-Zealand Development Sequence of Yellow-Brown Sands. *Australian Journal of Soil Research* **1993,** *31*, (5), 641-654.

Wang, F. H. L.; Guidry, L. J., Effect of Oxidation-Reduction Condition of Wettability Alteration. *SPE Formation Evaluation* **1994**, 140-148.

Wang, Z.; Wu, L.; Wu, Q. J., Water-Entry Value as an Alternative Indicator of Soil Water-Repellency and Wettability. *Journal of Hydrology* **2000,** *231-232*, 76-83.

Ward, A. D.; Ottewill, R. H.; Hazlett, R. D., An Investigation into the Stability of Aqueous Films Separating Hydrocarbon Drops from Quartz Surfaces. *Journal of Petroleum Science and Engineering* **1999,** *24*, 213-220.

Watson, C. L.; Letey, J., Indices for Characterizing Soil Water Repellency Based Upon Contact Angle-Surface Tension Relationships. *Soil Sci. Soc. Amer. Proc.* **1970,** *34*, 841-844.

Weaver, C. E., *Clays, Muds, and Shales*. Elsevier: New York, 1989.

Weber, W. J. J.; McGinley, P. M.; Katz, L. E., A Distributed Reactivity Model for Sorption to Soils and Sediments. 1. Conceptual Basis and Equilibrium Assessments. *Environmental Science & Technology* **1992,** *26*, 1955-1962.

Wessel, A. T., On Using the Effective Contact Angle and the Water Drop Penetration Time for Classification of Water Repellency in Dune Soils. *Earth Surface Processes and Landforms* **1988,** *13*, 555-561.

Wilson, J. L.; Conrad, S. H., Mason, William R.; Peplinski, W.; Hagan, E. *Laboratory Investigation of Residual Liquid Organics from Spills, Leaks, and the Disposal of Hazardous Wastes in Groundwater*; EPA/600/6-90/004; Robert S. Kerr Environmental Laboratory: Socorro, NM, April 1990, 1990; p 255.

Wright, K.; Cygan, R. T.; Slater, B., Structure of the (1014) Surfaces of Calcite, Dolomite and Magnesite under Wet and Dry Conditions. *Physical Chemistry and Chemical Physics* **2001,** *3*, 839-844.

Wu, W., Baseline Studies of the Clay Minerals Society Source Clays: Colloid and Surface Phenomena. *Clays and Clay Minerals* **2001,** *49*, (5), 446-452.

Yaws, C. L., *Chemical Properties Handbook: Physical, Thermodynamic, Environmental, Transport, Safety, and Health Related Properties for Organic and Inorganic Chemicals*. McGraw Hill: New York, **1999**, p 779.

Young, G. J.; Bursh, T. P., Immersion Calorimetry Studies of the Interaction of Water with Silica Surfaces. *Journal of Colloid Science* **1960,** *15*, 361-369.

Yuan, G.; Soma, M.; Seyama, H.; Theng, B. K. G.; Lavkulich, L. M.; Takamatsu, T., Assessing the Surface Composition of Soil Particles from Some Podzolic Soils by X-ray Photoelectron Spectroscopy. *Geoderma* **1998,** *86*, 169-181.

Zhang, S.; Lee, W. E., Improving the Water-Wettability and Oxidation Resistance of Graphite Using Al_2O_3/SiO_2 Sol-Gel Coatings. *Journal of the European Ceramic Society* **2003,** *23*, 1215-1221.

Zhou, Z. A.; Hussein, H.; Xu, S.; Czarnecki, J.; Masliyah, J. H., Interaction of Ionic Species and Fine Solids with a Low Energy Hydrophobic Surface from Contact Angle Measurement. *Journal of Colloid and Interface Science* **1998,** *204*, 342-349.